

# Species-selective Interactions of Histamine H<sub>2</sub> Receptors with Guanidine-type Agonists: Molecular Modelling, Site- directed Mutagenesis and Pharmacological Analysis

## Dissertation

zur Erlangung des Doktorgrades der Naturwissenschaften (Dr. rer. nat.)  
der Naturwissenschaftlichen Fakultät IV – Chemie und Pharmazie –  
der Universität Regensburg



vorgelegt von  
**Hendrik Preuß**  
aus Rudolstadt

2007



Die vorliegende Arbeit entstand in der Zeit von Januar 2003 bis Juni 2007 unter der Leitung von Herrn Prof. Dr. A. Buschauer, Herrn Prof. Dr. S. Dove und Herrn Prof. Dr. R. Seifert am Institut für Pharmazie der Naturwissenschaftlichen Fakultät IV – Chemie und Pharmazie – der Universität Regensburg.

Das Promotionsgesuch wurde eingereicht im Juni 2007.

Tag der mündlichen Prüfung: 9. Juli 2007

Prüfungsausschuss:

Prof. Dr. A. Mannschreck	(Vorsitzender)
Prof. Dr. A. Buschauer	(Erstgutachter)
Prof. Dr. S. Dove	(Zweitgutachter)
Prof. Dr. R. Seifert	(Drittprüfer)

*für Cornelia*



An dieser Stelle möchte ich mich bedanken bei:

Herrn Prof. Dr. A. Buschauer für die Gelegenheit, an einem so interessanten Projekt arbeiten zu dürfen, für seine wissenschaftlichen Anregungen sowie für seine Hilfsbereitschaft und konstruktive Kritik beim Verfassen dieser Arbeit,

Herrn Prof. Dr. S. Dove für seine fachliche Anleitung, wissenschaftliche Diskussionen sowie für seine Hilfsbereitschaft und konstruktive Kritik beim Verfassen dieser Arbeit,

Herrn Prof. Dr. R. Seifert für die Möglichkeit zur Durchführung der molekularpharmakologischen Untersuchungen, für seine fachliche Anleitung, wissenschaftliche Anregungen sowie für die konstruktive Kritik beim Verfassen der pharmakologischen Teile dieser Arbeit,

Herrn Prof. Dr. G. Bernhardt für seine fachliche Hilfe am  $\beta$ -Counter und an der HPLC-Anlage,

Frau Dr. A. Straßer für zahlreiche wissenschaftliche Diskussionen und ihre Unterstützung bei der Durchführung der Moleküldynamik sowie der Durchsicht des daraus hervorgegangenen Kapitels,

Herrn Prof. Dr. A. Pedretti (Università degli Studi di Milano) für die Zusendung der aktuellsten Versionen von VEGA ZZ,

Herrn Prof. Dr. I. Gantz (University of Michigan) für die Bereitstellung des CMVneo-cH<sub>2</sub>R Vektors,

Herrn Prof. Dr. R. Leurs (Vrije Universiteit Amsterdam) für die Bereitstellung des pcDNA-rH<sub>2</sub>R Vektors,

meinen Bürokollegen Herrn Dr. A. Botzki und Frau M. E. Silva für zahlreiche wissenschaftliche Diskussionen und ihre Hilfe bei Problemstellungen des Molecular Modelling,

Frau A. Kraus und Herrn Dr. P. Ghorai für die Bereitstellung der H<sub>2</sub>R-Agonisten,

Herrn Dr. E. Schneider und Herrn David Schnell für ihre Hilfe bei pharmakologischen Problemstellungen und die [ $\gamma$ -<sup>32</sup>P]GTP-Herstellung sowie besonders Frau G. Wilberg für die Anfertigung zahlreicher Western Blots und ihre Unterstützung auf dem Gebiet der Sf9-Zellkultur und Frau A. Seefeld für ihre Hilfe bei der Durchführung von GTPase assays,

Herrn Prof. Dr. J. Heilmann, Frau Dr. M. Hubensack, Frau Dr. M. Bäuml, Frau K. Nickl, Herrn PD Dr. F. Demirci und Herrn Dr. D. Heigl für die angenehme Zeit bei der Betreuung des PB III-Praktikums,

Herrn P. Richthammer für seine Hilfe bei technischen Problemen,

Frau S. Heinrich und Frau M. Luginger für ihre Unterstützung bei organisatorischen Problemen,

allen Mitgliedern des Lehrstuhls für ihre Kollegialität, Hilfsbereitschaft und das gute Arbeitsklima,

dem Graduiertenkolleg 760 der DFG für die finanzielle Unterstützung und wissenschaftliche Förderung,

meinen Freunden und Kollegen Dr. Edith Hofinger, Dr. Ralf Ziemek, Dr. Stefan Braun, Dr. Manuela Menke, Dr. Christian Horn, Patrick Igel und Christine Müller für die schöne Zeit in Regensburg,

ganz besonders meinen Eltern, meiner Schwester, meinen Großeltern und allen weiteren Familienmitgliedern für ihre Unterstützung und Hilfe,

und vor allem Cornelia.

# Contents

<b>1</b>	<b>Introduction</b>	<b>1</b>
1.1	G protein coupled receptors	1
1.2	Signal transduction of GPCRs	2
1.3	Constitutive activity and models of GPCR activation	4
1.4	Histamine and the histamine receptor family	6
1.4.1	Historical perspective	6
1.4.2	Histamine	7
1.4.3	Histamine receptors	9
1.4.4	The histamine H <sub>2</sub> receptor	13
1.4.4.1	Molecular pharmacological characterization	13
1.4.4.2	H <sub>2</sub> R distribution, functions, and signaling pathways	15
1.4.5	Histamine H <sub>2</sub> receptor agonists	17
1.4.5.1	Interactions of HA and small agonists with the H <sub>2</sub> R	17
1.4.5.2	Imidazolylpropylguanidines	19
1.5	References	22
<b>2</b>	<b>Scope and Objectives</b>	<b>29</b>
2.1	References	31
<b>3</b>	<b>Computational Methods</b>	<b>33</b>
3.1	GPCR homology models in pharmacological sciences	33
3.2	Sequence alignment	34
3.3	Construction of 3D structures	35
3.4	Validation of homology models	36
3.5	References	37

---

<b>4 3D Structure Models of Human and Guinea Pig Histamine H<sub>2</sub> Receptors: Analysis of Species-selective Interactions with Guanidine-type Agonists and Virtual Screening.....</b>	<b>39</b>
4.1 Introduction .....	39
4.2 Materials and Methods .....	41
4.2.1 Sequence alignment .....	41
4.2.2 Generation of 3D structure models of the hH <sub>2</sub> R and gpH <sub>2</sub> R .....	42
4.2.3 Structural refinement of the models .....	43
4.2.4 Docking of H <sub>2</sub> R agonists .....	43
4.2.5 Preparation of compound databases .....	44
4.2.6 Application of the LUDI software for virtual screening .....	45
4.3 Results.....	45
4.3.1 Characterization of three-dimensional homology models of hH <sub>2</sub> R and gpH <sub>2</sub> R ....	45
4.3.1.1 Analysis of the stereochemical quality .....	45
4.3.1.2 Conserved intramolecular interactions in rhodopsin and the H <sub>2</sub> R .....	47
4.3.2 Analysis of the binding modes of imidazolylpropylguanidines and N <sup>G</sup> -acylated derivatives with H <sub>2</sub> R species isoforms .....	51
4.3.2.1 Similar binding modes of agonists at hH <sub>2</sub> R and gpH <sub>2</sub> R.....	51
4.3.2.2 Distinct interactions of guanidine-type agonists with hH <sub>2</sub> R and gpH <sub>2</sub> R species isoforms .....	53
4.3.2.3 Impact of the alkyl chain length on species-selective interactions .....	54
4.3.3 Virtual screening for potent and selective acylguanidine-type hH <sub>2</sub> R agonists .....	55
4.4 Discussion .....	58
4.5 References .....	60
 <b>5 Molecular Dynamics Simulations of the Human Histamine H<sub>2</sub> Receptor in a Hydrated POPC Bilayer.....</b>	 <b>65</b>
5.1 Introduction .....	65
5.2 Materials and Methods .....	67
5.2.1 Construction of an hH <sub>2</sub> R-POPC-water system.....	67
5.2.2 Docking of ARP into the pre-equilibrated hH <sub>2</sub> R-POPC-water system.....	68
5.2.2.1 Preparation of the ligand .....	68
5.2.2.2 Preparation of the receptor structure and docking procedure .....	68
5.2.3 Parameters for MD simulations with GROMACS.....	69
5.3 Results.....	69
5.3.1 Equilibration of the hH <sub>2</sub> R-POPC-water system .....	69
5.3.1.1 NVT ensemble.....	70

5.3.1.2 <i>NPT</i> ensemble.....	70
5.3.1.3 Analysis of system parameters.....	71
5.3.1.4 Structural analysis of the POPC bilayer .....	72
5.3.2 MD simulations of the ligand-free and the ARP-docked hH <sub>2</sub> R models .....	77
5.3.2.1 System parameters and POPC bilayer structure.....	78
5.3.2.2 Arrangement of secondary structure elements.....	79
5.3.2.3 Analysis of conserved intramolecular interactions.....	83
5.3.2.4 Internal water molecules .....	86
5.3.2.5 Interactions of ARP with the hH <sub>2</sub> R binding pocket .....	88
5.4 Discussion .....	92
5.4.1 Setup of the simulation system .....	92
5.4.2 Application of restraints on protein atoms during MD simulations .....	93
5.4.3 Characterization of the ligand-free and the ARP-bound hH <sub>2</sub> R models .....	93
5.4.4 Dynamic model of the hH <sub>2</sub> R binding site for guanidine-type agonists .....	95
5.4.5 Conclusion .....	96
5.5 References .....	97
<b>6 Pharmacological Methods .....</b>	<b>103</b>
6.1 Materials .....	103
6.2 Generation of recombinant baculoviruses, cell culture, and membrane preparation.....	104
6.3 SDS-PAGE and immunoblot analysis.....	104
6.4 Steady-state GTPase activity assay .....	104
6.5 AC activity assay .....	105
6.6 Preparation of [ $\gamma$ - <sup>32</sup> P]GTP .....	106
6.7 Miscellaneous .....	106
6.8 References .....	107
<b>7 Constitutive Activity and Ligand Selectivity of Human, Guinea Pig, Rat, and Canine Histamine H<sub>2</sub> Receptors.....</b>	<b>109</b>
7.1 Introduction .....	109
7.2 Materials and Methods .....	112
7.2.1 Materials .....	112
7.2.2 Construction of the cDNAs for rH <sub>2</sub> R and rH <sub>2</sub> R-G <sub>saS</sub> .....	112
7.2.3 Construction of the cDNAs for cH <sub>2</sub> R and cH <sub>2</sub> R-G <sub>saS</sub> .....	113
7.3 Results.....	115
7.3.1 Immunological detection of recombinant proteins in Sf9 cell membranes .....	115

7.3.2 Efficacies and potencies of agonists at H <sub>2</sub> R-G <sub>saS</sub> species isoforms derived from the GTPase assay .....	117
7.3.3 Potencies and inverse agonist efficacies of antagonists at H <sub>2</sub> R-G <sub>saS</sub> species isoforms derived from the GTPase assay .....	119
7.3.4 Constitutive activities of hH <sub>2</sub> R-G <sub>saS</sub> , gpH <sub>2</sub> R-G <sub>saS</sub> , rH <sub>2</sub> R-G <sub>saS</sub> , and cH <sub>2</sub> R-G <sub>saS</sub> in the GTPase assay .....	120
7.3.5 Ambiguous response of metiamide in the GTPase assay .....	123
7.3.6 Regulation of AC activities in membranes expressing fused and non-fused H <sub>2</sub> R species isoforms.....	124
7.4 Discussion .....	127
7.4.1 Increased constitutive activity of the cH <sub>2</sub> R compared to hH <sub>2</sub> R, gpH <sub>2</sub> R, and rH <sub>2</sub> R .....	127
7.4.2 Ligand-specific interactions at H <sub>2</sub> R species isoforms .....	128
7.4.3 Conclusion .....	129
7.5 References .....	130
<b>8 Point Mutations of Cys-17 and Ala-271 in the Human Histamine H<sub>2</sub> Receptor.....</b>	<b>133</b>
8.1 Introduction .....	133
8.2 Materials and Methods .....	135
8.2.1 Materials .....	135
8.2.2 Construction of the cDNA for hH <sub>2</sub> R-C17Y-G <sub>saS</sub> .....	135
8.2.3 Construction of the cDNA for hH <sub>2</sub> R-C17Y-A271D-G <sub>saS</sub> .....	136
8.2.4 Reverse transcription .....	136
8.3 Results.....	137
8.3.1 Immunological detection of recombinant proteins in Sf9 cell membranes .....	137
8.3.2 Analysis of the mRNA in Sf9 membranes expressing hH <sub>2</sub> R-C17Y-G <sub>saS</sub> and hH <sub>2</sub> R-C17Y-A271D-G <sub>saS</sub> .....	138
8.3.3 Efficacies and potencies of agonists at hH <sub>2</sub> R-G <sub>saS</sub> , gpH <sub>2</sub> R-G <sub>saS</sub> , hH <sub>2</sub> R-C17Y-G <sub>saS</sub> , and hH <sub>2</sub> R-C17Y-A271D-G <sub>saS</sub> .....	139
8.3.4 Potencies and inverse agonist efficacies of antagonists at hH <sub>2</sub> R-G <sub>saS</sub> , gpH <sub>2</sub> R-G <sub>saS</sub> , hH <sub>2</sub> R-C17Y-G <sub>saS</sub> , and hH <sub>2</sub> R-C17Y-A271D-G <sub>saS</sub> .....	142
8.3.5 Regulation of AC activities in membranes expressing hH <sub>2</sub> R-G <sub>saS</sub> , gpH <sub>2</sub> R-G <sub>saS</sub> , hH <sub>2</sub> R-C17Y-G <sub>saS</sub> , and hH <sub>2</sub> R-C17Y-A271D-G <sub>saS</sub> .....	143
8.4 Discussion .....	145
8.4.1 Impaired coupling in membranes expressing hH <sub>2</sub> R-C17Y-G <sub>saS</sub> .....	145
8.4.2 Increased constitutive activity in membranes expressing hH <sub>2</sub> R-C17Y-A271D-G <sub>saS</sub> .....	146

8.4.3 Species-selectivity of guanidines and $N^G$ -acylguanidines at wild-type and mutant $H_2R-G_{saS}$ .....	147
8.4.4 Conclusion .....	148
8.5 References .....	149
<b>9 Point Mutations in the Second Extracellular Loops of Human and Guinea Pig Histamine <math>H_2</math> Receptors .....</b>	<b>151</b>
9.1 Introduction .....	151
9.2 Materials and Methods .....	154
9.2.1 Materials .....	154
9.2.2 Construction of the cDNA for gp $H_2R$ -hE2- $G_{saS}$ .....	154
9.2.3 Construction of the cDNA for h $H_2R$ -gpE2- $G_{saS}$ .....	155
9.2.4 Construction of the cDNA for h $H_2R$ -K173A- $G_{saS}$ .....	156
9.2.5 Construction of the cDNA for h $H_2R$ -K175A- $G_{saS}$ .....	156
9.3 Results.....	157
9.3.1 Immunological detection of recombinant proteins in Sf9 cell membranes .....	157
9.3.2 GTPase activities in Sf9 membranes expressing wild-type and mutant $H_2R-G_{saS}$ .....	158
9.4 Discussion .....	161
9.5 References .....	162
<b>10 Summary .....</b>	<b>165</b>
<b>11 Appendix .....</b>	<b>167</b>
Appendix 1: Principles of Molecular Mechanics and MD Simulations .....	167
Appendix 2: Parameters for MD simulations in GROMACS .....	173
Appendix 3: List of publications and presentations.....	176





## Abbreviations

3D	three-dimensional
AC	adenylyl cyclase
AMT	amthamine
ANOVA	analysis of variance
APT	aminopotentidine
ARP	arpromidine
ATP	adenosine triphosphate
BET	betahistine
bp	base pair(s)
cAMP	cyclic 3',5'-adenosine monophosphate
cH <sub>2</sub> R	canine histamine H <sub>2</sub> receptor
CIM	cimetidine
CoMFA	comparative molecular field analysis
DHA	dihydroalprenolol
DIM	dimaprit
e1, e2, e3	1 <sup>st</sup> , 2 <sup>nd</sup> , and 3 <sup>rd</sup> extracellular loops of a G protein coupled receptor
EC <sub>50</sub>	agonist concentration which induces 50% of the maximum effect
EDTA	ethylenediaminetetraacetic acid
FAM	famotidine
GDP	guanosine diphosphate
GPCR	G protein coupled receptor
GTP	guanosine triphosphate
gpH <sub>2</sub> R	guinea pig histamine H <sub>2</sub> receptor
gpH <sub>2</sub> R-hE2-G <sub>saS</sub>	fusion protein of the guinea pig histamine H <sub>2</sub> receptor bearing Asp-167→Gly-167, Asp-169→His-169, Ile-171→Thr-171, and Val-172→Ser-172 mutations, and the short splice variant of G <sub>sa</sub>
FLAG	octapeptide epitope for the labeling of proteins
G <sub>sa</sub>	α-subunit of the G <sub>s</sub> protein that mediates adenylyl cyclase activation
G <sub>saS</sub>	short splice variant of the G <sub>s</sub> protein G <sub>sa</sub>
GROMACS	Groningen Machine for Chemical Simulations
H <sub>1</sub> R, H <sub>2</sub> R, H <sub>3</sub> R, H <sub>4</sub> R	histamine receptor subtypes
(c/gp/h/r)H <sub>2</sub> R-G <sub>saS</sub>	fusion proteins of histamine H <sub>2</sub> receptor species isoforms and the short splice variant of G <sub>sa</sub>
HA	histamine
hH <sub>2</sub> R	human histamine H <sub>2</sub> receptor
hH <sub>2</sub> R-C17Y-A271D-G <sub>saS</sub>	fusion protein of the human histamine H <sub>2</sub> receptor bearing a Cys→Tyr mutation at position 17 and an Ala→Asp mutation at position 271 and the short splice variant of G <sub>sa</sub>

hH <sub>2</sub> R-C17Y-G <sub>saS</sub>	fusion protein of the human histamine H <sub>2</sub> receptor bearing a Cys→Tyr mutation at position 17 and the short splice variant of G <sub>sa</sub>
hH <sub>2</sub> R-gpE2-G <sub>saS</sub>	fusion protein of the human histamine H <sub>2</sub> receptor bearing Gly-167→Asp-167, His-169→Asp-169, Thr-171→Ile-171, and Ser-172→Val-172 mutations, and the short splice variant of G <sub>sa</sub>
hH <sub>2</sub> R-K173A-G <sub>saS</sub>	fusion protein of the human histamine H <sub>2</sub> receptor bearing a Lys-173→Ala-173 mutation, and the short splice variant of G <sub>sa</sub>
hH <sub>2</sub> R-K175A-G <sub>saS</sub>	fusion protein of the human histamine H <sub>2</sub> receptor bearing a Lys-175→Ala-175 mutation, and the short splice variant of G <sub>sa</sub>
i1, i2, i3	1 <sup>st</sup> , 2 <sup>nd</sup> , and 3 <sup>rd</sup> intracellular loops of a G protein coupled receptor
IAPT	iodoaminopotentidine
IMP	impromidine
K <sub>B</sub>	dissociation constant (functional assay)
L <sub>α</sub>	fluid phase of a lipid bilayer
MD	molecular dynamics
mRNA	messenger ribonucleic acid
NPT ensemble	constant number of atoms ( <i>N</i> ), pressure ( <i>P</i> ), and temperature ( <i>T</i> )
NVT ensemble	constant number of atoms ( <i>N</i> ), volume ( <i>V</i> ), and temperature ( <i>T</i> )
P <sub>i</sub>	inorganic phosphate
PAGE	polyacrylamide gel electrophoresis
PCR	polymerase chain reaction
POPC	1-palmitoyl-2-oleoyl- <i>sn</i> -glycero-3-phosphatidylcholine
QSAR	quantitative structure-activity relationships
r <sup>2</sup>	correlation coefficient
RAN	ranitidine
R <sub>gyration</sub>	radius of gyration
rH <sub>2</sub> R	rat histamine H <sub>2</sub> receptor
RMSD	root mean square deviation
rpm	revolutions per minute
S.D.	standard deviation
SASA	solvent-accessible surface area
S <sub>CD</sub>	order parameter
SDS	sodiumdodecylsulfate
S.E.M.	standard error of the mean
Sf9	<i>Spodoptera frugiperda</i> insect cell line
<i>sn</i>	stereospecific numbering (lipid nomenclature)
TM	transmembrane domain of a G protein coupled receptor
TM1-TM7	numbering of transmembrane domains of a G protein coupled receptor
Tris	tris(hydroxymethyl)aminomethan
vdW	van der Waals

# Chapter 1

## Introduction

### 1.1 G protein coupled receptors

G protein coupled receptors (GPCRs) represent one of the most important drug targets for pharmacological intervention and play key roles in cellular signaling networks (Hebert and Bouvier, 1998). It is estimated that more than 50% of the current therapeutic agents on the market are targeted at these receptors (Drews, 2000). The completion of the human genome project (International Human Genome Sequencing Consortium, 2004) has enabled the identification of more than 800 genes that belong to the GPCR superfamily which accounts for about 2% of the human genome (Fredriksson and Schiöth, 2005). The significance of GPCRs as drug targets lies in their physiological roles as cell-surface receptors responsible for transducing exogenous signals into cellular responses enabling the communication between individual cells, tissues or organs (Fang et al., 2003; Wise et al., 2002).

There are two main requirements for a protein to be classified as a GPCR. The first requirement concerns the existence of seven sequence stretches of about 25 to 35 residues comprising a high degree of hydrophobicity. These sequences should build seven  $\alpha$ -helices that span the cell membrane in an anti-clockwise manner when viewed from the extracellular side, forming a receptor, or a recognition and connection unit, enabling an extracellular ligand to exert a specific effect into the cell (Fredriksson et al., 2003). Following the term GPCR, the second main requirement would be the ability of the receptor to interact with a G protein. However, phylogenetic analysis uncovered many GPCRs to modulate G protein independent pathways (Fredriksson et al., 2003). Therefore, the term seven transmembrane (TM) receptors would be more technically correct. Both terms are used by the International Union of Pharmacology Committee on Receptor Nomenclature and Drug Classification (NC-

IUPHAR) (Humphrey and Barnard, 1998; Foord et al., 2005).

GPCRs are known as extremely versatile receptors for extracellular messengers as diverse as biogenic amines, purines and nucleic acid derivatives, lipids, peptides and proteins, odorants, pheromones, tastants, ions like calcium and protons, and even photons in the case of rhodopsin (Jacoby et al., 2006). GPCRs can roughly be separated into GPCRs responding to sensory signals of external origin (chemosensory GPCRs) and GPCRs responding to signals produced by endogenous ligands. Based on phylogenetic and ligand-receptor relationships the repertoire of human GPCRs is classified into three main subclasses/families, A, B, C, or 1, 2, 3, respectively<sup>1</sup>. The rhodopsin-like class 1 is the largest subgroup and contains the opsins, olfactory GPCRs, small-molecules/peptide hormone GPCRs, and glycoprotein hormone GPCRs. The binding sites of the endogenous small-molecule ligands are located within the TM bundle, whereas binding of peptides and glycoproteins occurs at the N-terminus, the extracellular loop regions, and the superior parts of the TM helices (Kristiansen, 2004). The secretin-like receptor class 2 contains GPCRs for peptides such as secretin, calcitonin, and parathyroid hormone. This family is characterized by a large N-terminus which is involved in ligand binding. The small glutamate class 3 comprises the metabotropic glutamate receptor, the  $\gamma$ -aminobutyric acid type B receptor,  $\text{Ca}^{2+}$ -sensing receptors, and pheromone and taste receptors. The ligand binding site of this family is located in the very large N-terminal region, which is composed of the so-called venus flytrap module that shares sequence similarity with bacterial periplasmic amino acid binding proteins (Jacoby et al., 2006). Another separate class comprises the human frizzled/smoothed receptors controlling cell development and proliferation mediated by the secreted glycoproteins Wnt and hedgehog.

Up to now, 244 human GPCRs with known ligands were identified, whereas 163 human GPCRs have no known ligand and are therefore still orphan receptors (Fredriksson and Schiöth, 2006).

## 1.2 Signal transduction of GPCRs

Upon extracellular binding of an agonist, GPCRs undergo a conformational change into an activated state which specifically interacts with a precoupled or free heterotrimeric G protein, consisting of a  $G_\alpha$ -subunit and a  $G_{\beta\gamma}$  heterodimer, located at the cytosolic side of the membrane (Hamm, 1998; Kostenis, 2006; Sprang, 1997).

When interacting with a GPCR in an active state, the conformation of the G protein  $\alpha$ -subunit is changed leading to the release of GDP (Figure 1.1). The resulting ternary complex of

---

<sup>1</sup> Both terminologies are synonymously used by the NC-IUPHAR.

agonist, GPCR, and G protein is characterized by high agonist affinity and promotes binding of GTP to  $G_{\alpha}$ . The binding of GTP to  $G_{\alpha}$  induces a conformational change in this subunit, resulting in dissociation of the heterotrimer into  $G_{\alpha}$ -GTP and the  $G_{\beta\gamma}$  complex. Different subtypes of activated  $G_{\alpha}$ -GTP can selectively stimulate ( $G_{\alpha s}$ ) or inhibit ( $G_{\alpha i}$ ) adenylyl cyclase (AC), activate phospholipase C $\beta$  ( $G_{\alpha q}$ ), or interact with guanine nucleotide exchange factors ( $G_{\alpha 12/13}$ ). As a result, the production of second messengers such as cyclic 3',5'-adenosine monophosphate (cAMP), diacylglycerol (DAG), and inositol-1,4,5-triphosphate (IP<sub>3</sub>) is modulated. These second messengers can induce a fast cellular response, such as a change in the intracellular ion concentration or the regulation of enzyme activity, or cause a long-term biological effect by modulating transcription factors, thereby regulating gene expression. The  $G_{\beta\gamma}$  subunit is also known to trigger cellular effects, *e.g.* via interaction with phospholipase C $\beta$ , AC or ion channels. The slow intrinsic GTPase activity of the  $G_{\alpha}$ -subunit leads to hydrolysis of GTP into GDP and P<sub>i</sub>, thus terminating the  $G_{\alpha}$ -induced effector activation and allowing the re-association of the subunits for the start of a new cycle.

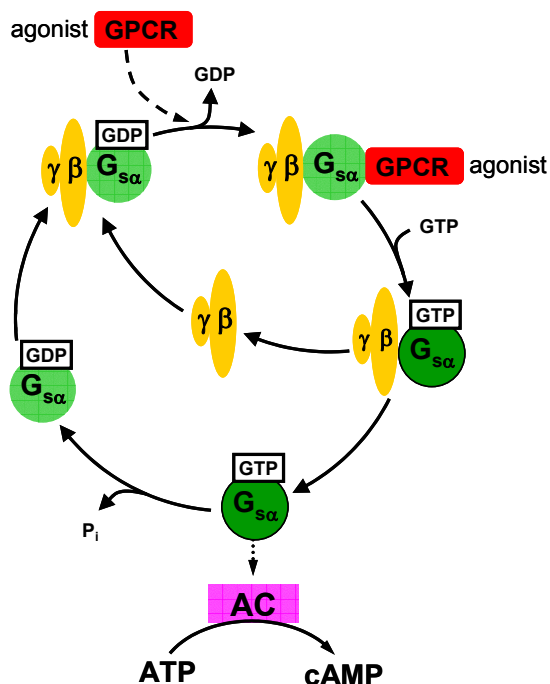


**Figure 1.1:**  $G_{s\alpha}$  protein activation/deactivation cycle after GPCR stimulation by an agonist. Adapted from Seifert, 2005.

One ubiquitous feature of signaling through GPCRs is the loss of cellular sensitivity following continuous stimulation. Such desensitization processes include phosphorylation of GPCRs by G protein coupled receptor kinases (GRK) followed by  $\beta$ -arrestin binding that uncouple the receptor at the plasma membrane from the G protein. Subsequent internalization of the receptor via clathrin-coated vesicles ultimately leads to sorting of the receptor either back to the plasma membrane (receptor recycling) or to lysosomes for degradation. GPCR phosphorylation is also mediated by second messenger dependent protein kinases.

The investigation of the mechanisms of agonist-induced receptor signaling, desensitization, internalization, trafficking, and recycling resulted in the discovery of many proteins that interact with GPCRs and which are collectively called G protein coupled receptor interacting proteins (GIPs) (Bockaert and Pin, 1999; Bockaert et al., 2004). GIPs form large protein networks with GPCRs called receptosomes. Investigations on mechanistic principles associated with receptosomes and their potential relevance for drug discovery are subject of current research (Jacoby et al., 2006).

### 1.3 Constitutive activity and models of GPCR activation

Constitutive activity can be defined as the ability of a GPCR to spontaneously (*i.e.* in the absence of an agonist) adopt an active conformation which activates G proteins (Samama et al., 1993; Lefkowitz et al., 1993). Until now, constitutive activity is observed in more than 60 wild-type GPCRs, and a large number of disease-causing GPCR mutations with increased constitutive activity has been identified (Seifert and Wenzel-Seifert, 2002).

The extended ternary complex model (ETC model) (Samama et al., 1993; Lefkowitz et al., 1993) which is also referred to as the two-state model of receptor activation (Leff, 1995), describes the ability of a GPCR to isomerize from an inactive ( $R$ ) to an active ( $R^*$ ) state of which only  $R^*$  can effectively interact with and activate G proteins. Both states coexist according to an allosteric constant  $L = [R^*] / [R]$  (Figure 1.2 A). The magnitude of  $L$  defines

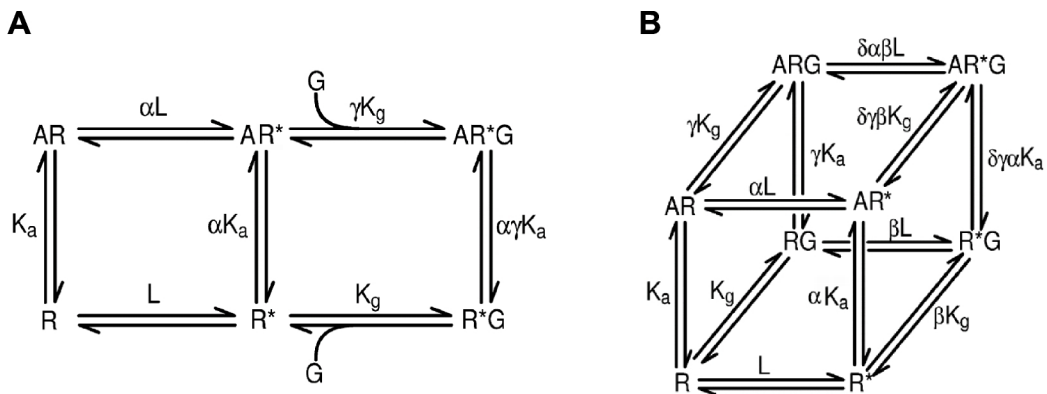


**Figure 1.2:** A, Extended ternary complex model of GPCR activation. The equilibrium between  $R$  and  $R^*$  is given by the allosteric constant  $L$ . Ligands have an affinity (association) constant  $K_a$  for  $R$  and  $\alpha K_a$  for  $R^*$ . G proteins have an affinity (association) constant  $K_g$  for  $R^*$  and  $\gamma K_g$  for  $AR^*$ . The response producing species are the agonist-free and the agonist-occupied complexes  $R^*G$  and  $AR^*G$ . B, Cubic ternary complex model. The inactive receptor  $R$  interacts (precouples) with the G protein to form the non-signaling complexes  $RG$  and  $ARG$ . The constant  $\delta$  reflects the specific state of the active ligand-bound receptor/G protein complex.

the ease of a spontaneous formation of the  $R^*$  state, *i.e.* the degree of constitutive activity. Full agonists maximally stabilize the  $R^*$  state and cause a maximally efficient GDP/GTP exchange at a G protein which, in turn, evokes maximum physiological response, called efficacy, in the biological system (Kenakin, 2002) (Figure 1.3 A, B). Conversely, full inverse agonists maximally stabilize the  $R$  state and reduce basal GDP/GTP exchange. Neutral antagonists do not alter the equilibrium between  $R$  and  $R^*$  and do not change basal G protein activity. Partial agonists and partial inverse agonists have lower efficacies than full agonists and full inverse agonists, respectively.

A more thermodynamically refined model of GPCR activation is established by the cubic ternary complex model (CTC model; Figure 1.2 B) (Weiss et al., 1996a, b, c). This model allows both the active and inactive receptor species to interact with G proteins. Of all theoretically possible receptor states, only the complexes between the activated receptor  $R^*$

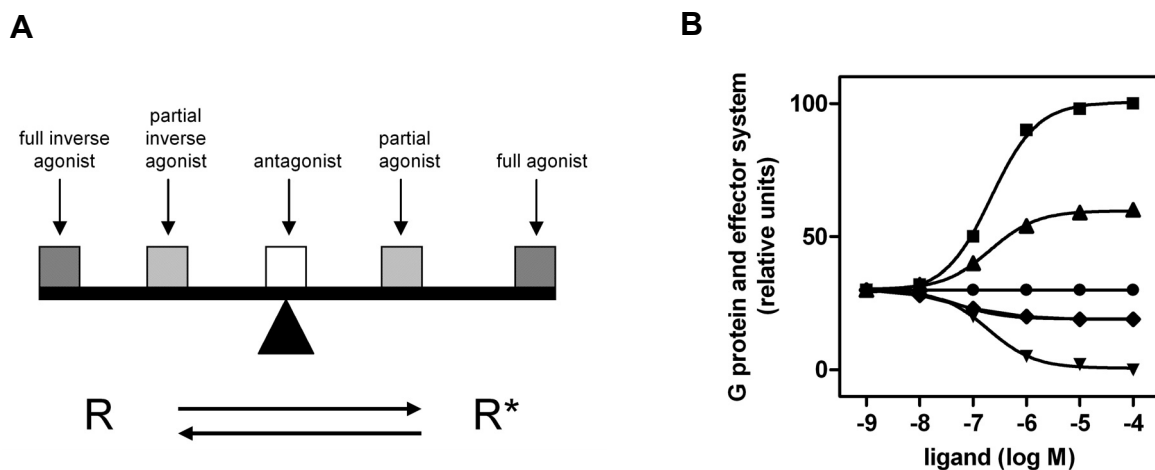


**Figure 1.3:** The two state model of GPCR activation. A, GPCRs are able to isomerize from an inactive state ( $R$ ) to an active state ( $R^*$ ). Ligands are classified according to their capability of shifting the equilibrium to either side of both states. B, differential responses in an effector system upon binding of full agonists (■), partial agonists (▲), antagonists (●), partial inverse agonists (◆), and full inverse agonists (▼). Adapted from Seifert, 2005.

and the G protein,  $AR^*G$  and  $R^*G$ , are assumed to give rise to G protein activation and thus physiological response.

To date, there is increasing evidence that GPCRs can adopt more than one active state (reviewed in Perez and Karnik, 2005). For example, the concept of agonist-directed trafficking of a receptor stimulus refers to the ability of structurally diverse agonists to activate different G protein-mediated signaling (Kenakin, 1995). Moreover, Swaminath et al. investigated catecholamine-induced  $\beta_2$ -adrenoceptor activation by kinetically distinguishable

active conformational states (Swaminath et al., 2004). GPCRs are thus assumed to adopt multiple active conformations with distinct biological activities.

## 1.4 Histamine and the histamine receptor family

### 1.4.1 Historical perspective

Histamine (HA, Figure 1.5), 2-(1*H*-imidazol-4-yl)ethylamine, was first synthesized in 1908 (Windaus and Vogt, 1908). HA was isolated from ergot in 1910 (Barger and Dale, 1910) and pharmacologically characterized during the following years (Dale and Laidlaw, 1910, 1911, 1919). In these early studies, fundamental effects of HA were elaborated, such as stimulation of smooth muscles from the gut and respiratory tract, vasodepression, stimulation of cardiac contractility, and induction of shock-like syndrome when injected into animals. In 1927, HA was isolated from liver and lung, thereby verifying for the first time HA to be an endogenous substance (Best et al., 1927). The first in a series of compounds that blocked the action of HA on vascular dilation and smooth muscle contraction during an anaphylactic response were developed in the 1930s (Fourneau and Bovet, 1933; Bovet and Staub, 1937). Subsequently, many other chemicals with similar actions have been identified. Some of these compounds (e.g. mepyramine, diphenhydramine) were introduced to clinical use in allergic conditions like hay fever. As these classical “antihistamines” were not able to block certain effects of HA such as the stimulation of gastric acid secretion, Ash and Schild suggested that HA acts via two distinct receptor subtypes (Ash and Schild, 1966). This prediction was confirmed when Black and co-workers developed burimamide (Figure 1.4), the first compound described to antagonize the HA-stimulated gastric acid secretion and the HA-induced relaxation of the electrically stimulated rat uterus (Black et al., 1972). Burimamide was shown to be a highly specific, competitive antagonist of the actions of HA on non-H<sub>1</sub> receptor containing tissues and led to the definition of these receptors as histamine H<sub>2</sub> receptors. For the treatment of gastric and duodenal ulcer, more potent H<sub>2</sub>R antagonists were chemically derived from burimamide, resulting in the development of metiamide (Black et al., 1973) and the first launched H<sub>2</sub>R antagonist, cimetidine (Brimblecombe et al., 1975). Together with the subsequently developed compounds ranitidine, famotidine, nizatidine and roxatidine, H<sub>2</sub>R antagonists became blockbuster drugs for the treatment of gastric and duodenal ulcers. In most cases, these compounds contain a basically substituted aromatic or heteroaromatic system, connected via a flexible chain to a planar structure, which is polar and uncharged at physiological pH.



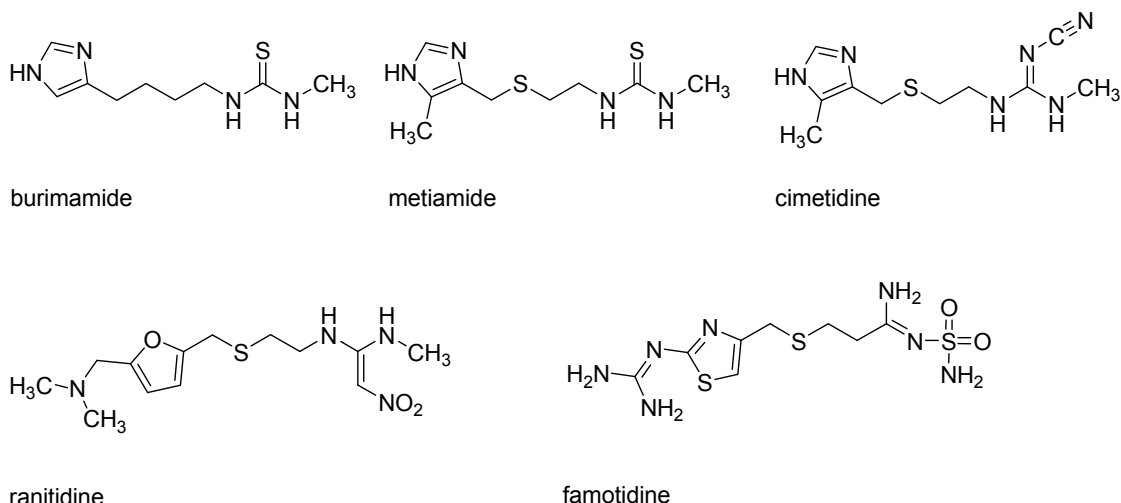


**Figure 1.4:** Structures of H<sub>2</sub>R antagonists/inverse agonists.

In 1983, the group of Schwartz has shown that HA inhibits its own release from depolarized slices of rat cerebral cortex, an action that was proposed to be mediated by a new subtype, the histamine H<sub>3</sub> receptor (Arrang et al., 1983). This suggestion was confirmed and the receptor was characterized in 1987 by the discovery that (*R*)- $\alpha$ -methylhistamine was a potent agonist and that thioperamide was a very selective competitive antagonist (Arrang et al., 1987). During the 1990s, progress in the field of molecular biology enabled cloning of H<sub>1</sub>R (Yamashita et al., 1991), H<sub>2</sub>R (Gantz et al., 1991a), and H<sub>3</sub>R (Lovenberg et al., 1999). A DNA sequence with homology to the H<sub>3</sub>R (35%) was identified, that was cloned and later termed H<sub>4</sub>R (Oda et al., 2000). The existence of the new receptor was confirmed by other workgroups (Liu et al., 2001; Morse et al., 2001; Nguyen et al., 2001; Zhu et al., 2001). A very recent retrospect about the history of HA and its receptors is given by Parsons and Ganellin (Parsons and Ganellin, 2006).

### 1.4.2 Histamine

Histamine is one of the most important mediators involved in various physiological and pathological conditions, including neurotransmission and numerous brain functions, secretion of pituitary hormones, regulation of gastrointestinal and circulatory functions, and inflammatory reactions (Leurs et al., 1995). High concentrations of HA are found in the skin, lung, and the gastrointestinal tract. In the hematopoietic system, mast cells and basophils store HA in specific granules where it is closely associated with anionic proteoglycans and chondroitin-4-sulfate. In this form, it can be released in large amounts during degranulation in response to various immunological or non-immunological stimuli. Alternatively, HA is liberated upon destruction of these cells or by chemical substances (HA liberators). In the stomach, HA is

produced in the enterochromaffin-like cells (ECL) and regulates gastric acid secretion. In the central nervous system (CNS), histaminergic neurons are located in the tuberomammillary nucleus of the posterior hypothalamus. They are involved in the regulation of brain functions such as sleep/wakefulness, emotion, learning, memory, locomotor activity, nociception, food intake, etc. (Haas and Panula, 2003). Recently, other cellular sources of HA have been discovered (Dy and Schneider, 2004) in which HA is immediately released without prior storage. The production of the so-called “neo-synthesized HA” is modulated by cytokines and was identified in hematopoietic cells, macrophages, platelets, dendritic cells, and T cells.

HA is synthesized in the cytosol by decarboxylation of histidine by *L*-histidine decarboxylase (HDC) (EC 4.1.1.22), which requires binding of the cofactor pyridoxal-5-phosphate (Figure 1.5). The vesicular monoamine transporter VMAT2 is responsible for the transport of HA from the cytosol into the secretory granules (Kazumori et al., 2004).

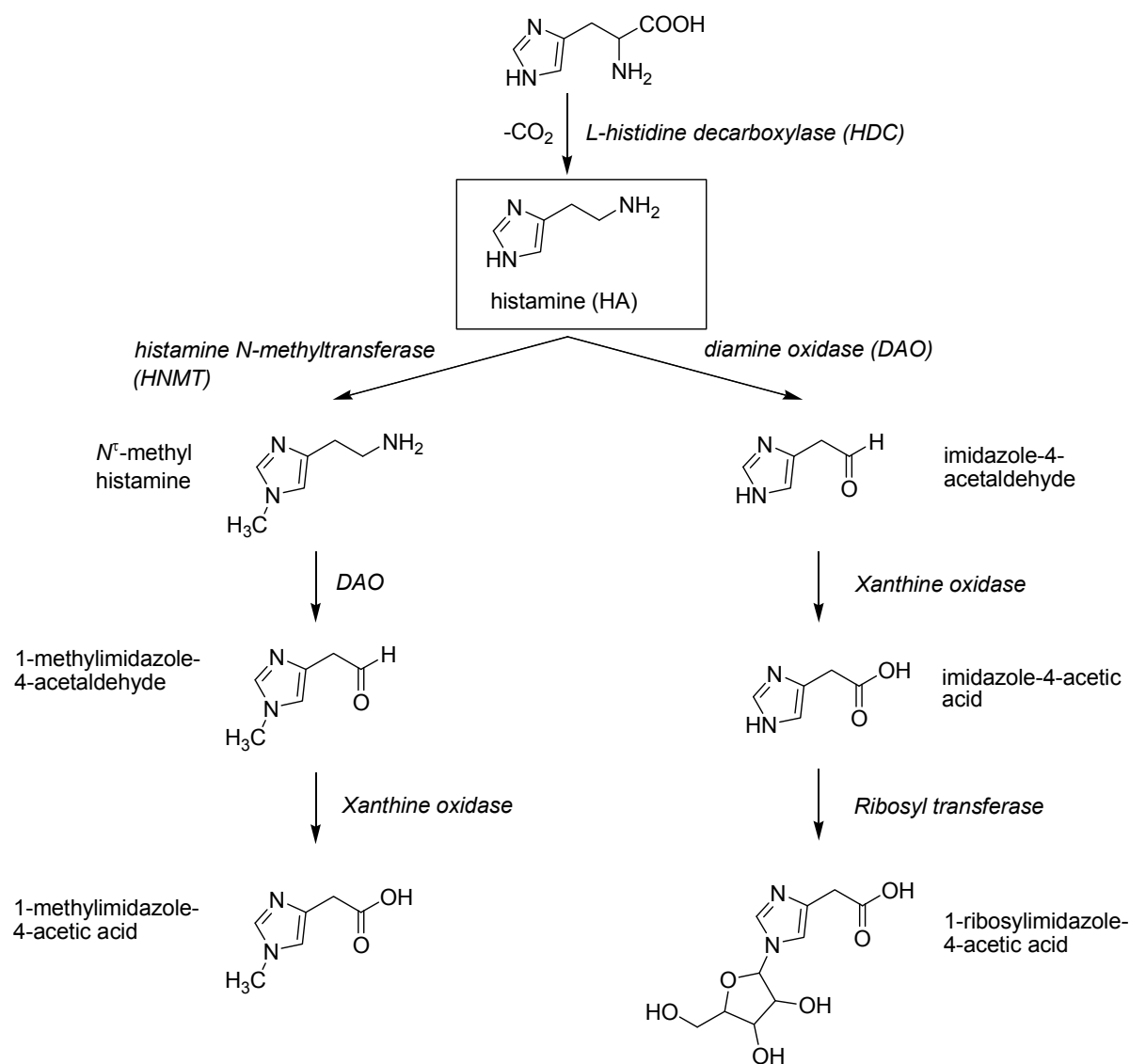


**Figure 1.5:** Biosynthesis and metabolism of histamine.

HA is inactivated by oxidative deamination or methylation to form imidazole-4-acetaldehyde and  $N^{\tau}$ -methylhistamine. These reactions are catalyzed by diamine oxidase (DAO, EC 1.4.3.6) and histamine  $N$ -methyltransferase (HNMT, EC 2.1.1.8), respectively (Beaven, 1982). HNMT transfers a methyl group from *S*-adenosyl-*L*-methionine to the  $N^{\tau}$  of the imidazole ring. Imidazole-4-acetaldehyde is oxidized to form imidazole-4-acetic acid. Imidazole-4-acetic acid and  $N^{\tau}$ -methylhistamine are further metabolized to 1-ribosylimidazole-4-acetic acid and 1-methylimidazole-4-acetic acid, respectively. At present it is not clear if HNMT is translocated to the plasma membrane to metabolize HA or if reuptake of HA occurs by means of organic cation transporters (OCT)-2 or -3 (Ogasawara et al., 2006). The inactive metabolites are excreted in the urine.

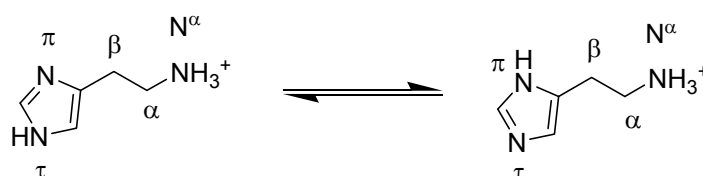


**Figure 1.6:** Tautomerism of HA in the monocationic form.

HA has two basic centres and fully protonated HA is a dication: the side chain amino group is a strong base ( $pK_{a2} = 9.40$ ); the imidazole ring is a weak base ( $pK_{a1} = 5.80$ ) (Ganellin, 1992). Under physiological conditions ( $pH = 7.4$ ) the monocation predominates and is the form most likely to be acting at histamine receptors. The imidazole ring of HA can exist in two tautomeric forms (Figure 1.6), with the proton on the N proximal ( $N^{\pi}$ -H tautomer) or distal ( $N^{\tau}$ -H tautomer). In aqueous solution about 80% of HA monocation is in the  $N^{\tau}$ -H tautomeric form (Ganellin, 1973).

### 1.4.3 Histamine receptors

Histamine receptors belong to class 1 GPCRs (rhodopsin-like) and are classified in the four subtypes  $H_1R$ ,  $H_2R$ ,  $H_3R$ , and  $H_4R$  (Foord et al., 2005). The average sequence homology between the subtypes is relatively low (20%).  $H_3R$  and  $H_4R$  share the highest sequence homology of about 40% (58% homology in the TM regions) (Hough, 2001). An overview of the most important properties of histamine receptors is given in Table 1.1.

$H_1R$  agonists can be divided into three groups (Figure 1.7): small agonists such as 2-methylhistamine, 2-(2-thiazolyl)ethanamine, and betahistidine derived from HA, agonists with aromatic substituents in position 2 of the imidazole ring such as 2-(3-trifluoromethylphenyl)histamine, and the histaprodifens such as suprahistaprodifen.  $H_1R$

**Table 1.1:** Overview of human histamine receptors.

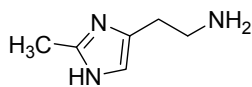
<b>H<sub>1</sub>R</b>	
Gene localization	3p25
Amino acids	487
Agonists	2-methylhistamine, 2-(3-trifluoromethylphenyl)histamine, histaprodifen(s)
Antagonists/inv. ag.	chlorpromazine, chlorpheniramine, mepyramine, cetirizine, astemizole, clemastine, terfenadine, loratadine, tripolidine
Expression	airway and vascular smooth muscles, nerve cells, hepatocytes, endothelial and epithelial cells, neutrophils, hematopoietic cells
Signal transduction	coupling to $G_{\alpha_{q/11}}$ , PLC $\uparrow$ , production of DAG and IP <sub>3</sub> , $[Ca^{2+}]_{\uparrow}$ , PKC $\uparrow$
Actions	rhinitis, conjunctivitis, urticaria, asthma, anaphylaxis, bronchoconstriction and vascular permeability in the lung, immune response
<b>H<sub>2</sub>R</b>	
Gene localization	5
Amino acids	359
Agonists	4-methylhistamine, dimaprit, amthamine, impromidine, arpromidine
Antagonists/inv. ag.	cimetidine, ranitidine, tiotidine, famotidine, aminopotentidine
Expression	gastric parietal cells, right atrial and ventricular muscle, airway and vascular smooth muscles, nerve cells, promyelocytic leukemic cells, hematopoietic cells
Signal transduction	coupling to $G_{\alpha_s}$ , AC $\uparrow$ , $[cAMP]_{\uparrow}$ , protein kinases $\uparrow$ , $[Ca^{2+}]_{\uparrow}$ ; alternative coupling to $G_{\alpha_{q/11}}$
Actions	gastric acid secretion, chronotropic and inotropic activity, vascular permeability, bronchodilation, hypotension, cell proliferation, differentiation, immune response
<b>H<sub>3</sub>R</b>	
Gene localization	20
Amino acids	445
Agonists	( <i>R</i> )- $\alpha$ -methylhistamine, imetit, immapip
Antagonists/inv. ag.	thioperamide, ciproxyfan, clobenpropit, iodoproxyfan, JNJ-5207852
Expression	histaminergic neurons, eosinophils, dendritic cells, monocytes, low concentrations in peripheral tissues
Signal transduction	coupling to $G_{\alpha_{i/o}}$ , AC $\downarrow$ , $[cAMP]_{\downarrow}$
Actions	pre-synaptic autoreceptor (controlling HA release) and heteroreceptor (controlling release of dopamine, serotonin, noradrenaline, GABA, acetylcholine)
<b>H<sub>4</sub>R</b>	
Gene localization	18q11.2
Amino acids	390
Agonists	OUP-16, iodophenpropit, imetit
Antagonists/inv. ag.	JNJ-77771202, thioperamide
Expression	hematopoietic and immunocompetent cells, low expression in brain, liver, and lung
Signal transduction	coupling to $G_{\alpha_{i/o}}$ , AC $\downarrow$ , $[cAMP]_{\downarrow}$ , $[Ca^{2+}]_{\uparrow}$ , MAPK $\uparrow$
Actions	chemotaxis in mast cells and eosinophiles, control of IL-16 production by CD8 <sup>+</sup> lymphocytes

agonists are important experimental tools to analyze H<sub>1</sub>R function in cellular and organ systems (Hill et al., 1997; Seifert et al., 2003). H<sub>1</sub>R antagonists are commonly divided into sedating first-generation (e.g. chlorpheniramine, chlorpromazine) and non-sedating second-generation (e.g. cetirizine) antagonists. Today, especially the second-generation H<sub>1</sub>R antagonists are of great importance for the treatment of allergic diseases (Hill et al., 1997). In our group, for the development of fluorescent H<sub>1</sub>R ligands the H<sub>1</sub>R antagonist mepyramine was conjugated with several fluorophores such as nitrobenzoxadiazole or carboxyfluorescein (Li et al., 2003; Schneider, 2005).

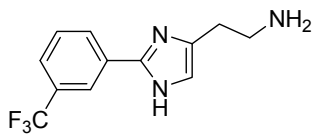
A detailed characterization of the H<sub>2</sub>R is given in chapter 1.4.4.

The H<sub>3</sub>R is mainly expressed in the CNS and acts as a presynaptic autoreceptor mediating a negative feedback on HA synthesis and release from histaminergic neurons. Additionally, H<sub>3</sub>Rs are expressed in several other neurons acting as presynaptic heteroreceptors (Hill et al., 1997). Selective H<sub>3</sub>R agonists such as (*R*)- $\alpha$ -methylhistamine, imetit, and imnepip may be useful for the treatment of insomnia or myocardial ischaemic arrhythmias, or as antinociceptiva. H<sub>3</sub>R antagonists can be divided into imidazole-containing (e.g. thioperamide, ciproxyfan) and non-imidazole (e.g. JNJ-5207852) antagonists. Generally, the latter group of H<sub>3</sub>R antagonists is characterized by increased selectivity over the H<sub>4</sub>R, a better susceptibility to cross the blood-brain-barrier, and a lower affinity to cytochrome P450. Detailed reviews about medicinal chemical and pharmacological aspects of H<sub>3</sub>R agonists (De Esch and Belzar, 2004), imidazole-containing (Stark et al., 2004), and non-imidazole H<sub>3</sub>R (Cowart et al., 2004) antagonists are available.

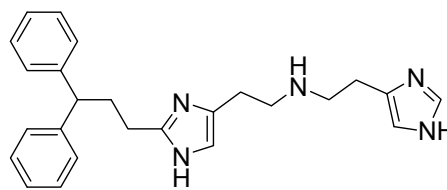
H<sub>4</sub>Rs are predominantly expressed in bone marrow and peripheral hematopoietic cells, regulating several events in immune response (e.g. increase in eosinophile chemotaxis, increase in IL-16 production). Due to the high homology with the H<sub>3</sub>R, many H<sub>3</sub>R ligands also bind to the H<sub>4</sub>R. OUP-16 was the first highly selective H<sub>4</sub>R agonist (Hashimoto et al., 2003) and the indolylpiperazine derivative JNJ-7777120 the first selective H<sub>4</sub>R antagonist (Jablonowski et al., 2003). Ligands targeting the H<sub>4</sub>R may be useful for the treatment of allergic rhinitis, asthma, dermatitis, and autoimmune diseases such as rheumatoid arthritis and multiple sclerosis.

**H<sub>1</sub>R agonists:**

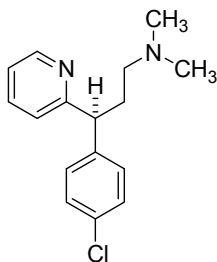
2-methylhistamine



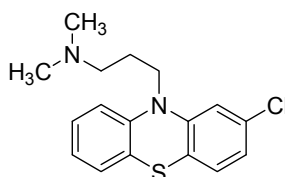
2-(3-trifluoromethylphenyl)histamine



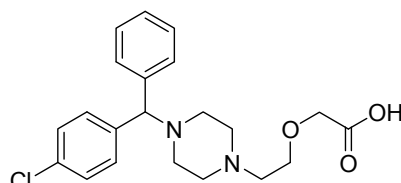
suprahistaprodifen

**H<sub>1</sub>R antagonists/inverse agonists:**

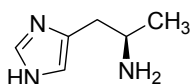
(+) -chlorpheniramine



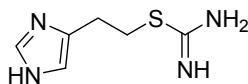
chlorpromazine



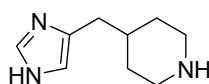
cetirizine

**H<sub>3</sub>R agonists:**

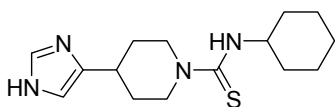
(R)-α-methylhistamine



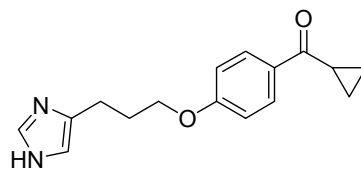
imetit



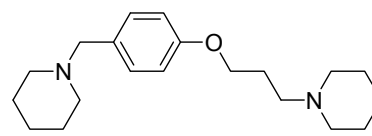
immepip

**H<sub>3</sub>R antagonists/inverse agonists:**

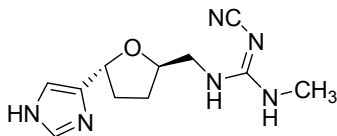
thioperamide



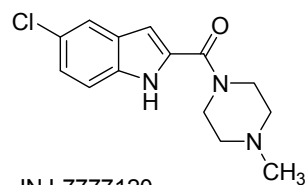
ciproxifan



JNJ-5207852

**H<sub>4</sub>R agonist:**

OUP-16

**H<sub>4</sub>R antagonist:**

JNJ-7777120

**Figure 1.7:** Structures of selected histamine receptor agonists and antagonists/inverse agonists.

## 1.4.4 The histamine H<sub>2</sub> receptor

### 1.4.4.1 Molecular pharmacological characterization

To date, H<sub>2</sub>Rs of the following species have been cloned: canine (Gantz et al., 1991a), human (Gantz et al., 1991b), rat (Ruat et al., 1991), guinea pig (Traiffort et al., 1995), and mouse (Kobayashi et al., 1996). The nucleotide sequences (genomic DNA) of gorilla, chimpanzee, and orang-utan H<sub>2</sub>R species isoforms were submitted to the EMBL/GenBank/DDBJ databases in 2000 by Kitano et al. Genomic Southern Blotting identified the human H<sub>2</sub>R to be located on chromosome 5 (Traiffort et al., 1995). The intronless gene encodes for 358 (rat, mouse) or 359 (human, canine, guinea pig, gorilla, chimpanzee, orang-utan) amino acids. H<sub>2</sub>R species isoforms share a considerably high sequence identity of more than 80%.

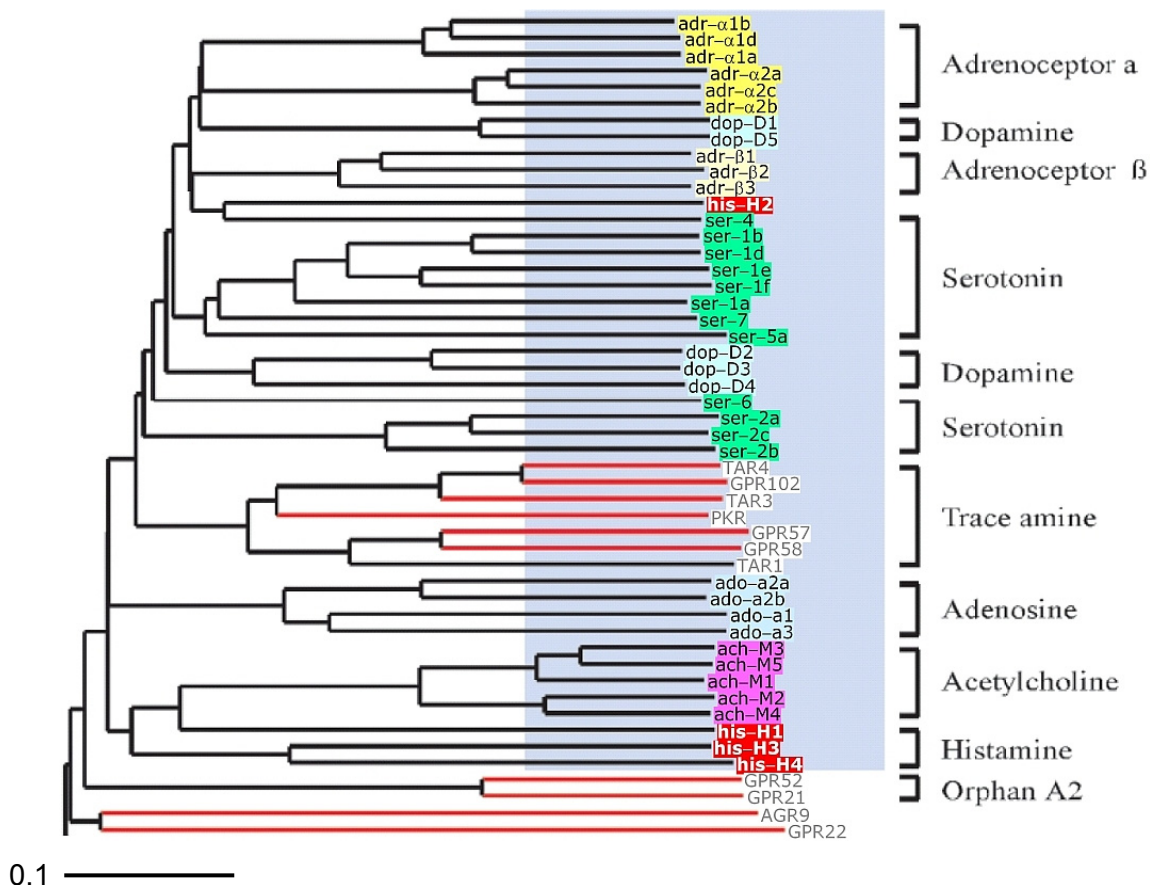


**Figure 1.8:** Phylogenetic tree of class 1 aminergic GPCRs. Black lines correspond to receptors with known ligands and red lines to those with unknown ligands (orphan receptors). Adapted from Vassilatis et al., 2003. The ruler at the bottom indicates the horizontal distance equal to 10% sequence divergence.

Phylogenetic analysis of class 1 aminergic GPCRs indicates the histamine receptor family as a heterogeneous group (Figure 1.8) (Vassilatis et al., 2003). H<sub>3</sub>R and H<sub>4</sub>R cluster together representing close relatedness. The H<sub>1</sub>R is more related to muscarinic acetylcholine receptors than to the histamine H<sub>3</sub> and H<sub>4</sub> subtypes. The H<sub>2</sub>R is placed in a very distant position closest to the serotonin 5-HT<sub>4</sub>R and the  $\beta$ -adrenergic receptors.

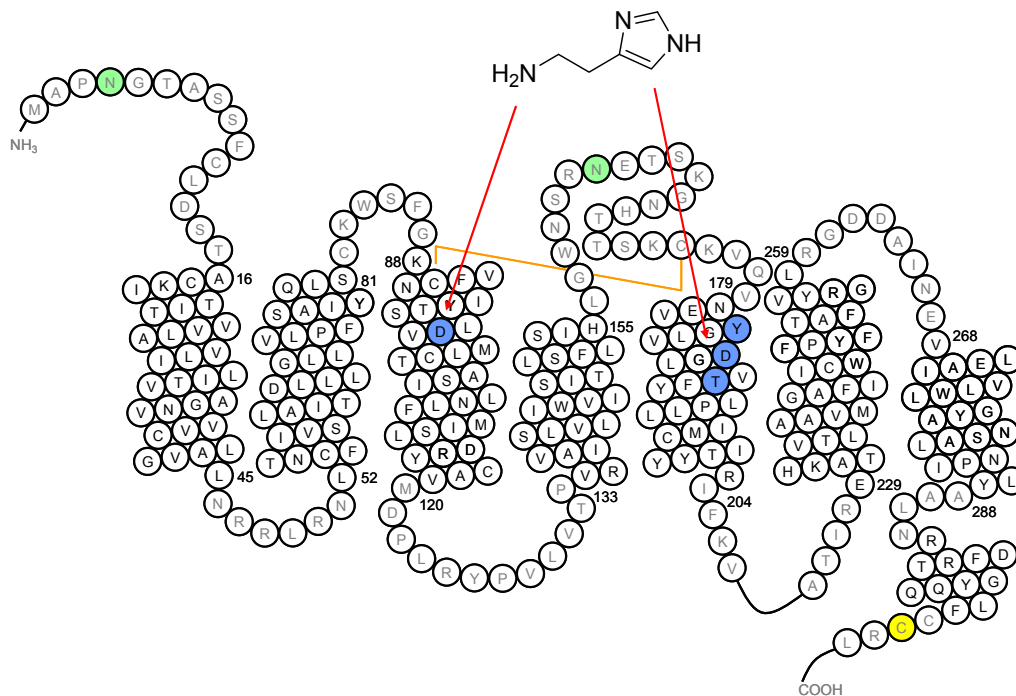


**Figure 1.9:** Snake representation of the human H<sub>2</sub>R. Asn-4 and Asn-162 (green) are being N-glycosylated, and Cys-305 (yellow) is being palmitoylated. A disulfide bond between Cys-91 and Cys-174 is represented by an orange line. Asp-98, Tyr-182, Asp-186, and Thr-190 that probably interact with HA are colored in blue. 16 amino acids of i3 and 51 amino acids of the C-terminus are omitted for reasons of clarity.

The secondary structure of the human H<sub>2</sub>R as suggested from sequence alignment with bovine rhodopsin is shown in Figure 1.9. The receptor is composed of seven TM domains that are connected by three extracellular (e1, e2, e3) and three intracellular (i1, i2, i3) loops. The N-terminus is located at the extracellular and the C-terminus at the intracellular side of the membrane. A disulfide bond that is highly conserved in class 1 GPCRs connects the extracellular end of TM3 with e2. The endogenous ligand HA binds to the H<sub>2</sub>R in a cavity between TM3 and TM5 (see chapter 1.4.5.1). As it is observed in all GPCRs, the H<sub>2</sub>R is subjected to post-translational modifications and regulatory mechanisms. Extracellular N-glycosylation occurs at Asn-4 (N-terminus) and at Asn-162 (e2). It has been shown that N-



glycosylation is not required for cell surface localization of the receptor, ligand binding, or functional coupling to G proteins (Fukushima et al., 1995). The H<sub>2</sub>R is palmitoylated at Cys-305 of the C-terminus which is important for proper membrane targeting of the receptor (Fukushima et al., 2001a). Upon agonist exposure, the H<sub>2</sub>R is internalized in a cAMP-independent pathway (Smit et al., 1995). Pharmacological characterization of C-terminally truncated canine H<sub>2</sub>Rs revealed Thr-315 to be involved in agonist-induced internalization (Fukushima et al., 1997a). Agonist-induced desensitization was first detected by the group of Fukushima (Fukushima et al., 1993) and was recently found to be mediated by phosphorylation via the G protein receptor kinases GRK2 and GRK3 (Rodriguez-Pena et al., 2000; Shayo et al., 2001). Although distinct regions of the H<sub>2</sub>R C-terminus are known to be important for GPCR signaling and down-regulation (Smit et al., 1996a), C-terminal truncation did not abolish agonist-induced H<sub>2</sub>R desensitization suggesting that this part is not involved in GRK2 and GRK3 mediated desensitization (Rodriguez-Pena et al., 2000). H<sub>2</sub>R dimerization and oligomerization was elucidated by Western Blot analysis in COS7 and Sf9 cells (Fukushima et al., 1997b).

Allelic variations of the human H<sub>2</sub>R gene have been observed (Orange et al., 1996a). The impact of an H<sub>2</sub>R polymorphism with a base exchange of A649 to G, causing a point mutation of Asn-217 to Asp, on the incidence of schizophrenia was discussed (Orange et al., 1996b) but could not be confirmed in recent studies (Ito et al., 2000). However, this H<sub>2</sub>R gene variant displayed low basal activity and resistance to upregulation upon antagonist exposure indicating an altered receptor function (Fukushima et al., 2001b).

Constitutive activity of the H<sub>2</sub>R was reported first by Smit (Smit et al., 1996b) for the rat species isoform leading to a reclassification of the H<sub>2</sub>R antagonists cimetidine and ranitidine to be inverse agonists. Two years later, constitutive activity and structural instability of the human H<sub>2</sub>R were discovered (Alewijns et al., 1998). Using the technique of fusion proteins (Milligan, 2000), it was shown that the magnitude of constitutive activity is similar when the human H<sub>2</sub>R couples to the long and the short splice variants of G<sub>sα</sub> (Wenzel-Seifert et al., 2001). Differences in the constitutive activities of wild-type and mutant H<sub>2</sub>R species isoforms are subject of this work (chapters 7 and 8).

#### *1.4.4.2 H<sub>2</sub>R distribution, functions, and signaling pathways*

H<sub>2</sub>Rs are located on the parietal cells of the gastric mucosa and mediate the HA-induced increase in gastric acid secretion (Gespach et al., 1982; Soll and Berglinde, 1987). Thus, H<sub>2</sub>R antagonists belong to the most important drugs for the treatment of gastric ulcers (Black et al., 1972). At the right atrial and the ventricular muscle of the heart, H<sub>2</sub>R stimulation leads to an increase in the slow inward Ca<sup>2+</sup> current (Levi and Aloatti, 1988) thereby causing the

positive chronotropic and positive inotropic effects of HA. Accordingly, measuring the change in the heart rate of the spontaneously beating guinea pig right atrium upon H<sub>2</sub>R ligand exposure was used as a standard H<sub>2</sub>R model in organ pharmacology. H<sub>2</sub>R-mediated smooth muscle relaxation has been documented in airway, uterine, and vascular smooth muscles (Levi et al., 1982; Jolly and Desmecht, 2003). Moreover, H<sub>2</sub>R<sub>s</sub> are distributed in hippocampal pyramidal cells in the brain. The direct effect of H<sub>2</sub>R stimulation on neuronal membranes is usually excitatory or potentiates excitation (Haas and Panula, 2003). HA blocks Ca<sup>2+</sup>-dependent K<sup>+</sup> conductance, leading to a long-lasting afterhyperpolarization and affecting the accommodation of firing (Haas and Konnerth, 1983). Synaptic transmission in the hippocampus is potentiated and the firing of several types of neurons is enhanced for many hours after exposure to HA or the H<sub>2</sub>R agonist impromidine (Brown et al., 2001; Selbach et al., 1997). Promyelocytic leukemic cells express H<sub>2</sub>R<sub>s</sub> and activation leads to functional differentiation to mature granulocytes (Seifert et al., 1992; reviewed in Klinker et al., 1996). Thus, H<sub>2</sub>R agonists are discussed to be useful for the treatment of acute promyelocytic leukemia. Finally, there is a complex network in the histaminergic system regulating hematopoiesis and immune responses (for recent reviews consider Dy and Schneider, 2004; Jutel et al., 2002; Schneider et al., 2002; Akdis and Simons, 2006). This type of regulation is particularly relevant in the context of the differentiation of T helper 1 (TH1) and T helper 2 (TH2) cell differentiation with impact on autoimmunity and tumor immunotherapy. TH1 cells show predominant, but not exclusive, expression of H<sub>1</sub>R, whereas TH2 cells show upregulation of H<sub>2</sub>R (Jutel et al., 2001). The H<sub>2</sub>R on TH2 cells acts as a negative regulator of proliferation as well as IL-4 and IL-13 production.

The H<sub>2</sub>R couples to G<sub>sα</sub> to activate AC which, in turn, leads to an increase in cAMP production (Figure 1.10) (Hill et al., 1997; Del Valle and Gantz, 1997). cAMP activates protein kinases, which phosphorylate regulatory proteins, leading to an influx of Ca<sup>2+</sup> in cardiac myocytes. Alternatively, an increase in intracellular Ca<sup>2+</sup> concentration mediated by the action of phospholipase C (PLC) has been observed (Del Valle et al., 1992; Wang et al., 1996). It has been demonstrated in subsequent studies that the H<sub>2</sub>R is capable of coupling to both G<sub>sα</sub> and G<sub>αq/11</sub> signaling pathways (Leopoldt et al., 1997; Kühn et al., 1996).

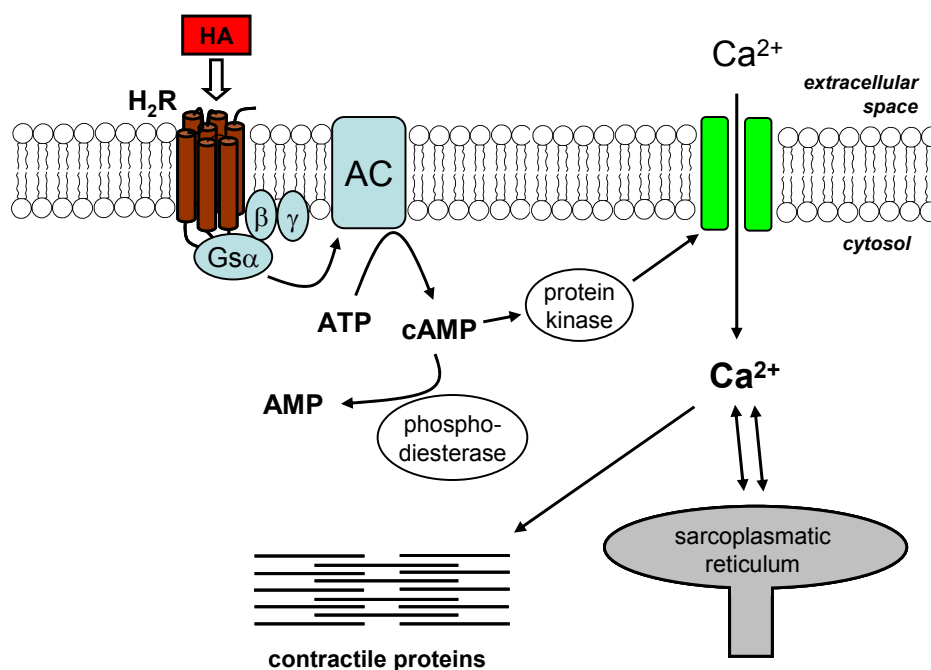


**Figure 1.10:** H<sub>2</sub>R-mediated signaling in a cardiac myocyte.

## 1.4.5 Histamine H<sub>2</sub> receptor agonists

### 1.4.5.1 Interactions of HA and small agonists with the H<sub>2</sub>R

The historical model for the agonistic binding site of the H<sub>2</sub>R was based on a postulated activation mechanism (Weinstein et al., 1976). The cationic ammonium group in the HA side chain and the N<sup>+</sup>-H group of the imidazole acted as proton donors, whereas the N<sup>π</sup> atom acted as a proton acceptor. Participation of the ammonium group in H-bonding with a negative charge on the receptor leads to a decrease in positive charge, which was thought to induce a tautomeric change in the imidazole ring system from N<sup>+</sup>-H to N<sup>π</sup>-H (in its neutral form, HA is mainly found as the N<sup>π</sup>-H tautomer). A consequence of this tautomeric shift was the donation of a proton from the receptor to the agonist on one side, while on the other side a proton would be donated from the agonist to the receptor. Controversial concepts were developed to understand the binding modes of the isothiurea derivative dimaprit (Figure 1.11) (Parsons et al., 1977) and the 2-amino-4-methylthiazolyle derivative amthamine (Durant et al., 1977; Green et al., 1978; Eriks et al., 1993).

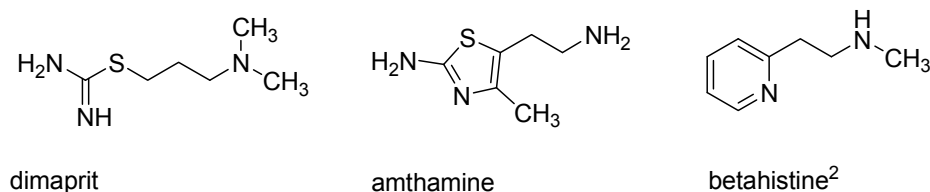


**Figure 1.11:** Structures of small H<sub>2</sub>R agonists.

In the model of Eriks et al., the partially positively charged sulfur atom of amthamine interacts with a negatively charged site of the receptor whereas the N<sup>+</sup> atom accepts a proton from a proton-donating site of the receptor (Eriks et al., 1993). An analogous binding mode of HA requires that the N<sup>π</sup>-H tautomer is the biologically active form (Nederkoorn et al., 1994). This model implies that a tautomeric shift is no prerequisite for H<sub>2</sub>R stimulation and is thus able to explain the agonistic activities of all known H<sub>2</sub>R agonists, including non-tautomeric compounds like betahistine and a series of 5-(2-aminoethyl)thiazole derivatives. Recently, Giraldo showed that the two mechanistic models of H<sub>2</sub>R activation by HA (“Weinstein-model” vs. “Eriks-model”) are compatible if the amino acid residues which constitute the recognition site of the receptor are present in different acid-base conjugate forms (Giraldo, 1999). Mutational studies on the H<sub>2</sub>R indicated an ionic interaction of the protonated amino group of HA with Asp-98 in TM3 (Gantz et al., 1992). The second and third site of the three-point activation model could principally be formed by the couples Asp-186/Thr-190 (Gantz et al., 1992) or Tyr-182/Asp-186 (Nederkoorn et al., 1996a, b) in TM5. Molecular mechanics and *ab initio* studies revealed that Tyr-182 and Asp-186 most likely interact with the imidazole ring of HA (Figure 1.12).

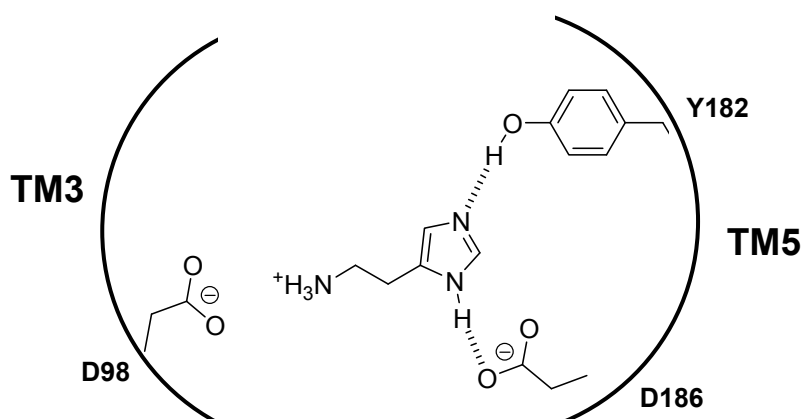


**Figure 1.12:** Interaction of HA in the binding site of the H<sub>2</sub>R according to the model of Nederkoorn (Nederkoorn et al., 1996a). HA is present in the N<sup>π</sup>-H tautomeric form.

<sup>2</sup> Non-selective H<sub>2</sub>R agonist.

### 1.4.5.2 Imidazolylpropylguanidines

Impromidine (IMP) (Durant et al., 1985) was the first highly potent and selective H<sub>2</sub>R agonist (Figure 1.13) (Durant et al., 1978). The compound is about 50-fold more potent than HA in increasing the heart rate of the isolated guinea pig right atrium and approaches 100% of HA intrinsic activity. IMP is a guanidine derivative with two different imidazolylalkyl substituents. The imidazolylpropylguanidine structure acts as weak partial agonist with low potency ( $pD_2 = 4.65$ ; rel. potency = 0.04; i.a. = 0.3) (Parsons et al., 1975), and the 2-[(5-methyl-1*H*-imidazol-4-yl)methylthio]ethyl guanidine moiety is a structural feature of the H<sub>2</sub>R antagonist cimetidine (Figure 1.4) showing no agonistic H<sub>2</sub>R activity. Thus, the cimetidine-like moiety in IMP is assumed to contribute to high potency and affinity whereas the imidazolylpropylguanidine is the major determinant of agonistic activity.

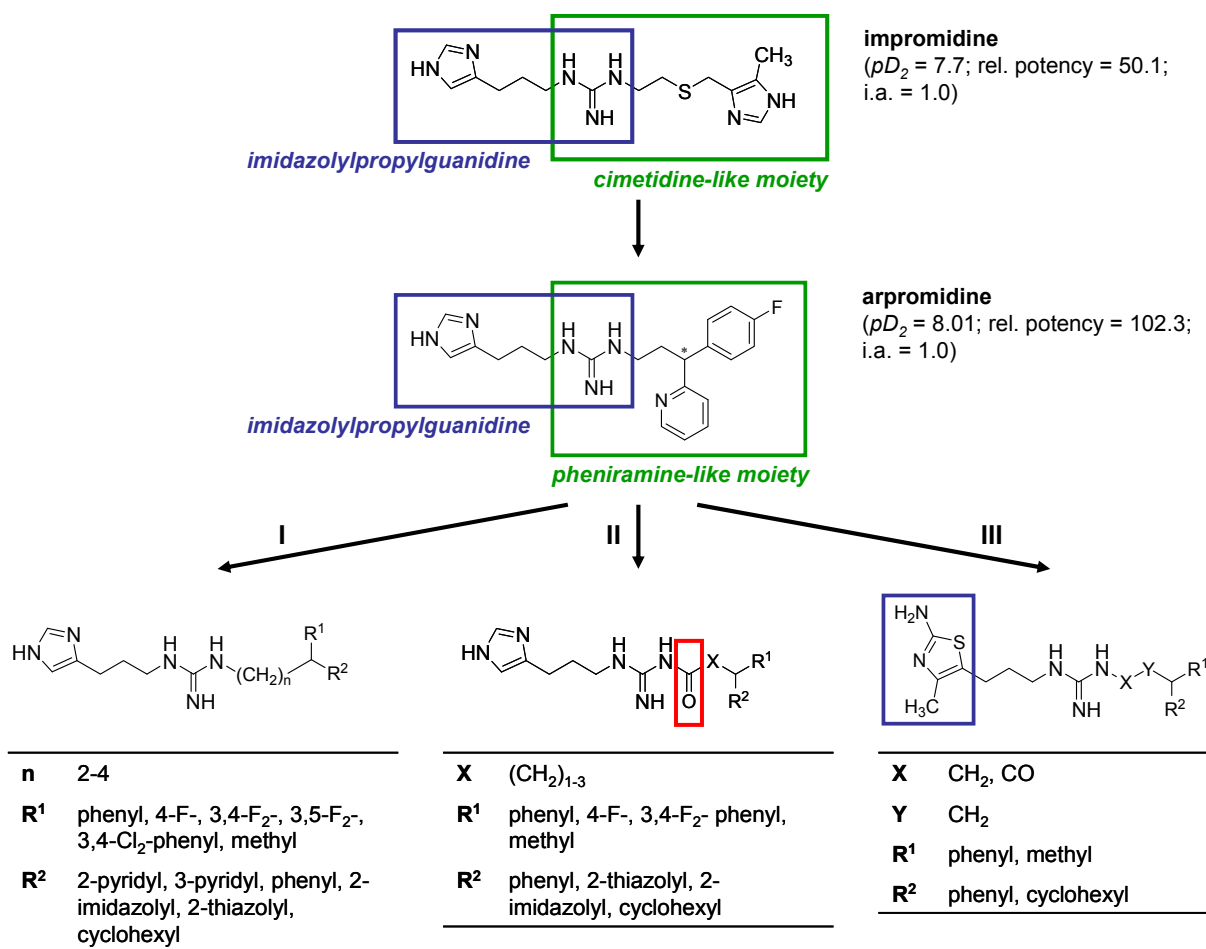


**Figure 1.13:** Flow chart of the development of potent and selective H<sub>2</sub>R agonistic guanidines. H<sub>2</sub>R activities of IMP and ARP were measured at the isolated spontaneously beating guinea pig right atrium (data taken from Buschauer, 1989); rel. potency, potency relative to HA = 1; i.a. intrinsic activity.

About twenty years ago the development of new H<sub>2</sub>R agonists was encouraged by clinical investigations suggesting a therapeutic potential of such compounds. By studying IMP, Baumann et al. demonstrated that H<sub>2</sub>R stimulation could be an effective treatment in patients suffering from severe catecholamine-insensitive congestive heart failure (Baumann et al., 1984). Arpromidine (ARP) and related *N*-[3-(1*H*-imidazol-4-yl)propyl]-*N'*-[3-phenyl-3-(2-pyridyl)-propyl] guanidines were the most interesting substances of a large series of so-called 'cardiohistaminergics' developed as positive inotropic vasodilators (Buschauer, 1989; Buschauer and Baumann, 1991). The ARP-like H<sub>2</sub>R agonists, in particular the 3,4- and 3,5-difluorinated analogues, proved to be superior to IMP in potency, hemodynamic profile, and side effects when tested in the guinea pig under physiological conditions and in a pathophysiological model of severe congestive heart failure (vasopressin-induced acute heart failure) (Felix et al., 1991). In ARP, the cimetidine-like moiety of IMP is replaced by the pheniramine-like [3-phenyl-3-(2-pyridyl)propyl]guanidine group (Figure 1.7) which is a weak H<sub>1</sub>R antagonist. The hybrid molecule is about 100 times more potent than HA on the guinea pig right atrium and exerts an H<sub>1</sub>R antagonistic profile comparable to that of pheniramine on the guinea pig ileum.

The structure-activity relationships of ARP-type H<sub>2</sub>R agonists (Figure 1.13, path I) can be summarized as follows (Dove et al., 2004):

- The imidazolylpropylguanidine moiety is essential for the H<sub>2</sub>R agonistic activity.
- Highest potency is observed in compounds with a three-membered carbon chain between the guanidine group and R<sup>1</sup>/R<sup>2</sup>.
- Substituents at the phenyl and pyridyl rings in R<sup>2</sup> position are mostly unfavorable for H<sub>2</sub>R agonistic activity, but different aromatics or heteroaromatics such as 2-imidazolyl and 2-thiazolyl may replace phenyl and pyridyl.
- Appropriate substitution at phenyl rings in R<sup>1</sup> may increase potency. Highest potency in the guinea pig atrium was found in the 3,4-F<sub>2</sub>, 3,4-Cl<sub>2</sub>, and 3,5-F<sub>2</sub> substituted compounds.
- The aromatic ring systems in R<sup>1</sup> and R<sup>2</sup> may be replaced by cyclohexyl and methyl substituents.

IMP, ARP and related guanidines are strong bases ( $pK_a \sim 13$ ) and thus nearly quantitatively protonated at physiological pH. To yield compounds with improved pharmacokinetic properties, particularly oral bioavailability and penetration across the blood-brain-barrier, *N*<sup>G</sup>-acylated imidazolylpropylguanidines were developed (Figure 1.13, path II) (Ghorai, 2005). Such agonists may be useful pharmacological tools to gain novel insight into the functions of the H<sub>2</sub>R in the brain. A large series of *N*<sup>G</sup>-acylated guanidines with reduced basicity

( $pK_a \sim 8$ ) was synthesized and pharmacologically characterized (Ghorai, 2005; Xie et al., 2006a, b). The  $N^G$ -acylated derivatives contain diverse mono- and diarylalkanoyl, heteroarylalkanoyl, and cyclohexylalkanoyl substituents, and most of these compounds display potencies and efficacies similar to their non-acylated analogs (Ghorai, 2005). Thus,  $N^G$ -acylation can be considered as a bioisosteric exchange.  $N^1$ -(3-Cyclohexylbutanoyl)- $N^2$ -[3-(1*H*-imidazol-4-yl)propyl]guanidine (UR-AK57, Figure 1.14) turned out to be the most potent human  $H_2R$  agonist identified so far ( $EC_{50}$  of 23 nM in a GTPase activity assay at human  $H_2R$ - $G_{s\alpha}$  fusion protein expressed in Sf9 insect cells) (Xie et al., 2006b). At the human  $H_1R$  this compound did not act as antagonist but rather as a partial agonist.  $N^G$ -acylated guanidines are absorbed from the gastrointestinal tract and are capable of penetrating across the blood-brain-barrier as measured by HPLC-MS analysis after administration to mice (Keller, personal communication). Very recently, several  $N^G$ -acylated imidazolylpropyl-guanidines have been identified as very potent  $H_4R$  agonists (Ghorai, 2005; Seifert, personal communication).

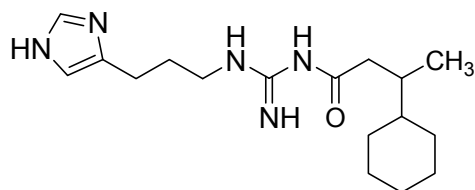


**Figure 1.14:** Structure of the  $H_2R$  agonistic compound UR-AK57.

An important step towards the development of highly potent and selective  $H_2R$  agonists was achieved by replacing the common imidazole ring of the guanidines by a 2-amino-4-methylthiazole group (Figure 1.13, path III). As such an exchange did not abolish the  $H_2R$  agonistic activity of small compounds (HA  $\rightarrow$  amthamine), a corresponding bioisosteric replacement was also possible in the case of the bulky guanidines. A series of ARP-related compounds with a 3-(4-methyl-2-aminothiazol-5-yl)propyl group displayed remarkably increased selectivity over the  $H_3R$  (Eriks et al., 1991). A similar strategy was successfully applied to the series of  $N^G$ -acylated compounds yielding  $N$ -acyl- $N'$ -[3-(2-amino-4-methylthiazol-5-yl)propyl]guanidines that were similarly potent and efficacious as their imidazolyl analogs but devoid of  $H_3R$  activity (Ghorai, 2005).

## 1.5 References

- Akdis CA and Simons FE (2006) Histamine receptors are hot in immunopharmacology. *Eur J Pharmacol* **533**:69-76.
- Alewijnse AE, Smit MJ, Hoffmann M, Verzijl D, Timmerman H and Leurs R (1998) Constitutive activity and structural instability of the wild-type human H<sub>2</sub> receptor. *J Neurochem* **71**:799-807.
- Arrang JM, Garbarg M and Schwartz JC (1983) Auto-inhibition of brain histamine release mediated by a novel class (H<sub>3</sub>) of histamine receptor. *Nature* **302**:832-837.
- Arrang JM, Garbarg M, Lancelot JC, Lecomte JM, Pollard H, Robba M, Schunack W and Schwartz JC (1987) Highly potent and selective ligands for histamine H<sub>3</sub>-receptors. *Nature* **327**:117-123.
- Ash ASF and Schild HO (1966) Receptors mediating some actions of histamine. *Br J Pharmacol* **27**:427-439.
- Barger G and Dale HM (1910) The presence in ergot and physiological activity of  $\beta$ -iminazolyethylamine. *J Physiol Paris* **40**:38-40.
- Baumann G, Permanetter B and Wirtzfeld A (1984) Possible value of H<sub>2</sub>-receptor agonists for treatment of catecholamine-insensitive congestive heart failure. *Pharmacol Ther* **24**:165-177.
- Beaven MA (1982) Factors regulating availability of histamine at tissue receptors, in *Pharmacology of histamine receptors* (Ganellin CR and Parsons EM eds) pp 103-145, Wright PSG, Bristol, London, Boston.
- Best CH, Dale HH, Dudley HW and Thorpe WV (1927) The nature of the vasodilator constituents of certain tissue extracts. *J Physiol* **62**:397-417.
- Black JW, Duncan WA, Durant CJ, Ganellin CR and Parsons EM (1972) Definition and antagonism of histamine H<sub>2</sub>-receptors. *Nature* **236**:385-390.
- Black JW, Duncan WA, Emmett JC, Ganellin CR, Hesselbo T, Parsons ME and Wyllie JH (1973) Metiamide—an orally active histamine H<sub>2</sub>-receptor antagonist. *Agents Actions* **3**:133-137.
- Bockaert J and Pin JP (1999) Molecular tinkering of G protein-coupled receptors: an evolutionary success. *EMBO J* **18**:1723-1729.
- Bockaert J, Dumuis A, Fagni L and Marin P (2004) GPCR-GIP networks: A first step in the discovery of new therapeutic drugs? *Curr Opin Drug Discovery Dev* **7**:649-657.
- Bovet D and Staub AM (1937) Action protectrice des éthers phénolique au cours de l'intoxication histaminique. *C R Soc Biol* **124**:547-549.
- Brimblecombe RW, Duncan WAM, Durant GJ, Ganellin CR, Parsons EM and Black JW (1975) The pharmacology of cimetidine; a new histamine H<sub>2</sub>-receptor antagonist. *Br J Pharmacol* **53**:435-436.
- Brown RE, Stevens DR and Haas HL (2001) The physiology of brain histamine. *Prog Neurobiol* **63**:637-672.
- Buschauer A (1989) Synthesis and in vitro pharmacology of arpromidine and related phenyl(pyridylalkyl)guanidines, a potential new class of positive inotropic drugs. *J Med Chem* **32**:1963-1970.
- Buschauer A and Baumann G (1991) Structure-activity relationships of histamine H<sub>2</sub>-agonists, a new class of positive inotropic drugs. *Agents Actions Suppl* **33**:231-256.
- Cowart M, Altenbach R, Black L, Faghiih R, Zhao C and Hancock AA (2004) Medicinal chemistry and biological properties of non-imidazole histamine H<sub>3</sub> antagonists. *Mini Rev Med Chem* **4**:979-992.
- Dale HH and Laidlaw PP (1910) The physiological action of  $\beta$ -iminazolyethylamine. *J Physiol* **41**:318-344.
- Dale HH and Laidlaw PP (1911) Further observations on the action of  $\beta$ -iminazolyethylamine. *J Physiol* **43**:182-195.



- Dale HH and Laidlaw PP (1919) Histamine shock. *J Physiol* **52**:355-390.
- De Esch IJ and Belzar KJ (2004) Histamine H<sub>3</sub> receptor agonists. *Mini Rev Med Chem* **4**:955-963.
- Del Valle J and Gantz I (1997) Novel insights into histamine H<sub>2</sub> receptor biology. *Am J Physiol* **273**:G987-996.
- Del Valle J, Wang L, Gantz I and Yamada T (1992) Characterization of H<sub>2</sub> histamine receptor: linkage to both adenylate cyclase and [Ca<sup>2+</sup>]<sub>i</sub> signaling systems. *Am J Physiol* **263**:G967-972.
- Dove S, Elz S, Seifert R and Buschauer A (2004) Structure-activity relationships of histamine H<sub>2</sub> receptor ligands. *Mini Rev Med Chem* **4**:941-954.
- Drews J (2000) Drug discovery: a historical perspective. *Science* **287**:1960-1964.
- Durant GJ, Ganellin CR and Parsons ME (1977) Dimaprit, (S-[3-(N,N-dimethylamino)propyl]-isothioureia). A highly specific histamine H<sub>2</sub>-receptor agonist. Part 2. Structure-activity considerations. *Agents Actions* **7**:39-43.
- Durant GJ, Duncan WA, Ganellin CR, Parsons ME, Blakemore RC and Rasmussen AC (1978) Impromidine (SK&F 92676) is a very potent and specific agonist for histamine H<sub>2</sub> receptors. *Nature* **276**:403-405.
- Durant GJ, Ganellin CR, Hills DW, Miles PD, Parsons ME, Pepper ES and White GR (1985) The histamine H<sub>2</sub> receptor agonist impromidine: synthesis and structure-activity considerations. *J Med Chem* **28**:1414-1422.
- Dy M and Schneider E (2004) Histamine-cytokine connection in immunity and hematopoiesis. *Cytokine Growth Factor Rev* **15**:393-410.
- Eriks JC, Sterk GJ, van der Aar EM, van Acker SA, van der Goot H and Timmerman H (1991) 4- or 5-(ω-aminoalkyl) thiazoles and derivatives; new selective H<sub>2</sub>-receptor agonists. *Agents Actions Suppl* **33**:301-314.
- Eriks JC, van der Goot H and Timmerman H (1993) New activation model for the histamine H<sub>2</sub> receptor, explaining the activity of the different classes of histamine H<sub>2</sub> receptor agonists. *Mol Pharmacol* **44**:886-894.
- Fang Y, Lahiri J and Picard L (2003) G protein-coupled receptor microarrays for drug discovery. *Drug Discov Today* **8**:755-761.
- Felix SB, Buschauer A and Baumann G (1991) Therapeutic value of H<sub>2</sub>-receptor stimulation in congestive heart failure. Hemodynamic effects of BU-E-76, BU-E-75 and arpromidine (BU-E-50) in comparison to impromidine. *Agents Actions Suppl* **33**:257-269.
- Foord SM, Bonner TI, Neubig RR, Rosser EM, Pin JP, Davenport AP, Spedding M and Harmar AJ (2005) International Union of Pharmacology. XLVI. G protein-coupled receptor list. *Pharmacol Rev* **57**:279-288.
- Fourneau E and Bovet T (1933) Recherches sur l'action sympatholytique d'un nouveau dérivé du dioxane. *Arch Int Pharmacodyn* **46**:179-191.
- Fredriksson R and Schiöth HB (2005) The repertoire of G-protein-coupled receptors in fully sequenced genomes. *Mol Pharmacol* **67**:1414-1425.
- Fredriksson R and Schiöth HB (2006) G protein-coupled receptors in the human genome., in *Ligand design for G protein-coupled receptors* (Rognan D ed) pp 1-26, Wiley-VCH, Weinheim.
- Fredriksson R, Lagerström MC, Lundin LG and Schiöth HB (2003) The G-protein-coupled receptors in the human genome form five main families. Phylogenetic analysis, paralogon groups, and fingerprints. *Mol Pharmacol* **63**:1256-1272.
- Fukushima Y, Oka Y, Katagiri H, Saitoh T, Asano T, Ishihara H, Matsuhashi N, Kodama T, Yazaki Y and Sugano K (1993) Desensitization of canine histamine H<sub>2</sub> receptor expressed in Chinese hamster ovary cells. *Biochem Biophys Res Commun* **190**:1149-1155.
- Fukushima Y, Oka Y, Saitoh T, Katagiri H, Asano T, Matsuhashi N, Takata K, van Breda E, Yazaki Y and Sugano K (1995) Structural and functional analysis of the canine histamine H<sub>2</sub> receptor by site-directed mutagenesis: N-glycosylation is not vital for its action. *Biochem J* **310** (Pt 2):553-558.

- Fukushima Y, Asano T, Takata K, Funaki M, Ogihara T, Anai M, Tsukuda K, Saitoh T, Katagiri H, Aihara M, Matsuhashi N, Oka Y, Yazaki Y and Sugano K (1997a) Role of the C terminus in histamine H<sub>2</sub> receptor signaling, desensitization, and agonist-induced internalization. *J Biol Chem* **272**:19464-19470.
- Fukushima Y, Asano T, Saitoh T, Anai M, Funaki M, Ogihara T, Katagiri H, Matsuhashi N, Yazaki Y and Sugano K (1997b) Oligomer formation of histamine H<sub>2</sub> receptors expressed in Sf9 and COS7 cells. *FEBS Lett* **409**:283-286.
- Fukushima Y, Saitoh T, Anai M, Ogihara T, Inukai K, Funaki M, Sakoda H, Onishi Y, Ono H, Fujishiro M, Ishikawa T, Takata K, Nagai R, Omata M and Asano T (2001a) Palmitoylation of the canine histamine H<sub>2</sub> receptor occurs at Cys(305) and is important for cell surface targeting. *Biochim Biophys Acta* **1539**:181-191.
- Fukushima Y, Saitoh T, Anai M, Tsukuda K, Onishi Y, Sakoda H, Inukai K, Ogihara T, Funaki M, Ono H, Fujishiro M, Ishikawa T, Nagai R, Omata M and Asano T (2001b) G649, an allelic variant of the human H<sub>2</sub> receptor with low basal activity, is resistant to upregulation upon antagonist exposure. *Pharmacogenomics J* **1**:78-83.
- Ganellin CR (1973) The tautomer ratio of histamine. *J Pharm Pharmacol* **25**:787-792.
- Ganellin CR (1992) Pharmacochemistry of H<sub>1</sub> and H<sub>2</sub> Receptors, in *The histamine receptor* (Schwartz JC and Haas HL eds) pp 1-56, Wiley-Liss, New York.
- Gantz I, Schaffer M, Del Valle J, Logsdon C, Campbell V, Uhler M and Yamada T (1991a) Molecular cloning of a gene encoding the histamine H<sub>2</sub> receptor. *Proc Natl Acad Sci U S A* **88**:429-433.
- Gantz I, Munzert G, Tashiro T, Schaffer M, Wang L, Del Valle J and Yamada T (1991b) Molecular cloning of the human histamine H<sub>2</sub> receptor. *Biochem Biophys Res Commun* **178**:1386-1392.
- Gantz I, Del Valle J, Wang LD, Tashiro T, Munzert G, Guo YJ, Konda Y and Yamada T (1992) Molecular basis for the interaction of histamine with the histamine H<sub>2</sub> receptor. *J Biol Chem* **267**:20840-20843.
- Gespach C, Bouhours D, Bouhours JF and Rosselin G (1982) Histamine interaction on surface recognition sites of H<sub>2</sub>-type in parietal and non-parietal cells isolated from the guinea pig stomach. *FEBS Lett* **149**:85-90.
- Ghorai P (2005) Arpromidine-related acylguanidines: synthesis and structure-activity relationships of a new class of guanidine-type histamine H<sub>2</sub> receptor agonists with reduced basicity. Doctoral thesis. University of Regensburg, Germany.  
<http://www.opus-bayern.de/uni-regensburg/volltexte/2006/561/>
- Giraldo J (1999) A pH-dependent model of the activation mechanism of the histamine H<sub>2</sub> receptor. *Biochem Pharmacol* **58**:343-353.
- Green JP, Johnson CL and Weinstein H (1978) Histamine as a neurotransmitter., in *Psychopharmacology, a generation of progress* (Lipton MA, Di Mascio A and Killam KF eds) pp 319-322, Raven Press, New York.
- Haas HL and Konnerth A (1983) Histamine and noradrenaline decrease calcium-activated potassium conductance in hippocampal pyramidal cells. *Nature* **302**:432-434.
- Haas H and Panula P (2003) The role of histamine and the tuberomamillary nucleus in the nervous system. *Nat Rev Neurosci* **4**:121-130.
- Hamm HE (1998) The many faces of G protein signaling. *J Biol Chem* **273**:669-672.
- Hashimoto T, Harusawa S, Araki L, Zuiderveld OP, Smit MJ, Imazu T, Takashima S, Yamamoto Y, Sakamoto Y, Kurihara T, Leurs R, Bakker RA and Yamatodani A (2003) A selective human H<sub>4</sub>-receptor agonist: (-)-2-cyano-1-methyl-3-[(2R,5R)-5- [1H-imidazol-4(5)-yl]tetrahydrofuran-2-yl] methylguanidine. *J Med Chem* **46**:3162-3165.
- Hebert TE and Bouvier M (1998) Structural and functional aspects of G protein-coupled receptor oligomerization. *Biochem Cell Biol* **76**:1-11.
- Hill SJ, Ganellin CR, Timmerman H, Schwartz JC, Shankley NP, Young JM, Schunack W, Levi R and Haas HL (1997) International Union of Pharmacology. XIII. Classification of histamine receptors. *Pharmacol Rev* **49**:253-278.

- Hough LB (2001) Genomics meets histamine receptors: new subtypes, new receptors. *Mol Pharmacol* **59**:415-419.
- Humphrey PP and Barnard EA (1998) International Union of Pharmacology. XIX. The IUPHAR receptor code: a proposal for an alphanumeric classification system. *Pharmacol Rev* **50**:271-277.
- International Human Genome Sequencing Consortium (2004) Finishing the euchromatic sequence of the human genome. *Nature* **431**:931-945.
- Ito C, Morisset S, Krebs MO, Olie JP, Loo H, Poirier MF, Lannfelt L, Schwartz JC and Arrang JM (2000) Histamine H<sub>2</sub> receptor gene variants: lack of association with schizophrenia. *Mol Psychiatry* **5**:159-164.
- Jablonowski JA, Grice CA, Chai W, Dvorak CA, Venable JD, Kwok AK, Ly KS, Wei J, Baker SM, Desai PJ, Jiang W, Wilson SJ, Thurmond RL, Karlsson L, Edwards JP, Lovenberg TW and Carruthers NI (2003) The first potent and selective non-imidazole human histamine H<sub>4</sub> receptor antagonists. *J Med Chem* **46**:3957-3960.
- Jacoby E, Bouhelal R, Gerspacher M and Seuwen K (2006) The 7 TM G-protein-coupled receptor target family. *ChemMedChem* **1**:761-782.
- Jolly S and Desmecht D (2003) Functional identification of epithelial and smooth muscle histamine-dependent relaxing mechanisms in the bovine trachea, but not in bronchi. *Comp Biochem Physiol C Toxicol Pharmacol* **134**:91-100.
- Jutel M, Watanabe T, Klunker S, Akdis M, Thomet OA, Malolepszy J, Zak-Nejmark T, Koga R, Kobayashi T, Blaser K and Akdis CA (2001) Histamine regulates T-cell and antibody responses by differential expression of H<sub>1</sub> and H<sub>2</sub> receptors. *Nature* **413**:420-425.
- Jutel M, Watanabe T, Akdis M, Blaser K and Akdis CA (2002) Immune regulation by histamine. *Curr Opin Immunol* **14**:735-740.
- Kazumori H, Ishihara S, Rumi MA, Ortega-Cava CF, Kadowaki Y and Kinoshita Y (2004) Transforming growth factor alpha directly augments histidine decarboxylase and vesicular monoamine transporter 2 production in rat enterochromaffin-like cells. *Am J Physiol Gastrointest Liver Physiol* **286**:514.
- Kenakin T (1995) Agonist-receptor efficacy. II. Agonist trafficking of receptor signals. *Trends Pharmacol Sci* **16**:232-238.
- Kenakin T (2002) Drug efficacy at G protein-coupled receptors. *Annu Rev Pharmacol Toxicol* **42**:349-379.
- Klinker JF, Wenzel-Seifert K and Seifert R (1996) G-protein-coupled receptors in HL-60 human leukemia cells. *Gen Pharmacol* **27**:33-54.
- Kobayashi T, Inoue I, Jenkins NA, Gilbert DJ, Copeland NG and Watanabe T (1996) Cloning, RNA expression, and chromosomal location of a mouse histamine H<sub>2</sub> receptor gene. *Genomics* **37**:390-394.
- Kostenis E (2006) G proteins in drug screening: from analysis of receptor-G protein specificity to manipulation of GPCR-mediated signalling pathways. *Curr Pharm Des* **12**:1703-1715.
- Kristiansen K (2004) Molecular mechanisms of ligand binding, signaling, and regulation within the superfamily of G-protein-coupled receptors: molecular modeling and mutagenesis approaches to receptor structure and function. *Pharmacol Ther* **103**:21-80.
- Kühn B, Schmid A, Harteneck C, Gudermann T and Schultz G (1996) G proteins of the G<sub>q</sub> family couple the H<sub>2</sub> histamine receptor to phospholipase C. *Mol Endocrinol* **10**:1697-1707.
- Leff P (1995) The two-state model of receptor activation. *Trends Pharmacol Sci* **16**:89-97.
- Lefkowitz RJ, Cotecchia S, Samama P and Costa T (1993) Constitutive activity of receptors coupled to guanine nucleotide regulatory proteins. *Trends Pharmacol Sci* **14**:303-307.
- Leopoldt D, Harteneck C and Nürnberg B (1997) G proteins endogenously expressed in Sf 9 cells: interactions with mammalian histamine receptors. *Naunyn Schmiedeberg's Arch Pharmacol* **356**:216-224.

- Leurs R, Smit MJ and Timmerman H (1995) Molecular pharmacological aspects of histamine receptors. *Pharmacol Ther* **66**:413-463.
- Levi RC and Alloatti G (1988) Histamine modulates calcium current in guinea pig ventricular myocytes. *J Pharmacol Exp Ther* **246**:377-383.
- Levi R, Owen DAA and Trzeciakowski J (1982) Action of histamine on the heart and vasculature., in *Pharmacology of histamine receptors* (Ganellin CR and Parsons EM eds) pp 236-297, Wright, Bristol, England.
- Li L, Kracht J, Peng S, Bernhardt G and Buschauer A (2003) Synthesis and pharmacological activity of fluorescent histamine H<sub>1</sub> receptor antagonists related to mepyramine. *Bioorg Med Chem Lett* **13**:1245-1248.
- Liu C, Ma X, Jiang X, Wilson SJ, Hofstra CL, Blevitt J, Pyati J, Li X, Chai W, Carruthers N and Lovenberg TW (2001) Cloning and pharmacological characterization of a fourth histamine receptor (H<sub>4</sub>) expressed in bone marrow. *Mol Pharmacol* **59**:420-426.
- Lovenberg TW, Roland BL, Wilson SJ, Jiang X, Pyati J, Huvar A, Jackson MR and Erlander MG (1999) Cloning and functional expression of the human histamine H<sub>3</sub> receptor. *Mol Pharmacol* **55**:1101-1107.
- Milligan G (2000) Insights into ligand pharmacology using receptor-G-protein fusion proteins. *Trends Pharmacol Sci* **21**:24-28.
- Morse KL, Behan J, Laz TM, West RE, Jr., Greenfeder SA, Anthes JC, Umland S, Wan Y, Hipkin RW, Gonsiorek W, Shin N, Gustafson EL, Qiao X, Wang S, Hedrick JA, Greene J, Bayne M and Monsma FJ, Jr. (2001) Cloning and characterization of a novel human histamine receptor. *J Pharmacol Exp Ther* **296**:1058-1066.
- Nederkoorn PH, Vernooijs P, Donne-Op den Kelder GM, Baerends EJ and Timmerman H (1994) A new model for the agonistic binding site on the histamine H<sub>2</sub>-receptor: the catalytic triad in serine proteases as a model for the binding site of histamine H<sub>2</sub>-receptor agonists. *J Mol Graph* **12**:242-256.
- Nederkoorn PH, van Lenthe JH, van der Goot H, Donne-Op den Kelder GM and Timmerman H (1996a) The agonistic binding site at the histamine H<sub>2</sub> receptor. I. Theoretical investigations of histamine binding to an oligopeptide mimicking a part of the fifth transmembrane  $\alpha$ -helix. *J Comput Aided Mol Des* **10**:461-478.
- Nederkoorn PH, van Gelder EM, Donne-Op den Kelder GM and Timmerman H (1996b) The agonistic binding site at the histamine H<sub>2</sub> receptor. II. Theoretical investigations of histamine binding to receptor models of the seven  $\alpha$ -helical transmembrane domain. *J Comput Aided Mol Des* **10**:479-489.
- Nguyen T, Shapiro DA, George SR, Setola V, Lee DK, Cheng R, Rauser L, Lee SP, Lynch KR, Roth BL and O'Dowd BF (2001) Discovery of a novel member of the histamine receptor family. *Mol Pharmacol* **59**:427-433.
- Oda T, Morikawa N, Saito Y, Masuho Y and Matsumoto S (2000) Molecular cloning and characterization of a novel type of histamine receptor preferentially expressed in leukocytes. *J Biol Chem* **275**:36781-36786.
- Ogasawara M, Yamauchi K, Satoh Y, Yamaji R, Inui K, Jonker JW, Schinkel AH and Maeyama K (2006) Recent advances in molecular pharmacology of the histamine systems: organic cation transporters as a histamine transporter and histamine metabolism. *J Pharmacol Sci* **101**:24-30.
- Orange PR, Heath PR, Wright SR and Pearson RC (1996a) Allelic variations of the human histamine H<sub>2</sub> receptor gene. *Neuroreport* **7**:1293-1296.
- Orange PR, Heath PR, Wright SR, Ramchand CN, Kolkeiwicz L and Pearson RC (1996b) Individuals with schizophrenia have an increased incidence of the H<sub>2</sub>R 649G allele for the histamine H<sub>2</sub> receptor gene. *Mol Psychiatry* **1**:466-469.
- Parsons ME and Ganellin CR (2006) Histamine and its receptors. *Br J Pharmacol* **147 Suppl 1**:S127-135.

- Parsons ME, Blakemore RC, Durant GJ, Ganellin CR and Rasmussen AC (1975) Proceedings: 3-(4(5)-imidazolyl) propylguanidine (SK&F 91486) - a partial agonist at histamine H<sub>2</sub>-receptors. *Agents Actions* **5**:464.
- Parsons ME, Owen DA, Ganellin CR and Durant GJ (1977) Dimaprit -(S-[3-(N,N-dimethylamino)-prophyl]isothiourea) - a highly specific histamine H<sub>2</sub>-receptor agonist. Part 1. Pharmacology. *Agents Actions* **7**:31-37.
- Perez DM and Karnik SS (2005) Multiple signaling states of G-protein-coupled receptors. *Pharmacol Rev* **57**:147-161.
- Rodriguez-Pena MS, Timmerman H and Leurs R (2000) Modulation of histamine H<sub>2</sub> receptor signalling by G-protein-coupled receptor kinase 2 and 3. *Br J Pharmacol* **131**:1707-1715.
- Ruat M, Traiffort E, Arrang JM, Leurs R and Schwartz JC (1991) Cloning and tissue expression of a rat histamine H<sub>2</sub>-receptor gene. *Biochem Biophys Res Commun* **179**:1470-1478.
- Samama P, Cotecchia S, Costa T and Lefkowitz RJ (1993) A mutation-induced activated state of the  $\beta_2$ -adrenergic receptor. Extending the ternary complex model. *J Biol Chem* **268**:4625-4636.
- Schneider E (2005) Development of Fluorescence-Based Methods for the Determination of Ligand Affinity, Selectivity and Activity at G-Protein Coupled Receptors. Doctoral thesis. University of Regensburg, Germany.
- Schneider E, Rolli-Derkinderen M, Arock M and Dy M (2002) Trends in histamine research: new functions during immune responses and hematopoiesis. *Trends Immunol* **23**:255-263.
- Seifert R (2005) Constitutive activity of  $\beta$ -adrenoceptors: analysis in membrane systems., in *G Protein-coupled Receptors as Drug Targets. Analysis of Activation and Constitutive Activity* (Seifert R and Wieland T eds) pp 123-140, Wiley-VCH, Weinheim.
- Seifert R and Wenzel-Seifert K (2002) Constitutive activity of G-protein-coupled receptors: cause of disease and common property of wild-type receptors. *Naunyn Schmiedebergs Arch Pharmacol* **366**:381-416.
- Seifert R, Hoer A, Schwaner I and Buschauer A (1992) Histamine increases cytosolic Ca<sup>2+</sup> in HL-60 promyelocytes predominantly via H<sub>2</sub> receptors with an unique agonist/antagonist profile and induces functional differentiation. *Mol Pharmacol* **42**:235-241.
- Seifert R, Wenzel-Seifert K, Bürckstümmer T, Pertz HH, Schunack W, Dove S, Buschauer A and Elz S (2003) Multiple differences in agonist and antagonist pharmacology between human and guinea pig histamine H<sub>1</sub>-receptor. *J Pharmacol Exp Ther* **305**:1104-1115.
- Selbach O, Brown RE and Haas HL (1997) Long-term increase of hippocampal excitability by histamine and cyclic AMP. *Neuropharmacology* **36**:1539-1548.
- Shayo C, Fernandez N, Legnazzi BL, Monczor F, Mladovan A, Baldi A and Davio C (2001) Histamine H<sub>2</sub> receptor desensitization: involvement of a select array of G protein-coupled receptor kinases. *Mol Pharmacol* **60**:1049-1056.
- Smit MJ, Timmerman H, Alewijnse AE, Punin M, van den Nieuwenhof I, Blauw J, van Minnen J and Leurs R (1995) Visualization of agonist-induced internalization of histamine H<sub>2</sub> receptors. *Biochem Biophys Res Commun* **214**:1138-1145.
- Smit MJ, Timmerman H, Blauw J, Beukers MW, Roovers E, Jacobs EH, Hoffmann M and Leurs R (1996a) The C terminal tail of the histamine H<sub>2</sub> receptor contains positive and negative signals important for signal transduction and receptor down-regulation. *J Neurochem* **67**:1791-1800.
- Smit MJ, Leurs R, Alewijnse AE, Blauw J, Van Nieuw Amerongen GP, Van De Vrede Y, Roovers E and Timmerman H (1996b) Inverse agonism of histamine H<sub>2</sub> antagonist accounts for upregulation of spontaneously active histamine H<sub>2</sub> receptors. *Proc Natl Acad Sci U S A* **93**:6802-6807.
- Soll AH and Berglinth T (1987) Physiology of isolated gastric glands and parietal cells: receptors and effectors regulating function., in *Physiology of the Gastrointestinal Tract* (Johnson LR ed) pp 883-909, Raven Press, New York.
- Sprang SR (1997) G protein mechanisms: insights from structural analysis. *Annu Rev Biochem* **66**:639-678.

- Stark H, Kathmann M, Schlicker E, Schunack W, Schlegel B and Sippl W (2004) Medicinal chemical and pharmacological aspects of imidazole-containing histamine H<sub>3</sub> receptor antagonists. *Mini Rev Med Chem* **4**:965-977.
- Swaminath G, Xiang Y, Lee TW, Steenhuis J, Parnot C and Kobilka BK (2004) Sequential binding of agonists to the  $\beta_2$  adrenoceptor. Kinetic evidence for intermediate conformational states. *J Biol Chem* **279**:686-691.
- Traiffort E, Vizuete ML, Tardivel-Lacombe J, Souil E, Schwartz JC and Ruat M (1995) The guinea pig histamine H<sub>2</sub> receptor: gene cloning, tissue expression and chromosomal localization of its human counterpart. *Biochem Biophys Res Commun* **211**:570-577.
- Vassilatis DK, Hohmann JG, Zeng H, Li F, Ranchalis JE, Mortrud MT, Brown A, Rodriguez SS, Weller JR, Wright AC, Bergmann JE and Gaitanaris GA (2003) The G protein-coupled receptor repertoires of human and mouse. *Proc Natl Acad Sci U S A* **100**:4903-4908.
- Wang L, Gantz I and Del Valle J (1996) Histamine H<sub>2</sub> receptor activates adenylate cyclase and PLC via separate GTP-dependent pathways. *Am J Physiol* **271**:G613-620.
- Weinstein H, Chou D, Johnson CL, Kang S and Green JP (1976) Tautomerism and the receptor action of histamine: a mechanistic model. *Mol Pharmacol* **12**:738-745.
- Weiss JM, Morgan PH, Lutz MW and Kenakin TP (1996a) The Cubic Ternary Complex Receptor-Occupancy Model I. Model Description. *J Theor Biol* **178**:151-167.
- Weiss JM, Morgan PH, Lutz MW and Kenakin TP (1996b) The Cubic Ternary Complex Receptor-Occupancy Model II. Understanding Apparent Affinity. *J Theor Biol* **178**:169-182.
- Weiss JM, Morgan PH, Lutz MW and Kenakin TP (1996c) The cubic ternary complex receptor-occupancy model. III. resurrecting efficacy. *J Theor Biol* **181**:381-397.
- Wenzel-Seifert K, Kelley MT, Buschauer A and Seifert R (2001) Similar apparent constitutive activity of human histamine H<sub>2</sub>-receptor fused to long and short splice variants of G<sub>sα</sub>. *J Pharmacol Exp Ther* **299**:1013-1020.
- Windaus A and Vogt W (1908) Synthesis of Imidazolyethylamine. *Ber Dtsch Ges* **40**:3691.
- Wise A, Gearing K and Rees S (2002) Target validation of G-protein coupled receptors. *Drug Discov Today* **7**:235-246.
- Xie SX, Ghorai P, Ye QZ, Buschauer A and Seifert R (2006a) Probing ligand-specific histamine H<sub>1</sub>- and H<sub>2</sub>-receptor conformations with N<sup>6</sup>-acylated Imidazolypropylguanidines. *J Pharmacol Exp Ther* **317**:139-146.
- Xie SX, Kraus A, Ghorai P, Ye QZ, Elz S, Buschauer A and Seifert R (2006b) N<sup>1</sup>-(3-cyclohexylbutanoyl)-N<sup>2</sup>-[3-(1H-imidazol-4-yl)propyl]guanidine (UR-AK57), a potent partial agonist for the human histamine H<sub>1</sub>- and H<sub>2</sub>-receptors. *J Pharmacol Exp Ther* **317**:1262-1268.
- Yamashita M, Fukui H, Sugama K, Horio Y, Ito S, Mizuguchi H and Wada H (1991) Expression cloning of a cDNA encoding the bovine histamine H<sub>1</sub> receptor. *Proc Natl Acad Sci U S A* **88**:11515-11519.
- Zhu Y, Michalovich D, Wu H, Tan KB, Dytko GM, Mannan IJ, Boyce R, Alston J, Tierney LA, Li X, Herrity NC, Vawter L, Sarau HM, Ames RS, Davenport CM, Hieble JP, Wilson S, Bergsma DJ and Fitzgerald LR (2001) Cloning, expression, and pharmacological characterization of a novel human histamine receptor. *Mol Pharmacol* **59**:434-441.

## Chapter 2

### Scope and Objectives

*N*-[3-(1*H*-imidazol-4-yl)propyl]guanidines such as arpromidine are the most potent agonists at the H<sub>2</sub>R known so far and possibly useful as positive inotropic drugs for the treatment of severe congestive heart failure, as agents inducing cell differentiation in acute myelogenous leukemia, and as anti-inflammatory drugs. Recently, a novel class of less basic *N*<sup>G</sup>-acylated derivatives with improved pharmacokinetic properties, *i.e.* oral bioavailability and the capability of penetrating across the blood-brain-barrier, was developed. In a membrane steady-state GTPase activity assay at fusion proteins of H<sub>2</sub>R and the short splice variant of G<sub>sq</sub>, G<sub>sqS</sub>, guanidines and *N*<sup>G</sup>-acylguanidines were considerably more potent and efficacious at the guinea pig (gp) than at the human (h) species isoform (Kelley et al., 2001; Xie et al., 2006a, b). By contrast, histamine and the small H<sub>2</sub>R agonists dimaprit and amthamine do not exhibit species-selectivity.

The aim of this thesis was to investigate molecular mechanisms underlying distinct functions of H<sub>2</sub>R species isoforms. Deeper insight into species-selective interactions of guanidine-type agonists with the human and guinea pig H<sub>2</sub>R will facilitate the development of novel agonists with increased hH<sub>2</sub>R potency and selectivity. Due to the present lack of GPCR crystal structures, investigations must be based on homology models derived from bovine rhodopsin (Palczewski et al., 2000). Predictions emerging from computational modelling provided a basis for subsequent experimental molecular pharmacological studies.

Due to the homology of GPCRs in the structurally conserved regions of the seven TM domains, the methodology of homology modelling was expected to yield reliable three-dimensional structural models of hH<sub>2</sub>R and gpH<sub>2</sub>R. Conserved intramolecular interactions including specific water molecules that were predicted to confer structural stability to the transmembrane-spanning domains and to play a role in receptor function had to be analyzed according to experimental data. A detailed inspection of the binding pocket was to identify

distinct amino acids selectively interacting with guanidine-type agonists. A virtual screening approach for appropriate substituents for the variable mono- or diarylalkanoyl groups of  $N^G$ -acylated guanidines was expected to result in agonists with increased hH<sub>2</sub>R potency and selectivity.

Molecular dynamics (MD) simulation is an established computational method to analyze the conformational dynamics of membrane proteins. MD simulations of the ligand-free and the arpromidine-docked hH<sub>2</sub>R models are to generate energetically favourable conformations representing the transition of the hH<sub>2</sub>R from an inactive towards an active state, predicted to occur on a nanosecond time scale. Since explicit consideration of the protein environment is a crucial prerequisite for reliable simulations, the hH<sub>2</sub>R model was aimed to be embedded in a 1-palmitoyl-2-oleoyl-*sn*-glycero-3-phosphatidylcholine bilayer solvated by water. The results from the simulations were expected to help on further refining dynamic models of the binding mode of guanidine-type agonists.

The experimental part of this thesis was aimed at the pharmacological characterization of H<sub>2</sub>R species isoforms of human, guinea pig, rat, and canine. Recombinant proteins were to be expressed using a baculovirus/Sf9 insect cells expression system. Measurement of steady-state GTPase activity in membranes expressing H<sub>2</sub>R-G<sub>sαS</sub> fusion proteins was selected as this system was previously shown to be reliable and very sensitive to analyze ligand potencies and efficacies. The constitutive activities of the various H<sub>2</sub>R species isoforms had to be quantified with the GTPase assay and supplemented by adenylyl cyclase activity assays at membranes expressing fused and non-fused H<sub>2</sub>R<sub>s</sub>. Results from these studies had to be analyzed with help of the generated receptor models.

Mutant hH<sub>2</sub>R-G<sub>sαS</sub> fusion proteins with Cys-17 and Ala-271 at the extracellular ends of TM1 and TM7, respectively, mutated into the corresponding gpH<sub>2</sub>R residues, Tyr-17 and Asp-271, had to be generated and characterized since these residues were predicted to contribute to the species-selectivity of guanidine-type agonists (Kelley et al., 2001). The elusive role of the second extracellular loop for binding H<sub>2</sub>R agonists was planned to be analyzed by additional site-directed mutagenesis experiments.

In summary, this thesis was aimed at further characterizing the structure and function of H<sub>2</sub>R species isoforms as well as the ligand-receptor interactions, the structure-activity and structure-selectivity relationships of guanidine-type agonists by an interdisciplinary approach comprising molecular modelling, *in-vitro* mutagenesis, and pharmacological assays.



## 2.1 References

- Kelley MT, Bürckstümmer T, Wenzel-Seifert K, Dove S, Buschauer A and Seifert R (2001) Distinct interaction of human and guinea pig histamine H<sub>2</sub>-receptor with guanidine-type agonists. *Mol Pharmacol* **60**:1210-1225.
- Palczewski K, Kumasaka T, Hori T, Behnke CA, Motoshima H, Fox BA, Le Trong I, Teller DC, Okada T, Stenkamp RE, Yamamoto M and Miyano M (2000) Crystal structure of rhodopsin: A G protein-coupled receptor. *Science* **289**:739-745.
- Xie SX, Ghorai P, Ye QZ, Buschauer A and Seifert R (2006a) Probing ligand-specific histamine H<sub>1</sub>- and H<sub>2</sub>-receptor conformations with N<sup>G</sup>-acylated imidazolylpropylguanidines. *J Pharmacol Exp Ther* **317**:139-146.
- Xie SX, Kraus A, Ghorai P, Ye QZ, Elz S, Buschauer A and Seifert R (2006b) N<sup>1</sup>-(3-cyclohexylbutanoyl)-N<sup>2</sup>-[3-(1H-imidazol-4-yl)propyl]guanidine (UR-AK57), a potent partial agonist for the human histamine H<sub>1</sub>- and H<sub>2</sub>-receptors. *J Pharmacol Exp Ther* **317**:1262-1268.



## Chapter 3

# Computational Methods

### 3.1 GPCR homology models in pharmacological sciences

In spite of remarkable advances in the fields of biology and pharmacology of GPCRs, progress on the structures of this protein family is rather limited. To date, the only high-resolution crystal structures of a GPCR are of bovine rhodopsin which was resolved for the first time in the year 2000 with 2.80 Å resolution (Palczewski et al., 2000). Meanwhile, four additional structures of bovine rhodopsin have been published. Coordinate files of these structures can be retrieved from the Brookhaven Protein Data Base (PDB) (Bernstein et al., 1977) by the identity codes 1F88 (Palczewski et al., 2000), 1HZX (Teller et al., 2001), 1L9H (Okada et al., 2002), 1GZM (Li et al., 2004), and 1U19 (Okada et al., 2004). Rhodopsin is better suited for structural studies than most other GPCRs because it is possible to obtain large quantities of highly enriched protein from bovine retina. Rhodopsin is also a remarkably stable GPCR, retaining function under conditions that denature many other GPCRs (Kobilka, 2007).

The lack of detailed structural information about GPCRs initiated the quest for three dimensional (3D) structural models. Knowledge-based approaches were developed to predict 3D structures of proteins that are based on experimental data of 3D structures of homologous reference proteins. Class 1 GPCRs (Foord et al., 2005) are homologous with rhodopsin (Mirzadegan et al., 2003) and are also referred to the term rhodopsin-like. Accordingly, crystal structures of bovine rhodopsin were frequently and successfully used to build homology models of class 1 GPCRs. Such models have been shown to provide unique insight into molecular mechanisms of GPCR function and activity (Kristiansen, 2004). For example, predictions about the specific roles of distinct amino acids for the regulation of

GPCR activity can be derived (Figure 3.1). These predictions can subsequently be used as a guideline for the construction and characterization of point mutations. Thus there is a tight correspondence between suggestions from homology models and the experimental field of molecular pharmacology. Furthermore, homology models offer the possibility to study ligand-receptor interactions at an atomic level that can direct the *de novo* design of new leads, e.g. by application of flexible docking and virtual screening methods (Bissantz et al., 2003).

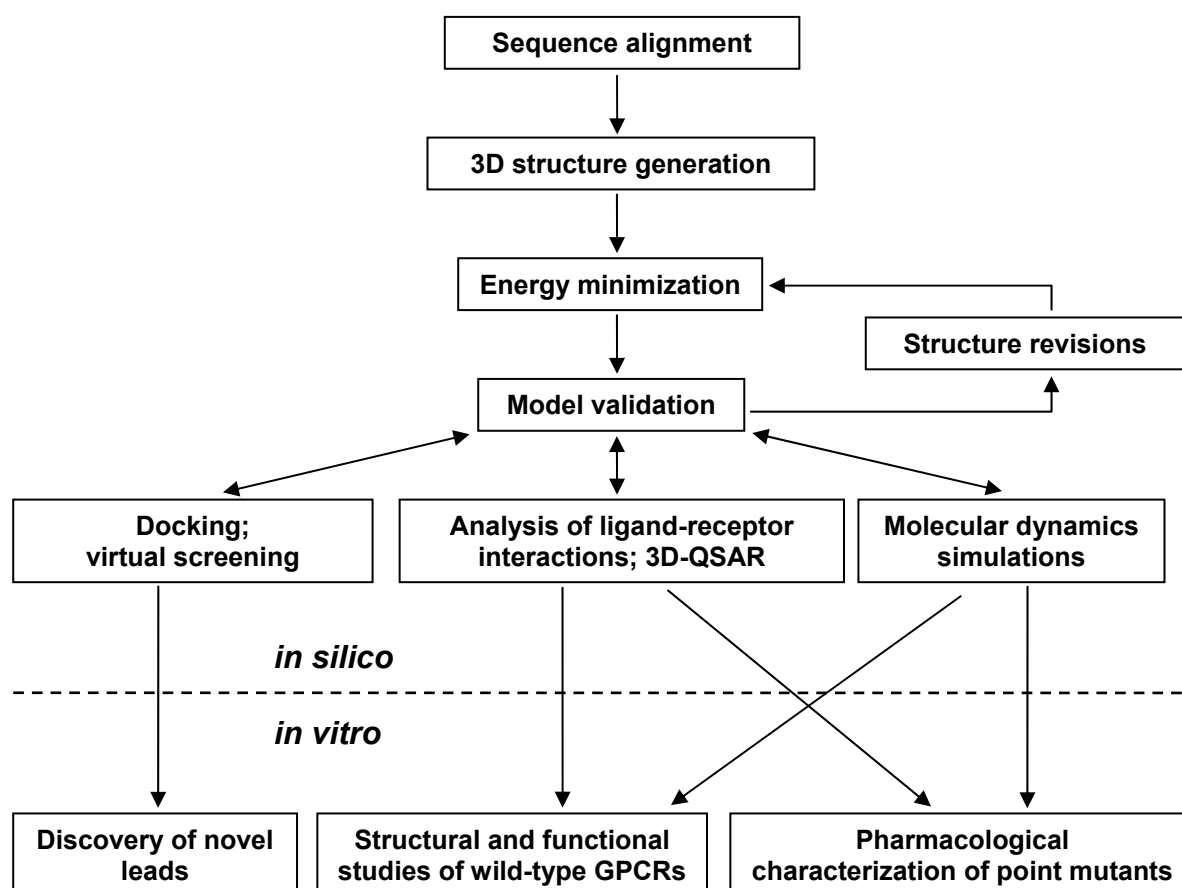


**Figure 3.1:** Flowchart of steps in homology modelling and possible applications of homology models in computational (*in silico*) and *in vitro* pharmacological fields of research.

## 3.2 Sequence alignment

The first step in homology modelling is the alignment of the amino acid sequence of the target protein with that of the template protein. Correspondences between amino acids are the basis for transferring the coordinates of the template to the target. Several prediction algorithms are available that help to identify structurally conserved hydrophobic

(intramembraneous) and less-conserved polar (loop) regions, and may therefore be useful in assisting in the sequence alignment.

Automatic sequence alignment tools are frequently used to search for an optimal similarity of sequences. Sequence comparisons are carried out either pairwise (e.g. ALIGN (Devereux et al., 1984)) or as a multi-sequence alignment (e.g. CLUSTAL W (Thompson et al., 1994)). Most sequence alignment algorithms more or less try to retrace the evolutionary process involved in converting one sequence into another. For this operation homology matrices are used that specify the weight for aligning a particular type of amino acid with another. These homology matrices make use of the most probable amino acid substitutions according to physical, chemical, or statistical properties. In cases of different sequence lengths and variations in the locations of conserved regions, gaps are introduced into the alignment. To minimize the number of gaps, a gap-penalty function is used.

### 3.3 Construction of 3D structures

The most important steps in the process of generating 3D structures of GPCRs are summarized as follows:

- *Construction of structurally conserved regions.* In gap-free regions of the sequence alignment, the backbone atom coordinates of the target model can be directly retrieved from the template structure. For GPCR modelling approaches, structurally conserved regions are the TM domains and potentially short loop regions.
- *Construction of structurally variable regions.* Loop regions and the N-termini and C-termini of GPCRs display low sequence homology and often contain gaps and deletions. A convenient method for constructing such regions is to search for appropriate peptide segments in a 3D structure database (loop search). With this approach, homologous loop segments can be selected that align with anchor regions and fit into the spatial environment of the target model. Alternatively, loops can be generated by *de novo* strategies, e.g. using simulating annealing methods.
- *Addition of amino acid side chains and adjustment of side chain conformations and protonation states.* Generally, identical and homologous amino acids in homologous proteins are proposed to adopt similar side chain conformations. Hence, the conformations of such residues may be retrieved by adjusting the conformation to that of the corresponding residue in the template structure. In cases of non-conserved amino

acid exchanges rotamer libraries can assist in the selection of reasonable side chain conformations. Rotamer libraries such as the Lovell library (Lovell et al., 2000) implemented in Sybyl 7.1 (Tripos, St. Louis, MO) contain a collection of statistically favored side chain conformations from which the most frequent one without clashes with other residues can be selected. Polar residues are preferably located in loop and terminal regions of GPCRs that point into the aqueous medium. Thus, the protonation states of these residues can be adjusted according to their  $pK_a$  values in water. By contrast, polar residues in the interior of the TM bundle most often are conserved and undergo distinct intramolecular interactions or form H-bonds with structurally important water molecules (Okada et al., 2002). The protonation states of these residues must therefore be individually adjusted.

- *Structural refinement using energy minimization and MD simulations.* Energy minimization techniques are used to remove strain from the protein structure and to transfer it in an energetically relaxed conformation. Energy minimization is based on the calculation of the potential energy in a molecular system using force fields. MD simulations are used to elaborate the conformational space of macromolecules. The principles of both methods are described in more detail in the Appendix 1 (chapter 11).

### 3.4 Validation of homology models

After GPCR homology models are generated and structurally optimized, validation of the resulting models is an essential task to guarantee applicability of the models for the particular purposes of the project. The most important parameters to be evaluated are summarized in Figure 3.2.

For an evaluation of the stereochemical quality of a structure model, programs such as PROCHECK (Laskowski et al., 1993) and WHATCHECK (Hoof et al., 1996) have been developed. A Ramachandran plot is frequently used to check the correctness of the backbone  $\phi$  and  $\psi$  torsion angles. A bump check is to detect and remove bad van der Waals contacts between adjacent residues and should already be carried out prior to energy minimization and MD simulations. An overall estimation of structural differences between the backbone structures of the protein model and the template can be obtained by calculating the root mean square deviation (*RMSD*) of all backbone or  $C_\alpha$  atoms. When conducting MD

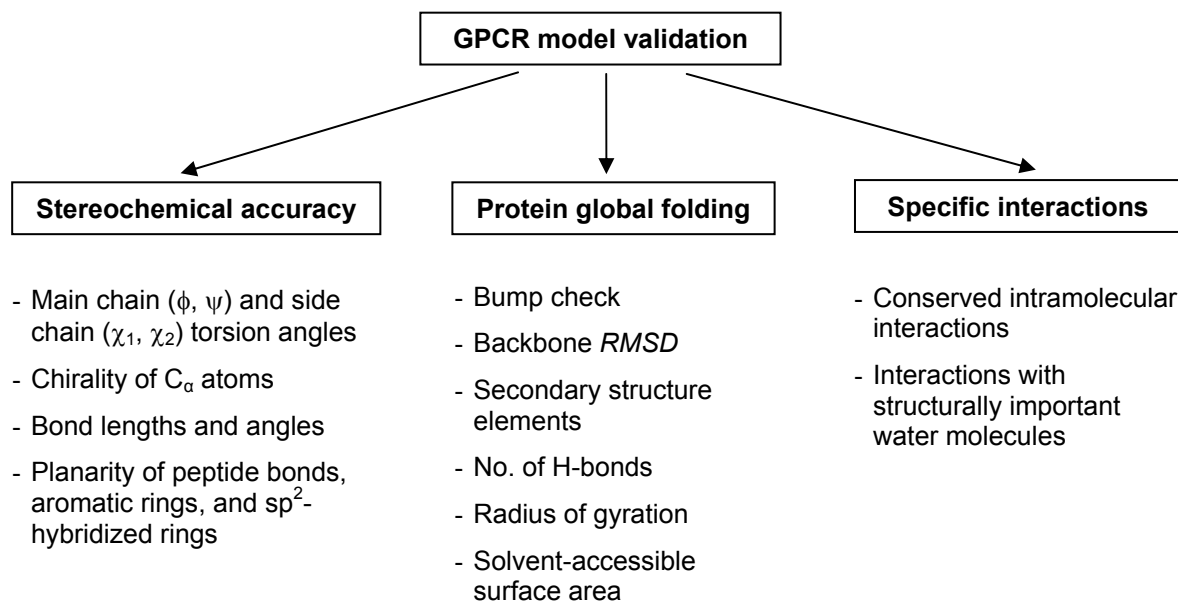


**Figure 3.2:** Overview of parameters for the validation of GPCR homology models.

simulations, stability of secondary structural elements is an important parameter that can be calculated by means of a dssp plot (Kabsch and Sander, 1983). Additionally, the total number of intramolecular H-bonds, the radius of gyration, and the solvent-accessible surface area give valuable measures of the protein global folding. Finally, distinct interactions between adjacent residues and between residues and structurally important water molecules that are predicted to be conserved and that may play a functional role in GPCR function and/or structural arrangement of the TM domains have to be controlled and eventually enforced by application of restraints.

### 3.5 References

- Bernstein FC, Koetzle TF, Williams GJ, Meyer EF, Brice MC, Rodger JR, Kennard O, Shimanouchi T and Tasumi M (1977) The protein data bank: a computer-based archival file for macromolecular structures. *J Mol Biol* **112**:535-542.
- Bissantz C, Bernard P, Hibert M and Rognan D (2003) Protein-based virtual screening of chemical databases. II. Are homology models of G-Protein Coupled Receptors suitable targets? *Proteins* **50**:5-25.
- Devereux J, Haeberli P and Smithies O (1984) A comprehensive set of sequence analysis programs for the VAX. *Nucleic Acids Res* **12**:387-395.
- Foord SM, Bonner TI, Neubig RR, Rosser EM, Pin JP, Davenport AP, Spedding M and Harmar AJ (2005) International Union of Pharmacology. XLVI. G protein-coupled receptor list. *Pharmacol Rev* **57**:279-288.
- Hooft RW, Vriend G, Sander C and Abola EE (1996) Errors in protein structures. *Nature* **381**:272.

- Kabsch W and Sander C (1983) Dictionary of protein secondary structure: pattern recognition of hydrogen-bonded and geometrical features. *Biopolymers* **22**:2577-2637.
- Kobilka BK (2007) G protein coupled receptor structure and activation. *Biochim Biophys Acta* **1768**:794-807.
- Kristiansen K (2004) Molecular mechanisms of ligand binding, signaling, and regulation within the superfamily of G-protein-coupled receptors: molecular modeling and mutagenesis approaches to receptor structure and function. *Pharmacol Ther* **103**:21-80.
- Laskowski RA, MacArthur MW, Moss DS and Thornton JM (1993) PROCHECK: a program to check the stereochemical quality of protein structures. *J Appl Cryst* **26**:283-291.
- Li J, Edwards PC, Burghammer M, Villa C and Schertler GF (2004) Structure of bovine rhodopsin in a trigonal crystal form. *J Mol Biol* **343**:1409-1438.
- Lovell SC, Word JM, Richardson JS and Richardson DC (2000) The penultimate rotamer library. *Proteins* **40**:389-408.
- Mirzadegan T, Benko G, Filipek S and Palczewski K (2003) Sequence analyses of G-protein-coupled receptors: similarities to rhodopsin. *Biochemistry* **42**:2759-2767.
- Okada T, Fujiyoshi Y, Silow M, Navarro J, Landau EM and Shichida Y (2002) Functional role of internal water molecules in rhodopsin revealed by X-ray crystallography. *Proc Natl Acad Sci U S A* **99**:5982-5987.
- Okada T, Sugihara M, Bondar AN, Elstner M, Entel P and Buss V (2004) The retinal conformation and its environment in rhodopsin in light of a new 2.2 Å crystal structure. *J Mol Biol* **342**:571-583.
- Palczewski K, Kumasaka T, Hori T, Behnke CA, Motoshima H, Fox BA, Le Trong I, Teller DC, Okada T, Stenkamp RE, Yamamoto M and Miyano M (2000) Crystal structure of rhodopsin: A G protein-coupled receptor. *Science* **289**:739-745.
- Teller DC, Okada T, Behnke CA, Palczewski K and Stenkamp RE (2001) Advances in determination of a high-resolution three-dimensional structure of rhodopsin, a model of G-protein-coupled receptors (GPCRs). *Biochemistry* **40**:7761-7772.
- Thompson JD, Higgins DG and Gibson TJ (1994) CLUSTAL W: improving the sensitivity of progressive multiple sequence alignment through sequence weighting, position-specific gap penalties and weight matrix choice. *Nucleic Acids Res* **22**:4673-4680.



## Chapter 4

# 3D Structure Models of Human and Guinea Pig Histamine H<sub>2</sub> Receptors: Analysis of Species-selective Interactions with Guanidine-type Agonists and Virtual Screening

### 4.1 Introduction

*N*-[3-(1*H*-imidazol-4-yl)propyl]guanidines are the most potent and selective agonists at the histamine H<sub>2</sub> receptor (H<sub>2</sub>R) known so far (Dove et al., 2004). Measuring the positive chronotropic response on the spontaneously beating guinea pig right atrium served as a standard method for the pharmacological characterization of the H<sub>2</sub>R agonists. Quantitative structure-activity relationship (QSAR) approaches were applied to correlate agonist potencies (expressed as *pD*<sub>2</sub> values) with structural properties. A Free-Wilson analysis of a series of unbranched impromidine-like and branched arpromidine (ARP)-like agonists led to first results about favorable and unfavorable arrangements of aromatic rings and substituent effects (Franke and Buschauer, 1992). Subsequently, a more powerful Hansch analysis was applied to a large series of 141 guanidine-type agonists (Dove and Buschauer, 1998) indicating that spatial effects like folding and branching as well as electrostatic interactions of heteroatoms like S, O, and N are the main forces for optimal binding of the compounds. Particularly, affinity-increasing effects of a branch three methylene units distant from the

guanidino group and introduction of a nitrogen atom in one of the two aromatic rings as well as an unfavorable influence of substituents at the heteroaryl ring were elucidated. More complex steric and electrostatic effects on receptor binding were detected by a 3D-QSAR approach submitting the agonists to a comparative molecular field analysis (CoMFA) (Dove and Buschauer, 1998, 1999). For this purpose, the 3D structures of 142 compounds were aligned based on their common imidazolylpropylguanidine groups. A refined alignment could be generated with the weighted field fit method (Dove and Buschauer, 1999). As a result, steric and electrostatic field variables contributing to H<sub>2</sub>R agonism were calculated. With this method, distinct effects of the two aromatic rings in *N*-(imidazolylpropyl)-*N*<sup>G</sup>-(diarylalkyl)guanidines were described. Accordingly, one of the aromatic rings was predicted to point into an “upper” binding region where bulk enhances activity. Substitution with negatively charged groups in *meta* and *para* position of this ring may further increase potency. A second “lower” binding region was predicted to be occupied by the other ring system where introduction of bulky groups generally decreases potency.

The results from 3D-QSAR studies were subsequently used to analyze the binding modes of guanidine-type agonists in the H<sub>2</sub>R binding pocket. For this purpose, a homology model of the seven transmembrane (TM) domains of the gpH<sub>2</sub>R was generated using the crystal structure of bovine rhodopsin as template (Kelley et al., 2001). In a membrane steady-state GTPase activity assay at fusion proteins of H<sub>2</sub>R and the short splice variant of G<sub>sa</sub>, G<sub>saS</sub>, the guanidines and their *N*<sup>G</sup>-acylated derivatives were determined to be considerably more potent and efficacious at the guinea pig than at the human H<sub>2</sub>R-G<sub>saS</sub> (Kelley et al., 2001). From the generated structure model, the non-conserved residues Asp-271(7.36)<sup>1</sup> and Tyr-17(1.31) were proposed to selectively interact in the guinea pig species isoform thereby stabilizing an active guanidine-bound receptor conformation. This hypothesis was subsequently confirmed by site-directed mutagenesis experiments (Kelley et al., 2001).

In the present study, 3D structure models of the gpH<sub>2</sub>R and hH<sub>2</sub>R were generated using the crystal structure of bovine rhodopsin as template. In addition to the previous model, the N-terminus of the proteins and all extracellular and intracellular loops connecting the TM domains were considered. For a further analysis of the binding modes of guanidine-type agonists and their *N*<sup>G</sup>-acylated derivatives, the extracellular loop regions were expected to be in spatial proximity to the agonists and thus to contribute to ligand-receptor interactions. In addition, the model of the human receptor was used to perform a virtual screening to develop more potent and selective hH<sub>2</sub>R agonists.

---

<sup>1</sup> Residues within TM domains are named according to the Ballesteros/Weinstein nomenclature (Ballesteros and Weinstein, 1995). The most conserved residue in each TM is numbered as X.50 where X is the number of the respective TM domain.

## 4.2 Materials and Methods

### 4.2.1 Sequence alignment

An initial amino acid sequence alignment of bovine rhodopsin with hH<sub>2</sub>R (Gantz et al., 1991) and gpH<sub>2</sub>R (Traiffort et al., 1995) was generated with CLUSTAL W (Thompson et al., 1994) (Figure 4.1). A multi-sequence alignment of a large series of aminergic GPCRs provided by the GPCR database (<http://www.gpcr.org/7tm>) was used as a reference to accomplish necessary corrections. Class 1 aminergic GPCRs and rhodopsin share the highest conservation within the seven  $\alpha$ -helical TM domains (sequence identity of 19.6% and 21.1% between bovine rhodopsin and hH<sub>2</sub>R and gpH<sub>2</sub>R, respectively). Since a much higher conservation exists within structurally conserved regions (Mirzadegan et al., 2003) those microdomains were used to refine the alignment. Examples of structurally conserved regions are the most conserved residues in each TM domain and highly conserved motifs such as the (E/D)RY motif in TM3, the CWxP(F/Y) motif in TM6, the NPxxY(x)<sub>5,6</sub>F motif in TM7 and the short  $\alpha$ -helical segment H8 at the C-terminus of the receptor. The final sequence alignment was in good agreement with a previous alignment of several GPCRs with bovine rhodopsin (Ballesteros et al., 2001a).

			N-term		TM1		i1	
b.Rhod.	1	MNGTEGPNFYVPFSNKTGVVRS	PFEAPQYYLAE	PWQFSMLAAYMFLLIMLGFPIN	FTLYVTVQHKKLRT			
hH2R	1	-----	MAPNGT.SSFC.DSTACKITITVVLAV..	LITVAG.VVVCLAVGLNRR..	N			
gpH2R	1	-----	MAFNQTV.SFCMDFTVYKVTISVILII..	LVTVAG.VVVCLAVGLNRR..	S			
			TM2	e1	TM3			
b.Rhod.	71	PLNYILLNLAVADLF	FMVFGGFTTTL	YTSLSHG	YFVGPTGCNLEGGFATL	GGEIALWSLVVLA	AIERYVVVC	
hH2R	52	LT.CFIVS..IT..	LLGLLVLPFSAIQ.SCKWS..	KVF..	IYTSLDVMLCTASILN.FMISLD..	CA.M		
gpH2R	52	LT.CFIVS...T..	LLGLLVLPFSAIQ.SCKWS.SKVF..	IYTSLDVMLCTASILN.FMISLD..	CA.T			
			i2	TM4	e2			
b.Rhod.	141	KPMSNFRFGE-NHAIMGVAFTW	VMALACAAPPLV-GW-SRYIPE-GMQC--	SCGIDYYTPHEETNNESFV				
hH2R	122	D.LRYPVLVTPVRVAISLVLI..	ISITLSFLSIHL..N..NETSK.NHTTSK.KVQV-----	..VYG				
gpH2R	122	D.LRYPVLITPARVAISLV.I..	ISITLSFLSIHL..N..NETSKDNDTIVK.KVQV-----	..VYG				
			TM5	i3	TM6			
b.Rhod.	205	IYMFVVHFIIPL	LIVIFFCYGQLVFTVKEAAAQQQE----	SATTQKAEKEVTRMVIIMVIAFLICWLPYAG				
hH2R	184	LVDGL.T.YL..	LIMCIT.YR.FKVAR	DQ.KRINHISWK.A.IR-.HKA.VTLAAVMG..I...F..FT				
gpH2R	184	LVDGL.T.YL..	LIMCIT.FR.FKIAR.Q.RRINHIGSWK.A.IR-.HKA.VTLAAVMG..I...F..FT					
			e3	TM7	H8			
b.Rhod.	271	VAFYIFTHQGSDFGPI	FMTIPAFFAKTSAVYN	NPVIYIMMNKQFRNCMVTTLC	CGKNPLGDD	EASTTVSKT		
hH2R	253	AFV.RGLRGDDAINEVLEA.VLWLGYANSAL..	IL.AAL.RD..	TGYQQLF..RLANRNSHKT.LRSNAS				
gpH2R	253	.FV.RGLKGDDAVNEV.EDVVLWLGYANSAL..	IL.AAL.RD..	TAYHQLF..RLASHNSH.T.LRLNNS				
			C-term					
b.Rhod.	341	ETSQVAPA-348						
hH2R	323	QL.RTQSREPRQQEEKPLKLQVWSGTEVTAPQGATDR	359					
gpH2R	323	QLNRSQCQEPWQEDKPLNLQVWSGTEVTAPQGATNR	359					

**Figure 4.1:** Sequence alignment of bovine rhodopsin with hH<sub>2</sub>R and gpH<sub>2</sub>R. Dots in the sequences indicate identity with bovine rhodopsin. Amino acids shown with grey shading represent the most conserved amino acid in each TM domain.

#### 4.2.2 Generation of 3D structure models of the hH<sub>2</sub>R and gpH<sub>2</sub>R

For the construction of hH<sub>2</sub>R and gpH<sub>2</sub>R homology models, three crystal structures of bovine rhodopsin (pdb accession numbers 1F88 (Palczewski et al., 2000), 1HZX (Teller et al., 2001), and 1L9H (Okada et al., 2002)) were used as templates. The sequence of bovine rhodopsin was mutated into the corresponding sequences of hH<sub>2</sub>R and gpH<sub>2</sub>R at positions without gaps and deletions, *i.e.* TM1 to TM7, extracellular loops e1 and e3, intracellular loop i1, N-terminus, and C-terminus up to Phe-303. Since the H<sub>2</sub>R C-terminus is by 29 residues longer than the C-terminus of bovine rhodopsin and since both sequences share a very low homology in this part, predictions about the peptide structure following H8 would be highly speculative. Therefore, the last 56 C-terminal residues were not considered in the construction of the models. The remaining intracellular and extracellular loops (e2, i2, i3) were added by the Loop Search tool implemented in Sybyl 7.1 (Tripos, St. Louis, MO). This tool searches a binary PDB variant of 3D protein structures for homologous sequences that

align with the termini before and after the lacking loops. Five buried water molecules positioned close to conserved residues were retained from the crystal structure of bovine rhodopsin (pdb accession number 1L9H) (Okada et al., 2002). Two water molecules (Wat2a and Wat2b) were not implemented in the new H<sub>2</sub>R models, since these molecules are involved in the interaction of the retinal-Schiff base with rhodopsin and interact with specific residues in e2 that are not conserved in the H<sub>2</sub>R.

### 4.2.3 Structural refinement of the models

Using a local geometry check (PROTABLE, implemented in Sybyl 7.1), all side chain conformations were inspected and, if necessary, corrected to achieve proper chirality and to avoid steric hindrance. Generally, the ionic states of basic (Arg, Lys) and acidic (Glu, Asp) residues was applied. As an exception, Asp-64(2.50) in TM2 was set to the uncharged form to account for the predicted H-bond network (Teller et al., 2001). The receptor model was energy-minimized with the Amber 7.0 force field using Amber charges and a dielectric constant of 4. In the first minimization steps, the positions of all backbone atoms of the TM domains and H8 were fixed. Conserved H-bond and ionic interactions between distinct residues (Table 4.2) and between water molecules and residues were enforced by application of distance restraints using a force constant of 100 kcal mol<sup>-1</sup> Å<sup>-2</sup>. In that way, the backbones of loops and terminal regions as well as amino acid side chains were allowed to relax during energy minimization. An initial minimization was performed using the steepest descent method followed by a second minimization by the Powell method. During subsequent steps, all protein atoms were allowed to move and constraints were successively released. In the final minimization, the protein was allowed to relax without constraints down to an RMS gradient of less than 0.05 kcal mol<sup>-1</sup> Å<sup>-1</sup>.

### 4.2.4 Docking of H<sub>2</sub>R agonists

Previous 3D-QSAR data obtained by CoMFA (Dove and Buschauer, 1999) and results from site-directed mutagenesis (Kelley et al., 2001) were considered on manually docking ARP and UR-PG136 (Figure 4.2) into the binding sites of the gpH<sub>2</sub>R and the hH<sub>2</sub>R (DOCK, implemented in Sybyl 7.1). Attempts of docking the ligands into the ligand-free receptor models failed due to steric clashes with the backbone of e2. Thus the conformation of e2 was carefully rearranged. Amber 7.0 atom types and Gasteiger-Hückel charges were assigned to the agonists. Missing Amber 7.0 parameters were derived by analogy with the Tripos force field. The ligand-receptor complexes were energy-minimized with the Amber 7.0 force field using Amber charges and a dielectric constant of 4. In the first minimization steps, the

positions of all backbone atoms of the TM domains and H8 were fixed. In addition to the distance constraints applied on the ligand-free receptor models, a force constant of 100 kcal mol<sup>-1</sup> Å<sup>-2</sup> was applied to enforce an interaction of the imidazolylpropyl moiety of ARP and UR-PG136, respectively, with Asp-98(3.32), Tyr-182(5.38), and Asp-186(5.42). An initial minimization was performed using the steepest descent method followed by a second minimization by the Powell method. During subsequent minimization steps, all protein atoms were allowed to move and constraints were successively released until an RMS gradient of less than 0.05 kcal mol<sup>-1</sup> Å<sup>-1</sup> was achieved.

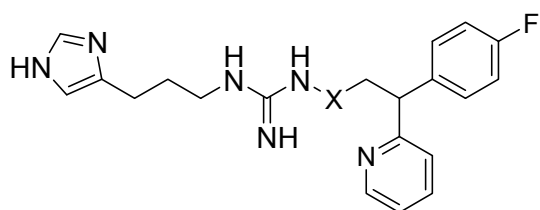


**Figure 4.2:** Structures of ARP and its N<sup>6</sup>-acylated analogue UR-PG136.

	<b>X</b>
arpromidine (ARP)	CH <sub>2</sub>
UR-PG136	CO

#### 4.2.5 Preparation of compound databases

The CStar 2004 (<http://www.chemstar.ru>; ChemStar, Ltd.), the ambinter (<http://www.ambinter.com>; Ambinter SARL, Paris, France), and the LeadQuest (<http://leadquest.com>; Tripos Inc., St. Louis, MA, USA) 2D libraries of commercially available compounds, and the ibscreen (<http://www.ibscreen.com>; InterBioScreen) 2D chemical library for screening programs were pre-processed to remove salts, metals, and isotopes by use of the ChemFinder Pro 6.0 software (CambridgeSoft, Cambridge, MA, USA). To generate a compound fragment library a molecular weight filter of MW ≤ 250 g mol<sup>-1</sup> was applied. To eliminate multiple entries, the libraries were subsequently combined to a unified database with 26051 records. 2D structures were converted into 3D by use of the CORINA software (<http://www.mol-net.de>; Molecular Networks GmbH, Erlangen, Germany). Here, small fragments such as counter-ions in salts and solvent molecules were removed. Existing stereoisomers (up to six) were generated. Nitrogen inversion was allowed to consider multiple ring conformations. In this way, 6544 isomers were added. The resulting database with 32589 entries was prepared with the LUDI module GENFRA (Böhm, 1992, 1993) for applicability of the LUDI virtual screening software package (Accelrys Inc., San Diego, USA). A link library was generated with link sites at methyl atoms to connect the fragments in the database with a reference ligand docked into the hH<sub>2</sub>R homology model during the LUDI run.

### 4.2.6 Application of the LUDI software for virtual screening

For virtual screening approaches, the hH<sub>2</sub>R homology model in complex with UR-PG136 was used as starting structure. A link mode was applied to search for small molecule fragments using our fragment library (chapter 4.2.5) and a fragment library provided by Accelrys. The 4-F-phenyl group of docked UR-PG136 was deleted to generate a link-site at the methylene group in position 3 of the *N*<sup>G</sup>-3-(2-pyridyl)propanoyl chain. In another approach, the 4-F-phenyl(2-pyridyl)methyl group of UR-PG136 was deleted to generate a link-site at the terminal methyl group of the *N*<sup>G</sup>-ethanoyl chain. The LUDI routine then linked appropriate molecule fragments from the databases to these sites. A sphere of 8 Å radius was defined around the link atom in the binding site of the hH<sub>2</sub>R. The values of the most important LUDI parameters were as follows: the maximal RMS distance of the fit between the fragment and the interaction site was 0.8 Å, the number of lipophilic and polar interaction sites was set to 25, and the maximal alignment angle formed by a bond in the fragment and the C-H bond that defines the link site in the partially built molecule was 14°. New conformations for the library fragments were generated by simultaneously altering two rotatable bonds in a molecule. For the remaining parameters default values were applied.

## 4.3 Results

### 4.3.1 Characterization of three-dimensional homology models of hH<sub>2</sub>R and gpH<sub>2</sub>R

#### 4.3.1.1 Analysis of the stereochemical quality

The stereochemical qualities of the hH<sub>2</sub>R and gpH<sub>2</sub>R homology models (Figure 4.3 A) were analyzed using the PROCHECK software (Laskowski et al., 1993). A summary of this analysis is listed in Table 4.1. In both models, more than 80% of the backbone  $\phi$ - and  $\psi$ -angles coincide with the most favoured regions as illustrated in the corresponding Ramachandran plots (Figure 4.3 B). All of the analysis parameters shown are within the expected limitations and represent a proper stereochemical quality of both receptor models.

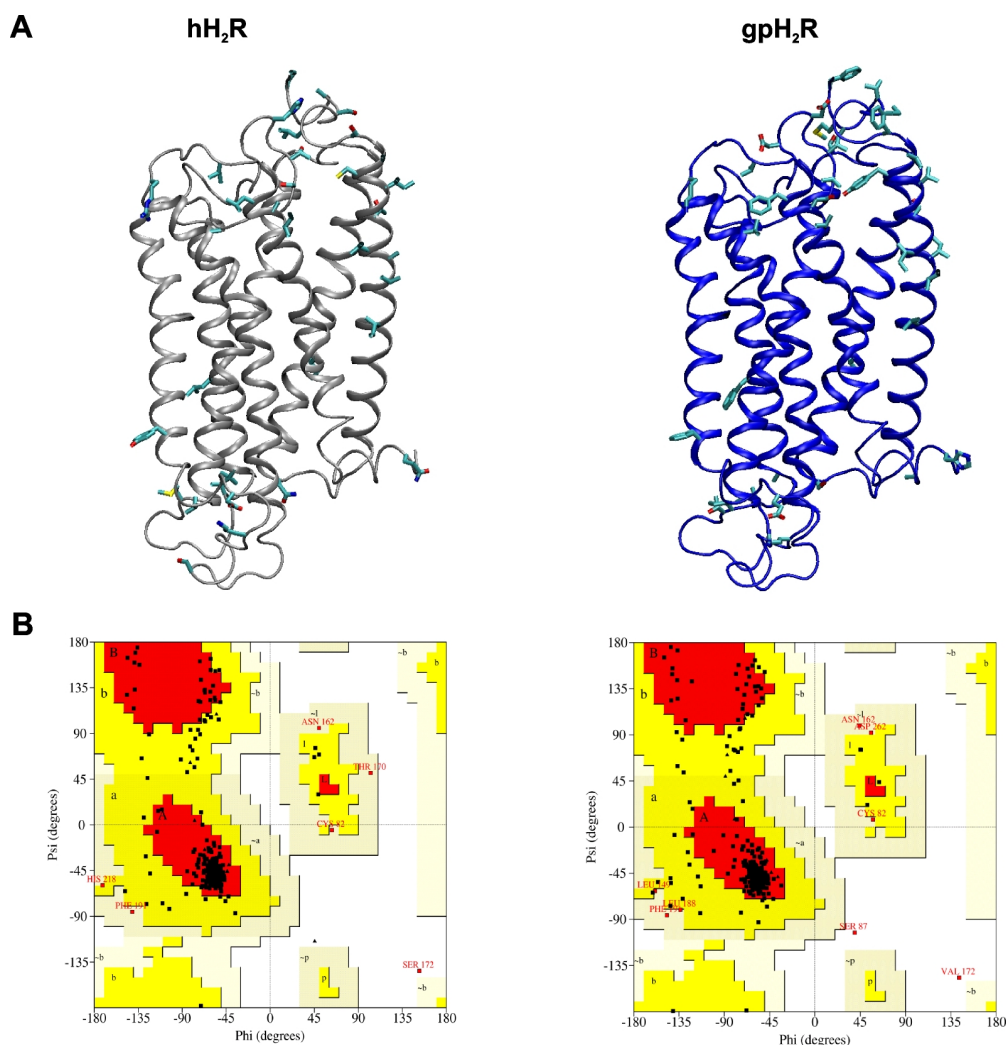


**Figure 4.3:** A, Side view of the secondary structures of the hH<sub>2</sub>R and gpH<sub>2</sub>R models. The side chains of residues differing in the sequences of both species-isoforms are shown in stick representation; B, Ramachandran plots of hH<sub>2</sub>R (left hand side) and gpH<sub>2</sub>R (right hand side) models showing the distribution of  $\phi$ - and  $\psi$ - torsion angles of amino acids. Glycines are shown as triangles and all remaining residues except prolines are shown as squares. Red fields, most favoured regions; yellow fields, additional allowed regions; grey fields, generously allowed regions; white fields, disallowed regions. A and a,  $\alpha$ -helix; B and b,  $\beta$ -strand; L and l, left-hand  $\alpha$ -helix; p, allowed  $\epsilon$ .

**Table 4.1:** PROCHECK analysis of the hH<sub>2</sub>R and gpH<sub>2</sub>R homology models.

Parameter	hH <sub>2</sub> R	gpH <sub>2</sub> R
Residues in most favored regions (A, B, L)	233 (83.5%)	228 (80.8%)
Residues in additional allowed regions (a, b, l, p)	40 (14.3%)	46 (16.4%)
Residues in generously allowed regions ( $\sim$ a, $\sim$ b, $\sim$ l, $\sim$ p)	5 (1.8%)	6 (2.1%)
Residues in disallowed regions	1 (0.4%)	2 (0.7%)
Bad contacts	0	0
Main chain bond length within limits (%)	100	100
Main chain bond angles within limits (%)	87.8	85.8
Planar groups within limits	96.6	94.7



#### 4.3.1.2 Conserved intramolecular interactions in rhodopsin and the H<sub>2</sub>R

The crystal structure of bovine rhodopsin contains a number of interhelical contacts that are assumed to be conserved among class 1 GPCRs (Filipek et al., 2003; Okada et al., 2001; Mirzadegan et al., 2003; Palczewski, 2006). Such conserved interactions are predicted to confer stability to the TM domains and presumably play a functional role in receptor activity. For the generation of the H<sub>2</sub>R models, some of these interactions were constrained during energy minimization. Conserved intramolecular interactions were analyzed by calculating the distances between the respective residues in the generated models (Table 4.2). Okada et al. proposed conserved interhelical contacts to be mediated by a few water molecules buried in the TM bundle (Okada et al., 2002). Therefore, five of these functional water molecules were transferred from rhodopsin to the new H<sub>2</sub>R models. A schematic representation of the resulting network of water-mediated H-bonds is shown in Figure 4.4. A cluster of the water molecules Wat1a, Wat1b, and Wat1c (names of water molecules match those of corresponding water molecules in the crystal structure of bovine rhodopsin (Okada et al., 2002)) connected residues in TM2 and TM3, TM2 and TM7, and TM6 and TM7. TM6 and TM7 were additionally linked via Wat3, and Wat4 was predicted to link TM1 and TM2.

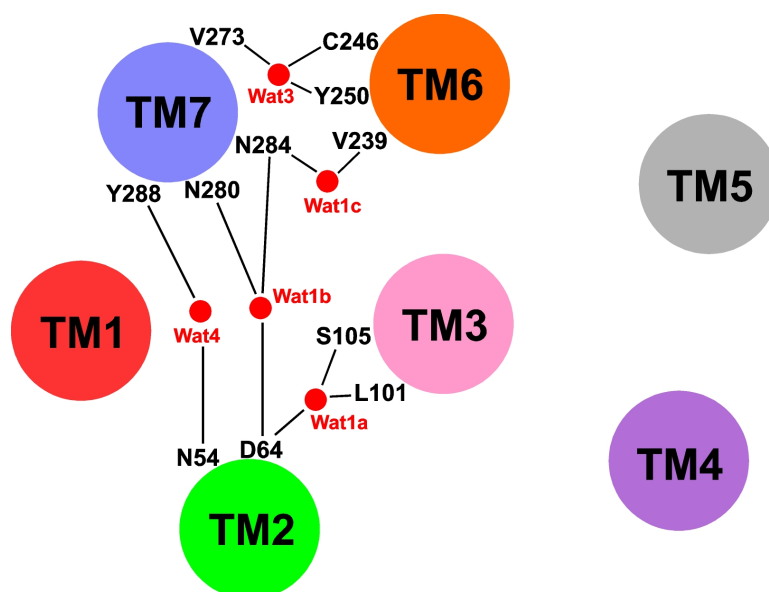


**Figure 4.4:** Schematic representation of water-mediated H-bonds in hH<sub>2</sub>R and gpH<sub>2</sub>R. The names of water molecules match those of corresponding water molecules in the crystal structure of bovine rhodopsin (Okada et al., 2002).

In inactive GPCR conformations, Arg(3.50) of the highly conserved (E/D)RY motif at the intracellular end of TM3 was predicted to form ionic interactions with adjacent

Glu(3.49)/Asp(3.49) and with Glu(6.30) at the intracellular end of TM6 (Ballesteros et al., 2001b). This network of interactions was proposed to be disrupted upon GPCR activation, ultimately leading to an anticlockwise rotation when viewed from the extracellular side and outward movement of TM6 (Visiers et al., 2002; Hubbell et al., 2003). H<sub>2</sub>R mutations of Arg-116(3.50) gave rise to a highly instable receptor with increased constitutive activity, suggesting that disruption of interactions in the (E/D)RY motif leads to the formation of active, but instable receptor conformations (Alewijse et al., 2000). In the H<sub>2</sub>R models, ionic interactions between Asp-115(3.49), Arg-116(3.50), and Glu-229(6.30) were established. Additional ionic interactions were formed between Glu-229(6.30) and the non-conserved Arg-228(6.29) as well as between Arg-228(6.29) and Asp-294(7.59) (Figure 4.5 A).

**Table 4.2:** Conserved intramolecular interactions in the hH<sub>2</sub>R and gpH<sub>2</sub>R models.

Domain	Residues	Type <sup>a</sup>	Min. distance (Å) <sup>b</sup>	
			hH <sub>2</sub> R	gpH <sub>2</sub> R
TM1	N36(1.50) - T32(1.46)	h	2.90*	2.91*
TM1-TM2	N36(1.50) - D64(2.50)	h	2.83*	2.84*
TM1-TM7	N36(1.50) - S281(7.46)	h	3.03	2.97
TM2	I57(2.43) - L60(2.46)	vdW	4.83	4.55
TM2-TM6	I57(2.43) - V239(6.40)	vdW	6.80	7.19
TM2-TM4	S59(2.45) - W143(4.50)	h	3.03	3.06
TM3-TM7	Y94(3.28) - Y278(7.43)	h	3.18	3.31
TM3	L109(3.43) - I112(3.46)	vdW	4.70	4.33
TM3-TM6	L109(3.43) - V239(6.40)	vdW	4.16	3.97
TM3	D115(3.49) - R116(3.50)	i	3.04*	3.09*
TM3-TM6	R116(3.50) - E229(6.30)	i	2.91*	2.92*
TM7-H8	Y288(7.53) - F295(7.60)	ar	3.47	3.87
TM7-H8	A289(7.54) - R296(7.61)	h	3.00	3.01
TM7-H8	A290(7.55) - R296(7.61)	h	2.93	3.32

<sup>a</sup> type of interactions; h, H-bond; i, ionic interaction; vdW, van der Waals interaction; ar, aromatic interaction

<sup>b</sup> Distance between the nearest heavy atoms of interacting residues

\* Distances between residues were constrained during energy-minimization (chapter 4.2.3).

TM1 and TM2 strongly interacted via the highly conserved residues Asn-36(1.50) and Asp-64(2.50) (Figure 4.5 B). N<sub>δ2</sub>-H of Asn-36(1.50) additionally formed H-bonds with the backbone oxygens of Thr-32(1.46) and Ser-281(7.46) similar to corresponding interactions in bovine rhodopsin (Pardo et al., 2007; Bissantz, 2003). Asp-64(2.50) interacted via Wat1b with the backbone-O of Asn-280(7.45) and with the backbone-NH of Asn-284(7.49) thus

linking TM2 and TM7. Asn-284(7.49) is a member of the highly conserved NPxxY(x)<sub>5,6</sub>F motif and was previously shown to play a critical role in receptor activation (Govaerts et al., 2001; Urizar et al., 2005). In the inactive state, the side chain of this residue is predicted to point towards TM6 (Pardo et al., 2007) which is in agreement with the Wat1c-mediated H-bond to Val-239(6.40) in the H<sub>2</sub>R models. Upon receptor activation, Asn-284(7.49) is predicted to adopt a different conformation then interacting with Asp-64(2.50) (chapter 5.3.2.3). Tyr-288(7.53) and Phe-295(7.60) are also part of the NPxxY(x)<sub>5,6</sub>F motif and are suggested to form an aromatic interaction in the inactive state of rhodopsin. Upon transition to meta I/meta II this interaction is proposed to be disrupted (Fritze et al., 2003). In the H<sub>2</sub>R models both residues were in spatial proximity. Additionally, the hydroxyl group of Tyr-288(7.53) interacted with the conserved Asn-54(2.40) via Wat4 thus linking the cytoplasmic ends of TM2 and TM7.

The CWxP(F/Y) motif in TM6 is another functionally important microdomain in class 1 GPCRs. The structure of metarhodopsin I was recently determined by electron crystallography (Ruprecht et al., 2004) showing that Trp(6.48) undergoes a conformational transition from pointing towards TM7 in the inactive state to pointing towards TM5 in an active conformation. The orientation of Trp(6.48) in the inactive state of the H<sub>1</sub>R was predicted to be determined by an interaction with the conserved Asn(7.45) (Jongejan et al., 2005). In the H<sub>2</sub>R models, the side chain of Trp-247(6.48) was directed towards TM7 although a direct interaction with Asn-280(7.45) was not observed (Figure 4.5 C). However, since the side chain of Asn-280(7.45) was allowed to rotate around the  $\chi_1$ -angle a corresponding interaction would be possible. In agreement with the crystal structure of rhodopsin, Wat3 mediated H-bond interactions of Tyr-250(6.51) and Cys-246(6.47) with the backbone oxygen of Val-273(7.38). These interactions presumably stabilize the exceptionally sharp Pro-kink (triggered by the highly conserved Pro-249(6.50)) of 35° in TM6 (Pardo et al., 2007). Wat1a mediated an interaction of the carboxylate group of Asp-64(2.50) with the backbone-O of Leu-101(3.35). In the H<sub>2</sub>R models, the hydroxyl group of Ser-105(3.39) participated in this H-bond network. Previously it was proposed that Ser(3.39) or Thr(3.39) could contribute to a sodium binding site in rhodopsin-like GPCRs (Okada et al., 2002; Neve et al., 2001).

Another network of conserved interhelical interactions in rhodopsin is constituted by Asn(2.45), Ser(3.42), Thr(4.49), and Trp(4.50) (Palczewski et al., 2000). In the H<sub>2</sub>R, the OH oxygen of Ser-59(2.45) interacted with the conserved Trp-143(4.50) thus linking TM2 and TM4 (Figure 4.5 D). By analogy to H-bond interactions between the conserved Arg(7.61) in H8 and the backbone oxygens of Ile(7.54) and Met(7.55) in rhodopsin (Teller et al., 2001), Arg-296(7.61) was identified to interact with Ala-289(7.54) and Ala-290(7.55) in the H<sub>2</sub>R models (Table 4.2). Glu(3.28) forms the counterion to the Schiff-base of retinal with

Lys(7.43). The corresponding H<sub>2</sub>R residues, Tyr-94(3.28) and Tyr-278(7.43), interacted via their side chain atoms. A large number of hydrophobic interhelical contacts exists in rhodopsin, mainly between TM1-TM2, TM2-TM7, TM3-TM4, TM5-TM6, TM6-TM7 (Filipek et al., 2003). Met (6.40) was identified to be surrounded by a Leu cluster including Leu(2.43), Leu(2.46), Leu(3.43), and Leu(3.46) (Okada et al., 2001). Mutation of Leu(3.43) resulted in increased constitutive activity in several GPCRs (Tao et al., 2000; Lu and Hulme, 1999), supporting a general function of hydrophobic interactions between these residues in maintaining the ground state of GPCRs (Okada et al., 2001). In agreement with these studies, the corresponding hydrophobic residues in the H<sub>2</sub>R models, Val-239(6.40), Ile-57(2.43), Leu-60(2.46), Leu-109(3.43), and Ile-112(3.46), were in close proximity to each other (Figure 4.5 D).

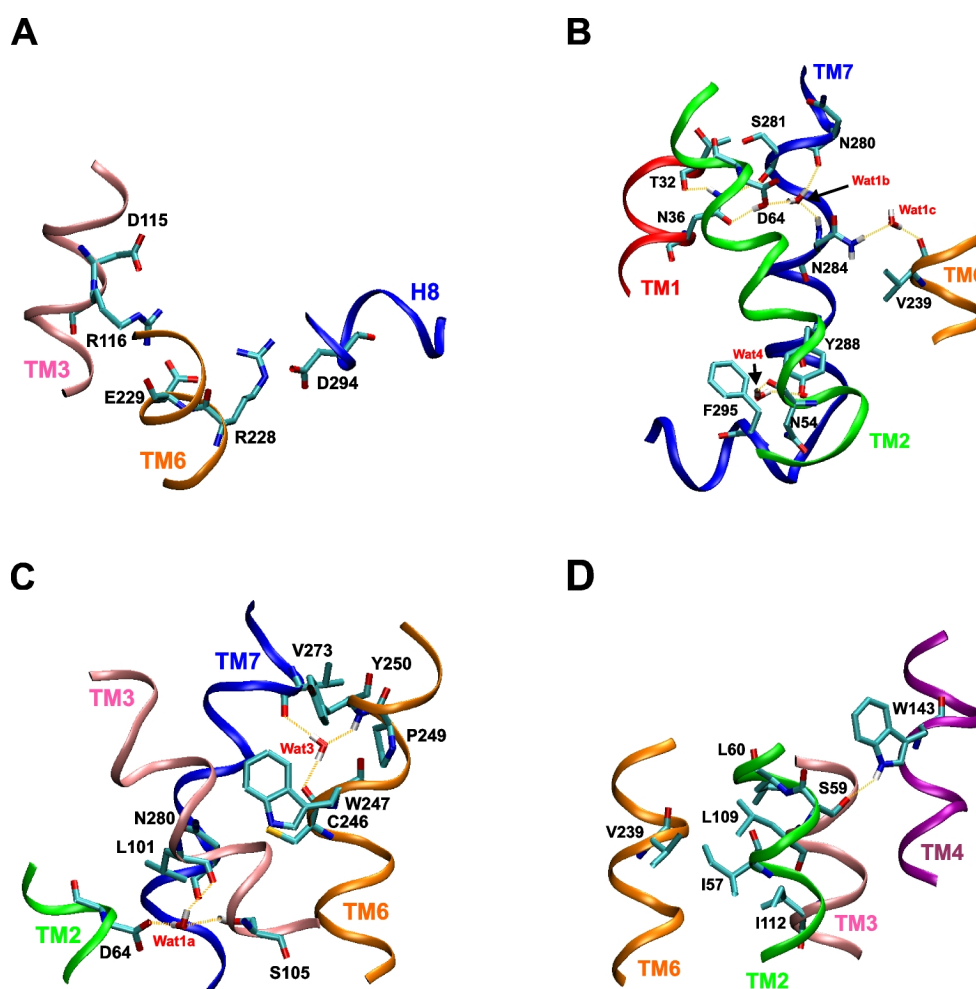


**Figure 4.5:** Conserved interactions in the hH<sub>2</sub>R. A, interactions of the (E/D)RY motif at the intracellular end of TM3; B, interactions of the NPxxY(x)<sub>5,6</sub>F motif in TM7; C, interactions of the CWxP(F/Y) motif in TM6; D, hydrophobic latch between residues in TM2, TM3, and TM6, and interaction between Ser-59(2.45) and Trp-143(4.50).

### 4.3.2 Analysis of the binding modes of imidazolypropylguanidines and *N*<sup>G</sup>-acylated derivatives with H<sub>2</sub>R species isoforms

#### 4.3.2.1 Similar binding modes of agonists at hH<sub>2</sub>R and gpH<sub>2</sub>R

ARP and its *N*<sup>G</sup>-acylated analogue UR-PG136 shared a similar binding mode in the H<sub>2</sub>R models (Figure 4.6), suggesting a common binding mechanism of the two compound classes.

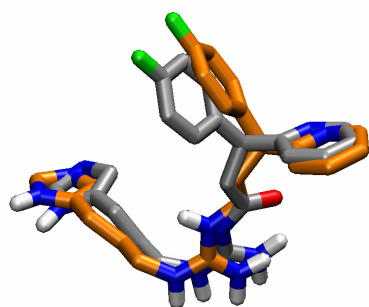


**Figure 4.6:** Conformations of ARP (carbon atoms in orange) and UR-PG136 (carbon atoms in grey) in the binding pocket of the H<sub>2</sub>R.

Most amino acids interacting with guanidine-type agonists are identical in hH<sub>2</sub>R and gpH<sub>2</sub>R species isoforms (Kelley et al., 2001). The complex of ARP in the binding site of the hH<sub>2</sub>R is shown in Figure 4.7. In guanidine-type H<sub>2</sub>R agonists, the common imidazolypropylguanidine moiety is proposed to mimic binding of HA (Dove et al., 2004). Accordingly, the strongly basic guanidino group of the compounds underwent an ionic interaction with the highly conserved Asp-98(3.32). The N<sup>π</sup>-H atom of the imidazole ring interacted with the carboxylate group of Asp-186(5.42), and the N<sup>τ</sup> atom accepted a proton from the hydroxyl group of Tyr-182(5.38) in TM5 which is in agreement with the established binding model of HA at the H<sub>2</sub>R (Nederkoorn et al., 1996a, b). Residues of the CWxP(F/Y) motif in TM6 probably participate in ligand binding and receptor activation in many class 1 GPCRs (Shi and Javitch, 2002). In agreement with these studies, Trp-247(6.48) and Tyr-250(6.51) faced the imidazolypropylguanidine moiety of ARP in the H<sub>2</sub>R model. Asn-293(6.55) in the β<sub>2</sub>AR (Wieland et al., 1996) and Phe-436(6.55) in the H<sub>1</sub>R (Wieland et al., 1999) have been suggested to interact with the β-OH group of epinephrine and with the imidazolyethyl group of HA, respectively. The corresponding residue in the H<sub>2</sub>R, Phe-254(6.55), was in close proximity to the imidazolypropyl moiety of ARP. The pyridyl ring of ARP was predicted to point into a “lower” binding region where bulk mainly decreases activity (Dove et al., 2004). In the hH<sub>2</sub>R model, the pyridyl moiety was surrounded by a cluster of aromatic and hydrophobic residues in TM2, TM3, and TM7. A conserved Trp(7.40) in TM7 should be involved in ligand-binding of the β<sub>1</sub>AR (Wong et al., 1988) and the 5-HT<sub>1A</sub> receptors (Roth et al., 1997).

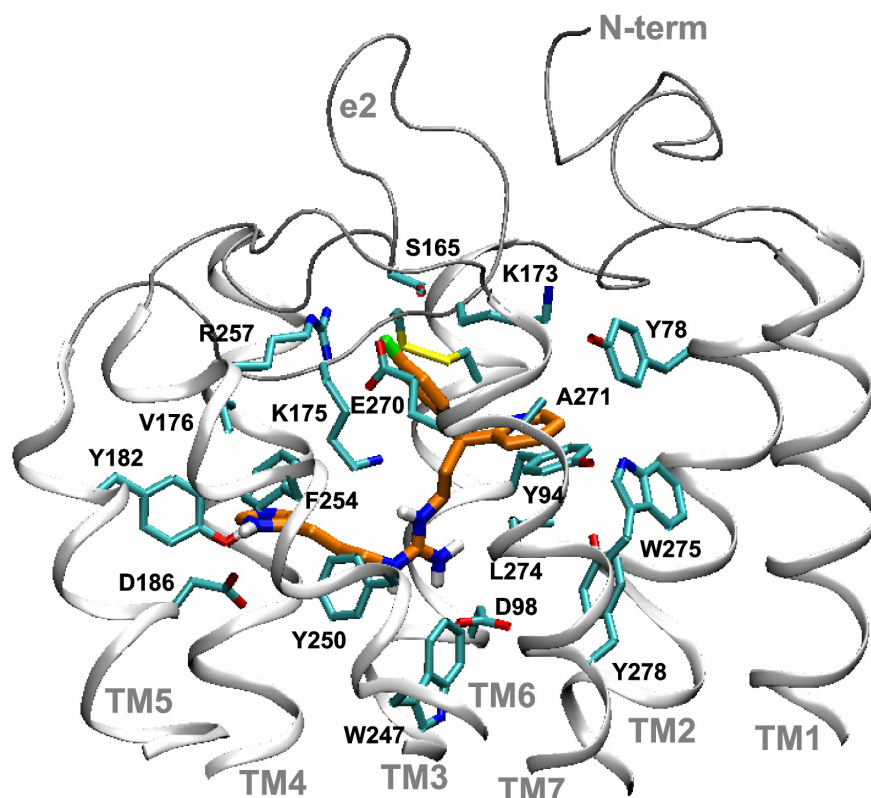


**Figure 4.7:** Side view of the hH<sub>2</sub>R model in complex with ARP. The putative agonist binding site and the extracellular components of the hH<sub>2</sub>R are shown. ARP (carbon atoms in orange) was manually docked into the putative binding pocket. Grey ribbon, transmembrane domains TM1-TM7; thin grey lines, extracellular loops e1, e2, and e3, and N-terminus (N-term). Amino acid side chains in a sphere of 3 Å radius around ARP are displayed.

In the M<sub>3</sub> muscarinic acetylcholine receptor (Wess et al., 1991), the dopamine D<sub>2</sub> receptor (Fu et al., 1996), and the 5-HT<sub>2A</sub> receptor (Roth et al., 1997), ligands may interact with a conserved Tyr(7.43). By analogy, the corresponding residues in the H<sub>2</sub>R, Trp-275(7.40) and Tyr-278(7.43), pointed towards the pyridyl moiety of ARP. In aminergic class 1 GPCRs, diverse residues in position 7.39 have shown to belong to the binding sites of ligands (Shi and Javitch, 2002). In agreement with these studies, Leu-274(7.39) was in close proximity to ARP in the hH<sub>2</sub>R model. Tyr-78(2.64) and Tyr-94(3.28) at the extracellular ends of TM2 and TM3, respectively, surrounded the pyridyl ring of ARP. Residues at corresponding positions have previously shown to interact with ligands of aminergic GPCRs (Shi and Javitch, 2002). The 4-F-phenyl group of ARP was proposed to point into a second “upper” binding region, where bulk may enhance agonist activity (Dove and Buschauer, 1999). Arg-257(6.58) at the extracellular end of TM6 was in an appropriate position to serve as H-bond donor for an interaction with the 4-F-phenyl group of ARP. Glu-270(7.35) close to the 4-F-phenyl group possibly participates in this network of interactions (Kelley et al., 2001; Dove et al., 2004). The backbone of e2 folded down between the extracellular ends of the TM domains and

formed a lid over the H<sub>2</sub>R binding pocket (Figure 4.7). The lower part of this loop contains Cys-174 forming a disulfide bond with Cys-91(3.25). The side chain of the adjacent Lys-175 pointed into a cavity close to the imidazolylpropylguanidine moiety of ARP suggesting participation of this residue in interaction with the ligand. The  $\epsilon$ -amino group of Lys-173 did not face ARP although the flexible alkyl chain would allow for an interaction with the 4-F-phenyl or the pyridyl ring. Ser-165 in e2 also covered the ARP binding pocket and furthermore interacted with Glu-270(7.35).

#### 4.3.2.2 *Distinct interactions of guanidine-type agonists with hH<sub>2</sub>R and gpH<sub>2</sub>R species isoforms*

In Figure 4.8, the ARP-bound hH<sub>2</sub>R and gpH<sub>2</sub>R models are shown in a superimposed form. The positions of backbone atoms and side chain orientations were very similar in both receptor models, as RMSD values of 0.86 Å and 1.31 Å were calculated for all C $\alpha$ -atoms and all protein atoms, respectively. In agreement with a previous 3D model of the seven TM domains of the gpH<sub>2</sub>R (Kelley et al., 2001), an interaction between Tyr-17(1.31) and Asp-271(7.36) at the extracellular ends of TM1 and TM7, respectively, was selectively formed in the gpH<sub>2</sub>R model. In the model of the human receptor a corresponding interhelical interaction was absent due to the presence of Cys-17(1.31) and Ala-271(7.36). The gpH<sub>2</sub>R model further suggested interactions of Asp-271(7.36) with Trp-275(7.40) and with the amino group of Lys-173 in e2. Strikingly, this species-selective network of interactions was also observed in the ligand-free gpH<sub>2</sub>R model (not shown), suggesting a ligand-independent stabilization of an active gpH<sub>2</sub>R conformation. To test this hypothesis, an hH<sub>2</sub>R double mutation with Cys-17(1.31)→Tyr-17(1.31) and Ala-271(7.36)→Asp-271(7.36) exchanges was generated and pharmacologically characterized (chapter 8).



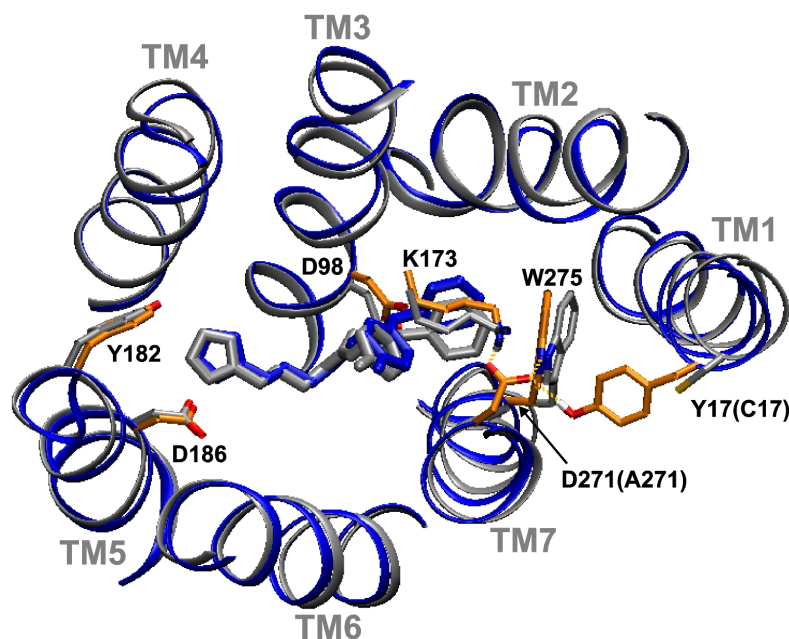


**Figure 4.8:** Top-view from the extracellular side of the superimposed ARP-bound hH<sub>2</sub>R and gpH<sub>2</sub>R models. The secondary structures of hH<sub>2</sub>R and gpH<sub>2</sub>R are shown as grey and blue ribbons, respectively. For reasons of clarity, loop regions are not shown. In the hH<sub>2</sub>R model, residue side chains and ARP are coloured in grey. In the gpH<sub>2</sub>R model, residue side chains are coloured in orange, and docked ARP is shown in blue. For residues differing in both species isoforms, the gpH<sub>2</sub>R residue name is given first, followed by the corresponding hH<sub>2</sub>R name (in brackets).

#### 4.3.2.3 Impact of the alkyl chain length on species-selective interactions

The possibly more open and flexible pocket around Ala-271(7.36) in hH<sub>2</sub>R may explain the inverse impact of the chain length between the guanidino and the phenyl group in the *N*<sup>G</sup>-(phenylalkanoyl)guanidines UR-AK67 and UR-AK22 (Table 4.3) on the activity in the steady-state GTPase assay at hH<sub>2</sub>R-G<sub>saS</sub> and gpH<sub>2</sub>R-G<sub>saS</sub> fusion proteins. Elongation of the alkyl chain in UR-AK67 by one methylene unit reduced the potency at gpH<sub>2</sub>R-G<sub>saS</sub> by ~3-fold, while both compounds were similarly potent at hH<sub>2</sub>R-G<sub>saS</sub>. An analogous tendency was observed with the *N*<sup>G</sup>-[3-phenyl-3-(2-pyridyl)propyl]guanidine moiety in BU-E-42 and the homologous *N*<sup>G</sup>-[4-phenyl-4-(2-pyridyl)butyl]guanidine portion in BU-E-43. Agonist potency was approximately 3-fold decreased at gpH<sub>2</sub>R-G<sub>saS</sub> upon elongation of the alkyl chain but slightly increased at hH<sub>2</sub>R-G<sub>saS</sub>. According to previous CoMFA studies (Dove and Buschauer, 1999), the unbranched alkyl side chain of the guanidines was suggested to interact with the “lower” pyridyl binding site close to amino acid position 271. In the model of the hH<sub>2</sub>R the flexible pocket around Ala-271(7.36) and Cys-17(1.31) should allow the accommodation of a longer alkyl chain than in the gpH<sub>2</sub>R where the proposed interaction between Asp-271(7.36) and Tyr-17(1.31) limits the accessible receptor volume. In agreement with this hypothesis, at



an Ala-271(7.36)→Asp-271(7.36) mutant of the hH<sub>2</sub>R-G<sub>saS</sub>, BU-E-43 was about 4-fold less potent than BU-E-42 (BU-E-42: EC<sub>50</sub> = 80 ± 10 nM; BU-E-43: EC<sub>50</sub> = 280 ± 40 nM) (Kelley et al., 2001).

**Table 4.3:** Structures of guanidine-type agonists with variable chain lengths and agonist potencies at H<sub>2</sub>R-G<sub>saS</sub> species isoforms derived from the GTPase activity assay.

Cpd.	X	Y	R <sup>1</sup>	R <sup>2</sup>	hH <sub>2</sub> R-G <sub>saS</sub>	gpH <sub>2</sub> R-G <sub>saS</sub>
					EC <sub>50</sub> (nM)	
UR-AK67	CO	(CH <sub>2</sub> ) <sub>2</sub>	phenyl	-	67 ± 9 <sup>a</sup>	21 ± 2 <sup>a</sup>
UR-AK22	CO	(CH <sub>2</sub> ) <sub>3</sub>	phenyl	-	72 ± 23 <sup>a</sup>	56 ± 5 <sup>a</sup>
BU-E-42	CH <sub>2</sub>	CH <sub>2</sub>	phenyl	2-pyridyl	420 ± 70 <sup>b</sup>	70 ± 20 <sup>b</sup>
BU-E-43	CH <sub>2</sub>	(CH <sub>2</sub> ) <sub>2</sub>	phenyl	2-pyridyl	280 ± 70 <sup>b</sup>	190 ± 60 <sup>b</sup>

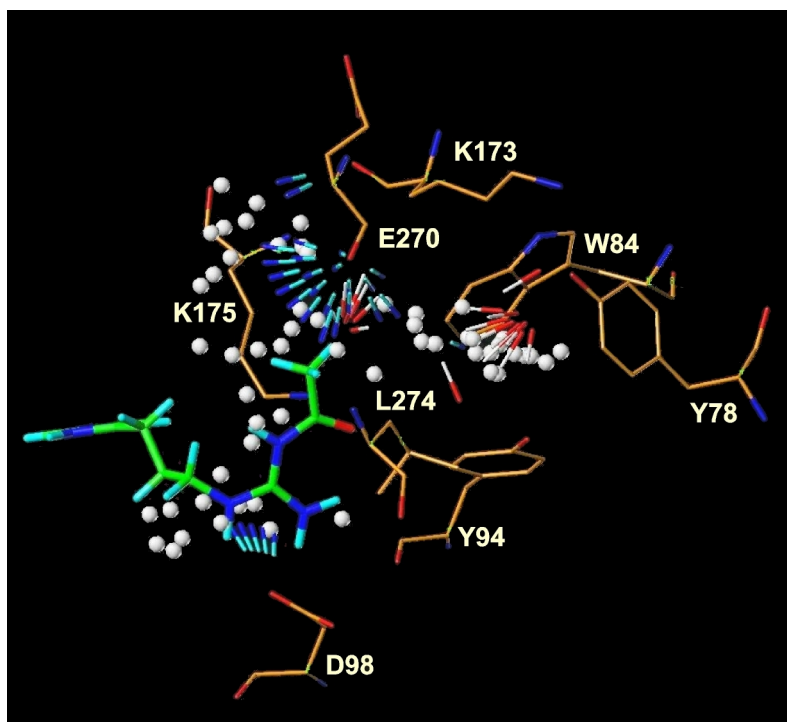
<sup>a</sup> Data were taken from Xie et al., 2006.

<sup>b</sup> Data were taken from Kelley et al., 2001.

### 4.3.3 Virtual screening for potent and selective acylguanidine-type hH<sub>2</sub>R agonists

To guide the synthesis of *N*<sup>G</sup>-acylated imidazolylpropylguanidines towards more potent and hH<sub>2</sub>R-selective derivatives, a structure based virtual screening was performed using the LUDI program. Since potencies and selectivities of guanidine-type agonists are mainly determined by structural variations at the *N*<sup>G</sup>-mono- or -diaryl-alkanoyl side chains, the purpose of the approach was to identify appropriate substituents for this substructure while leaving the *N*-[3-(1*H*-imidazol-4-yl)propyl]guanidine moiety unchanged (Figure 4.9).

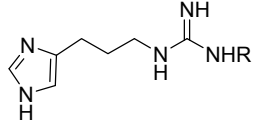
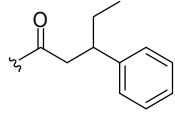
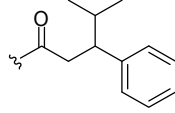
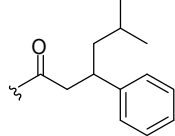
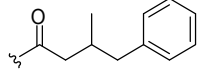
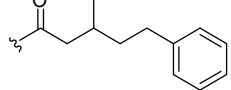
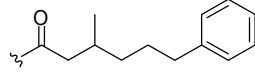
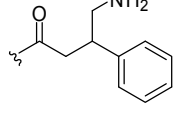
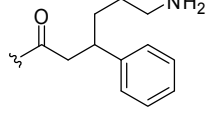
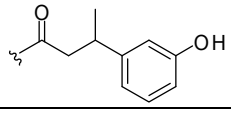
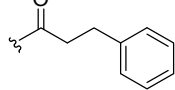
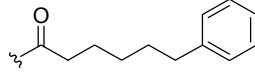
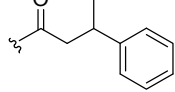
LUDI calculations generated 91 hits of which fragments were selected by means of synthetical feasibility and chemical stability. Fragments of already known agonists were rejected. Finally, nine compounds have been selected for synthesis and pharmacological characterization (Table 4.4). Compounds **1-6** represent *N*-[3-(1*H*-imidazol-4-yl)propyl]-*N*<sup>G</sup>-(phenylalkanoyl)guanidines with an alkyl branch at position 3 of the phenylalkanoyl chain. In the hH<sub>2</sub>R model, this alkanoyl side chain is flanked by the backbones of e2 and TM7 and the side chains of Lys-175 and Glu-270(7.35). In the steady-state GTPase activity assay at hH<sub>2</sub>R-G<sub>saS</sub>, the ethyl- (**1**), isopropyl- (**2**), and isobutyl- (**3**) substituted agonists were more potent than the unbranched analogue **10** (Table 4.4).



**Figure 4.9:** Interaction sites inside the binding pocket of the hH<sub>2</sub>R model generated by LUDI. White spheres, lipophilic interaction sites; red, H-bond acceptors; blue, H-bond donors. After UR-PG136 was docked into the hH<sub>2</sub>R binding site, the (4-F-phenyl-2-pyridyl)methyl group was deleted to generate a link-site for a virtual screening for appropriate fragments (chapter 4.2.6).

Whereas the three alkyl-branched compounds were similarly potent at the human receptor, the efficacy of the bulkiest compound **3** was reduced. At gpH<sub>2</sub>R-G<sub>saS</sub>, the unsubstituted compound **10** was about 4-fold more potent than at hH<sub>2</sub>R-G<sub>saS</sub>. The potency differences between the species isoforms tended to be reduced in the cases of the 3-alkyl substituted derivatives **1-3**. In compounds **4**, **5**, and **6**, the alkanoyl spacer between the phenyl ring and the guanidine group was successively increased. At both H<sub>2</sub>R species isoforms 3-methyl substitution in compounds **4** and **5** yielded a slight potency increase when compared with the corresponding unbranched compounds UR-AK67 and UR-AK22 (Table 4.3), respectively. However, with the maximal chain length of five C atoms between the phenyl and the carbonyl moieties, the unbranched compound **11** was ~5-fold more potent at hH<sub>2</sub>R-G<sub>saS</sub> than its 3-methyl branched analogue **6**. The potencies of compounds **4**, **5**, and **6** were only slightly increased at the guinea pig compared to the human H<sub>2</sub>R. Compounds **7** and **8** contain primary amine functions which were suggested to interact with the carboxylate group of Glu-270(7.35). In addition, the amino group was thought to be an appropriate linker atom for fluorescence labelling. Introduction of this function, however, yielded a considerable loss in potency at hH<sub>2</sub>R-G<sub>saS</sub> (increased EC<sub>50</sub> values of compounds **7** and **8** compared to the EC<sub>50</sub> value of compound **1**). Both compounds **7** and **8** were about 8-fold more potent at

**Table 4.4:** Efficacies ( $E_{\text{Max}}$ ) and potencies of  $N^G$ -acylated imidazolylpropylguanidines, predicted by virtual screening (**1-9**), and reference compounds (**10-12**), at hH<sub>2</sub>R-G<sub>saS</sub> and gpH<sub>2</sub>R-G<sub>saS</sub> in the GTPase activity assay. Data shown are the means  $\pm$  S.D. of two experiments performed in duplicates.

Cpd.		hH <sub>2</sub> R-G <sub>saS</sub>		gpH <sub>2</sub> R-G <sub>saS</sub>	
		$E_{\text{Max}}^a$	EC <sub>50</sub> (nM)	$E_{\text{Max}}^a$	EC <sub>50</sub> (nM)
HA		1.00	990 $\pm$ 92	1.00	850 $\pm$ 340
	<b>R<sup>b</sup></b>				
<b>1</b>		0.64 $\pm$ 0.25	37 $\pm$ 29	0.78 $\pm$ 0.11	11 $\pm$ 6
<b>2</b>		0.72	33 $\pm$ 3	0.72 $\pm$ 0.11	30 $\pm$ 4
<b>3</b>		0.30 $\pm$ 0.06	24 $\pm$ 5	0.72 $\pm$ 0.11	13 $\pm$ 11
<b>4</b>		0.55 $\pm$ 0.03	27 $\pm$ 7	0.86 $\pm$ 0.08	10 $\pm$ 2
<b>5</b>		0.49 $\pm$ 0.24	50 $\pm$ 64	0.59 $\pm$ 0.19	23 $\pm$ 12
<b>6</b>		0.31 $\pm$ 0.02	30 $\pm$ 23	0.58 $\pm$ 0.14	13 $\pm$ 4
<b>7</b>		0.62 $\pm$ 0.06	750 $\pm$ 420	0.82 $\pm$ 0.04	102 $\pm$ 65
<b>8</b>		0.68 $\pm$ 0.01	170 $\pm$ 81	0.89 $\pm$ 0.08	21 $\pm$ 8
<b>9</b>		0.82 $\pm$ 0.13	47 $\pm$ 41	0.97 $\pm$ 0.01	4 $\pm$ 1
<b>10<sup>c</sup></b>		0.84 $\pm$ 0.03	100 $\pm$ 16	1.05 $\pm$ 0.11	23 $\pm$ 1
<b>11</b>		0.44 $\pm$ 0.22	6 $\pm$ 1	0.42 $\pm$ 0.10	19 $\pm$ 14
<b>12<sup>c</sup></b>		0.87 $\pm$ 0.01	67 $\pm$ 2	1.03 $\pm$ 0.06	12 $\pm$ 1

<sup>a</sup> Efficacy relative to HA (= 1.00)

<sup>b</sup> All compounds were synthesized and pharmacologically characterized by Anja Kraus (Dept. of Med./Pharm. Chemistry II, University of Regensburg) and will be part of her doctoral thesis.

<sup>c</sup> Data were taken from Xie et al., 2006.

gpH<sub>2</sub>R-G<sub>saS</sub> than at hH<sub>2</sub>R-G<sub>saS</sub>. Compounds **1-8** were partial agonists at hH<sub>2</sub>R-G<sub>saS</sub> and gpH<sub>2</sub>R-G<sub>saS</sub> with increased efficacies at gpH<sub>2</sub>R-G<sub>saS</sub> compared to hH<sub>2</sub>R-G<sub>saS</sub>. In compound **9**, a hydroxyl group in *m*-position of the aromatic ring was suggested to interact with the backbone carbonyl group of Lys-173 in e2. At hH<sub>2</sub>R-G<sub>saS</sub> the potency of this compound was not increased compared to its non-hydroxylated analogue **12**. At gpH<sub>2</sub>R-G<sub>saS</sub> however, this compound was ~3-fold more potent than **12** and ~12-fold more potent than at hH<sub>2</sub>R-G<sub>saS</sub>. In this series, compound **9** was the only full agonist at gpH<sub>2</sub>R-G<sub>saS</sub> exhibiting only partial agonism at the human species isoform.

Taken together, introduction of ethyl-, isopropyl-, and isobutyl substituents at position 3 of the 3-phenylpropanoyl chain increased the potencies at hH<sub>2</sub>R-G<sub>saS</sub> vs. gpH<sub>2</sub>R-G<sub>saS</sub> whereas the polar substituents in compounds **7-9** strongly enhanced gpH<sub>2</sub>R-G<sub>saS</sub> selectivity. These results further support the hypothesis of a network of ionic and/or H-bond interactions of Asp-271(7.36) with Tyr-17(1.31), Trp-275(7.40), and Lys-173. A positively charged amino group or an H-bond donor may directly or indirectly participate in this network, whereas due to a more hydrophobic binding pocket interactions with aliphatic substituents are preferred in the case of the hH<sub>2</sub>R.

## 4.4 Discussion

Three-dimensional homology models of hH<sub>2</sub>R and gpH<sub>2</sub>R were generated using the crystal structure of bovine rhodopsin as template. Five water molecules predicted to play a functional role for the stabilization of interhelical contacts in class 1 GPCRs (Okada et al., 2002) were transferred to the receptor models. In the generated models conserved intramolecular interactions were formed according to present concepts of GPCR structure and function. At the intracellular end of TM6, Glu-229(6.30) formed a network of ionic interactions with residues of the conserved (E/D)RY motif in TM3 which is proposed to stabilize the inactive state of GPCRs (Bissantz, 2003). Glu-229(6.30) additionally interacted with the consecutive residue Arg-228(6.29), and the model further proposed an interaction of Arg-228(6.29) with Asp-294(7.59) in H8. Strikingly, many class 1 GPCRs contain a basic residue at position 6.29, and a stabilizing role of this residue in the network of ionic interactions has been proposed (Ballesteros et al., 2001b). Since Arg-228(6.29) is not conserved among all H<sub>2</sub>R species isoforms (e.g. the canine H<sub>2</sub>R contains Gly-228(6.29)), the selective formation of this network of interactions may be responsible for differences in the constitutive activities between H<sub>2</sub>R species isoforms (chapter 7.4.1).

The receptor models were used to analyze the binding modes of *N*-[3-(1*H*-imidazol-4-yl)propyl]guanidines and their *N*<sup>G</sup>-acylated derivatives. Introduction of an electron-

withdrawing carbonyl group adjacent to the strongly basic guanidine moiety did not significantly change the pharmacological activities of most of these agonists rendering this structural modification as a bioisosteric exchange (Ghorai, 2005). In agreement with these studies, no specific interaction of the acyl moiety was obvious. Accordingly, the binding modes of ARP and its *N*<sup>G</sup>-acylated analogue UR-PG136 in the H<sub>2</sub>R binding pocket were very similar. In agreement with a previous 3D model of the TM domains of the gpH<sub>2</sub>R (Kelley et al., 2001), the HA-like imidazolylpropyl group interacted with residues in TM3, TM5, and TM6, and the binding site for the variable *N*<sup>G</sup>-diarylalkyl or *N*<sup>G</sup>-diarylalkanoyl groups was formed by amino acids in TM2, TM3, TM6, and TM7. In addition to residues within the TM domains, the H<sub>2</sub>R models suggested amino acids in e2 to contribute to the binding pocket of the agonists. Particularly, Lys-173 and Lys-175 in the lower part of this loop are candidates to contact ARP. Contribution of residues in e2 to the ligand binding sites was previously shown for several aminergic GPCRs (Shi and Javitch, 2004; Kim et al., 1996; Scarselli et al., 2007). The role of e2 on H<sub>2</sub>R activity was experimentally investigated by the generation and pharmacological characterization of receptor mutants (chapter 9).

Recently, an ionic interaction between Asp-271(7.36) and Tyr-17(1.31) was proposed to stabilize an active conformation of the guanidine-bound gpH<sub>2</sub>R (Kelley et al., 2001). In addition to the formation of this interaction, the present gpH<sub>2</sub>R model suggested that Trp-275(7.40) and Lys-173 participate in this network. Due to the presence of Ala-271(7.36) and Cys-17(1.31) in the human species isoform, corresponding interactions were not observed in the hH<sub>2</sub>R model, corroborating the current concept that these two amino acids are important determinants for the species-selective activity of guanidine-type H<sub>2</sub>R agonists. A virtual screening for appropriate substituents at the carbonyl group of *N*<sup>G</sup>-acylated imidazolylpropylguanidines was performed to develop more potent and selective agonists for the hH<sub>2</sub>R. Introduction of ethyl-, isopropyl-, and isobutyl substituents at position 3 of the *N*<sup>G</sup>-(3-phenylpropanoyl) group proved to be favorable in terms of enhanced potencies at the hH<sub>2</sub>R, whereas the more hydrophilic *N*<sup>G</sup>-[3-(aminoalkyl)-3-phenylpropanoyl]guanidines displayed an increased potency at the guinea pig species isoform.

In summary, 3D structure models of human and guinea pig H<sub>2</sub>R species isoforms enabled us to gain novel insight into the structure and function of the H<sub>2</sub>R and facilitated the molecular analysis of species-selective interactions with guanidine-type agonists. Structure based virtual screening was able to predict substituents conferring high potency and selectivity to the compounds. The success of the virtual screening approaches was restricted due to few limitations of the generated models. First, for LUDI calculations, the hH<sub>2</sub>R protein was treated as a rigid body, disregarding the existence of rotatable bonds. Errors in the preliminary adjustment of residue side chain orientations may thus have biased the placement of compound fragments in the binding pocket. Second, due to the low sequence homology

between the loop regions of class 1 GPCRs it is generally difficult to provide reliable predictions about the three-dimensional structure of such loops when using the crystal structure of bovine rhodopsin as template. In this context, the course of the e2 backbone is of particular relevance due to its proximity to the H<sub>2</sub>R binding pocket. Finally, the crystal structure of bovine rhodopsin in complex with 11-*cis* retinal represents an inactive receptor conformation (Palczewski et al., 2000). It is widely accepted that GPCR activation involves large changes in the arrangements of the TM helices. These changes mainly occur within the intracellular portions of TM3, TM6, and TM7 (Hubbell et al., 2003) but recent data also predict alteration of extracellular parts including the binding pocket (Schwartz et al., 2006). Molecular dynamics simulations can thus be useful to study the transitions of the H<sub>2</sub>R towards active guanidine-bound conformations (chapter 5).

## 4.5 References

- Alewijnse AE, Timmerman H, Jacobs EH, Smit MJ, Roovers E, Cotecchia S and Leurs R (2000) The effect of mutations in the DRY motif on the constitutive activity and structural instability of the histamine H<sub>2</sub> receptor. *Mol Pharmacol* **57**:890-898.
- Ballesteros JA and Weinstein H (1995) Integrated methods for the construction of three dimensional models and computational probing of structure-function relations in G-protein coupled receptors. *Methods Neurosci* **25**:366-428.
- Ballesteros JA, Shi L and Javitch JA (2001a) Structural mimicry in G protein-coupled receptors: implications of the high-resolution structure of rhodopsin for structure-function analysis of rhodopsin-like receptors. *Mol Pharmacol* **60**:1-19.
- Ballesteros JA, Jensen AD, Liapakis G, Rasmussen SG, Shi L, Gether U and Javitch JA (2001b) Activation of the  $\beta_2$ -adrenergic receptor involves disruption of an ionic lock between the cytoplasmic ends of transmembrane segments 3 and 6. *J Biol Chem* **276**:29171-29177.
- Bissantz C (2003) Conformational changes of G protein-coupled receptors during their activation by agonist binding. *J Recept Signal Transduct Res* **23**:123-153.
- Böhm HJ (1992) The computer program LUDI: a new method for the de novo design of enzyme inhibitors. *J Comput Aided Mol Des* **6**:61-78.
- Böhm HJ (1993) A novel computational tool for automated structure-based drug design. *J Mol Recognit* **6**:131-137.
- Dove S and Buschauer A (1998) Imidazolypropylguanidines as histamine H<sub>2</sub> receptor agonists: 3D-QSAR of a large series. *Pharm Acta Helv* **73**:145-155.
- Dove S and Buschauer A (1999) Improved alignment by weighted field fit in CoMFA of histamine H<sub>2</sub> receptor agonistic imidazolypropylguanidines. *Quant Struct-Act Relat* **18**:329-341.
- Dove S, Elz S, Seifert R and Buschauer A (2004) Structure-activity relationships of histamine H<sub>2</sub> receptor ligands. *Mini Rev Med Chem* **4**:941-954.
- Filipek S, Stenkamp RE, Teller DC and Palczewski K (2003) G protein-coupled receptor rhodopsin: a prospectus. *Annu Rev Physiol* **65**:851-879.
- Franke R and Buschauer A (1992) Quantitative structure-activity relationships in histamine H<sub>2</sub>-agonists related to impromidine and arpromidine. *Eur J Med Chem* **27**:443-448.

- Fritze O, Filipek S, Kuksa V, Palczewski K, Hofmann KP and Ernst OP (2003) Role of the conserved NPxxY(x)<sub>5,6</sub>F motif in the rhodopsin ground state and during activation. *Proc Natl Acad Sci U S A* **100**:2290-2295.
- Fu D, Ballesteros JA, Weinstein H, Chen J and Javitch JA (1996) Residues in the seventh membrane-spanning segment of the dopamine D<sub>2</sub> receptor accessible in the binding-site crevice. *Biochemistry* **35**:11278-11285.
- Gantz I, Munzert G, Tashiro T, Schäffer M, Wang L, DelValle J and Yamada T (1991) Molecular cloning of the human histamine H<sub>2</sub> receptor. *Biochem Biophys Res Commun* **178**:1386-1392.
- Ghorai P (2005) Arpromidine-related acylguanidines: synthesis and structure-activity relationships of a new class of guanidine-type histamine H<sub>2</sub> receptor agonists with reduced basicity. Doctoral thesis. University of Regensburg, Germany.  
<http://www.opus-bayern.de/uni-regensburg/volltexte/2006/561/>
- Govaerts C, Lefort A, Costagliola S, Wodak SJ, Ballesteros JA, Van Sande J, Pardo L and Vassart G (2001) A conserved Asn in transmembrane helix 7 is an on/off switch in the activation of the thyrotropin receptor. *J Biol Chem* **276**:22991-22999.
- Hubbell WL, Altenbach C, Hubbell CM and Khorana HG (2003) Rhodopsin structure, dynamics, and activation: a perspective from crystallography, site-directed spin labeling, sulfhydryl reactivity, and disulfide cross-linking. *Adv Protein Chem* **63**:243-290.
- Jongejan A, Bruysters M, Ballesteros JA, Haaksma E, Bakker RA, Pardo L and Leurs R (2005) Linking agonist binding to histamine H<sub>1</sub> receptor activation. *Nat Chem Biol* **1**:98-103.
- Kelley MT, Bürckstümmer T, Wenzel-Seifert K, Dove S, Buschauer A and Seifert R (2001) Distinct interaction of human and guinea pig histamine H<sub>2</sub>-receptor with guanidine-type agonists. *Mol Pharmacol* **60**:1210-1225.
- Kim J, Jiang Q, Glashofer M, Yehle S, Wess J and Jacobson KA (1996) Glutamate residues in the second extracellular loop of the human A<sub>2a</sub> adenosine receptor are required for ligand recognition. *Mol Pharmacol* **49**:683-691.
- Laskowski RA, MacArthur MW, Moss DS and Thornton JM (1993) PROCHECK: a program to check the stereochemical quality of protein structures. *J Appl Cryst* **26**:283-291.
- Lu ZL and Hulme EC (1999) The functional topography of transmembrane domain 3 of the M<sub>1</sub> muscarinic acetylcholine receptor, revealed by scanning mutagenesis. *J Biol Chem* **274**:7309-7315.
- Mirzadegan T, Benko G, Filipek S and Palczewski K (2003) Sequence analyses of G-protein-coupled receptors: similarities to rhodopsin. *Biochemistry* **42**:2759-2767.
- Nederkoorn PH, van Lenthe JH, van der Goot H, Donne-Op den Kelder GM and Timmerman H (1996a) The agonistic binding site at the histamine H<sub>2</sub> receptor. I. Theoretical investigations of histamine binding to an oligopeptide mimicking a part of the fifth transmembrane alpha-helix. *J Comput Aided Mol Des* **10**:461-478.
- Nederkoorn PH, van Gelder EM, Donne-Op den Kelder GM and Timmerman H (1996b) The agonistic binding site at the histamine H<sub>2</sub> receptor. II. Theoretical investigations of histamine binding to receptor models of the seven alpha-helical transmembrane domain. *J Comput Aided Mol Des* **10**:479-489.
- Neve KA, Cumbay MG, Thompson KR, Yang R, Buck DC, Watts VJ, DuRand CJ and Teeter MM (2001) Modeling and mutational analysis of a putative sodium-binding pocket on the dopamine D<sub>2</sub> receptor. *Mol Pharmacol* **60**:373-381.
- Okada T, Ernst OP, Palczewski K and Hofmann KP (2001) Activation of rhodopsin: new insights from structural and biochemical studies. *Trends Biochem Sci* **26**:318-324.
- Okada T, Fujiyoshi Y, Silow M, Navarro J, Landau EM and Shichida Y (2002) Functional role of internal water molecules in rhodopsin revealed by X-ray crystallography. *Proc Natl Acad Sci U S A* **99**:5982-5987.
- Palczewski K (2006) G protein-coupled receptor rhodopsin. *Annu Rev Biochem* **75**:743-767.

- Palczewski K, Kumasaka T, Hori T, Behnke CA, Motoshima H, Fox BA, Le Trong I, Teller DC, Okada T, Stenkamp RE, Yamamoto M and Miyano M (2000) Crystal structure of rhodopsin: A G protein-coupled receptor. *Science* **289**:739-745.
- Pardo L, Deupi X, Dolker N, Lopez-Rodriguez ML and Campillo M (2007) The role of internal water molecules in the structure and function of the rhodopsin family of G protein-coupled receptors. *Chembiochem* **8**:19-24.
- Roth BL, Shoham M, Choudhary MS and Khan N (1997) Identification of conserved aromatic residues essential for agonist binding and second messenger production at 5-hydroxytryptamine<sub>2A</sub> receptors. *Mol Pharmacol* **52**:259-266.
- Ruprecht JJ, Mielke T, Vogel R, Villa C and Schertler GF (2004) Electron crystallography reveals the structure of metarhodopsin I. *EMBO J* **23**:3609-3620.
- Scarselli M, Li B, Kim SK and Wess J (2007) Multiple residues in the second extracellular loop are critical for M<sub>3</sub> muscarinic acetylcholine receptor activation. *J Biol Chem* **282**:7385-7396.
- Schwartz TW, Frimurer TM, Holst B, Rosenkilde MM and Eling CE (2006) Molecular mechanism of 7TM receptor activation-a global toggle switch model. *Annu Rev Pharmacol Toxicol* **46**:481-519.
- Shi L and Javitch JA (2002) The binding site of aminergic G protein-coupled receptors: the transmembrane segments and second extracellular loop. *Annu Rev Pharmacol Toxicol* **42**:437-467.
- Shi L and Javitch JA (2004) The second extracellular loop of the dopamine D<sub>2</sub> receptor lines the binding-site crevice. *Proc Natl Acad Sci U S A* **101**:440-445.
- Tao YX, Abell AN, Liu X, Nakamura K and Segaloff DL (2000) Constitutive activation of G protein-coupled receptors as a result of selective substitution of a conserved leucine residue in transmembrane helix III. *Mol Endocrinol* **14**:1272-1282.
- Teller DC, Okada T, Behnke CA, Palczewski K and Stenkamp RE (2001) Advances in determination of a high-resolution three-dimensional structure of rhodopsin, a model of G-protein-coupled receptors (GPCRs). *Biochemistry* **40**:7761-7772.
- Thompson JD, Higgins DG and Gibson TJ (1994) CLUSTAL W: improving the sensitivity of progressive multiple sequence alignment through sequence weighting, position-specific gap penalties and weight matrix choice. *Nucleic Acids Res* **22**:4673-4680.
- Traiffort E, Vizuite ML, Tardivel-Lacombe J, Souil E, Schwartz JC and Ruat M (1995) The guinea pig histamine H<sub>2</sub> receptor: gene cloning, tissue expression and chromosomal localization of its human counterpart. *Biochem Biophys Res Commun* **211**:570-577.
- Urizar E, Claeysen S, Deupi X, Govaerts C, Costagliola S, Vassart G and Pardo L (2005) An activation switch in the rhodopsin family of G protein-coupled receptors: the thyrotropin receptor. *J Biol Chem* **280**:17135-17141.
- Visiers I, Ebersole B, Dracheva S, Ballesteros JA, Sealfon S and Weinstein H (2002) Structural motifs as functional microdomains in G-protein-coupled receptors: Energetic considerations in the mechanism of activation of the serotonin 5-HT<sub>2A</sub> receptor by disruption of the ionic lock of the arginine cage. *Int J Quantum Chem* **88**:65-75.
- Wess J, Gdula D and Brann MR (1991) Site-directed mutagenesis of the M<sub>3</sub> muscarinic receptor: identification of a series of threonine and tyrosine residues involved in agonist but not antagonist binding. *EMBO J* **10**:3729-3734.
- Wieland K, Zuurmond HM, Krasel C, Ijzerman AP and Lohse MJ (1996) Involvement of Asn-293 in stereospecific agonist recognition and in activation of the  $\beta_2$ -adrenergic receptor. *Proc Natl Acad Sci U S A* **93**:9276-9281.
- Wieland K, Laak AM, Smit MJ, Kühne R, Timmerman H and Leurs R (1999) Mutational analysis of the antagonist-binding site of the histamine H<sub>1</sub> receptor. *J Biol Chem* **274**:29994-30000.
- Wong SK, Slaughter C, Ruoho AE and Ross EM (1988) The catecholamine binding site of the  $\beta$ -adrenergic receptor is formed by juxtaposed membrane-spanning domains. *J Biol Chem* **263**:7925-7928.



Xie SX, Kraus A, Ghorai P, Ye QZ, Elz S, Buschauer A and Seifert R (2006) *N*<sup>1</sup>-(3-cyclohexylbutanoyl)-*N*<sup>2</sup>-[3-(1*H*-imidazol-4-yl)propyl]guanidine (UR-AK57), a potent partial agonist for the human histamine H<sub>1</sub>- and H<sub>2</sub>-receptors. *J Pharmacol Exp Ther* **317**:1262-1268.



## Chapter 5

# Molecular Dynamics Simulations of the Human Histamine H<sub>2</sub> Receptor in a Hydrated POPC Bilayer

### 5.1 Introduction

Bovine rhodopsin is the only GPCR from which crystal structures are presently available (Palczewski et al., 2000; Teller et al., 2001; Okada et al., 2002; Li et al., 2004; Okada et al., 2004). Despite relatively low sequence homologies with rhodopsin, GPCRs are expected to adopt similar general folding characteristics by means of structural mimicry (Ballesteros et al., 2001). Accordingly, different amino acids or alternate microdomains may be compatible with similar deviations from regular  $\alpha$ -helical structure, thereby resulting in related tertiary structures. The conformational changes in the transmembrane spanning (TM) domains upon receptor activation and the interaction of the intracellular surface with G proteins are proposed to be similar among all class 1 GPCRs. The receptor selectivity of agonists and antagonists however, is assumed to originate from local variabilities within the TM domains and extracellular binding regions of the ligands. The corresponding conservation gradient within a GPCR molecule, based on the primary sequences of 270 class 1 GPCRs, indicates that the extracellular parts are least conserved, while considerable conservation exists toward the cytoplasmic sides (Mirzadegan et al., 2003). At present, the crystal structure of bovine rhodopsin is established as a useful template for constructing homology models of rhodopsin-like GPCRs (Bissantz et al., 2003; Fanelli and De Benedetti, 2005). However,

substantial deviations in the conformations of the GPCR binding sites were predicted to require further modifications of the initial template (Ballesteros et al., 2001).

Recently, Huber et al. suggested that the conformation of rhodopsin in the crystal unit cell may be considerably different from the conformations of rhodopsin under physiological conditions (Huber et al., 2004). Particularly, the presence of detergent molecules ( $\beta$ -nonylglucoside), the crystallization adjuvant heptane-1,2,3-triol, and several heavy atoms such as zinc and mercury (Palczewski et al., 2000; Teller et al., 2001; Okada et al., 2002) may act as packing constraints. Thus, computational methods describing the dynamic behaviour of proteins are necessary to recognize and remove such packing constraints.

Molecular dynamics (MD) simulation is an established computational methodology to analyze the conformational dynamics of membrane proteins. MD simulations can provide information about the conformational properties of molecular systems and the way in which the conformation changes with time (Leach, 2001). Thus this technique may be useful to gain insight into the relationship between structure and biological function (Faraldo-Gomez et al., 2002; Hansson et al., 2002; Karplus and McCammon, 2002; Gumbart et al., 2005; Ash et al., 2004). At present, numerous dynamic studies on membrane proteins such as transmembrane peptides, fusion proteins, channel and pore proteins, transporters, ion pumps, ATP-synthases, and GPCRs, have been performed (for recent reviews consider Kandt et al., 2007; Ash et al., 2004; Gumbart et al., 2005). Since the function of membrane proteins is influenced by the membrane environment through electrostatic, hydrophobic and van der Waals interactions and through the internal pressure of the membrane, explicit consideration of the protein environment is a crucial prerequisite for reliable MD studies of such proteins (Gumbart et al., 2005). This is supported by experiments suggesting that organisms vary the lipid composition of their membranes to modulate protein function (Albert et al., 1996; Mitchell et al., 1992). Moreover, specific protein and lipid interactions are related to the domain organization of biomembranes in rafts (Simons and Ikonen, 2000; Ostrom and Insel, 2004; Simons and Ikonen, 1997). In the case of rhodopsin photoactivation, the thermodynamic equilibrium between the meta I and meta II conformations strongly depends on the lipid composition of the membrane (Beach et al., 1984), and a native-like lipid mixture results in optimal function (Wiedmann et al., 1988). Huber et al. suggested a possible microscopic mechanism for lipid effects on rhodopsin activation, based on site-specific conformational changes of rhodopsin close to the lipid/protein interfaces (Huber et al., 2004). In addition to an explicit consideration of the lipid bilayer, hydration with water and ions are needed to mimic a realistic environment of membrane proteins. In particular, when simulating under vacuum conditions, polar and charged residues on the protein surface potentially do not exhibit extended conformations to account for expected interactions with the hydrophilic water shell but rather fold back into the protein surface producing artificial H-bond patterns

(Mehler et al., 2002).

The choice of the lipid model mimicking the bilayer is not a trivial task, since distinct properties, e.g. the degree of unsaturation and the lengths of the carbon chains, may critically alter the interactions with the protein. In a recent MD simulation of rhodopsin embedded in a bilayer containing cholesterol and different lipids comprising poly-unsaturated acyl chains it was shown that lipids near the protein preferentially reorient such that their unsaturated chains interact with the protein (Pitman et al., 2005).

In the present study, the human H<sub>2</sub>R (hH<sub>2</sub>R) was subjected to MD simulations both in its ligand-unoccupied form mimicking the inactive state of the receptor, and in complex with the H<sub>2</sub>R agonist arpromidine (ARP, Figure 4.2). 1-Palmitoyl-2-oleoyl-*sn*-glycero-3-phosphatidylcholine (POPC) was used as a lipid model to simulate the membrane environment of the hH<sub>2</sub>R. The system was hydrated by water molecules and counter ions were explicitly considered. The purpose of this study was to characterize the structure and function of the hH<sub>2</sub>R and to validate the results on the basis of present concepts of GPCR activation mechanisms. Finally, the resulting dynamic hH<sub>2</sub>R models were used to provide an improved model for the binding mode of ARP and related imidazolypropylguanidines.

## 5.2 Materials and Methods

### 5.2.1 Construction of an hH<sub>2</sub>R-POPC-water system

A homology model of the ligand-free hH<sub>2</sub>R (chapter 4.3) was embedded in a 1-palmitoyl-2-oleoyl-*sn*-glycero-3-phosphatidylcholine (POPC) (Figure 5.3 A) bilayer. In the first step, the software package VEGA ZZ release 2.0.8.60 (Pedretti et al., 2002, 2004; <http://www.ddl.unimi.it>) was used to place the hH<sub>2</sub>R model into the centre of a triclinic box of 79 Å x 82 Å x 78 Å dimensions. A bilayer consisting of 81 POPC molecules was then constructed around the receptor model. To prepare for an optimal fit of the receptor with the lipid molecules, the van der Waals radii of both partners were allowed to overlap by 1.5 Å.

The software package GROMACS version 3.2 (van der Spoel et al., 2004, 2005; Bekker et al., 1993; Berendsen et al., 1995; Lindahl et al., 2001) (Department of Biophysical Chemistry, University of Groningen, Nijenborgh 4, 9747 AG Groningen, The Netherlands) was used to optimize the hH<sub>2</sub>R-POPC complex, first with the steepest descent and then with the conjugate gradient method. A new triclinic box of 70 Å x 83 Å x 70 Å dimensions was generated around the hH<sub>2</sub>R-POPC system, subsequently solvated with 7345 single-point charge (spc) water molecules (command genbox). In the course of this procedure, apart from

the upper and lower regions of the box representing the extracellular and intracellular parts of the biological system, remaining space at the interface between protein and lipids and at the box edges has been filled with water. Accordingly, 634 water molecules in a layer of 18 Å thickness in the regions of the lipophilic POPC carbon chains were removed, thus yielding a number of 6711 water molecules. After subsequent minimization steps, 10 water molecules were exchanged by 10 chloride ions according to the electrostatic potential to achieve a total charge of zero of the system (command genion). Finally, five conserved water molecules were transferred from the initial hH<sub>2</sub>R homology model (chapter 4.3.1) to the new system. Subsequently, the complete hH<sub>2</sub>R-POPC-water system was optimized until the maximum force was smaller than 100 kJ mol<sup>-1</sup> nm<sup>-1</sup>. The total number of atoms in the system was 27390.

## 5.2.2 Docking of ARP into the pre-equilibrated hH<sub>2</sub>R-POPC-water system

### 5.2.2.1 Preparation of the ligand

With help of the PRODRG software (Schüttelkopf and van Aalten, 2004), a coordinate file of ARP in the pdb format was converted into the corresponding GROMACS structure and topology file. Atom types and Gasteiger-Hückel charges were assigned to the ligand, according to the GROMOS force field parameters. To achieve both appropriate positioning and conformation in the binding cavity, the ARP atom coordinates were transferred from the initial hH<sub>2</sub>R-ARP model (chapter 4.2.4) to the new structure file.

### 5.2.2.2 Preparation of the receptor structure and docking procedure

For docking ARP, an hH<sub>2</sub>R-POPC-water system was selected as starting structure consisting of the pre-equilibrated POPC bilayer and water shells (chapter 5.3.2). For an optimal fit of the ligand in the binding pocket, the torsion angles of Asp-98(3.32), Tyr-182(5.38), Tyr-250(6.51), Phe-254(6.55), and Trp-275(7.40) were carefully modified. To approach the proposed activated state of the hH<sub>2</sub>R, the total charge of Asp-115(3.49) was set to zero. 18 water molecules within the binding pocket were removed. Subsequently, all entries in the coordinate and topology files of ARP were added to the corresponding files of the hH<sub>2</sub>R. Since the generated ligand-receptor complex comprised a total charge of +2 (considering the positive charge of the guanidine group in ARP), two chloride ions were added to achieve an overall charge of zero in the system. Finally, the complex of ARP and hH<sub>2</sub>R in the hydrated lipid bilayer was energy-minimized until the maximum force was smaller than 100 kJ mol<sup>-1</sup> nm<sup>-1</sup>, first with the steepest-descent and then with the conjugate gradient method.

### 5.2.3 Parameters for MD simulations with GROMACS

A topology file for a POPC molecule and the corresponding lipid parameters (Berger et al., 1997), containing the interaction parameters between the lipid atoms and the modified GROMOS87 force field, have been taken from the group of Prof. Tieleman (<http://moose.bio.ucalgary.ca>; Department of Biological Sciences, 2500 University Drive NW, Calgary, AB T2N 1N4, Canada). All MD simulations were thus performed applying the GROMOS87 force field. The LINCS algorithm (Hess et al., 1997) was applied to allow for a timestep of 2 fs (constraints on all bonds). The cut-off distance for the generation of the short-range neighbour list for calculating the van der Waals interactions was set to 1.0 nm. The neighbour list was updated every 10 steps of the calculations. Periodic boundary conditions were applied in all directions of the simulation box. The Particle Mesh Ewald method (Darden et al., 1993; Essmann et al., 1995) was used to calculate the long-range electrostatic interactions. The distance for the Lennard Jones cut-off was set to 1.4 nm. The Berendsen algorithm (Berendsen et al., 1984) was used to couple the system to an external heat bath of 300 K reference temperature with a coupling constant of 0.1 ps. Different macroscopic types of ensembles using various methods of pressure coupling were studied (chapter 5.3.1). A complete list of run parameters for MD simulations is provided in the Appendix 2 (chapter 11).

## 5.3 Results

### 5.3.1 Equilibration of the hH<sub>2</sub>R-POPC-water system

Prior to performing long-term MD simulations initial runs of MD simulations are generally necessary to equilibrate a system until constant physical values, e.g. potential energy, box volume, temperature, and pressure, are obtained. Macroscopic ensemble types most frequently used for MD simulations are the *NVT* (canonical) and the *NPT* (isobaric-isothermal) ensembles. In both systems, the number of atoms  $N$  in the system and the temperature  $T$  are kept constant. Additionally, in the *NVT* ensemble the volume  $V$  of the simulation box is fixed thus allowing the pressure in the system to adapt. Using the *NPT* ensemble, the pressure  $P$  in the system is adjusted to a reference value thus allowing the simulation box to adapt in its size. To select optimal parameters for MD simulations of the hH<sub>2</sub>R-POPC-water system, both ensemble types were compared.

### 5.3.1.1 *NVT ensemble*

By assessing an *NVT* ensemble, the dimensions of the box remained constant at 70 Å x 83 Å x 70 Å during 20 ps of equilibration time. By visual inspection severe disruptions of the bilayer structure became apparent (not shown). The hydrophobic lipid chains were disordered and space in the region of the lipid bilayer remained free. The density in the box was 889 kg m<sup>-3</sup> and a pressure of -670 bar was calculated. Due to the low density in the starting system setup, adaptation of the box vectors was crucial for appropriate MD simulations. Therefore, no further studies were performed using the *NVT* ensemble.

### 5.3.1.2 *NPT ensemble*

The Berendsen algorithm was applied to coupling the simulation system to an external pressure bath. Coordinates and box vectors were scaled every time step using a pressure coupling constant of 0.1 ps. 500 ps of equilibration time were applied to the hH<sub>2</sub>R-POPC-water system using various types of pressure coupling. In system 1, the pressure was coupled isotropically, *i.e.* all box vectors were scaled similarly. The positions of all hH<sub>2</sub>R heavy atoms were fixed using a force constant of 1000 kJ mol<sup>-1</sup> nm<sup>-2</sup> to allow for equilibration of only the POPC bilayer and water. In system 2, the pressure was coupled anisotropically, *i.e.* all three box vectors were scaled individually. Since there is no coupling between any of the directions in anisotropic pressure coupling, deformations of the membrane can occur (Kandt et al., 2007). Therefore, special attention was paid to the structure and the size of the phospholipid bilayer. Positional restraints were applied on the hH<sub>2</sub>R heavy atoms during the first 400 ps of simulation time. Additionally, within the first 200 ps the positions of POPC atoms were fixed in their y dimension perpendicular to the membrane layer and using a force constant of 1000 kJ mol<sup>-1</sup> nm<sup>-2</sup>. Thus the bilayer was allowed to move only in the x-z plane which should prevent an early reduction of the bilayer size. During the last 100 ps of equilibration, the whole system was allowed to move without any restraints. In system 3, semi-isotropic pressure coupling was assessed in x- and z-dimensions. Here, the box size was allowed to adapt only in x and z directions whereas the y-dimension of the box was fixed. Since with this setting the bilayer size was not expected to change, positional restraints were applied only on all hH<sub>2</sub>R heavy atoms (force constant of 1000 kJ mol<sup>-1</sup> nm<sup>-2</sup>). In all three systems, isothermal compressibility was set to  $4.5 \cdot 10^{-5}$  bar<sup>-1</sup> corresponding to the compressibility of water at 1 atm and a temperature of 300 K. A comparison of the final structures of the POPC bilayers in complex with the hH<sub>2</sub>R models after 500 ps equilibration time can be seen in Figure 5.1.



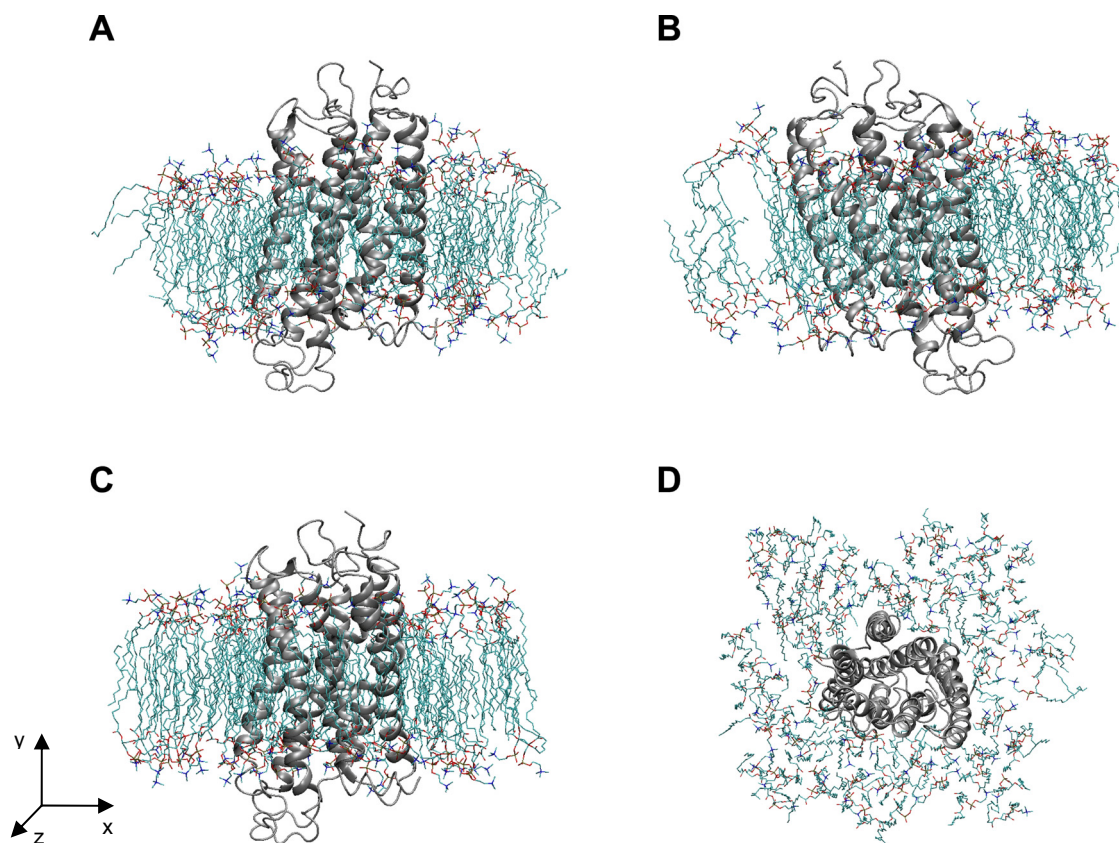


**Figure 5.1:** Structures of hH<sub>2</sub>R models embedded in a solvated POPC bilayer using different system setups. A, *NPT* ensemble with isotropic pressure coupling (system 1); B, *NPT* ensemble with semi-isotropic pressure coupling (system 3); C and D, *NPT* ensemble with anisotropic pressure coupling in all dimensions (system 2). A, B, C, lateral view; D, view from the extracellular side. TM domains are shown as grey ribbon. For clarity, water molecules are not shown.

### 5.3.1.3 Analysis of system parameters

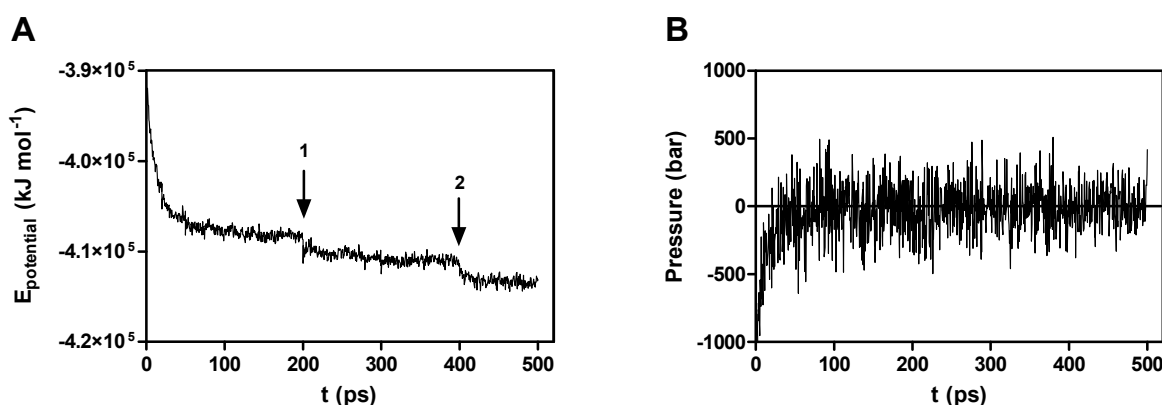
After 500 ps of equilibration, box volumes and densities were approximately similar in the three systems (Table 5.1). In system 3 the box y-dimension was highest matching the starting value. After releasing the strain on the POPC atom positions, the box y-dimension in system 2 was higher compared to system 1.

**Table 5.1:** Box dimensions and physical values in the different systems after equilibration.

	Box (Å) <sup>a</sup>			V (nm <sup>3</sup> ) <sup>b</sup>	Density (kg m <sup>-3</sup> ) <sup>a</sup>
	x	y	z		
system 1	66	78	66	345 ± 1	1043
system 2	65	81	65	345 ± 0	1047
system 3	65	83	65	346 ± 1	1039

<sup>a</sup> values corresponding to the final snapshot after equilibration<sup>b</sup> mean ± S.D. assessed during the last 100 ps of equilibration time

Approximately 150 ps of equilibration time were necessary to obtain constant potential energies in all systems. In Figure 5.2 A, the time course for the potential energy in system 2 is shown. Although depending on the restraints applied, in all systems the potential energies converged to an approximately similar value of  $-4.1 \cdot 10^5$  kJ mol<sup>-1</sup>. After ~50 ps of simulation time, the pressures converged to the reference value of 1 bar in all three systems, which is shown for system 2 in Figure 5.2 B.

**Figure 5.2:** Potential energy (A) and pressure (B) in system 2 during equilibration. **1**, release of positional restraints on POPC atoms; **2**, release of positional restraints on protein heavy atoms.

#### 5.3.1.4 Structural analysis of the POPC bilayer

MD simulations should characterize the POPC bilayer system in a state that resembles the fluid phase ( $L_\alpha$ ) naturally occurring at  $-5$  °C to  $+70$  °C (Wiener and White, 1991). In the case of rhodopsin, the membrane lipids are entirely in the  $L_\alpha$  state at physiological temperature (Deese et al., 1981; Miljanich et al., 1985; Ellena et al., 1986). To quantify the dynamics of the *sn*-1 and *sn*-2 carbon chains of POPC, the deuterium order parameter ( $S_{CD}$ ), originally

obtained from the quadrupolar splittings measured by <sup>2</sup>H NMR on phospholipids, was calculated. This value is related to the average orientation of the methylen groups and provides information about the order within the bilayer which helps in guiding the choice of simulation parameters and evaluating MD models. Order parameters are among the most accurately determined experimental properties and are readily available from simulations (Berendsen and Tieleman, 1998). Preliminary MD studies simulating the *L<sub>α</sub>* phase of a hydrated POPC bilayer revealed good agreement of calculated *S<sub>CD</sub>* values with experimental data (Heller et al., 1993; Huber et al., 2002, 2004). From MD trajectories order parameters can be directly calculated as

$$S_z = \frac{3}{2} \langle \cos^2 \theta_z \rangle - \frac{1}{2} \quad (5.1)$$

where  $\theta_z$  is the angle between the z-axis of the simulation box and the vector from C<sub>n-1</sub> to C<sub>n+1</sub>. *S<sub>x</sub>* and *S<sub>y</sub>* are defined in the same way. The brackets imply averaging over time and molecules. The shape of the palmitoyl chain curve is characterized by a typical plateau in the central region of the alkyl chain and by decreasing values for the terminal atoms representing an increase in configurational freedom with depth in the bilayer (Seelig and Seelig, 1980; Petrache et al., 2001) (Figure 5.3 B). Strikingly, order parameters in system 2 were in very good agreement with experimental data and were considerably lower in the cases of systems 1 and 3. The curve of the unsaturated *sn*-2 (oleoyl) chain shows a significant dip at carbon atoms 9 and 10 representing the *cis*-double bond (Seelig, 1977; Seelig and Seelig, 1980; Huber et al., 2002). Similar *S<sub>CD</sub>* values in the three systems were observed for the *sn*-2 chain carbon atoms 2-7 and 14-16, but the characteristic dips representing the double bound were less pronounced in system 2 compared to approximately similar values in systems 1 and 3.

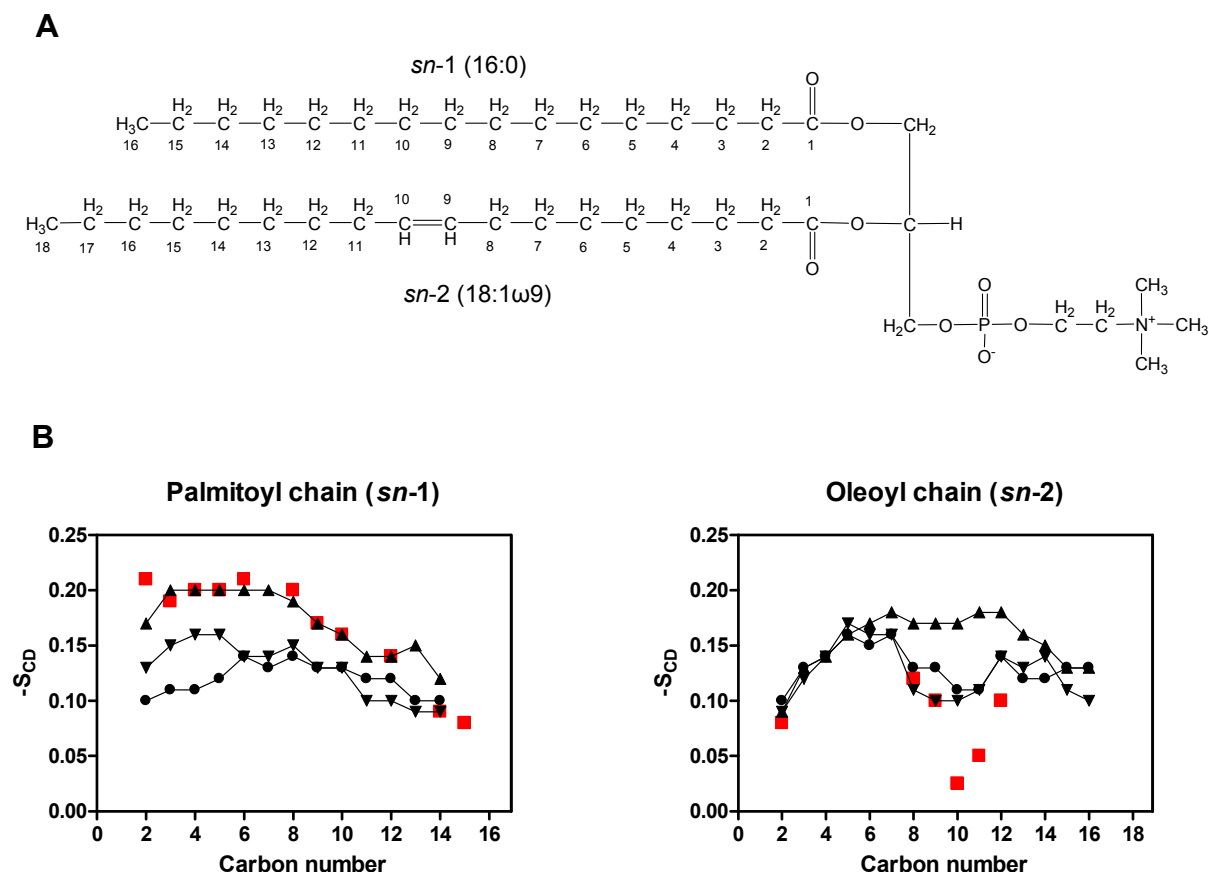


**Figure 5.3:** A, Chemical structure of 1-palmitoyl-2-oleoyl-*sn*-glycero-3-phosphatidylcholine (POPC); B, order parameters for carbon atoms in the *sn*-1 and *sn*-2 chains of POPC. Data are the means calculated from the last 50 ps equilibration time of system 1 ( $\blacktriangledown$ ), system 2 ( $\blacktriangle$ ), and system 3 ( $\bullet$ ). For comparison, experimental data are shown ( $\blacksquare$ ) (Seelig, 1977; Seelig and Seelig, 1980).

To further analyze the quality of mimicking the  $L_\alpha$  phase of the POPC bilayer, *RMSD* values of the POPC atoms were calculated during equilibration. Due to a high degree of disorder of the fatty acid chains, *RMSD* values of at least 20 Å were expected for MD simulations (Iadanza et al., 2002). Indeed, after an equilibration time of ~100 ps approximately similar *RMSD* values of 27 Å were determined in all systems. As can be seen in Figure 5.4, *RMSD* values of the POPC molecules were independent from positional restraints applied.

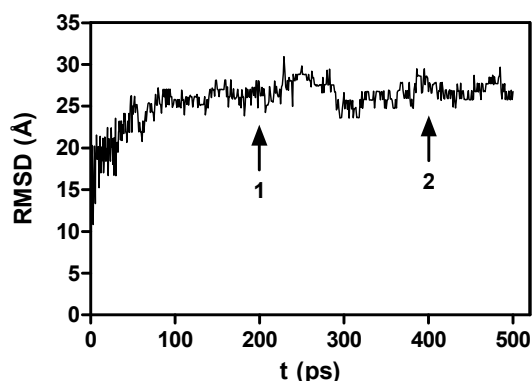


**Figure 5.4:** Trajectory of *RMSD* values of POPC atoms in system 2 during equilibration. **1**, release of positional restraints on POPC atoms; **2**, release of positional restraints on protein heavy atoms.

A common feature of membrane proteins is the accumulation of charged amino acids at both hydrophilic extensions of the membrane, whereas the protein surfaces at the interface with the hydrophobic lipid core mainly consist of hydrophobic residues (hydrophobic belt) (Rees et al., 1989; Wallin et al., 1997). In particular, positively charged arginine and lysine residues at the extracellular and intracellular sides are predicted to participate in ionic interactions with the negatively charged phospholipid head groups (Ballesteros et al., 2001). Thus, in MD simulations the protein should be oriented in such a way that its hydrophobic belt is aligned with the non-polar lipid tails (Kandt et al., 2007). Rhodopsin-like GPCRs were proposed to be in contact with the lipophilic membrane core in a slice of approximately 24 Å thickness (Baldwin et al., 1997). Results from neutron diffraction and X-ray diffraction experiments revealed a value of 27.1 Å for the thickness of the hydrocarbon core of a pure dioleoylphosphatidylcholine bilayer at a temperature of 30 °C (Nagle and Tristram-Nagle, 2000). To estimate the size of the lipophilic POPC membrane core, the distances between the average y-positions of the carbonyl carbon atoms in the upper and lower leaflets of the bilayer were calculated for both alkyl chains separately (Table 5.2). In systems 2 and 3, the thicknesses of the palmitoyl layers were similar but ~1 Å higher than in system 1. The oleoyl chains were of similar lengths in systems 1 and 2 and increased in system 3. Releasing the strain on POPC atoms in y-direction (system 2) resulted in a considerable reduction of the palmitoyl chain size by 4.3 Å ( $26.9 \pm 0.0$  Å when using positional restraints on POPC atoms) and that of the oleoyl chain by 1.7 Å ( $22.3 \pm 0.0$  Å when using positional restraints on POPC atoms). When inspected visually (Figure 5.1), the bilayer in system 1 appeared to be smaller than in the other two systems with the extracellular parts of the TM domains being located in the water shell. In system 2, arrangement of the phospholipid head groups allowed for adequate interactions with the charged residues on the hH<sub>2</sub>R surface (Figure 5.5).

**Table 5.2:** Analysis of the size of the lipophilic POPC bilayer core after equilibration. Values shown are the means  $\pm$  S.D. calculated from the last 100 ps of equilibration time.

	<b>d (Å)<sup>a</sup></b>	
	<b><i>sn-1</i></b>	<b><i>sn-2</i></b>
system 1	21.6 $\pm$ 0.2	20.5 $\pm$ 0.2
system 2	22.6 $\pm$ 0.2	20.6 $\pm$ 0.2
system 3	22.9 $\pm$ 0.2	22.0 $\pm$ 0.2

<sup>a</sup> Distance between the average y-positions of the *sn-1* and *sn-2* carbonyl carbon atoms, respectively, in the upper and lower leaflets of the POPC bilayer.

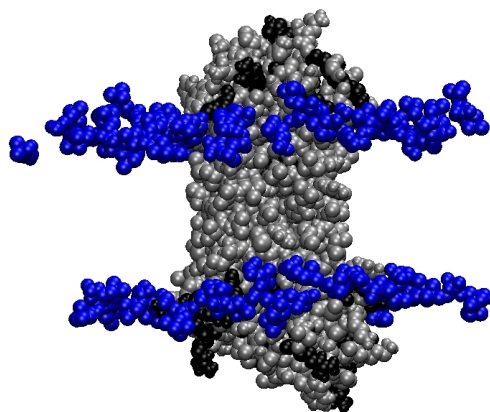


**Figure 5.5:** Distribution of charged residues (Arg, Lys, Glu, Asp; black) on the molecular surface of the hH<sub>2</sub>R model (grey) in system 2 after equilibration. Phosphatidylcholine groups of the POPC bilayer are shown in blue.

The solvent-accessible surface area (SASA) was calculated for the entire POPC bilayer and was used as a measure for the conformational fit between the alkyl chains in the lipophilic bilayer core. The lowest values of total and hydrophobic SASA were observed in system 2, indicating intensive van der Waals and hydrophobic interactions between adjacent carbon chains (Table 5.3). When releasing the strain on the POPC atoms, the hydrophobic SASA abruptly decreased (Figure 5.6), coinciding with the reduction in the lipophilic bilayer size. Thus, the resulting SASA difference was due to increased van der Waals contacts between the chain termini of opposite POPC bilayers. By contrast, the values for the hydrophilic SASA evenly increased during the equilibration time and approached the highest value in system 2 compared to systems 1 and 3, indicating that the polar head groups were most extensively solvated by water molecules.

**Table 5.3:** Analysis of the solvent-accessible surface area (SASA) of the POPC molecules using various system setups. Values shown are the means  $\pm$  S.D. calculated from the last 100 ps of equilibration time.

	SASA (nm <sup>2</sup> )		
	total	hydro-phobic	hydro-philic
system 1	315 $\pm$ 3	122 $\pm$ 3	157 $\pm$ 2
system 2	296 $\pm$ 2	107 $\pm$ 2	190 $\pm$ 2
system 3	308 $\pm$ 3	123 $\pm$ 2	185 $\pm$ 2

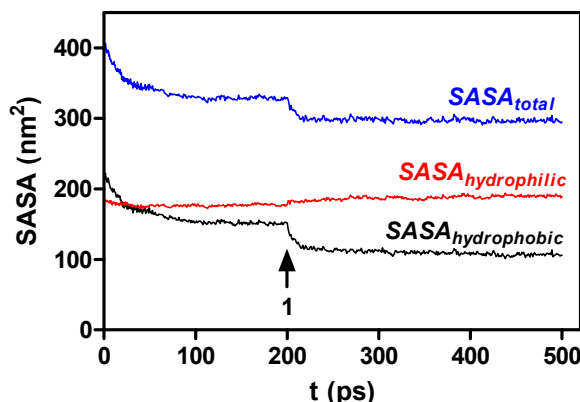


**Figure 5.6:** SASA of POPC molecules during equilibration of system 2. 1, release of positional restraints on POPC atoms.

### 5.3.2 MD simulations of the ligand-free and the ARP-docked hH<sub>2</sub>R models

Due to the superior performance in reproducing the dynamic and structural properties of the POPC membrane, for the following MD simulations the equilibrated hH<sub>2</sub>R-POPC-water complex from system 2 (*NPT* ensemble with anisotropic pressure coupling) was used. Both a model of the ligand-free hH<sub>2</sub>R and the hH<sub>2</sub>R in complex with docked ARP (hH<sub>2</sub>R-ARP) were subjected to total simulation periods of 5.0 ns each.

In preliminary MD runs, the backbones of TM7 and the extracellular half of TM5 did not remain in constant  $\alpha$ -helical structures but were disrupted during the first 1.0 ns. To achieve stable  $\alpha$ -helices within these TM domains, further equilibration steps of 200 ps lengths each were executed sequentially applying force constants of 750, 500, and 250 kJ mol<sup>-1</sup> nm<sup>-2</sup> on all protein atom positions, respectively, followed by a final step of 200 ps without application of restraints. During subsequent MD simulations, the ligand-free hH<sub>2</sub>R was allowed to move without any restraints. When ARP was docked into the hH<sub>2</sub>R binding pocket, the helicity of the extracellular part of TM5 was broken up within the first 500 ps of unrestrained simulations. To prevent this disruption, distance restraints between backbone atoms in the critical part of TM5 were applied using a force constant of 1000 kJ mol<sup>-1</sup> nm<sup>-2</sup>. To approach the proposed HA-like binding mode of the imidazolylpropylguanidine moiety of ARP and related guanidine-type H<sub>2</sub>R agonists (Dove et al., 2004), additional restraints were applied on the distances between the guanidine group of ARP and Asp-98(3.32) (Gantz et al., 1992) and between N <sup>$\pi$</sup> -H and N <sup>$\tau$</sup>  of the imidazole group with Asp-186(5.42) and Tyr-182(5.38) (Nederkoorn et al., 1996), respectively, using a force constant of 1000 kJ mol<sup>-1</sup> nm<sup>-2</sup>.

### 5.3.2.1 System parameters and POPC bilayer structure

Similar physical values of potential energy, temperature, and pressure were observed in both systems containing hH<sub>2</sub>R and hH<sub>2</sub>R-ARP, respectively, during the whole simulation time (Table 5.4). Snapshots after 5.0 ns revealed similar densities in both systems, whereas the y-dimension of the box was by 4 Å larger in the system of the ligand-free receptor compared to hH<sub>2</sub>R-ARP.

**Table 5.4:** Physical values and box dimensions in the systems containing hH<sub>2</sub>R and hH<sub>2</sub>R-ARP, respectively. Data shown are the means  $\pm$  S.D. from 5.0 ns simulation time.

	hH <sub>2</sub> R	hH <sub>2</sub> R-ARP
$E_{\text{pot}}$ (kJ mol <sup>-1</sup> )	$-4.10 \cdot 10^5 \pm 560$	$-4.10 \cdot 10^5 \pm 630$
$T$ (K)	$300 \pm 1$	$300 \pm 2$
$P$ (bar)	$3 \pm 150$	$0 \pm 160$
$V$ (nm <sup>3</sup> )	$342 \pm 0.4$	$341 \pm 0.4$
Density (kg m <sup>-3</sup> ) <sup>a</sup>	1052	1054
Box x, y, z (Å) <sup>a</sup>	62 x 86 x 65	63 x 82 x 65

<sup>a</sup> Values corresponding to the final snapshot after 5.0 ns of simulation time.

Order parameters of the POPC *sn*-1 and *sn*-2 chains were similar in both systems.  $S_{\text{CD}}$  values of the palmitoyl chains corresponded to the values during equilibration phase and agreed very well with experimental data. The dip in the graph of the oleoyl chain around carbon atoms 9 and 10 representing the *cis* double bond was considerably more pronounced than during the equilibration (Figure 5.7 and Figure 5.3 B).

Similar *RMSD* values of  $24.1 \pm 2.0$  Å and  $24.7 \pm 1.5$  Å were calculated for all POPC atoms in the systems with hH<sub>2</sub>R and hH<sub>2</sub>R-ARP, respectively, during the last 1.0 ns. When simulating the ligand-free hH<sub>2</sub>R, the thickness of the lipophilic bilayer core was  $23.1 \pm 0.3$  Å and  $22.9 \pm 0.3$  Å, respectively, using the palmitoyl and oleoyl carbonyl carbon atom positions as references. With the hH<sub>2</sub>R-ARP complex, corresponding values of 21.8 Å and 21.7 Å, respectively, were measured.



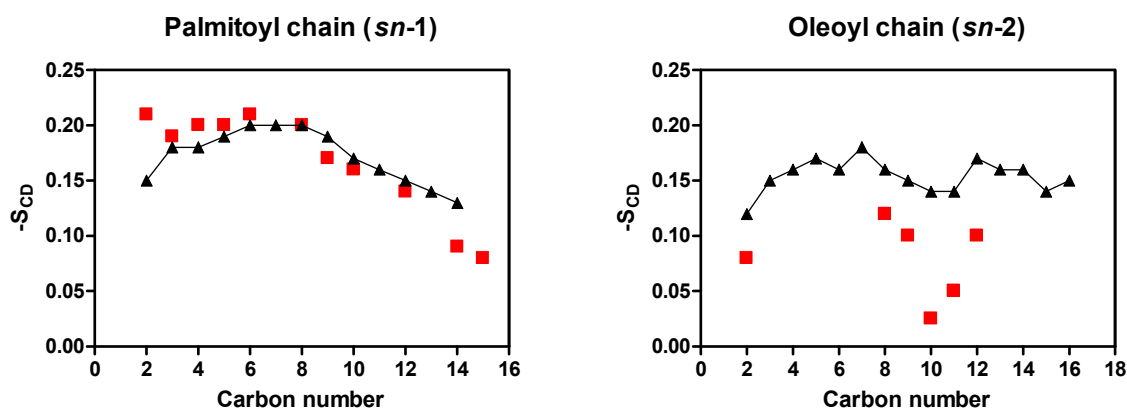


**Figure 5.7:** Order parameters for carbon atoms of POPC *sn*-1 and *sn*-2 alkyl chains. Data are the means calculated from the last 500 ps of 5.0 ns of MD simulations of the hH<sub>2</sub>R-ARP complex. For comparison, experimental data are shown (■) (Seelig, 1977; Seelig and Seelig, 1980).

### 5.3.2.2 Arrangement of secondary structure elements

Global folding of the ligand-free and the ARP-docked hH<sub>2</sub>R models were analyzed by calculating the total number of H-bonds, the radius of gyration ( $R_{\text{gyration}}$ ), and the total SASA of the protein. Docking of ARP into the hH<sub>2</sub>R binding pocket resulted in the disruption of 12 intramolecular H-bonds. The values shown in Table 5.5 were very similar in both systems, thus representing stable overall protein structures in both hH<sub>2</sub>R models.

**Table 5.5:** Protein global folding in the systems containing the ligand-free and the ARP-docked hH<sub>2</sub>R models. Data shown are the means  $\pm$  S.D. during 5.0 ns of simulation time.

	hH <sub>2</sub> R	hH <sub>2</sub> R-ARP
No. of H-bonds	254 $\pm$ 8	242 $\pm$ 7
$R_{\text{gyration}}$ (Å)	20.8 $\pm$ 0.1	20.8 $\pm$ 0.1
SASA <sub>protein</sub> (nm <sup>2</sup> )	155 $\pm$ 2	158 $\pm$ 2

The stability of secondary structural elements of the protein was calculated throughout the whole trajectories by means of dssp-plots (Kabsch and Sander, 1983). Strikingly, the TM domains of both hH<sub>2</sub>R models exhibited constant  $\alpha$ -helical patterns during 5.0 ns of MD simulations (Figure 5.8 A).

Two short antiparallel  $\beta$ -strands in the e2 loop (Glu-163 to Ser-165 and Lys-173 to Lys-175,

respectively) not present in the starting structure emerged during the last 2.5 ns of the simulation of the ligand-free hH<sub>2</sub>R (Figure 5.8 B). By analogy, the crystal structure of bovine rhodopsin (Palczewski et al., 2000) contains two  $\beta$ -strands at corresponding positions, *i.e.* between Arg-177 and Glu-181 and between Ser-186 and Asp-190, respectively (Figure 5.8 C). Intriguingly, analogous  $\beta$ -strands were not observed in the simulated hH<sub>2</sub>R-ARP complex.

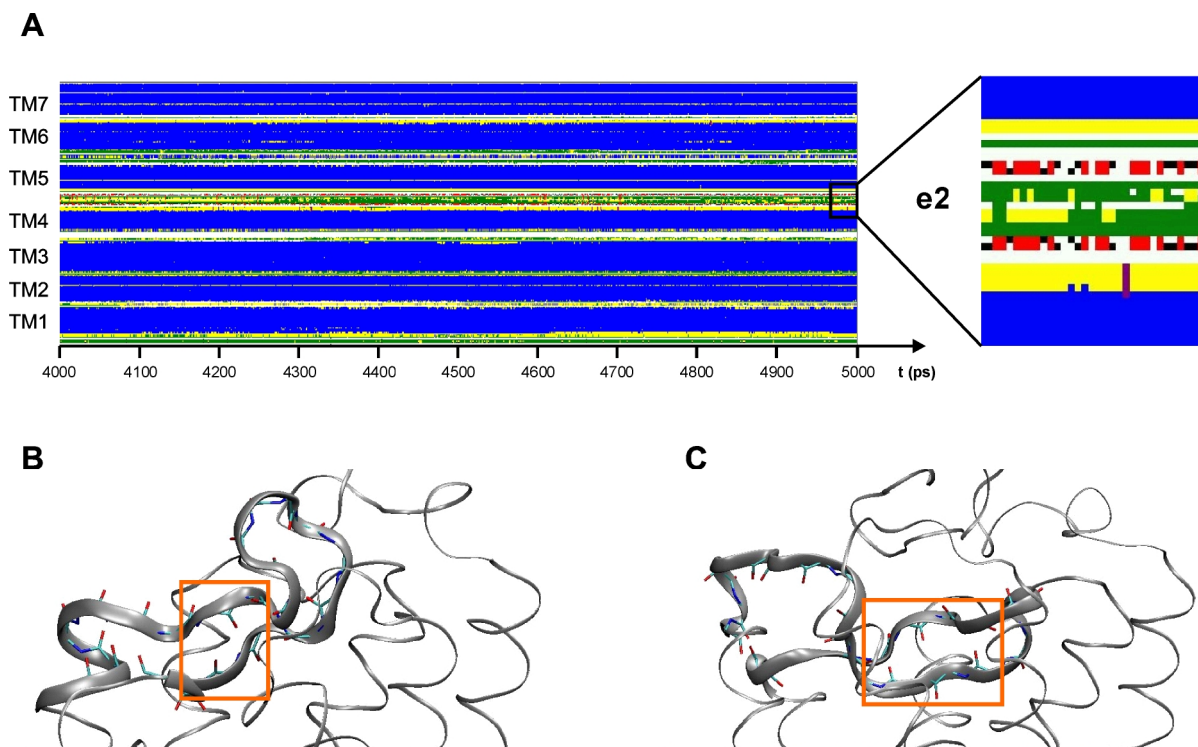


**Figure 5.8:** A, dssp-plot illustrating the dynamics of secondary structure elements of the ligand-free hH<sub>2</sub>R model during the last 1.0 ns of simulation time. Blue,  $\alpha$ -helix; red,  $\beta$ -strands; yellow, turn; green, bend; white, coil. B, backbone atoms of e2 in the hH<sub>2</sub>R model after MD simulations. Two short antiparallel  $\beta$ -strands are indicated by an orange box. C, backbone atoms of e2 in the crystal structure of bovine rhodopsin (Palczewski et al., 2000). Corresponding antiparallel  $\beta$ -strands are indicated by an orange box.

A comparison of *RMSD* values of backbone atoms in both models during MD simulations is shown in Figure 5.9. Within the first 3.0 ns, the *RMSD* of ligand-free hH<sub>2</sub>R increased and approached a constant value of  $1.88 \pm 0.06$  Å during the last 2.0 ns. By contrast, a constant *RMSD* of  $1.20 \pm 0.08$  Å was observed with hH<sub>2</sub>R-ARP during 0.5 to 3.0 ns of the simulation. The values then increased and approached a similar level as the unoccupied hH<sub>2</sub>R. Ligand-receptor interactions and, additionally, the restraints applied on the distances between Asp-98(3.32), Tyr-182(5.38), and Asp-186(5.42), respectively, and ARP reduced the flexibility of the backbone atoms in the first time period and became less essential during the following 2.0 ns.

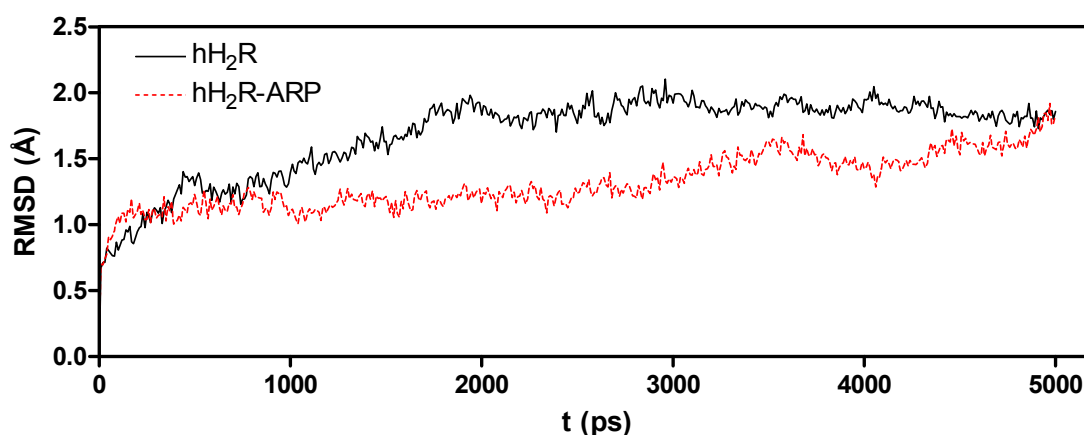


**Figure 5.9:** Trajectory of *RMSD* values of the backbones of the ligand-free and the ARP-docked hH<sub>2</sub>R models after least-square fit of all C<sub>α</sub> atoms during 5.0 ns of simulation time.

To identify differences in the flexibilities of entire protein domains, *RMSD* values of backbone atoms were calculated for the TM domains, loops, the N- and the C-terminus (Figure 5.10 A). In addition, information about flexibilities of the amino acids was obtained by computing average *RMSD* values for each residue separately (Figure 5.10 B). In both hH<sub>2</sub>R models, the TM domains were the most rigid structures. Large *RMSD* differences in the N-termini and TM1 domains coincide with considerably different spatial displacements as visualized in the energy-minimized models of the ligand-free hH<sub>2</sub>R and the hH<sub>2</sub>R-ARP complex after 3.0 ns of simulations (Figure 5.11). Whereas in the free hH<sub>2</sub>R the extracellular part of TM1 was shifted towards TM7, the intracellular parts of TM1 were similar in both models. The backbone positions of TM2 and TM3 were not significantly affected by the ligand as represented by only minor differences in the *RMSD* values. The low *RMSD* value of TM3 was due to the central course of this tilted  $\alpha$ -helix within the bundle of TM domains. In the ligand-free hH<sub>2</sub>R, TM4 was shifted in towards the lipid bilayer if compared with hH<sub>2</sub>R-ARP. The side chain of Trp-158 at the N-terminal region of e2 displayed higher flexibility in the hH<sub>2</sub>R-ARP complex than in the free receptor (Figure 5.10 B). This difference was attributed to the close proximity of this residue to the side chain of Asn-92(3.26) in the free receptor during the whole simulation. In hH<sub>2</sub>R-ARP, the side chain of Trp-158 turned away from Asn-92(3.26) and pointed into the phospholipid bilayer allowing higher conformational flexibility. The large *RMSD* differences between the e2 backbones of hH<sub>2</sub>R and hH<sub>2</sub>R-ARP (difference of 1.58 Å)

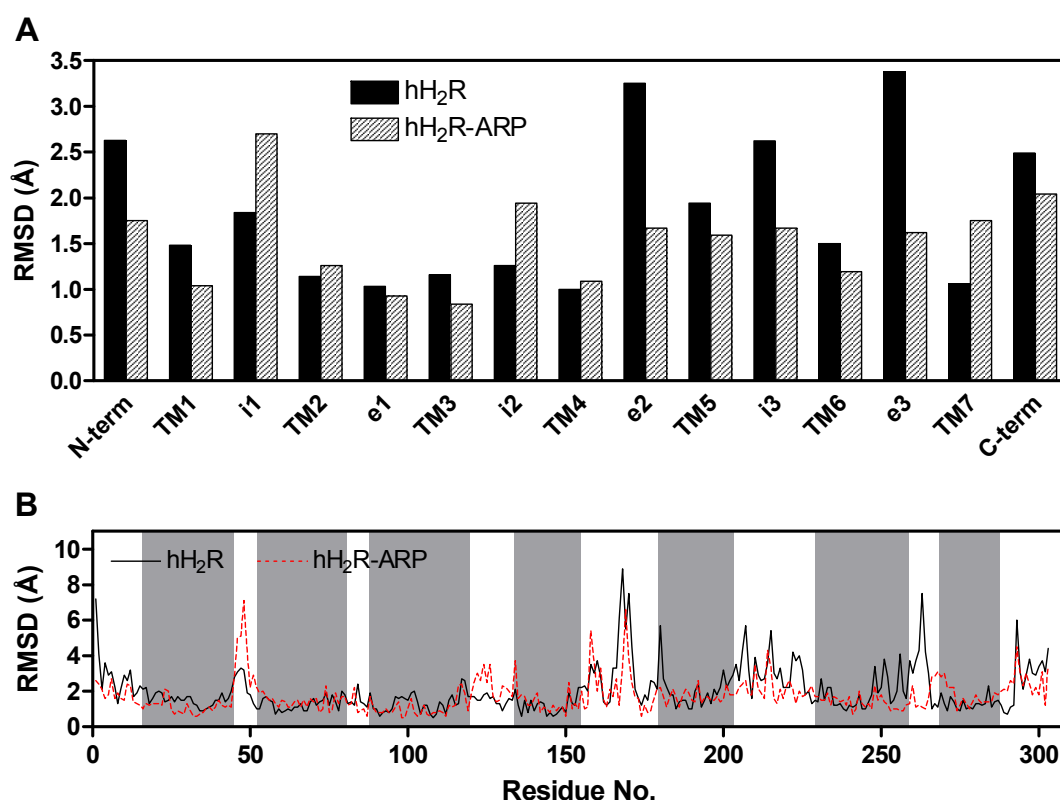


**Figure 5.10:** Domain- and residue-specific flexibility during the 3.0 to 4.0 ns simulation interval. A, Mean *RMSD* values of the backbone atoms of individual subsequences after least-square fit of all C<sub>α</sub> atoms. B, Mean *RMSD* values of all heavy atoms of each residue after least-square fit of all C<sub>α</sub> atoms. Residues within TM domains are shown as grey shading.

suggested participation of this loop in the binding mode of agonists (chapter 5.3.2.5). Asn-168, His-169, and Thr-170 formed the turn between the upper and the lower parts of e2 and exhibited very high *RMSD* values (up to 8.9 Å and 6.6 Å in the free and the hH<sub>2</sub>R-ARP models, respectively). These residues were completely solvated by the extracellular water shell and thus did not adopt distinct side chain conformations. The extracellular part of TM5 of the ligand-free receptor was shifted towards TM4, whereas the intracellular end slightly pointed out of the TM bundle, relative to the backbone position of TM5 in hH<sub>2</sub>R-ARP. Although the backbones of TM6 and the extracellular parts of TM7 adopted similar positions in both hH<sub>2</sub>R models, the flexibilities of residues in these domains were different. *RMSD* values of Phe-248(6.49), Phe-251(6.52), and Tyr-256(6.57) were considerably higher in the ligand-free hH<sub>2</sub>R (*RMSD* values of 3.4 Å, 3.8 Å, and 4.1 Å, respectively) than in the hH<sub>2</sub>R-ARP complex (*RMSD* values of 2.3 Å, 1.4 Å, and 0.9 Å, respectively). These residues are part of the conserved CWxP(F/Y) motif and pointed into the lipid environment whereas the adjacent Trp-247(6.48) and Tyr-250(6.51) belong to the ligand binding pocket. In the case of

Tyr-256(6.57) the very large *RMSD* difference was attributed to an interaction of the hydroxyl OH with the carboxyl group of Asp-263 in e3 that was stable during the entire simulation of hH<sub>2</sub>R-ARP (H-bond frequency of 93.4%). In the simulation of the ligand-free hH<sub>2</sub>R, this interaction was broken already at the beginning of the simulation (H-bond frequency of 2.8%) leading to random orientations of Tyr-256(6.57) and Asp-263. The terminal residues of e3 starting from Asn-266 and the first six residues of TM7 were considerably more flexible in the

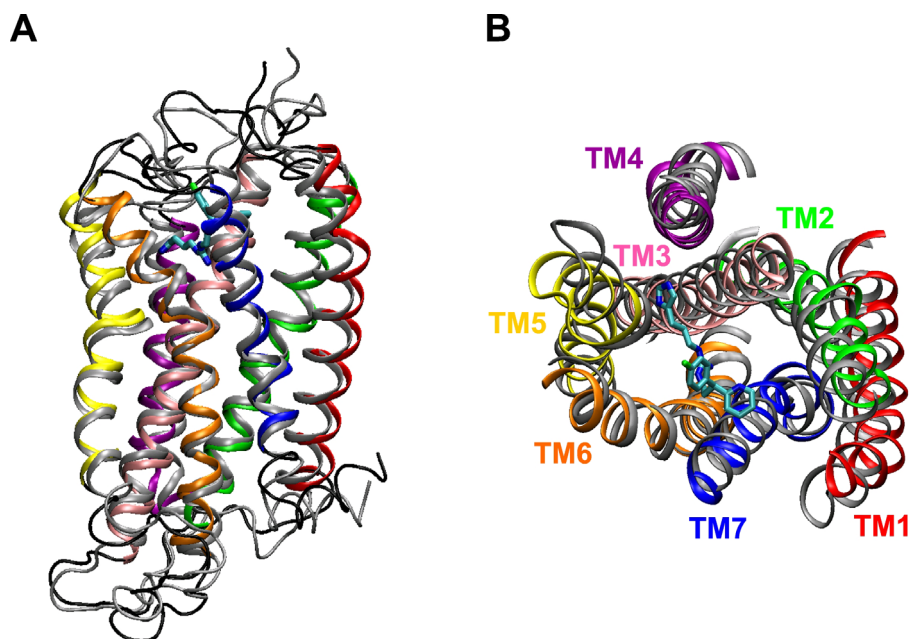


**Figure 5.11:** Comparison of the energy-minimized backbone structures of ligand-free hH<sub>2</sub>R (grey) and ARP-hH<sub>2</sub>R (colored) after 3.0 ns of MD simulations. A, side view; B, TM domains viewed from the extracellular side. Loop regions and the termini are not shown for reasons of clarity.

hH<sub>2</sub>R-ARP complex as represented by an average *RMSD* difference of 1.3 Å between the two receptors in this region. In the central part of TM7 similar *RMSD* values were observed in both models whereas the intracellular end of TM7, *i.e.* the sequence from Ile-286(7.51) to Asn-292(7.57), was more flexible in the ARP-bound receptor. The positions of the backbones of H8 were remarkably different in both receptor models. Residues in this short α-helix were solvated by the POPC head groups and water.

### 5.3.2.3 Analysis of conserved intramolecular interactions

Interactions between residues predicted to be conserved among aminergic GPCRs (chapter 4.3.1.2) were analyzed in Table 5.6. Low *RMSD* values, high H-bond frequencies, and low minimum distances between interacting residues were used as measures of the strengths of

interactions. Additional intramolecular interactions analyzed during the simulations are shown at the bottom of the list.

In the ligand-free hH<sub>2</sub>R a stable ionic interaction was observed between Asp-115(3.49) and Arg-116(3.50) of the conserved (E/D)RY motif mimicking the inactive state of the H<sub>2</sub>R (Alewijns et al., 2000). By protonating Asp-115(3.49) in the hH<sub>2</sub>R-ARP model according to an active state in GPCRs this interaction was inhibited (Figure 5.12 A). In spite of a short distance of ~3Å, the proposed ionic interaction between Arg-116(3.50) and Glu-229(6.30) in the ligand-free receptor (Bissantz, 2003) did not occur. However, the increased distance between both residues and the higher *RMSD* value of Arg-116(3.50) in the ARP-bound receptor indicated release of interhelical constraints within the intracellular ends of TM3 and TM6 which is in agreement with current concepts of GPCR activation (Bissantz, 2003). The MD simulation of the free hH<sub>2</sub>R revealed a stable interaction of Arg-228(6.29) with Asp-294(7.59). In correlation with the increased flexibility of the TM7 backbone, this hypothetical interaction was disrupted in the hH<sub>2</sub>R-ARP model. The side chains of Arg-228(6.29) and Glu-229(6.30) did not interact in both receptor models.

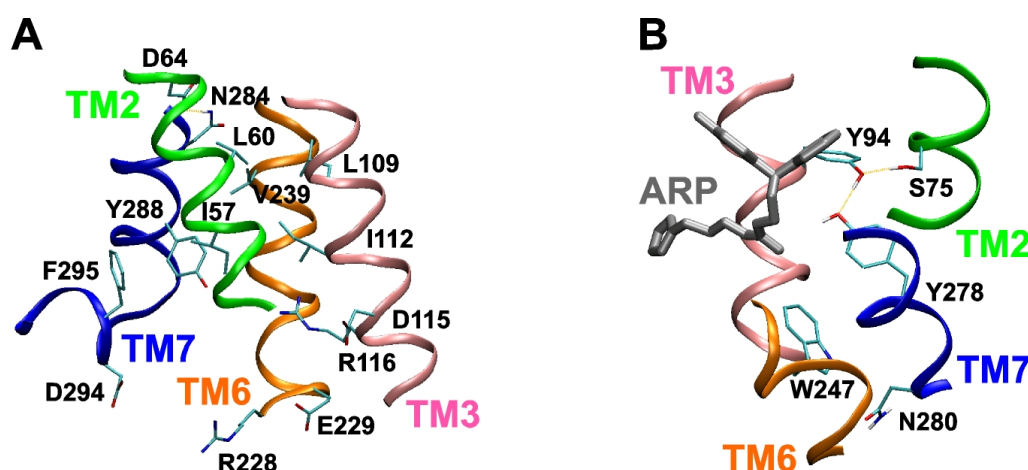


**Figure 5.12:** Arrangement of conserved residues in the hH<sub>2</sub>R-ARP complex after 3.0 ns of MD simulations (energy-minimized structure). A, intracellular parts of TM2, TM3, TM6, and TM7; B, interacting residues in the vicinity of ARP.

The conserved hydrophobic latch formed by Ile-57(2.43), Leu-60(2.46), Leu-109(3.43), Ile-112(3.46), and Val-239(6.40) adopted similar positions in the free and the liganded hH<sub>2</sub>R models. As an exception, the distance between Val-239(6.40) and Ile-57(2.43) was increased in the hH<sub>2</sub>R-ARP complex during MD simulation. An aromatic interaction between Tyr-288(7.53) and Phe-295(7.60) of the conserved NPxxY(x)<sub>5,6</sub>F motif predicted to represent the inactive state of bovine rhodopsin and other GPCRs (Fritze et al., 2003) was observed during simulation of the free hH<sub>2</sub>R. After docking of ARP, the *RMSD* value of Tyr-288(7.53)

was increased implicating disruption of this interaction, which is in agreement with the concept of a structural rearrangement after activation of bovine rhodopsin (Fritze et al., 2003). The NPxxY(x)<sub>5,6</sub>F motif also contains Asn-284(7.49). In the crystal structure of bovine rhodopsin and in the initial hH<sub>2</sub>R models (chapter 4.3.1.2) a water mediated interhelical interaction of this residue with the highly conserved Asp-64(2.50) was described. During MD simulations of both hH<sub>2</sub>R models, the H-bonds with this water molecule were lost (see chapter 5.3.2.4). Instead, the amide NH<sub>2</sub> group of Asn-284(7.49) and the carboxylate of Asp-64(2.50) underwent a stable direct interaction in the hH<sub>2</sub>R-ARP model (Figure 5.12 A) but not in the free receptor. Strikingly, this interaction was proposed to be formed during the transformation from the inactive to the active state of GPCRs (Bissantz, 2003; Lu et al., 2002) according to a series of mutational experiments with corresponding residues in the gonadotropin-releasing hormone receptor (Zhou et al., 1994), the 5-HT<sub>2A</sub> receptor (Sealfon et al., 1995), the thyrotropin-releasing hormone receptor (Perlman et al., 1997), and the tachykinin NK2 receptor (Donnelly et al., 1999). Whereas single point mutations of one of these residues disrupted receptor function, double-revertant mutants were able to restore functionality.

Trp-247(6.48) of the highly conserved CWxP(F/Y) motif in TM6 underwent a stable H-bond with Asn-280(7.45) in the ligand-free hH<sub>2</sub>R that was not present in the initial structure and did occur considerably less frequently in the hH<sub>2</sub>R-ARP complex (Figure 5.12 B). These results agree with the concept of different orientations of the side chain of Trp-247(6.48) in the inactive and the active states of the H<sub>1</sub>R (Jongejan et al., 2005) and other GPCRs (Pardo et al., 2007). Experimental support of a conformational transition of Trp(6.48) was derived from the structure of metarhodopsin I by electron crystallography (Ruprecht et al., 2004).

In the crystal structure of bovine rhodopsin, Glu-113(3.28) forms the counter-ion to the protonated Schiff-base of retinal and Lys-296(7.43) (Palczewski et al., 2000). The side chains of the corresponding H<sub>2</sub>R residues Tyr-94(3.28) and Tyr-278(7.43) interacted more frequently in hH<sub>2</sub>R-ARP than in the free receptor. Additionally, a stable H-bond was detected between the hydroxyl groups of Tyr-94(3.28) and Ser-75(2.61) in the hH<sub>2</sub>R-ARP complex but not in the free hH<sub>2</sub>R where instead of that the OH group of Ser-75(2.61) served as donor for the hydroxyl oxygen of Tyr-278(7.43).



**Table 5.6:** Analysis of important intramolecular interactions in the models of the ligand-free and the ARP-docked hH<sub>2</sub>R during 5.0 ns of MD simulations.

Residues	hH <sub>2</sub> R			hH <sub>2</sub> R-ARP		
	<i>RMSD</i> (Å) <sup>a</sup>	H-bond (%) <sup>b</sup>	Min. distance (Å) <sup>c</sup>	<i>RMSD</i> (Å) <sup>a</sup>	H-bond (%) <sup>b</sup>	Min. distance (Å) <sup>c</sup>
N36(1.50)-T32(1.46)	1.0; 1.3	68.5	1.97 ± 0.17	1.0; 0.6	36.6	2.08 ± 0.22
N36(1.50)-D64(2.50)	1.0; 1.1	< 1	3.14 ± 0.29	1.0; 1.4	< 1	2.83 ± 0.47
N36(1.50)-S281(7.46)	1.0; 1.3	28.7	2.36 ± 0.32	1.0; 1.5	60.2	2.16 ± 0.29
I57(2.43)-L60(2.46)	1.4; 0.8	vdW	3.12 ± 0.26	1.6; 1.5	vdW	3.15 ± 0.27
I57(2.43)-V239(6.40)	1.4; 0.9	vdW	5.87 ± 1.02	1.6; 1.2	vdW	8.64 ± 0.89
S59(2.45)-W143(4.50)	1.0; 1.3	57.2	2.25 ± 0.39	1.1; 1.1	55.6	2.29 ± 0.33
L60(2.46)-L109(3.43)	0.8; 0.7	vdW	3.91 ± 0.29	1.5; 0.8	vdW	4.32 ± 0.49
Y94(3.28)-Y278(7.43)	0.8; 1.1	12.6	2.80 ± 0.49	0.8; 1.0	79.6	2.00 ± 0.36
L109(3.43)-I112(3.46)	0.7; 0.7	vdW	3.11 ± 0.27	0.8; 0.6	vdW	3.16 ± 0.30
L109(3.43)-V239(6.40)	0.7; 0.9	vdW	4.25 ± 0.45	0.8; 1.2	vdW	3.80 ± 0.27
D115(3.49)-R116(3.50)	1.2; 1.2	79.4	n.a.	1.3; 2.3	< 1	n.a.
R116(3.50)-E229(6.30)	1.2; 1.5	< 1	2.97 ± 0.49	2.3; 1.7	< 1	3.56 ± 0.35
W247(6.48)-N280(7.45)	1.8; 1.3	52.7	2.06 ± 0.22	1.0; 1.8	5.8	2.74 ± 0.45
Y288(7.53)-F295(7.60)	1.2; 2.1	vdW	3.13 ± 0.56	2.0; 2.3	vdW	2.84 ± 0.32
A289(7.54)-R296(7.61)	0.8; 2.9	2.6	3.43 ± 1.00	2.1; 3.0	4.2	3.12 ± 0.29
A290(7.55)-R296(7.61)	0.7; 2.9	3.5	3.68 ± 1.25	2.0; 3.0	1.4	3.80 ± 0.83
<b>Additional interactions:</b>						
D64(2.50)-N284(7.49)	1.1; 2.3	16.2	3.86 ± 0.93	1.4; 1.4	81.6	2.35 ± 0.78
S75(2.61)-Y94(3.28)	1.2; 0.8	9.4	1.77 ± 0.19	0.8; 0.8	93.2	1.90 ± 0.26
S75(2.61)-Y278(7.43)	1.2; 1.1	68.6	1.94 ± 0.43	0.8; 1.0	< 1	2.89 ± 0.44
R228(6.29)-E229(6.30)	1.3; 1.5	< 1	n.a.	2.3; 1.7	< 1	n.a.
R228(6.29)-D294(7.59)	1.3; 3.1	77.1	2.42 ± 0.65	2.3; 3.1	9.4	5.19 ± 1.97

<sup>a</sup> *RMSD* mean values of single residues after least-square fit of all C<sub>α</sub>-atoms during 3.0 to 4.0 ns of simulation time.

<sup>b</sup> frequency of the presence of H-bonds between selected residues during 5.0 ns of simulation time. vdW, van der Waals interaction

<sup>c</sup> mean ± S.D. of the distance between the nearest atoms of selected residues during 5.0 ns of simulation time. n.a., not applicable, since both residues are consecutive.

#### 5.3.2.4 Internal water molecules

The frequency of H-bonds between residues and five internal water molecules predicted to be conserved and structurally important in class 1 GPCRs (Okada et al., 2002) were investigated (Table 5.7). Whereas an H-bond of Wat1a with Asp-64(2.50) was stable in both models during 5.0 ns, interactions of this water molecule with Ser-105(3.39) and



Leu-101(3.35) were reduced and lost, respectively. In the case of hH<sub>2</sub>R-ARP but not the free receptor, an additional water molecule interacted with the OH hydrogen of Ser-105(3.39). In both systems, interactions of Wat1b with Asn-280(7.45) and Asn-284(7.49) were lost and replaced by stable H-bonds with Asn-36(1.50) (H-bond frequencies of 91.4% and 66.6% in hH<sub>2</sub>R and hH<sub>2</sub>R-ARP, respectively). Interactions of Wat1b with Asp-64(2.50) were stable in both models. In the model of the ligand-free hH<sub>2</sub>R, Wat1c interacted with Asn-284(7.49) and, substituting for the absent H-bond with Val-239(6.40), with Asp-64(2.50) (H-bond frequency of 94.8%). In the hH<sub>2</sub>R-ARP model, this water molecule diffused into the water shell. Overall, at the interface between TM2, TM3, TM6, and TM7 two additional water molecules not present in the starting structure were observed during simulations of the ligand-free hH<sub>2</sub>R. These water molecules were located in the centre of the TM domains nearby the empty binding pocket that, by itself, was filled with 18 water molecules. By contrast, in the hH<sub>2</sub>R-ARP complex four additional water molecules were located at the intracellular ends of these TMs, presumably due to the increased flexibility of TM7. Wat3 strongly interacted with Cys-246(6.47), Tyr-250(6.51), and Val-273(7.38) in the free receptor. In hH<sub>2</sub>R-ARP, the corresponding H-bond frequencies were reduced. In both models, Wat4 moved into the water shell.

**Table 5.7:** Interactions of the hH<sub>2</sub>R with five internal water molecules during 5.0 ns of simulation time. Water molecules are named after corresponding water molecules in the crystal structure of bovine rhodopsin (pdb entry 1L9H) (Okada et al., 2002).

Water	Residue	hH <sub>2</sub> R	hH <sub>2</sub> R-ARP
H-bond (%) <sup>a</sup>			
Wat1a	D64(2.50)	86.8	82.4
	L101(3.35)	3	< 1
	S105(3.39)	12.1	29.0
Wat1b	D64(2.50)	83.1	72.0
	N280(7.45)	< 1	< 1
	N284(7.49)	< 1	< 1
Wat1c	V239(6.40)	< 1	-
	N284(7.49)	62.7	-
Wat3	C246(6.47)	98.3	38.0
	Y250(6.51)	97.2	41.0
	V273(7.38)	92.2	49.8
Wat4	D54(2.40)	-	-
	Y288(7.53)	-	-

<sup>a</sup> frequency of the presence of H-bonds between selected residues during 5.0 ns of simulation time.

### 5.3.2.5 Interactions of ARP with the hH<sub>2</sub>R binding pocket

To provide an improved model of the binding mode of ARP and related guanidine-type H<sub>2</sub>R agonists, residues were selected facing ARP most frequently during MD simulations. Every time-step of the simulation, residues holding a distance of less than 5 Å from the centre of mass of each ARP substructure were collected. Only residues meeting this distance criterion in more than 10% of all snapshots registered during 5.0 ns were considered to participate in binding ARP (Table 5.8).

In addition to the enforced interactions of Tyr-182(5.38), Asp-186(5.42), and Asp-98(3.32) with the imidazolylpropylguanidine moiety of ARP, also other residues frequently facing ARP were identical with the binding residues in the starting homology model (Figure 4.7 in chapter 4.3.2.1). Most of these residues were less flexible than in the ligand-free receptor, thus indicating stable interactions. The increased *RMSD* values of residues in TM7 were due to the high flexibility of this helix backbone (Figure 5.10). Val-176 in e2 and Trp-275(7.40) were approximately 4 to 5 Å distant from ARP and achieved the contact criterion with an incidence of less than 50%. Additional residues exposed to the binding crevice during the simulation that have not been considered in the previous H<sub>2</sub>R models will be explicitly characterized (Figure 5.13).

The imidazolyl group of ARP was in close proximity to Ser-153(4.60) and Thr-95(3.29), both selectively interacting when ARP was bound (frequency of 90% in the ARP-docked hH<sub>2</sub>R; no interaction in the ligand-free hH<sub>2</sub>R), and Val-99(3.33). By analogy, residues at position 3.29 may participate in the binding modes of the M<sub>1</sub> acetylcholine (Lu and Hulme, 1999) and the dopamine D<sub>4</sub> receptors (Schetz et al., 2000). Val-115(3.33) was shown to be part of the binding crevice of the dopamine D<sub>2</sub> receptor (Javitch et al., 1995a). The highly conserved Phe-191(5.47) (70% conservation among class 1 GPCRs) (Mirzadegan et al., 2003), one helical turn below Asp-186(5.42), was exposed to the binding site during the simulation. Phe(5.47) is known to be part of the binding sites of the dopamine D<sub>2</sub>R (Javitch et al., 1995b) and the 5-HT<sub>2A</sub> receptor (Shapiro et al., 2000).

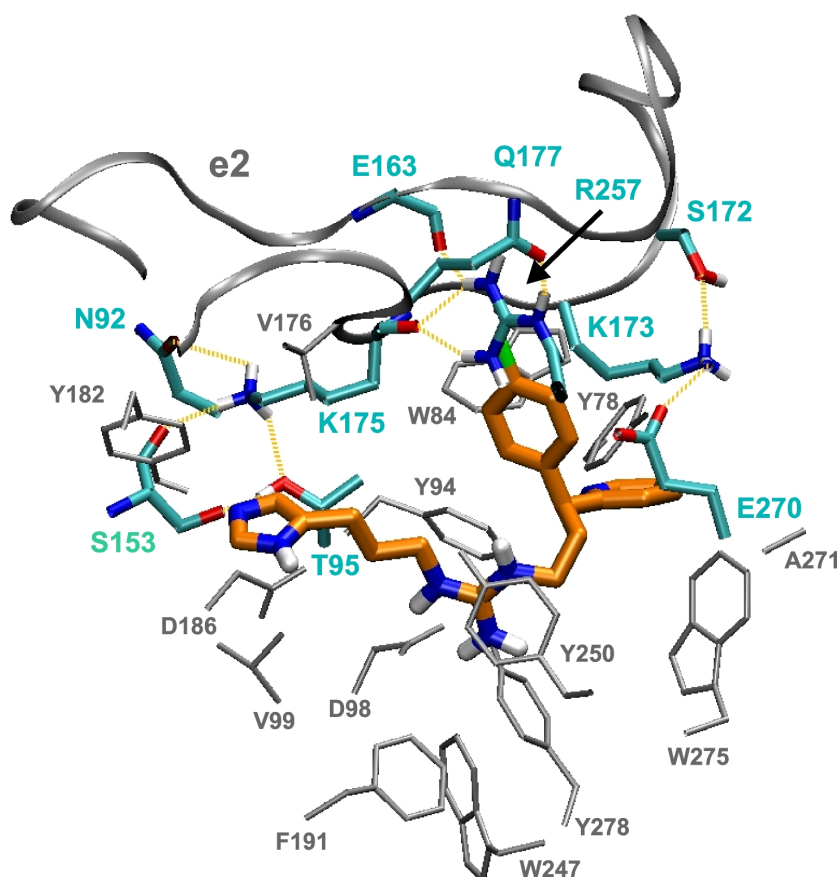


**Figure 5.13:** Side-view into the binding pocket of the hH<sub>2</sub>R in complex with ARP after 3.0 ns of MD simulations (energy-minimized structure). Carbon atoms of residues forming distinct intramolecular interactions are shown in cyan. Remaining residues participating in binding ARP are shown in grey. The backbone of e2 is shown as grey ribbon.

In a previous model of the gpH<sub>2</sub>R, the basic guanidine group of Arg-257(6.58) was proposed to interact with a partially negatively charged substituent at the "upper" phenyl ring of diarylalkylguanidines, potentially stabilized by the carboxylate function of Glu-270(7.35) (Kelley et al., 2001; Dove et al., 2004). However, during 5.0 ns of simulation a direct interaction between Arg-257(6.58) and ARP did not occur. In the ligand-free hH<sub>2</sub>R model, the charged side chains of Arg-257(6.58) and Glu-270(7.35) interacted with an incidence of 39%. The positioning of the 4-F-phenyl group of ARP inhibited this interaction. Alternatively, in the hH<sub>2</sub>R-ARP complex Arg-257(6.58) formed H-bonds to the side chain oxygen of Gln-177 (H-bond frequency of 22%) and the backbone oxygens of Glu-163 (35%) and Lys-175 (79%), all of them located in e2. The side chain of Glu-270(7.35) was solvated by a cluster of water molecules and adopted greater flexibility as represented by the high *RMSD* value. Trp-84 in e1 was identified to be in close contact with the 2-pyridyl and the 4-F-phenyl moieties of ARP during the whole simulation as a much lower *RMSD* value was calculated for this residue

when the ligand was bound compared to the free receptor.

Ser-165 and the four consecutive residues Lys-173, Cys-174, Lys-175, and Val-176 in the lower leaflet of e2 formed the top of the ARP binding pocket. Whereas in the starting model of the hH<sub>2</sub>R-ARP complex, Lys-175 pointed towards the imidazolylpropylguanidine moiety, the amino group of this residue did not face the ligand in the simulated system but interacted with the backbone-O of Ser-153(4.60) (frequency of 85%), with the OH group of Thr-95(3.29) (21%), and with the side chain O of Asn-92(3.26) (frequency of 2%) or a water molecule. The primary amine of Lys-173 interacted with the side chain O of Ser-172 (frequency of 50%) and less frequently with the carboxylate group of Glu-270(7.35) (frequency of 24%) and with solvent molecules from the surrounding water shell.

**Table 5.8:** Analysis of residues facing ARP most frequently during 5.0 ns of simulation time.

ARP substructure	Residue	Contacts (%) <sup>a</sup>	Min. dist. (Å) <sup>b</sup>	hH <sub>2</sub> R RMSD (Å) <sup>c</sup>	hH <sub>2</sub> R-ARP RMSD (Å) <sup>c</sup>
imidazolyl	Y182(5.38)	100	1.9 ± 0.2	2.2	(1.1)
imidazolyl	D186(5.42)	100	2.3 ± 0.3	1.4	(1.1)
imidazolyl, Im-propyl <sup>d</sup>	T95(3.29)	100	3.6 ± 0.2	1.0	0.8
imidazolyl	V99(3.33)	100	3.3 ± 0.2	1.6	0.5
imidazolyl	S153(4.60)	100	2.1 ± 0.3	1.2	1.3
imidazolyl, 4-F-C <sub>6</sub> H <sub>4</sub>	K175(e2)	86	3.2 ± 0.3	1.8	1.2
imidazolyl	V176(e2)	25	4.9 ± 0.4	1.5	0.8
imidazolyl	T190(5.46)	16	3.9 ± 0.4	1.0	1.5
Im-propyl <sup>d</sup>	Y250(6.51)	100	2.9 ± 0.2	2.2	1.8
guanidine	D98(3.32)	100	2.2 ± 0.4	1.7	(0.5)
guanidine	W247(6.48)	100	2.7 ± 0.4	1.8	1.0
guanidine	Y278(7.43)	69	3.6 ± 0.8	1.1	1.0
guanidine	F191(5.47)	25	4.3 ± 1.0	2.0	1.4
Ar <sub>2</sub> -propyl <sup>e</sup> , guanidine	L274(7.39)	100	3.3 ± 0.2	1.0	0.9
Ar <sub>2</sub> -propyl <sup>e</sup>	V273(7.38)	33	4.3 ± 0.4	1.4	2.2
2-pyridyl	Y78(2.64)	100	2.9 ± 0.2	0.9	1.3
2-pyridyl, 4-F-C <sub>6</sub> H <sub>4</sub>	E270(7.35)	100	3.2 ± 0.2	1.3	3.0
2-pyridyl, 4-F-C <sub>6</sub> H <sub>4</sub>	K173(e2)	100	3.4 ± 0.2	1.6	1.6
2-pyridyl, 4-F-C <sub>6</sub> H <sub>4</sub>	W84(e1)	98	3.1 ± 0.3	2.4	0.8
2-pyridyl	Y94(3.28)	82	3.6 ± 0.4	0.8	0.8
2-pyridyl	A271(7.36)	55	3.8 ± 0.2	0.9	2.2
2-pyridyl	W275(7.40)	33	4.1 ± 0.5	0.9	1.2
4-F-C <sub>6</sub> H <sub>4</sub>	R257(6.58)	100	2.8 ± 0.3	2.0	0.9
4-F-C <sub>6</sub> H <sub>4</sub>	C174(e2)	88	3.5 ± 0.3	1.2	0.6
4-F-C <sub>6</sub> H <sub>4</sub>	S165(e2)	80	3.7 ± 0.4	3.3	1.7

<sup>a</sup> Frequency of contacts between substructures of ARP with residues in the hH<sub>2</sub>R binding pocket. Every 10 ps during 5.0 ns simulation time, residues exhibiting a minimum distance of less than 5 Å relative to each ARP-substructure were collected. Only residues facing ARP in more than 10% of all snapshots were considered.

<sup>b</sup> mean ± S.D. of the distance between the nearest atoms of selected residues and ARP during 5.0 ns of simulation time.

<sup>c</sup> RMSD mean values of residues after least-square fit of all C<sub>α</sub>-atoms during 3.0 to 4.0 ns of simulation time. Values shown in brackets were biased due to the application of distance restraints (chapter 5.3.2).

<sup>d</sup> propyl group connecting the imidazolyl with the guanidine moiety of ARP

<sup>e</sup> propyl group connecting the guanidine with the 4-fluorophenyl group and the pyridin-2-yl moiety of ARP.

## 5.4 Discussion

### 5.4.1 Setup of the simulation system

Depending on the methodology of generating a model system containing protein and lipid, the starting conditions for equilibration and subsequent MD simulations are considerably different and need to be adjusted individually (Kandt et al., 2007). In this study, the POPC bilayer was assembled around a pre-defined surface of the hH<sub>2</sub>R homology model and was subsequently solvated by water molecules with explicit consideration of counter ions. Due to the low density in this setup, adaptation of the box volume was necessary, rendering the *NPT* ensemble type to be useful for the simulations. This is in agreement with previous MD simulations of a hydrated dipalmitoylphosphatidylcholine bilayer showing that application of the *NPT* ensemble allows a system to adjust the box sizes so that the internal virial matches the externally applied pressure. Accordingly, with this method only an approximation of the initial box size is needed because the system finds its size by itself, based on the force field (Tieleman and Berendsen, 1996). By contrast, with the *NVT* ensemble these volume corrections could not take place, leading to severe disruptions of the membrane structure mainly in the middle of the bilayer (which is most compressible).

Generally, in an *NPT* system the pressure can be coupled isotropically, semi-isotropically, and anisotropically. Kandt et al. claimed that application of isotropic pressure coupling is inappropriate for membrane simulations, since due to the proportional box scaling in this system only very small changes in the size are possible (Kandt et al., 2007). Nevertheless, this type of pressure coupling was successfully used for MD simulations of GPCRs embedded in hydrated lipid bilayers (Schlegel et al., 2005; Iadanza et al., 2002; Salo et al., 2004). Semi-isotropic and anisotropic pressure couplings allow surface area fluctuations of the bilayer and were recommended for membrane protein simulations (Kandt et al., 2007). However, under anisotropic conditions no coupling between any of the directions of pressure contributions takes place which can lead to large deformations of the whole simulation system.

For a structural analysis of the POPC bilayer using systems with various types of pressure coupling, calculation of the  $S_{CD}$  order parameter proved to be the most sensitive parameter. Using anisotropic conditions experimental order parameters of POPC carbon atoms in the  $L_{\alpha}$ -phase were approximated best. A characteristic reduction of the absolute  $S_{CD}$  values caused by the double bond of the *sn*-2 chain was more pronounced during 5.0 ns simulation compared to the preceding 500 ps of equilibration time which was due to relatively large time-scales processes of lipid bilayer dynamics (e.g. lipid diffusion and rotational

reorientation) need to occur (Anezo et al., 2003). Adjustment of the proper bilayer size turned out to be the most critical parameter when simulating with constant pressure since the scaling of the box vectors always caused a reduction of the bilayer thickness. Thus, during the simulations, the lipophilic bilayer core was by ~2-3 Å smaller than the proposed value of 24 Å (Baldwin et al., 1997). However, charged residues at both margins of the hH<sub>2</sub>R TM domains were mainly surrounded by the ionic phosphatidylcholine head groups, reflecting an appropriate positioning of the hH<sub>2</sub>R surface between the complex lipophilic-ionic-water interface of the membrane (Kandt et al., 2007).

### 5.4.2 Application of restraints on protein atoms during MD simulations

The TM domains of bovine rhodopsin contain several deviations from pure  $\alpha$ -helical structures that were predicted to be conserved among class 1 GPCRs (Ballesteros et al., 2001). Studying the dynamics of GPCRs, such helix irregularities can induce severe perturbations of secondary structural elements. For example, TM7 of bovine rhodopsin exhibits irregular helicity, mainly around Lys-296(7.43) to which retinal is covalently attached (Palczewski et al., 2000). According to the concept of structural mimicry it was suggested that the structure of TM7 in class 1 GPCRs that lack this interaction is similar to that of rhodopsin (Ballesteros et al., 2001). Performing MD simulations of the hH<sub>2</sub>R, the backbone of TM7 was only stable when positional restraints were applied on the protein backbone atoms that were successively released during the equilibration. Similarly, TM5 of rhodopsin contains an unusual kink around the non-conserved His-211(5.46), presumably due to an interaction with Glu-122(3.37). Strikingly, amino acid position 5.46 is located one helical turn below 5.42 facing the binding site crevice in aminergic GPCRs, and this unusual kink was predicted to be necessary to allow for an interaction of residue 5.42 with endogenous ligands (Ballesteros et al., 2001). In the simulation of the hH<sub>2</sub>R, both stability in the secondary structure of TM5 and stable interactions of Tyr-182(5.38) and Asp-186(5.42) with the imidazolyl group of ARP were only achieved when the distances of interacting atoms were restrained.

### 5.4.3 Characterization of the ligand-free and the ARP-bound hH<sub>2</sub>R models

During MD simulations of the ligand-free and the ARP-bound hH<sub>2</sub>R, the C-terminus of TM7 and the following short helix H8 were highly flexible and adopted different positions. By analogy, great mobility of the rhodopsin C-terminus including H8 was demonstrated by large B-factors in the crystal structure (Palczewski et al., 2000) as well as in NMR, spin-labelling, and further structural studies (Klein-Seetharamna et al., 2002; Langen et al., 1999; Cai et al., 1999; Altenbach et al., 2001; Altenbach et al., 1999; reviewed in Klein-Seetharaman, 2002

and Hubbell et al., 2003). MD simulations of rhodopsin were able to reproduce these observations (Crozier et al., 2003; Huber et al., 2004). In this respect, the high *RMSD* values of the corresponding domains in both hH<sub>2</sub>R systems agree very well with experimental data. Moreover, mutagenesis studies of specific amino acids in rhodopsin have shown the involvement of i2, i3, and the C-terminus in binding and activating transducin (Franke et al., 1990; Franke et al., 1992; Marin et al., 2000; Ernst et al., 2000; Fahmy et al., 2000), and Krishna et al. concluded that H8 acts as a membrane-dependent conformational switch domain upon photoactivation of rhodopsin (Krishna et al., 2002). Thus it may be possible that differential orientations of corresponding domains in the ARP-bound hH<sub>2</sub>R indeed represent an approximation to the active conformation being more susceptible for interacting with a G<sub>s</sub> protein. Results from our MD simulations clearly coinciding with current concepts of a common mechanism of GPCR activation (Bissantz, 2003) are the higher abundance of an H-bond between Asn-284(7.49) and Asp-64(2.50) and the loss of an aromatic interaction between Tyr-288(7.53) and Phe-295(7.60) in the ARP-bound receptor.

Activation of GPCRs is supposed to include a counterclockwise rotation of TM6 when viewed from the extracellular side and an outward movement of the cytoplasmic end of TM6 away from TM3 (Visiers et al., 2002; Bissantz, 2003). Upon this movement, the ionic lock between Asp(3.49) and Arg(3.50) of the conserved (E/D)RY motif and Glu(6.30) at the intracellular ends of TM3 and TM6 is proposed to be disrupted. This process is presumably supported by a proton uptake of Asp(3.49) (Ghanouni et al., 2000). During 5.0 ns of MD simulation no such large-scale movements of TM6 occurred in the hH<sub>2</sub>R-ARP model and were actually not expected to be observed since receptor activation after binding of a diffusible ligand follows rather slow kinetics including discrete intermediate conformational states (Swaminath et al., 2004). By analogy, meta I to meta II transition of rhodopsin upon photoactivation occurs in a millisecond time scale which is longer than usual computer simulations (Palczewski, 2006). However, as was shown for a simulation of rhodopsin in a dark-adapted state, MD simulation with agonists may simulate early events of activation (Crozier et al., 2003). In this respect, our MD simulation of hH<sub>2</sub>R-ARP starting from the inactive state of the receptor should represent perturbations necessary for the transition towards the active conformation. Thus, both longer simulation time and application of specific restraints on atoms enforcing the expected conformational changes would be required. MD simulations of the liganded hH<sub>2</sub>R however did agree with the concepts of an activated GPCR in that none of the residues Asp-115(3.49), Arg-116(3.50), and Glu-229(6.30) underwent directed interactions with other residues. The adjacent Arg-228(6.29) interacted with Asp-294(7.59) only in the free hH<sub>2</sub>R but pointed into the intracellular water shell when ARP was present. From these results it is not possible to conclude the impact of the non-conserved Arg-228(6.29) on differences in the constitutive activities of H<sub>2</sub>R species isoforms (chapters 4.3.1.2 and 7.4.1). Experimental



investigations, e.g. by mutagenesis studies are required. H-bond interactions between Trp-247(6.48) of the CWxP(F/Y) motif and Asn-280(7.45) selectively occurring in the ligand-free hH<sub>2</sub>R were also consistent with current concepts on receptor activation (Pardo et al., 2007).

Five internal water molecules in the crystal structure of bovine rhodopsin were predicted to have a functional role in class 1 GPCRs (Okada et al., 2002). In the dynamic models of the ligand-free and the ARP-bound hH<sub>2</sub>R, one and two of these molecules, respectively, dissociated into the surrounding water shell whereas the other water molecules stably remained at their positions. In return, additional water molecules entered the protein interior, depending on the presence of cavities (empty binding pocket of the unliganded hH<sub>2</sub>R) and the flexibility of TM domains and loops at the intracellular side (hH<sub>2</sub>R-ARP). Influx of water from the bulk was observed in previous MD simulations (Huber et al., 2004; Röhrig et al., 2002). Since these water molecules are in contact with polar residues, the possibility of a polar pathway through the rhodopsin protein was discussed (Huber et al., 2004).

#### 5.4.4 Dynamic model of the hH<sub>2</sub>R binding site for guanidine-type agonists

ARP is a potent and efficacious H<sub>2</sub>R agonist at the guinea-pig right atrium (Buschauer, 1989) and in a steady-state GTPase activity assay at H<sub>2</sub>R-G<sub>sαS</sub> fusion proteins (chapter 7.3.2). In this study, ARP was selected as a reference compound to study the binding mode of H<sub>2</sub>R agonistic diarylalkylguanidines at the hH<sub>2</sub>R. Since the initial models of hH<sub>2</sub>R and gpH<sub>2</sub>R (chapter 4.3.1) were energy-minimized conformations derived from the crystal structure of rhodopsin, these can only be considered as first approximations to H<sub>2</sub>R conformations that exist under physiological conditions. Although these initial models provided striking evidence about differences in the interactions of guanidine-type agonists with human and guinea pig H<sub>2</sub>R species isoforms that were confirmed experimentally (Kelley et al., 2001; chapter 8), a more realistic model for the H<sub>2</sub>R agonist binding site was expected to be provided by MD simulations. The probability of interactions to occur between distinct residues and pre-defined ARP-substructures were estimated by calculating the frequencies of close contacts, minimum distances between proximal partners, and *RMSD* values of the residues.

Apart from residues that were included in the previous model of the hH<sub>2</sub>R binding pocket, eight additional amino acids residing in e1, TM3, TM4, e2, TM5, and TM7 exhibited close contacts with ARP. Arg-257(6.58) and Glu-270(7.35) that were suggested to constitute a network of electrostatic interactions with a partially negatively charged substituent in *p*-position of the upper phenyl ring (Dove et al., 2004) underwent alternative interactions with residues in e2 during the simulation. In addition, in the binding pocket networks of H-bond interactions between Tyr-94(3.28), Tyr-278(7.43), and Ser-75(2.61) and between

Ser-153(4.60) and Thr-95(3.29) were selectively formed in the ARP-bound hH<sub>2</sub>R model. Possibly, these interactions are critical for the shape of the binding pocket and hence for the fit of agonists.

The top of the ARP binding pocket was formed by the backbone of the sequence from Lys-173 to Val-176 in the lower leaflet of e2 including Cys-174 that is covalently bound to Cys-91(3.25) via a disulfide bond. The side chains of Lys-173 and Lys-175 were in contact with adjacent residues in e2, the ends of TM3 and TM7, and with surrounding water molecules, and did not directly interact with ARP as was proposed from the previous hH<sub>2</sub>R model. hH<sub>2</sub>R point mutations of Lys-173 to Ala and Lys-175 to Ala were generated and pharmacologically characterized (chapter 9). With these mutants the efficacies and potencies of H<sub>2</sub>R agonists did not significantly differ from the corresponding data of the wild-type hH<sub>2</sub>R further corroborating that both residues do not directly face the H<sub>2</sub>R binding pocket.

In the dynamic model of the ligand-free hH<sub>2</sub>R two short antiparallel  $\beta$ -strands were formed in e2 similar to those that were observed in the crystal structure of bovine rhodopsin (Palczewski et al., 2000). Possibly these  $\beta$ -strands represent a functional microdomain enabled by structural mimicry (Ballesteros et al., 2001), and may also be present in other rhodopsin-like GPCRs. However, major differences between both e2 loop structures become apparent when comparing *RMSD* values of e2 from our MD simulation with corresponding data of an MD simulation of rhodopsin (Huber et al., 2004). Strikingly, the e2 loop of hH<sub>2</sub>R was much more flexible than that of rhodopsin when compared with the flexibilities of the respective TM domains and intracellular segments. The N-terminus of the rhodopsin sequence is by 19 amino acids longer than the N-terminus of the H<sub>2</sub>R sequence and contains two  $\beta$ -strands that are in close proximity to e2 in contrast to the spatial arrangement of e2 in hH<sub>2</sub>R that was mainly solvated by water molecules. Since the N-termini and the extracellular loops of rhodopsin and other class 1 GPCRs show rather low sequence homology, structure and dynamics of the e2 loops may generally be different.

### 5.4.5 Conclusion

3D-structure models of the hH<sub>2</sub>R in an unliganded and an agonist-bound state were studied by means of MD simulations with explicit consideration of the membrane and water. Boundary conditions were selected and optimized to reliably simulate a POPC bilayer in the fluid phase. The simulations with hH<sub>2</sub>R in complex with ARP did not reproduce large-scale movements of entire domains as were predicted to occur during a common GPCR activation process. The reason for this limitation is the relatively long time such rigid-body motions need to occur. Formation and breakage of distinct interactions dependent on the presence or absence of ARP in the hH<sub>2</sub>R binding pocket were in good agreement with experimental data

and previous computational studies. Therefore the ARP-bound hH<sub>2</sub>R model is proposed to represent perturbations, occurring in a nanosecond timescale after binding of agonists, that are necessary for the transition towards the active conformation.

The results of our MD simulations help on further refining dynamic models of the binding mode of guanidine-type agonists. They form a basis for pharmacological experiments with wild-type and mutant H<sub>2</sub>R species isoforms to improve our concepts about H<sub>2</sub>R and GPCR function in general on a molecular level.

## 5.5 References

- Albert AD, Young JE and Yeagle PL (1996) Rhodopsin-cholesterol interactions in bovine rod outer segment disk membranes. *Biochim Biophys Acta* **1285**:47-55.
- Alewijnse AE, Timmerman H, Jacobs EH, Smit MJ, Roovers E, Cotecchia S and Leurs R (2000) The effect of mutations in the DRY motif on the constitutive activity and structural instability of the histamine H<sub>2</sub> receptor. *Mol Pharmacol* **57**:890-898.
- Altenbach C, Cai K, Khorana HG and Hubbell WL (1999) Structural features and light-dependent changes in the sequence 306-322 extending from helix VII to the palmitoylation sites in rhodopsin: a site-directed spin-labeling study. *Biochemistry* **38**:7931-7937.
- Altenbach C, Klein-Seetharaman J, Cai K, Khorana HG and Hubbell WL (2001) Structure and function in rhodopsin: mapping light-dependent changes in distance between residue 316 in helix 8 and residues in the sequence 60-75, covering the cytoplasmic end of helices TM1 and TM2 and their connection loop CL1. *Biochemistry* **40**:15493-15500.
- Anezo C, de Vries AH, Hölting H-D, Tieleman DP and Marrink S-J (2003) Methodological issues in lipid bilayer simulations. *J Phys Chem B* **107**:9424-9433.
- Ash WL, Zlomislic MR, Oloo EO and Tieleman DP (2004) Computer simulations of membrane proteins. *Biochim Biophys Acta* **1666**:158-189.
- Baldwin JM, Schertler GF and Unger VM (1997) An alpha-carbon template for the transmembrane helices in the rhodopsin family of G-protein-coupled receptors. *J Mol Biol* **272**:144-164.
- Ballesteros JA, Shi L and Javitch JA (2001) Structural mimicry in G protein-coupled receptors: implications of the high-resolution structure of rhodopsin for structure-function analysis of rhodopsin-like receptors. *Mol Pharmacol* **60**:1-19.
- Beach JM, Pates RD, Ellena JF and Brown MF (1984) Flash photolysis studies of rhodopsin function in recombinant membranes. *Biophys J* **45**:292a.
- Bekker H, Berendsen HJC, Dijkstra EJ, Achterop S, van Drunen R, van der Spoel D, Sijbers A, Keegstra H, Reitsma B and Renardus MKR (1993) Gromacs: A parallel computer for molecular dynamics simulations., in *Physics Computing 92* (de Groot RA and Nadrichal J eds), World Scientific, Singapore.
- Berendsen HJ and Tieleman DP (1998) Molecular dynamics: studies of lipid bilayers, in *Encyclopedia of Computational Chemistry* (Schleyer PvR ed) pp 1639-1650, Wiley, J.
- Berendsen HJ, Postma JPM, DiNola A and Haak JR (1984) Molecular dynamics with coupling to an external bath. *J Chem Phys* **81**:3684-3690.
- Berendsen HJC, van der Spoel D and van Drunen R (1995) GROMACS: A message-passing parallel molecular dynamics implementation. *Comp Phys Comm* **91**:43-56.
- Berger O, Edholm O and Jahnig F (1997) Molecular dynamics simulations of a fluid bilayer of dipalmitoylphosphatidylcholine at full hydration, constant pressure, and constant temperature. *Biophys J* **72**:2002-2013.

- Bissantz C (2003) Conformational changes of G protein-coupled receptors during their activation by agonist binding. *J Recept Signal Transduct Res* **23**:123-153.
- Bissantz C, Bernard P, Hibert M and Rognan D (2003) Protein-based virtual screening of chemical databases. II. Are homology models of G-Protein Coupled Receptors suitable targets? *Proteins* **50**:5-25.
- Buschauer A (1989) Synthesis and in vitro pharmacology of arpromidine and related phenyl(pyridylalkyl)guanidines, a potential new class of positive inotropic drugs. *J Med Chem* **32**:1963-1970.
- Cai K, Klein-Seetharaman J, Farrens D, Zhang C, Altenbach C, Hubbell WL and Khorana HG (1999) Single-cysteine substitution mutants at amino acid positions 306-321 in rhodopsin, the sequence between the cytoplasmic end of helix VII and the palmitoylation sites: sulfhydryl reactivity and transducin activation reveal a tertiary structure. *Biochemistry* **38**:7925-7930.
- Crozier PS, Stevens MJ, Forrest LR and Woolf TB (2003) Molecular dynamics simulation of dark-adapted rhodopsin in an explicit membrane bilayer: coupling between local retinal and larger scale conformational change. *J Mol Biol* **333**:493-514.
- Darden T, York D and Pedersen L (1993) Particle mesh ewald: An N-log(N) method for ewald sums in large systems. *J Chem Phys* **98**:10089-10092.
- Deese AJ, Dratz EA and Brown MF (1981) Retinal rod outer segment lipids form bilayers in the presence and absence of rhodopsin: a <sup>31</sup>P NMR study. *FEBS Lett* **124**:93-99.
- Donnelly D, Maudsley S, Gent JP, Moser RN, Hurrell CR and Findlay JB (1999) Conserved polar residues in the transmembrane domain of the human tachykinin NK2 receptor: functional roles and structural implications. *Biochem J* **339** (Pt 1):55-61.
- Dove S, Elz S, Seifert R and Buschauer A (2004) Structure-activity relationships of histamine H<sub>2</sub> receptor ligands. *Mini Rev Med Chem* **4**:941-954.
- Ellena JF, Pates RD and Brown MF (1986) <sup>31</sup>P NMR spectra of rod outer segment and sarcoplasmic reticulum membranes show no evidence of immobilized components due to lipid-protein interactions. *Biochemistry* **25**:3742-3748.
- Ernst OP, Meyer CK, Marin EP, Henklein P, Fu WY, Sakmar TP and Hofmann KP (2000) Mutation of the fourth cytoplasmic loop of rhodopsin affects binding of transducin and peptides derived from the carboxyl-terminal sequences of transducin  $\alpha$  and  $\gamma$  subunits. *J Biol Chem* **275**:1937-1943.
- Essmann U, Perera L, Berkowitz ML, Darden T, Lee H and Pedersen LG (1995) A smooth particle mesh ewald potential. *J Chem Phys* **103**:8577-8592.
- Fahmy K, Sakmar TP and Siebert F (2000) Transducin-dependent protonation of glutamic acid 134 in rhodopsin. *Biochemistry* **39**:10607-10612.
- Fanelli F and De Benedetti PG (2005) Computational modeling approaches to structure-function analysis of G protein-coupled receptors. *Chem Rev* **105**:3297-3351.
- Faraldo-Gomez JD, Smith GR and Sansom MS (2002) Setting up and optimization of membrane protein simulations. *Eur Biophys J* **31**:217-227.
- Franke RR, König B, Sakmar TP, Khorana HG and Hofmann KP (1990) Rhodopsin mutants that bind but fail to activate transducin. *Science* **250**:123-125.
- Franke RR, Sakmar TP, Graham RM and Khorana HG (1992) Structure and function in rhodopsin. Studies of the interaction between the rhodopsin cytoplasmic domain and transducin. *J Biol Chem* **267**:14767-14774.
- Fritze O, Filipek S, Kuksa V, Palczewski K, Hofmann KP and Ernst OP (2003) Role of the conserved NPxxY(x)<sub>5,6</sub>F motif in the rhodopsin ground state and during activation. *Proc Natl Acad Sci U S A* **100**:2290-2295.
- Gantz I, DelValle J, Wang LD, Tashiro T, Munzert G, Guo YJ, Konda Y and Yamada T (1992) Molecular basis for the interaction of histamine with the histamine H<sub>2</sub> receptor. *J Biol Chem* **267**:20840-20843.

- Ghanouni P, Schambye H, Seifert R, Lee TW, Rasmussen SG, Gether U and Kobilka BK (2000) The effect of pH on  $\beta_2$  adrenoceptor function. Evidence for protonation-dependent activation. *J Biol Chem* **275**:3121-3127.
- Gumbart J, Wang Y, Aksimentiev A, Tajkhorshid E and Schulten K (2005) Molecular dynamics simulations of proteins in lipid bilayers. *Curr Opin Struct Biol* **15**:423-431.
- Hansson T, Oostenbrink C and van Gunsteren W (2002) Molecular dynamics simulations. *Curr Opin Struct Biol* **12**:190-196.
- Heller H, Schäfer M and Schulten K (1993) Molecular dynamics simulation of a bilayer of 200 lipids in the gel and in the liquid-crystal phases. *J Phys Chem* **97**:8343-8360.
- Hess B, Bekker H, Berendsen HJ and Fraaije JGEM (1997) LINCS: A linear constraint solver for molecular simulations. *J Comp Chem* **18**:1463-1472.
- Hubbell WL, Altenbach C, Hubbell CM and Khorana HG (2003) Rhodopsin structure, dynamics, and activation: a perspective from crystallography, site-directed spin labeling, sulfhydryl reactivity, and disulfide cross-linking. *Adv Protein Chem* **63**:243-290.
- Huber T, Rajamoorthi K, Kurze VF, Beyer K and Brown MF (2002) Structure of docosahexaenoic acid-containing phospholipid bilayers as studied by <sup>2</sup>H NMR and molecular dynamics simulations. *J Am Chem Soc* **124**:298-309.
- Huber T, Botelho AV, Beyer K and Brown MF (2004) Membrane model for the G-protein-coupled receptor rhodopsin: hydrophobic interface and dynamical structure. *Biophys J* **86**:2078-2100.
- Iadanza M, Hölting M, Ronsisvalle G and Hölting HD (2002)  $\kappa$ -Opioid receptor model in a phospholipid bilayer: molecular dynamics simulation. *J Med Chem* **45**:4838-4846.
- Javitch JA, Fu D, Chen J and Karlin A (1995a) Mapping the binding-site crevice of the dopamine D<sub>2</sub> receptor by the substituted-cysteine accessibility method. *Neuron* **14**:825-831.
- Javitch JA, Fu D and Chen J (1995b) Residues in the fifth membrane-spanning segment of the dopamine D<sub>2</sub> receptor exposed in the binding-site crevice. *Biochemistry* **34**:16433-16439.
- Jongejan A, Bruysters M, Ballesteros JA, Haaksma E, Bakker RA, Pardo L and Leurs R (2005) Linking agonist binding to histamine H<sub>1</sub> receptor activation. *Nat Chem Biol* **1**:98-103.
- Kabsch W and Sander C (1983) Dictionary of protein secondary structure: pattern recognition of hydrogen-bonded and geometrical features. *Biopolymers* **22**:2577-2637.
- Kandt C, Ash WL and Tieleman DP (2007) Setting up and running molecular dynamics simulations of membrane proteins. *Methods* **41**:475-488.
- Karplus M and McCammon JA (2002) Molecular dynamics simulations of biomolecules. *Nat Struct Biol* **9**:646-652.
- Kelley MT, Bürckstümmer T, Wenzel-Seifert K, Dove S, Buschauer A and Seifert R (2001) Distinct interaction of human and guinea pig histamine H<sub>2</sub>-receptor with guanidine-type agonists. *Mol Pharmacol* **60**:1210-1225.
- Klein-Seetharaman J (2002) Dynamics in rhodopsin. *Chembiochem* **3**:981-986.
- Klein-Seetharaman J, Reeves PJ, Loewen MC, Getmanova EV, Chung J, Schwalbe H, Wright PE and Khorana HG (2002) Solution NMR spectroscopy of [ $\alpha$ -<sup>15</sup>N]lysine-labeled rhodopsin: The single peak observed in both conventional and TROSY-type HSQC spectra is ascribed to Lys-339 in the carboxyl-terminal peptide sequence. *Proc Natl Acad Sci U S A* **99**:3452-3457.
- Krishna AG, Menon ST, Terry TJ and Sakmar TP (2002) Evidence that helix 8 of rhodopsin acts as a membrane-dependent conformational switch. *Biochemistry* **41**:8298-8309.
- Langen R, Cai K, Altenbach C, Khorana HG and Hubbell WL (1999) Structural features of the C-terminal domain of bovine rhodopsin: a site-directed spin-labeling study. *Biochemistry* **38**:7918-7924.
- Leach AR (2001) *Molecular Modelling: Principles and Applications*, 2nd ed. Prentice Hall, Harlow, UK.
- Li J, Edwards PC, Burghammer M, Villa C and Schertler GF (2004) Structure of bovine rhodopsin in a trigonal crystal form. *J Mol Biol* **343**:1409-1438.

- Lindahl E, Hess B and van der Spoel D (2001) Gromacs 3.0: A package for molecular simulation and trajectory analysis. *J Mol Mod* **7**:306-317.
- Lu ZL and Hulme EC (1999) The functional topography of transmembrane domain 3 of the M<sub>1</sub> muscarinic acetylcholine receptor, revealed by scanning mutagenesis. *J Biol Chem* **274**:7309-7315.
- Lu ZL, Saldanha JW and Hulme EC (2002) Seven-transmembrane receptors: crystals clarify. *Trends Pharmacol Sci* **23**:140-146.
- Marin EP, Krishna AG, Zvyaga TA, Isele J, Siebert F and Sakmar TP (2000) The amino terminus of the fourth cytoplasmic loop of rhodopsin modulates rhodopsin-transducin interaction. *J Biol Chem* **275**:1930-1936.
- Mehler EL, Periole X, Hassan SA and Weinstein H (2002) Key issues in the computational simulation of GPCR function: representation of loop domains. *J Comput Aided Mol Des* **16**:841-853.
- Miljanich GP, Brown MF, Mabrey-Gaud S, Dratz EA and Sturtevant JM (1985) Thermotropic behavior of retinal rod membranes and dispersions of extracted phospholipids. *J Membr Biol* **85**:79-86.
- Mirzadegan T, Benko G, Filipek S and Palczewski K (2003) Sequence analyses of G-protein-coupled receptors: similarities to rhodopsin. *Biochemistry* **42**:2759-2767.
- Mitchell DC, Straume M and Litman BJ (1992) Role of *sn*-1-saturated, *sn*-2-polyunsaturated phospholipids in control of membrane receptor conformational equilibrium: effects of cholesterol and acyl chain unsaturation on the metarhodopsin I in equilibrium with metarhodopsin II equilibrium. *Biochemistry* **31**:662-670.
- Nagle JF and Tristram-Nagle S (2000) Structure of lipid bilayers. *Biochim Biophys Acta* **1469**:159-195.
- Nederkoorn PH, van Gelder EM, Donne-Op den Kelder GM and Timmerman H (1996) The agonistic binding site at the histamine H<sub>2</sub> receptor. II. Theoretical investigations of histamine binding to receptor models of the seven alpha-helical transmembrane domain. *J Comput Aided Mol Des* **10**:479-489.
- Okada T, Fujiyoshi Y, Silow M, Navarro J, Landau EM and Shichida Y (2002) Functional role of internal water molecules in rhodopsin revealed by X-ray crystallography. *Proc Natl Acad Sci U S A* **99**:5982-5987.
- Okada T, Sugihara M, Bondar AN, Elstner M, Entel P and Buss V (2004) The retinal conformation and its environment in rhodopsin in light of a new 2.2 Å crystal structure. *J Mol Biol* **342**:571-583.
- Ostrom RS and Insel PA (2004) The evolving role of lipid rafts and caveolae in G protein-coupled receptor signaling: implications for molecular pharmacology. *Br J Pharmacol* **143**:235-245.
- Palczewski K (2006) G protein-coupled receptor rhodopsin. *Annu Rev Biochem* **75**:743-767.
- Palczewski K, Kumasaka T, Hori T, Behnke CA, Motoshima H, Fox BA, Le Trong I, Teller DC, Okada T, Stenkamp RE, Yamamoto M and Miyano M (2000) Crystal structure of rhodopsin: A G protein-coupled receptor. *Science* **289**:739-745.
- Pardo L, Deupi X, Dolker N, Lopez-Rodriguez ML and Campillo M (2007) The role of internal water molecules in the structure and function of the rhodopsin family of G protein-coupled receptors. *Chembiochem* **8**:19-24.
- Pedretti A, Villa L and Vistoli G (2002) VEGA: a versatile program to convert, handle and visualize molecular structure on Windows-based PCs. *J Mol Graph Model* **21**:47-49.
- Pedretti A, Villa L and Vistoli G (2004) VEGA-an open platform to develop chemo-bio-informatics applications, using plug-in architecture and script programming. *J Comput Aided Mol Des* **18**:167-173.
- Perlman JH, Colson AO, Wang W, Bence K, Osman R and Gershengorn MC (1997) Interactions between conserved residues in transmembrane helices 1, 2, and 7 of the thyrotropin-releasing hormone receptor. *J Biol Chem* **272**:11937-11942.
- Petrache HI, Salmon A and Brown MF (2001) Structural properties of docosahexaenoyl phospholipid bilayers investigated by solid-state <sup>2</sup>H NMR spectroscopy. *J Am Chem Soc* **123**:12611-12622.

- Pitman MC, Grossfield A, Suits F and Feller SE (2005) Role of cholesterol and polyunsaturated chains in lipid-protein interactions: molecular dynamics simulation of rhodopsin in a realistic membrane environment. *J Am Chem Soc* **127**:4576-4577.
- Rees DC, DeAntonio L and Eisenberg D (1989) Hydrophobic organization of membrane proteins. *Science* **245**:510-513.
- Röhrig UF, Guidoni L and Rothlisberger U (2002) Early steps of the intramolecular signal transduction in rhodopsin explored by molecular dynamics simulations. *Biochemistry* **41**:10799-10809.
- Ruprecht JJ, Mielke T, Vogel R, Villa C and Schertler GF (2004) Electron crystallography reveals the structure of metarhodopsin I. *Embo J* **23**:3609-3620.
- Salo OM, Lahtela-Kakkonen M, Gynther J, Jarvinen T and Poso A (2004) Development of a 3D model for the human cannabinoid CB<sub>1</sub> receptor. *J Med Chem* **47**:3048-3057.
- Schetz JA, Benjamin PS and Sibley DR (2000) Nonconserved residues in the second transmembrane-spanning domain of the D<sub>4</sub> dopamine receptor are molecular determinants of D<sub>4</sub>-selective pharmacology. *Mol Pharmacol* **57**:144-152.
- Schlegel B, Sippl W and Höltje HD (2005) Molecular dynamics simulations of bovine rhodopsin: influence of protonation states and different membrane-mimicking environments. *J Mol Model* **12**:49-64.
- Schüttelkopf AW and van Aalten DMF (2004) PRODRG - a tool for high-throughput crystallography of protein-ligand complexes. *Acta Crystallographica* **D60**:1355-1363.
- Sealfon SC, Chi L, Ebersole BJ, Rodic V, Zhang D, Ballesteros JA and Weinstein H (1995) Related contribution of specific helix 2 and 7 residues to conformational activation of the serotonin 5-HT<sub>2A</sub> receptor. *J Biol Chem* **270**:16683-16688.
- Seelig J (1977) Deuterium magnetic resonance: theory and application to lipid membranes. *Q Rev Biophys* **10**:353-418.
- Seelig J and Seelig A (1980) Lipid conformation in model membranes and biological membranes. *Q Rev Biophys* **13**:19-61.
- Shapiro DA, Kristiansen K, Kroeze WK and Roth BL (2000) Differential modes of agonist binding to 5-hydroxytryptamine<sub>2A</sub> serotonin receptors revealed by mutation and molecular modeling of conserved residues in transmembrane region 5. *Mol Pharmacol* **58**:877-886.
- Simons K and Ikonen E (1997) Functional rafts in cell membranes. *Nature* **387**:569-572.
- Simons K and Ikonen E (2000) How cells handle cholesterol. *Science* **290**:1721-1726.
- Swaminath G, Xiang Y, Lee TW, Steenhuis J, Parnot C and Kobilka BK (2004) Sequential binding of agonists to the  $\beta_2$  adrenoceptor. Kinetic evidence for intermediate conformational states. *J Biol Chem* **279**:686-691.
- Teller DC, Okada T, Behnke CA, Palczewski K and Stenkamp RE (2001) Advances in determination of a high-resolution three-dimensional structure of rhodopsin, a model of G-protein-coupled receptors (GPCRs). *Biochemistry* **40**:7761-7772.
- Tieleman DP and Berendsen HJC (1996) Molecular dynamics simulations of a fully hydrated dipalmitoylphosphatidylcholine bilayer with different macroscopic boundary conditions and parameters. *J Chem Phys* **105**:4871-4880.
- van der Spoel D, Lindahl E, Hess B, van Buuren AR, Apol E, Meulenhoff PJ, Tieleman DP, Sijbers ALTM, Feenstra KA, van Drunen R and Berendsen HJC (2004) *Gromacs user manual version 3.2*.
- van der Spoel D, Lindahl E, Hess B, Groenhof G, Mark AE and Berendsen HJC (2005) GROMACS: Fast, Flexible and Free. *J Comp Chem* **26**:1701-1718.
- Visiers I, Ballesteros JA and Weinstein H (2002) Three-dimensional representations of G protein-coupled receptor structures and mechanisms. *Methods Enzymol* **343**:329-371.
- Wallin E, Tsukihara T, Yoshikawa S, von Heijne G and Elofsson A (1997) Architecture of helix bundle membrane proteins: an analysis of cytochrome c oxidase from bovine mitochondria. *Protein Sci* **6**:808-815.

Wiedmann TS, Pates RD, Beach JM, Salmon A and Brown MF (1988) Lipid-protein interactions mediate the photochemical function of rhodopsin. *Biochemistry* **27**:6469-6474.

Wiener MC and White SH (1991) Fluid bilayer structure determination by the combined use of X-ray and neutron diffraction. I. Fluid bilayer models and the limits of resolution. *Biophys J* **59**:162-173.

Zhou W, Flanagan C, Ballesteros JA, Konvicka K, Davidson JS, Weinstein H, Millar RP and Sealfon SC (1994) A reciprocal mutation supports helix 2 and helix 7 proximity in the gonadotropin-releasing hormone receptor. *Mol Pharmacol* **45**:165-170.



## Chapter 6

# Pharmacological Methods

### 6.1 Materials

*N*<sup>G</sup>-acylated *N*-[3-(1*H*-imidazol-4-yl)propyl]guanidines and UR-AK57 were prepared as described (Ghorai, 2005; Xie et al., 2006a, b). IMP (Durant et al., 1978) was synthesized as described (Durant et al., 1985). ARP and BU-E-43 were synthesized as described (Buschauer, 1989). Aminopotentidine and iodoaminopotentidine were prepared as described (Hirschfeld et al., 1992). Suprahistaprodifen and 2-benzylhistamine were synthesized as described (Elz et al., 2000; Seifert et al., 2003). The structures of compounds were confirmed by elemental analysis (C, H, N), <sup>1</sup>H NMR, and mass spectrometry. Purity of compounds was >98% as determined by high-performance liquid chromatography or capillary electrophoresis. The anti-FLAG Ig (M1 monoclonal antibody) was from Sigma (St. Louis, MO). The anti-G<sub>sα</sub> Ig (C-terminal) was from Santa Cruz Biotechnology (Santa Cruz, CA), and the anti-6His Ig was from Clontech Laboratories (Mountain View, CA). [<sup>32</sup>P]P<sub>i</sub> (8500-9100 Ci/mmol orthophosphoric acid), [α-<sup>32</sup>P]ATP (800 Ci/mmol), and [<sup>3</sup>H]dihydroalprenolol (85-90 Ci/mmol) were from PerkinElmer Life Sciences (Boston, MA).

All unlabeled nucleotides, glycerol-3-phosphate dehydrogenase, triose phosphate isomerase, glyceraldehyde-3-phosphate dehydrogenase, and lactate dehydrogenase were from Roche (Indianapolis, IN). 3-Phosphoglycerate kinase, *L*-α-glycerol phosphate, histamine, betahistine, cimetidine, ranitidine, and famotidine were from Sigma. Amthamine was from Tocris Cookson (Ballwin, MO). Dimaprit was from RBI (Natick, MA). Burimamide and metiamide were from Dr. W. Schunack (Free University of Berlin, Germany). All restriction enzymes, T4 DNA ligase, and calf intestinal phosphatase were from New England Biolabs (Beverly, MA). Cloned *Pfu* DNA polymerase was from Stratagene (La Jolla, CA).

## 6.2 Generation of recombinant baculoviruses, cell culture, and membrane preparation

Baculoviruses encoding recombinant proteins were generated in Sf9 cells using the BaculoGOLD transfection kit (BD Pharmingen, San Diego, CA) according to the manufacturer's instructions. After initial transfection, high-titer virus stocks were generated by two sequential virus amplifications. Sf9 cells were cultured in 250-ml disposable Erlenmeyer flasks at 28 °C under rotation at 125 rpm in SF 900 II medium (Invitrogen, Carlsbad, CA) supplemented with 5% (v/v) fetal calf serum (BioWhittaker, Walkersville, MD) and 0.1 mg/ml gentamicin (BioWhittaker). Cells were maintained at a density of  $0.5$  to  $6.0 \cdot 10^6$  cells/ml. For infection, cells were sedimented by centrifugation and suspended in fresh medium. Cells were seeded at  $3.0 \cdot 10^6$  cells/ml and infected with a 1:100 dilution of high-titer baculovirus stocks encoding H<sub>2</sub>R<sub>s</sub>, G<sub>saS</sub>, or H<sub>2</sub>R-G<sub>saS</sub> proteins. Cells were cultured for 48 h before membrane preparation. Sf9 membranes were prepared as described previously (Seifert et al., 1998), using 1 mM EDTA, 0.2 mM phenylmethylsulfonyl fluoride, 10 µg/ml benzamidine, and 10 µg/ml leupeptin as protease inhibitors. Membranes were suspended in binding buffer (12.5 mM MgCl<sub>2</sub>, 1 mM EDTA, and 75 mM Tris/HCl, pH 7.4) and stored at -80 °C until use.

## 6.3 SDS-PAGE and immunoblot analysis

Membrane proteins were separated on SDS polyacrylamide gels containing 12% (w/v) acrylamide. Proteins were then transferred onto Immobilon-P transfer membranes (Millipore, Bedford, MA). Membranes were reacted with M1 antibody, anti-G<sub>sa</sub> Ig, or anti-6His Ig (1:1000 each). Immunoreactive bands were visualized by enhanced chemoluminescence (Pierce, Rockford, IL) using sheep anti-mouse IgG (M1 and anti-6His Ig) and donkey anti-rabbit IgG (anti-G<sub>sa</sub> Ig), respectively, coupled to peroxidase.

## 6.4 Steady-state GTPase activity assay

Membranes were thawed, sedimented, and resuspended in 10 mM Tris/HCl, pH 7.4. Assay tubes contained Sf9 membranes expressing H<sub>2</sub>R-G<sub>saS</sub> fusion proteins (10 µg of protein/tube), 1.0 mM MgCl<sub>2</sub>, 0.1 mM EDTA, 0.1 mM ATP, 100 nM GTP, 0.1 mM adenylyl imidodiphosphate, 5 mM creatine phosphate, 40 µg of creatine kinase, and 0.2% (w/v) bovine serum albumin in 50 mM Tris/HCl, pH 7.4, and H<sub>2</sub>R ligands at various concentrations. Reaction mixtures (80 µl) were incubated for 2 min at 25 °C before the addition of 20 µl of

[ $\gamma$ - $^{32}\text{P}$ ]GTP (0.1  $\mu\text{Ci}/\text{tube}$ ). All stock and work dilutions of [ $\gamma$ - $^{32}\text{P}$ ]GTP were prepared in 20 mM Tris/HCl, pH 7.4. Reactions were conducted for 20 min at 25 °C. Preliminary studies under basal conditions and with histamine, impromidine, and arpromidine showed that under these conditions GTP hydrolysis was linear. Reactions were terminated by the addition of 900  $\mu\text{l}$  of slurry consisting of 5% (w/v) activated charcoal and 50 mM  $\text{NaH}_2\text{PO}_4$ , pH 2.0. Charcoal absorbs nucleotides but not  $\text{P}_i$ . Charcoal-quenched reaction mixtures were centrifuged for 7 min at room temperature at 15000g. Six hundred microliters of the supernatant fluid of reaction mixtures were removed and [ $^{32}\text{P}$ ] was determined by liquid scintillation counting. Enzyme activities were corrected for spontaneous degradation of [ $\gamma$ - $^{32}\text{P}$ ]GTP. Spontaneous [ $\gamma$ - $^{32}\text{P}$ ]GTP degradation was determined in tubes containing all of the above described components plus a very high concentration of unlabeled GTP (1 mM) that, by competition with [ $\gamma$ - $^{32}\text{P}$ ]GTP, prevents [ $\gamma$ - $^{32}\text{P}$ ]GTP hydrolysis by enzymatic activities present in Sf9 membranes. Spontaneous [ $\gamma$ - $^{32}\text{P}$ ]GTP degradation was <1% of the total amount of radioactivity added using 20 mM Tris/HCl, pH 7.4, as solvent for [ $\gamma$ - $^{32}\text{P}$ ]GTP. The experimental conditions chosen ensured that not more than 10% of the total amount of [ $\gamma$ - $^{32}\text{P}$ ]GTP added was converted to  $^{32}\text{P}_i$ .

## 6.5 AC activity assay

AC activity in Sf9 membranes was determined as described previously (Houston et al., 2002). Briefly, membranes were thawed and sedimented by a 15-min centrifugation at 4 °C and 15000g to remove residual endogenous guanine nucleotides as far as possible, and were subsequently resuspended in binding buffer. Tubes contained Sf9 membranes expressing  $\text{H}_2\text{Rs}$  (100  $\mu\text{g}$  of protein/tube),  $\text{H}_2\text{Rs}$  coexpressed with mammalian  $\text{G}_{\text{saS}}$  (50  $\mu\text{g}$  of protein/tube), or  $\text{H}_2\text{R}$ - $\text{G}_{\text{saS}}$  fusion proteins (20  $\mu\text{g}$  of protein/tube), additionally 5 mM  $\text{MgCl}_2$ , 0.4 mM EDTA, and 30 mM Tris/HCl, pH 7.4. Assay tubes containing membranes and various additions in a total volume of 30  $\mu\text{l}$  were incubated for 3 min at 37 °C before starting reactions by the addition of 20  $\mu\text{l}$  of reaction mixture containing (final) [ $\alpha$ - $^{32}\text{P}$ ]ATP (0.3  $\mu\text{Ci}/\text{tube}$ ) plus 40  $\mu\text{M}$  unlabeled ATP, 2.7 mM mono(cyclohexyl)ammonium phosphoenolpyruvate, 0.125 IU of pyruvate kinase, 1 IU of myokinase, and 0.1 mM cAMP. Reactions were conducted for 20 min at 37 °C. Reactions were terminated by the addition of 20  $\mu\text{l}$  of 2.2 N HCl. Denatured protein was sedimented by a 3-min centrifugation at 25 °C and 15000g. Sixty-five microliters of the supernatant fluid were applied onto disposable columns filled with 1.3 g of neutral alumina (Sigma A-1522, super I, WN-6). [ $^{32}\text{P}$ ]cAMP was separated from [ $\alpha$ - $^{32}\text{P}$ ]ATP by elution of [ $^{32}\text{P}$ ]cAMP with 4 ml of 0.1 M ammonium acetate, pH 7.0. Recovery of [ $^{32}\text{P}$ ]cAMP was ~80%. Blank values were routinely ~0.01% of the total amount

of [ $\alpha$ - $^{32}\text{P}$ ]ATP added. [ $^{32}\text{P}$ ]cAMP was determined by liquid scintillation counting. The experimental conditions chosen ensured that not more than 1-3% of the total amount of [ $\alpha$ - $^{32}\text{P}$ ]ATP added was converted to [ $^{32}\text{P}$ ]cAMP.

## 6.6 Preparation of [ $\gamma$ - $^{32}\text{P}$ ]GTP

[ $\gamma$ - $^{32}\text{P}$ ]GTP was produced through substrate level phosphorylation of GDP during the enzymatic conversion of *L*- $\alpha$ -glycerol phosphate to 3-phosphoglycerate following a procedure described previously (Walseth and Johnson, 1979). The final concentrations of enzymes and reagents used were as follows: 43  $\mu\text{g/ml}$  glycerol-3-phosphate dehydrogenase (0.44 IU), 0.9  $\mu\text{g/ml}$  triose phosphate isomerase (0.27 IU), 34  $\mu\text{g/ml}$  glyceraldehyde-3-phosphate dehydrogenase (0.16 IU), 4.3  $\mu\text{g/ml}$  3-phosphoglycerate kinase (0.12 IU), 21  $\mu\text{g/ml}$  lactate dehydrogenase (0.69 IU), 12 mM  $\text{MgCl}_2$ , 27 mM dithiothreitol, 0.8 mM *L*- $\alpha$ -glycerolphosphate, 0.25 mM GDP, 0.5 mM  $\beta$ - $\text{NAD}^+$ , 1 mM pyruvic acid, and 0.1 mM EDTA in 10 mM Tris-HCl, pH 9.0. Immediately before use, a stock solution containing all enzymes was sedimented by a 15-min centrifugation at 14000 rpm and a temperature of 4 °C to remove supernatant ammonium sulfate. Phosphorylation was started by addition of 1.25 mCi [ $^{32}\text{P}$ ]P<sub>i</sub> (orthophosphoric acid) in a total volume of 60  $\mu\text{l}$  and was conducted for 15 min at 37 °C. The reaction was stopped by placing the reaction mixture on ice and adding 60  $\mu\text{l}$  of ice-cold EtOH. To monitor conversion of [ $^{32}\text{P}$ ]P<sub>i</sub> into [ $\gamma$ - $^{32}\text{P}$ ]GTP, a pipet tip was putted into the reaction mixture to collect a very small amount that was distributed in 1 ml of 50 mM  $\text{KH}_2\text{PO}_4$ , pH 2.0. 25  $\mu\text{l}$  of this solution were withdrawn for liquid scintillation counting representing the total amount of radioactivity added to the reaction mixture. A spatula full of charcoal was then added to the remaining solution. After mixing, [ $\gamma$ - $^{32}\text{P}$ ]GTP absorbed by charcoal was separated from [ $^{32}\text{P}$ ]P<sub>i</sub> by a 5-min centrifugation at 14000 rpm. 25  $\mu\text{l}$  of the supernatant were used for scintillation counting giving the amount of [ $^{32}\text{P}$ ]P<sub>i</sub> in the reaction mixture not being converted to [ $\gamma$ - $^{32}\text{P}$ ]GTP. The experimental conditions ensured that more than 99% of [ $^{32}\text{P}$ ]P<sub>i</sub> were converted to [ $\gamma$ - $^{32}\text{P}$ ]GTP. Appropriate aliquots of [ $\gamma$ - $^{32}\text{P}$ ]GTP were stored at -80 °C until use.

## 6.7 Miscellaneous

Protein concentrations were determined using the DC protein assay kit (Bio-Rad, Hercules, CA). [ $^3\text{H}$ ]Dihydroalprenolol saturation binding was performed as described (Seifert et al., 1998). All analyses of experimental data were performed with the Prism 4 program (GraphPad Software, San Diego, CA).  $K_B$  values were calculated using the Cheng and

Prusoff equation (Cheng and Prusoff, 1973). Expression levels of recombinant proteins were determined using the BioRad GS-710 Calibrated Imaging Densitometer and the software tool Quantity One Version 4.0.3 (Bio-Rad, Hercules, CA).

## 6.8 References

- Buschauer A (1989) Synthesis and in vitro pharmacology of arpromidine and related phenyl(pyridylalkyl)guanidines, a potential new class of positive inotropic drugs. *J Med Chem* **32**:1963-1970.
- Cheng Y and Prusoff WH (1973) Relationship between the inhibition constant ( $K_i$ ) and the concentration of inhibitor which causes 50 per cent inhibition ( $I_{50}$ ) of an enzymatic reaction. *Biochem Pharmacol* **22**:3099-3108.
- Durant GJ, Duncan WA, Ganellin CR, Parsons ME, Blakemore RC and Rasmussen AC (1978) Impromidine (SK&F 92676) is a very potent and specific agonist for histamine  $H_2$  receptors. *Nature* **276**:403-405.
- Durant GJ, Ganellin CR, Hills DW, Miles PD, Parsons ME, Pepper ES and White GR (1985) The histamine  $H_2$  receptor agonist impromidine: synthesis and structure-activity considerations. *J Med Chem* **28**:1414-1422.
- Elz S, Kramer K, Pertz HH, Detert H, ter Laak AM, Kühne R and Schunack W (2000) Histaprodifens: synthesis, pharmacological in vitro evaluation, and molecular modeling of a new class of highly active and selective histamine  $H_1$ -receptor agonists. *J Med Chem* **43**:1071-1084.
- Ghorai, P (2005) Arpromidine-related acylguanidines: synthesis and structure-activity relationships of a new class of guanidine-type histamine  $H_2$  receptor agonists with reduced basicity. Doctoral thesis. University of Regensburg, Germany.  
<http://www.opus-bayern.de/uni-regensburg/volltexte/2006/561/>
- Hirschfeld J, Buschauer A, Elz S, Schunack W, Ruat M, Traiffort E and Schwartz JC (1992) Iodoaminopotentidine and related compounds: a new class of ligands with high affinity and selectivity for the histamine  $H_2$  receptor. *J Med Chem* **35**:2231-2238.
- Houston C, Wenzel-Seifert K, Bürckstümmer T and Seifert R (2002) The human histamine  $H_2$ -receptor couples more efficiently to Sf9 insect cell  $G_s$ -proteins than to insect cell  $G_q$ -proteins: limitations of Sf9 cells for the analysis of receptor/ $G_q$ -protein coupling. *J Neurochem* **80**:678-696.
- Seifert R, Lee TW, Lam VT and Kobilka BK (1998) Reconstitution of  $\beta_2$ -adrenoceptor-GTP-binding-protein interaction in Sf9 cells: High coupling efficiency in a  $\beta_2$ -adrenoceptor- $G_{sq}$  fusion protein. *Eur J Biochem* **255**:369-382.
- Seifert R, Wenzel-Seifert K, Bürckstümmer T, Pertz HH, Schunack W, Dove S, Buschauer A and Elz S (2003) Multiple differences in agonist and antagonist pharmacology between human and guinea pig histamine  $H_1$ -receptor. *J Pharmacol Exp Ther* **305**:1104-1115.
- Walseth TF and Johnson RA (1979) The enzymatic preparation of [ $\alpha$ - $^{32}P$ ] nucleoside triphosphates, cyclic [ $^{32}P$ ] AMP, and cyclic [ $^{32}P$ ] GMP. *Biochim Biophys Acta* **562**:11-31.
- Xie SX, Ghorai P, Ye QZ, Buschauer A and Seifert R (2006a) Probing ligand-specific histamine  $H_1$ - and  $H_2$ -receptor conformations with  $N^G$ -acylated imidazolylpropylguanidines. *J Pharmacol Exp Ther* **317**:139-146.
- Xie SX, Kraus A, Ghorai P, Ye QZ, Elz S, Buschauer A and Seifert R (2006b)  $N^1$ -(3-cyclohexylbutanoyl)- $N^2$ -[3-(1H-imidazol-4-yl)propyl]guanidine (UR-AK57), a potent partial agonist for the human histamine  $H_1$ - and  $H_2$ -receptors. *J Pharmacol Exp Ther* **317**:1262-1268.



## Chapter 7

# Constitutive Activity and Ligand Selectivity of Human, Guinea Pig, Rat, and Canine Histamine H<sub>2</sub> Receptors

### 7.1 Introduction

The histamine H<sub>2</sub> receptor species isoforms of canine (Gantz et al., 1991a), human (Gantz et al., 1991b), rat (Ruat et al., 1991), and guinea pig (Traiffort et al., 1995) had been cloned. The four H<sub>2</sub>R species isoforms are closely related to each other, as is reflected by an overall amino acid sequence identity of more than 80%. The highest conservation exists within the seven  $\alpha$ -helical transmembrane (TM) domains (sequence identity of more than 90%), whereas the N-terminal domain together with the extracellular end of TM1 and the C-terminus are the least conserved regions (Figure 7.1).

Despite this high degree of structural similarity, *N*-[3-(1*H*-imidazol-4-yl)propyl]guanidines such as compounds **8-10** (Figure 7.2) differentially activate guinea pig (gpH<sub>2</sub>R) and human (hH<sub>2</sub>R) H<sub>2</sub> receptors. In a membrane steady-state GTPase activity assay using fusion proteins of H<sub>2</sub>R and the short splice variant of G<sub>sa</sub>, G<sub>saS</sub>, such H<sub>2</sub>R-selective agonists are considerably more potent and efficacious at gpH<sub>2</sub>R-G<sub>saS</sub> than at hH<sub>2</sub>R-G<sub>saS</sub> (Kelley et al., 2001). By contrast, the small H<sub>2</sub>R agonists histamine (**1**, HA), dimaprit (**2**, DIM), amthamine (**3**, AMT), and betahistine (**4**, BET) are unselective between these species. Recently, a novel class of *N*<sup>G</sup>-acylated imidazolylpropylguanidines as represented by compounds **11-16** was developed (Ghorai, 2005; Xie et al., 2006a). Generally, by introduction of a carbonyl group

		N-term	TM1	i1	TM2
hH <sub>2</sub> R	1	MAPNGTASSFCLDSTACKITITVVLAVLILITVAGNVVVCLAVGLNRRLRNLTNCFIVSLAITDLLLGLL			
gpH <sub>2</sub> R	1	..F...VP...M. <b>F</b> .VY.V..S.I.II..V.....S.....V.....			
rH <sub>2</sub> R	1	. <b>E</b> ...VH. <b>C</b> ... <b>M</b> . <b>L</b> .V..S... <b>TT</b> ...I..... <b>S</b> .....S.....A.....			
cH <sub>2</sub> R	1	. <b>IS</b> ... <b>G</b> ..... <b>PP</b> .R..VS... <b>T</b> .....I.....S.....S.....			
		e1	TM3	i2	TM4
hH <sub>2</sub> R	71	VLPFSAIYQLSCKWSFGKVFCNIYTSLDVMLCTASILNLFMISLDRYCAVMDPLRYPVLVTPVRVAISLV			
gpH <sub>2</sub> R	71	..... <b>S</b> ..... <b>T</b> .....I..A.....			
rH <sub>2</sub> R	71	..... <b>FT</b> ... <b>H</b> ..... <b>T</b> .....I.....			
cH <sub>2</sub> R	71	.....F.....R..... <b>T</b> .....I.....V...			
		TM4	e2	TM5	
hH <sub>2</sub> R	141	LIWVISITLSFLSIHLGWNSRNETSKGNHTTSCKKVQVNEVYGLVDGLVTFFYLPLLIMCITYYRIFKVAR			
gpH <sub>2</sub> R	141	F..... <b>D</b> . <b>D</b> . <b>IV</b> ..... <b>F</b> .....I..			
rH <sub>2</sub> R	141	F..... <b>G</b> . <b>RG</b> .. <b>D</b> . <b>F</b> -.....V.....I..			
cH <sub>2</sub> R	141	..... <b>SF</b> .. <b>IP</b> ..... <b>L</b> .....V.....I..			
		i3	TM6	e3	TM7
hH <sub>2</sub> R	211	DQAKRINHISWKAATIREHKATVTLAAVMGAFTICWFFPYFTAFVYRGLRGDDAINEVLEAIVLWLGYN			
gpH <sub>2</sub> R	211	E..R..... <b>G</b> .....V.....K...V...F. <b>DV</b> .....			
rH <sub>2</sub> R	210	E..... <b>G</b> .....V.....K...V... <b>AV</b> . <b>G</b> .....			
cH <sub>2</sub> R	211	.....H. <b>MG</b> ..... <b>G</b> .....V.....K...AF..V.....			
		C-term			
hH <sub>2</sub> R	281	SALNPILYAALNRDFRTGYQQFLFCCRLANRNSHKTSLSRNASQLSRTQSREPRQQEEKPLKLQVWSGTEV			
gpH <sub>2</sub> R	281	..... <b>A</b> .H..... <b>SH</b> .. <b>E</b> .. <b>L</b> . <b>N</b> ...N.S. <b>CQ</b> .. <b>W</b> .. <b>D</b> .. <b>N</b> .....			
rH <sub>2</sub> R	280	..... <b>A</b> ...H.KF. <b>SH</b> .. <b>L</b> . <b>N</b> . <b>L</b> . <b>P</b> .S.. <b>G</b> . <b>W</b> .....L			
cH <sub>2</sub> R	281	..... <b>T</b> ..... <b>A</b> ...R.. <b>P</b> . <b>SH</b> . <b>AQE</b> .. <b>S</b> .. <b>A</b> .N.. <b>MR</b> .....			
hH <sub>2</sub> R	351	TAPQGATDR	359		
gpH <sub>2</sub> R	351	..... <b>N</b> .	359		
rH <sub>2</sub> R	350	. <b>H</b> .. <b>NPI</b> .	358		
cH <sub>2</sub> R	351	... <b>R</b> .....	359		

**Figure 7.1:** Comparison of the amino acid sequences of hH<sub>2</sub>R, gpH<sub>2</sub>R, rH<sub>2</sub>R, and cH<sub>2</sub>R. Dots in the sequences of gpH<sub>2</sub>R, rH<sub>2</sub>R, and cH<sub>2</sub>R indicate identity with hH<sub>2</sub>R. Amino acids shown in white with black shading represent the interaction sites of HA with the H<sub>2</sub>R (Gantz et al., 1992; Nederkoorn et al., 1996). The most conserved residues in each TM domain are indicated in grey shading. Amino acids shown in regular font in the sequences of gpH<sub>2</sub>R, rH<sub>2</sub>R, and cH<sub>2</sub>R represent conservative exchanges. Amino acids shown in bold in the sequences of gpH<sub>2</sub>R, rH<sub>2</sub>R, and cH<sub>2</sub>R represent nonconservative exchanges.

adjacent to the guanidine moiety, the species-selectivity of the agonists is preserved (Xie et al., 2006a). Comparison of the corresponding agonist efficacies in the GTPase assay and at stabilizing the high-affinity ternary complex of the H<sub>2</sub>R with nucleotide-free G<sub>sq</sub> indicate that *N*-[3-(1*H*-imidazol-4-yl)propyl]guanidines and their *N*<sup>G</sup>-acylated analogs stabilize different ligand-specific active conformations of hH<sub>2</sub>R and gpH<sub>2</sub>R (Kelley et al., 2001; Xie et al., 2006a). However, it is not known whether these differences also apply for other H<sub>2</sub>R species isoforms. Moreover, H<sub>2</sub>R<sub>s</sub> are known to be constitutively active (Smit et al., 1996a; Alewijnse



et al., 1998), but the degree to which constitutive activity varies among several species isoforms remains elusive. To generate an expanded pharmacological profile of H<sub>2</sub>R species isoforms, we compare human, guinea pig, rat (r), and canine (c) H<sub>2</sub>R<sub>s</sub>.

Sf9 cell membranes expressing H<sub>2</sub>R-G<sub>sαS</sub> fusion proteins were used to measure steady-state GTPase activity. For this purpose, we studied several classes of H<sub>2</sub>R ligands (Figure 7.2). HA (**1**) and related small H<sub>2</sub>R agonists DIM (**2**), AMT (**3**), and BET (**4**) similarly interact with the binding site of H<sub>2</sub>R. The amino group of HA forms an ionic interaction with Asp-98(3.32) in TM3 and the imidazolyl ring presumably interacts with Tyr-182(5.38) and Asp-186(5.42) in TM5 (Figure 7.1). The guanidine-type H<sub>2</sub>R agonists impromidine (**8**, IMP), arpromidine (**9**, ARP), and BU-E-43 (**10**), as well as the *N*<sup>G</sup>-acylated derivatives **11–16** share a common *N*-[3-(1*H*-imidazol-4-yl)propyl]guanidine moiety that mimics binding of HA and thus is crucial for agonistic activity (Dove et al., 2004). The 2-(5-methylimidazol-4-ylmethylthio)ethyl moiety of IMP and the 3-(4-fluorophenyl)-3-(2-pyridyl)propyl group of ARP are supposed to interact with a pocket formed by multiple residues in TM2, TM3, TM6, and TM7 (chapters 4 and 5; Kelley et al., 2001).

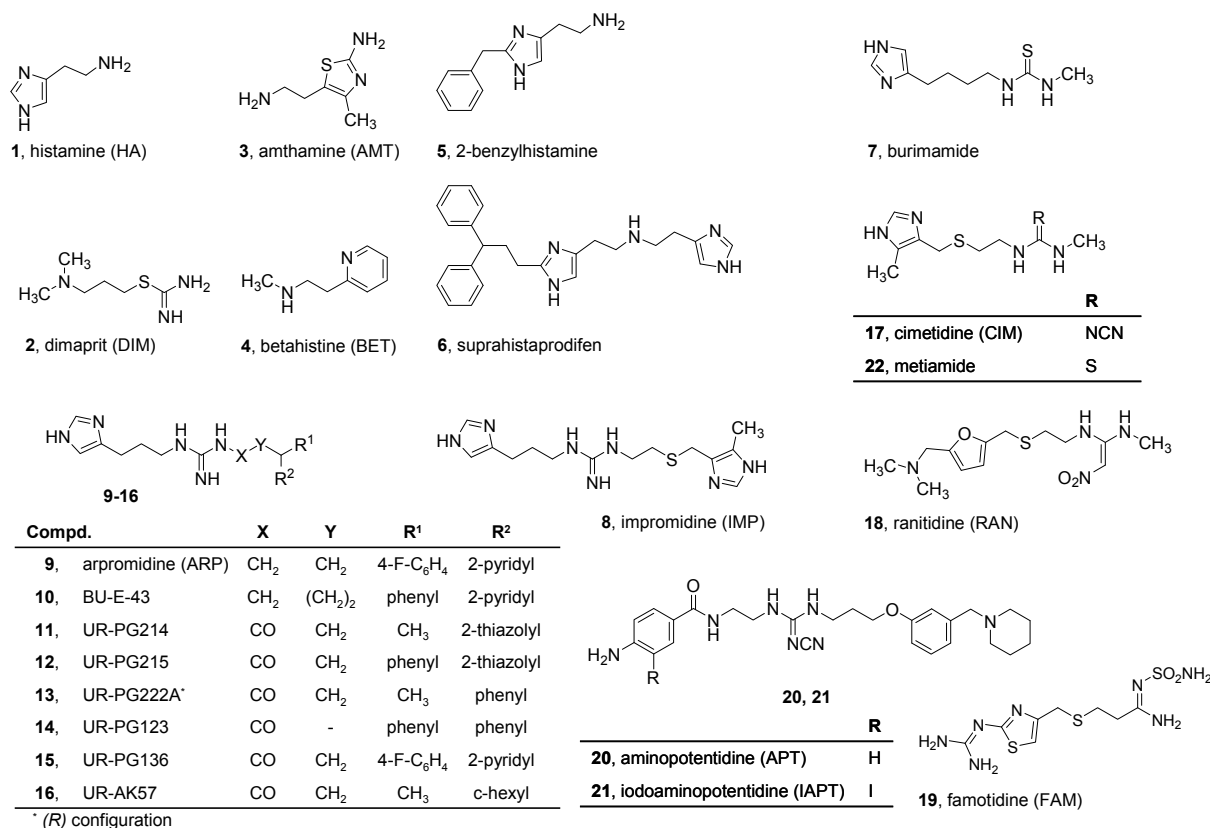


**Figure 7.2:** Structures of H<sub>2</sub>R agonists, partial agonists, and antagonists. **1–4**, small H<sub>2</sub>R agonists; **5** and **6**, H<sub>1</sub>R agonists with partial agonism at the H<sub>2</sub>R; **8–10**, guanidine-type H<sub>2</sub>R agonists; **11–16**, *N*<sup>G</sup>-acylated *N*-[3-(1*H*-imidazol-4-yl)propyl]guanidines with agonistic H<sub>2</sub>R activity; **7** and **17–22**, H<sub>2</sub>R antagonists.

The variable side chains of the ARP derivatives **10-16** consist of diverse mono- or diarylalkyl groups with different chain lengths between the aromatic ring system and the guanidine group. In compound **16** (Xie et al., 2006b), the aryl ring is replaced by a cyclohexyl moiety. Compound **13** is the pure (*R*)-enantiomer (eutomer). 2-Benzylhistamine (**5**) and suprahistaprodifen (**6**) represent H<sub>1</sub>R agonists with partial H<sub>2</sub>R agonism (Seifert et al., 2003). Burimamide (**7**) and metiamide (**22**) are neutral H<sub>2</sub>R antagonists, whereas cimetidine (**17**, CIM), ranitidine (**18**, RAN), famotidine (**19**, FAM), aminopotentidine (**20**, APT), and iodoaminopotentidine (**21**, IAPT) act as inverse agonists (Hill et al., 1997; Dove et al., 2004). Previous studies showed that the determination of adenylyl cyclase (AC) activity in Sf9 cell membranes is a very sensitive system to elucidate differences in the constitutive activities of GPCRs (Seifert et al., 1998b). Therefore, we also assessed AC activity in membranes expressing non-fused H<sub>2</sub>R<sub>s</sub> (coupling to endogenous G<sub>sα</sub>-like G proteins), in membranes coexpressing H<sub>2</sub>R and mammalian G<sub>sαS</sub>, and in membranes expressing H<sub>2</sub>R-G<sub>sαS</sub> fusion proteins.

## 7.2 Materials and Methods

### 7.2.1 Materials

The cDNA for the rH<sub>2</sub>R was kindly provided by Dr. R. Leurs (Leiden/Amsterdam Center for Drug Research, Department of Medicinal Chemistry, Vrije Universiteit Amsterdam, Amsterdam, The Netherlands) (Ruat et al., 1991). The cDNA for the cH<sub>2</sub>R was kindly provided by Dr. I. Gantz (University of Michigan, Medical School and Ann Arbor VA Medical Center, Ann Arbor, MI) (Gantz et al., 1991a). The generation of the baculoviruses encoding hH<sub>2</sub>R, gpH<sub>2</sub>R, hH<sub>2</sub>R-G<sub>sαS</sub>, and gpH<sub>2</sub>R-G<sub>sαS</sub> was described previously (Kelley et al., 2001; Houston et al., 2002). The baculoviruses encoding G<sub>sαS</sub> were kindly provided by Drs. R. Sunahara and A. G. Gilman (Department of Pharmacology, University of Southwestern Medical Center, Dallas, TX, USA). The generation of pGEM-3Z-SF-β<sub>1</sub>AR-G<sub>sαS</sub> and pVL1392-SF-β<sub>1</sub>AR-G<sub>sαS</sub> was described previously (Wenzel-Seifert et al., 2002). A description of the preparation of all remaining materials is given in chapter 6.1.

### 7.2.2 Construction of the cDNAs for rH<sub>2</sub>R and rH<sub>2</sub>R-G<sub>sαS</sub>

The cDNAs encoding for the proteins were generated by sequential overlap-extension PCRs. With pGEM-3Z-SF-gpH<sub>2</sub>R-G<sub>sαS</sub> as template, PCR 1A was used to amplify a DNA fragment

consisting of the cleavable signal peptide from influenza hemagglutinin (S), the FLAG epitope (F) recognized by the M1 monoclonal antibody, and the start codon of the rH<sub>2</sub>R. The sense primer annealed with 18 bp of pGEM-3Z prior to the 5'-end of SF. The antisense primer annealed with 15 bp of the 3'-end of SF and with ATG. In PCR 1B, the cDNA encoding the rH<sub>2</sub>R followed by a hexahistidine tag in 3'-position was generated. The hexahistidine tag was included to allow future purification and to provide additional protection against proteolysis (Seifert et al., 1998a). The sense primer consisted of 15 bp of the 3'-end of SF and the first 22 bp of the 5'-end of the rH<sub>2</sub>R. The antisense primer consisted of 18 bp of the C-terminus of the rH<sub>2</sub>R, the hexahistidine tag, the stop codon, and an *Xba* I site. The cDNA for the rH<sub>2</sub>R was extracted from pcDNA-rH<sub>2</sub>R after restriction digestion with *Hind* III and *Bgl* II and was used as template. In PCR 2, the products of PCR 1A and PCR 1B annealed in the region encoding SF and ATG. Here, the sense primer of PCR 1A and the antisense primer of PCR 1B were used. In that way, a fragment encoding SF, the rH<sub>2</sub>R, the hexahistidine tag, the stop codon, and an *Xba* I site was obtained. This fragment was digested with *Sac* I and *Xba* I and cloned into pGEM-3Z-SF-hH<sub>2</sub>R digested with *Sac* I and *Xba* I to yield pGEM-3Z-SF-rH<sub>2</sub>R. pGEM-3Z-SF-rH<sub>2</sub>R was digested with *Sac* I and *Xba* I and cloned into the baculovirus transfer vector pVL1392-SF-hH<sub>2</sub>R digested with *Sac* I and *Xba* I. With pGEM-3Z-SF-rH<sub>2</sub>R as template, the sense primer of PCR 1A, and an antisense primer encoding six histidines, in PCR 3A a fragment encoding SF, the cDNA for the rH<sub>2</sub>R, and the hexahistidine tag was generated. In PCR 3B, a fragment encoding the hexahistidine tag, the cDNA of G<sub>saS</sub>, the stop codon, and an *Xba* I site was generated. Here, the sense primer annealed with the hexahistidine tag and the start codon of G<sub>saS</sub>, and the antisense primer annealed with the cDNA encoding the 5 C-terminal amino acids of G<sub>saS</sub>, the stop codon, and an *Xba* I site. pGEM-3Z-SF-gpH<sub>2</sub>R-G<sub>saS</sub> was used as template. In PCR 4, the products of PCRs 3A and 3B annealed in the hexahistidine region, and the sense primer of PCR 1A and the antisense primer of PCR 3B were used. In that way, the complete cDNA for the rH<sub>2</sub>R-G<sub>saS</sub> fusion protein, consisting of SF, the cDNA for the rH<sub>2</sub>R, the hexahistidine tag, and the cDNA of G<sub>saS</sub> was amplified. The product of PCR 4 was digested with *Sac* I and *Bgl* II and cloned into pGEM-3Z-SF-β<sub>1</sub>AR-G<sub>saS</sub> digested with *Sac* I and *Bgl* II. Additionally, the PCR 4 product was digested with *Sac* I and *Bgl* II and directly cloned into pVL1392-SF-β<sub>1</sub>AR-G<sub>saS</sub> that was digested with *Sac* I and *Bgl* II and treated with calf intestinal phosphatase to yield the baculovirus transfer vector pVL1392-SF-rH<sub>2</sub>R-G<sub>saS</sub>.

### 7.2.3 Construction of the cDNAs for cH<sub>2</sub>R and cH<sub>2</sub>R-G<sub>saS</sub>

The strategy for the generation of the cDNAs for the epitope-tagged cH<sub>2</sub>R and cH<sub>2</sub>R-G<sub>saS</sub> was analogous to the strategy for the generation of the cDNAs for rH<sub>2</sub>R and rH<sub>2</sub>R-G<sub>saS</sub>. With

pGEM-3Z-SF-gpH<sub>2</sub>R-G<sub>ssS</sub> as template, in PCR 1A the SF region and the start codon of the cH<sub>2</sub>R were amplified. The sense primer annealed with 18 bp of pGEM-3Z prior to the 5'-end of SF, and the antisense primer annealed with 15 bp of the 3'-end of SF and with ATG. In PCR 1B, the cDNA encoding the sequence for the cH<sub>2</sub>R followed by the hexahistidine tag in 3'-position was generated. The sense primer consisted of 15 bp of the 3'-end of SF and the first 21 bp of the 5'-end of cH<sub>2</sub>R. The antisense primer consisted of 18 bp of the C-terminus of the cH<sub>2</sub>R, the hexahistidine tag, the stop codon, and an *Xba* I site. The cDNA for the cH<sub>2</sub>R was extracted from CMVneo-cH<sub>2</sub>R after digestion with *Bgl* II and was used as template. In PCR 2, the products of PCR 1A and PCR 1B annealed in the region encoding SF and ATG. Here, the sense primer of PCR 1A and the antisense primer of PCR 1B were used. In that way, a fragment encoding SF, the cH<sub>2</sub>R, the hexahistidine tag, the stop codon, and an *Xba* I site was obtained. This fragment was digested with *Sac* I and *Xba* I and cloned into pGEM-3Z-SF-hH<sub>2</sub>R digested with *Sac* I and *Xba* I to yield pGEM-3Z-SF-cH<sub>2</sub>R. pGEM-3Z-SF-cH<sub>2</sub>R was digested with *Sac* I and *Xba* I and cloned into the baculovirus transfer vector pVL1392-SF-hH<sub>2</sub>R digested with *Sac* I and *Xba* I. PCR 3 was used to generate a fragment encoding the C-terminus of the cH<sub>2</sub>R, the hexahistidine tag, and G<sub>ssS</sub>. The sense primer encoded the last 10 amino acids of the C-terminus of the cH<sub>2</sub>R, the hexahistidine tag, and the start codon of G<sub>ssS</sub>, and the antisense primer encoded the 5 C-terminal amino acids of G<sub>ssS</sub>, the stop codon, and an *Xba* I site. Here, pGEM-3Z-SF-hH<sub>2</sub>R-G<sub>ssS</sub> was used as template. This fragment was digested with *Xho* I and *Xba* I and cloned into pGEM-3Z-SF-cH<sub>2</sub>R digested with *Xho* I and *Xba* I to yield pGEM-3Z-SF-cH<sub>2</sub>R-G<sub>ssS</sub>. pGEM-3Z-SF-cH<sub>2</sub>R-G<sub>ssS</sub> was digested with *Sac* I and *Bgl* II and cloned into pVL1392-SF-β<sub>1</sub>AR-G<sub>ssS</sub> that was digested with *Sac* I and *Bgl* II and treated with calf intestinal phosphatase, to yield the baculovirus transfer vector pVL1392-SF-cH<sub>2</sub>R-G<sub>ssS</sub>.

#### 7.2.4 Generation of recombinant baculoviruses, cell culture, and membrane preparation

A description is given in chapter 6.2.

#### 7.2.5 SDS-PAGE and immunoblot analysis

A description is given in chapter 6.3.

### 7.2.6 Steady-state GTPase activity assay

A description is given in chapter 6.4.

### 7.2.7 AC activity assay

A description is given in chapter 6.5.

## 7.3 Results

### 7.3.1 Immunological detection of recombinant proteins in Sf9 cell membranes

The predicted molecular mass of the H<sub>2</sub>R is ~33 kDa (Gantz et al., 1991a, b; Fukushima et al., 1997). H<sub>2</sub>R species isoforms presumably exhibit similar glycosylation patterns, since the putative N-glycosylation sites for the H<sub>2</sub>R, Asn-4 and Asn-162, are fully conserved within their sequences (Figure 7.1) (Fukushima et al., 1995). However, only rH<sub>2</sub>R and hH<sub>2</sub>R migrated as the expected bands for monomeric GPCRs (Figure 7.3 A, B). Both bands occurred as doublets, representing different glycosylation forms (Houston et al., 2002). Additional bands were detected at ~70 kDa, presumably representing receptor dimers. A similar pattern of immunoreactive bands was previously observed for the hH<sub>2</sub>R (Houston et al., 2002). In contrast, both cH<sub>2</sub>R and gpH<sub>2</sub>R displayed strong doublet bands at ~60 kDa that coincide with the expected bands of differentially glycosylated H<sub>2</sub>R dimers, whereas the bands for monomers were absent. Additional bands were detected at ~150 kDa and above 250 kDa, possibly corresponding to H<sub>2</sub>R tetramers and higher oligomers, respectively. Dimerization and oligomerization of the cH<sub>2</sub>R has been described previously (Fukushima et al., 1997), but in those experiments, also receptor monomers were detected. Hence, gpH<sub>2</sub>R and cH<sub>2</sub>R possibly migrated atypically in SDS-PAGE, *i.e.* the bands at ~60 kDa and ~150 kDa could correspond to monomers and dimers, respectively, and not to dimers and tetramers. With the anti-6His Ig, in membranes expressing cH<sub>2</sub>R an additional doublet band at ~23 kDa was detected, and in rH<sub>2</sub>R- and hH<sub>2</sub>R membranes a ~27 kDa band was present. However, no such bands were detected in gpH<sub>2</sub>R membranes. The ~23-27 kDa bands may represent differentially and atypically migrating H<sub>2</sub>R monomers not recognized by the M1 antibody because of a lack of epitope exposure. By analogy to formyl peptide receptors (Wenzel-Seifert and Seifert, 2003), differences in the C-termini of H<sub>2</sub>R species isoforms may constitute the molecular basis for the species-selective migration pattern. Thus, H<sub>2</sub>R species

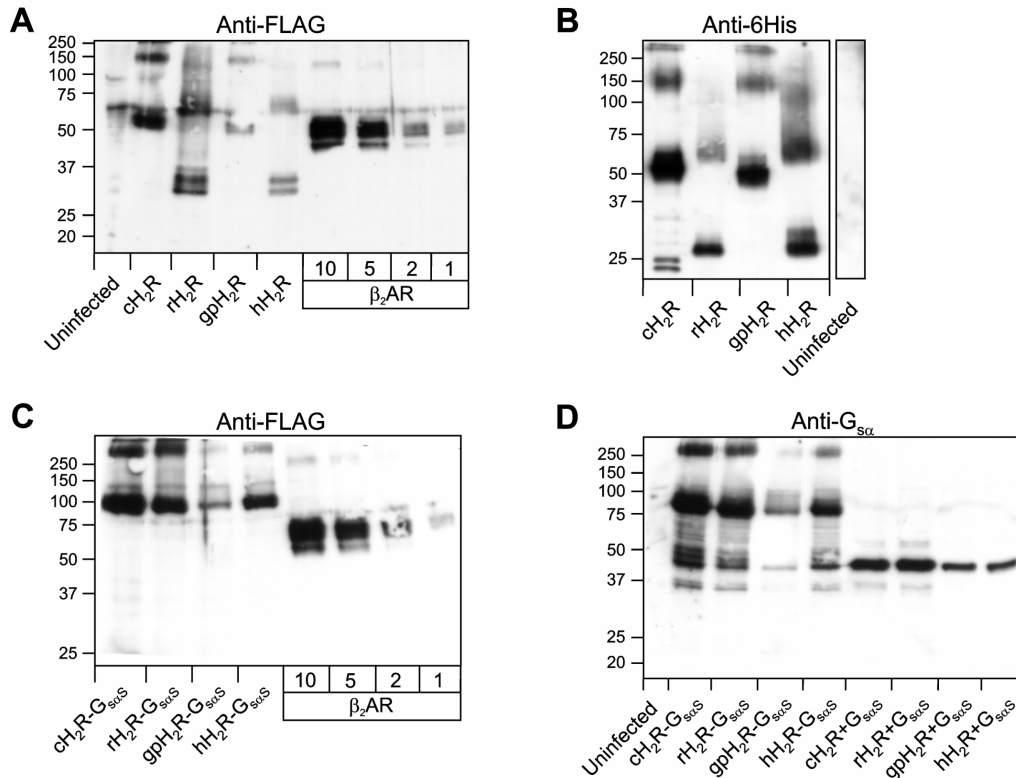


**Figure 7.3:** Immunological detection and analysis of the expression of recombinant proteins in Sf9 cells. In each lane, 10 µg of membrane protein was loaded onto the gel, unless otherwise indicated below membranes. Exceptionally, 40 µg of a membrane expressing gpH<sub>2</sub>R-G<sub>saS</sub> were loaded onto the gels in panels C and D. Numbers on the left of membranes designate masses of marker proteins in kDa. In A and C, 1, 2, 5, and 10 µg of protein of Sf9 membranes expressing the β<sub>2</sub>AR at 7.5 pmol mg<sup>-1</sup> (as determined by [<sup>3</sup>H]DHA saturation binding) were used as standard to assess the expression levels of H<sub>2</sub>R species isoforms. In D, membranes expressing H<sub>2</sub>R-G<sub>saS</sub> fusion proteins and membranes coexpressing H<sub>2</sub>R species and mammalian G<sub>saS</sub> were loaded onto the gel.

isoforms were well expressed in Sf9 membranes, but due to their widely different migration, it was impossible to precisely assess their expression levels using β<sub>2</sub>AR-membranes calibrated with [<sup>3</sup>H]dihydroalprenolol saturation binding as standard (Kelley et al., 2001).

H<sub>2</sub>R-G<sub>saS</sub> fusion proteins of canine, rat, guinea pig, and human occurred as strong bands at ~80 kDa (Figure 7.3 C). Since G<sub>saS</sub> has an apparent molecular mass of ~45 kDa (Graziano et al., 1989), these bands correspond to H<sub>2</sub>R-G<sub>saS</sub> monomers. Weaker bands were detected at ~110 kDa, most probably representing differently glycosylated fusion proteins. With all species additional bands at ~250 kDa were detected, presumably representing H<sub>2</sub>R-G<sub>saS</sub> dimers or oligomers. ch<sub>2</sub>R-G<sub>saS</sub> was expressed at ~5 pmol mg<sup>-1</sup>, rH<sub>2</sub>R-G<sub>saS</sub> at ~4 pmol mg<sup>-1</sup>, gpH<sub>2</sub>R-G<sub>saS</sub> at ~1 pmol mg<sup>-1</sup>, and hH<sub>2</sub>R-G<sub>saS</sub> at ~3 pmol mg<sup>-1</sup> using β<sub>2</sub>AR-membranes as standard. To account for the decreased expression level of gpH<sub>2</sub>R-G<sub>saS</sub>, in this case the amount of protein applied to the gel was adjusted to 40 µg.

Probing membranes expressing H<sub>2</sub>R-G<sub>saS</sub> species with the anti-G<sub>sa</sub> Ig yielded ~80 kDa and ~250 kDa bands (Figure 7.3 D) which are consistent with those bands observed with the anti-FLAG Ig. Additional bands appeared at ~45 kDa, representing atypically migrating or partially degraded fusion proteins. In all membranes coexpressing H<sub>2</sub>R species and G<sub>saS</sub>, the expected bands for G<sub>saS</sub> monomers were detected at ~45 kDa. The expression levels of G<sub>saS</sub> in membranes coexpressing H<sub>2</sub>R and G<sub>saS</sub> were estimated using the ~80 kDa peak intensities of H<sub>2</sub>R-G<sub>saS</sub> species as standard and were ~2 pmol mg<sup>-1</sup> in membranes coexpressing cH<sub>2</sub>R and G<sub>saS</sub>, ~2 pmol mg<sup>-1</sup> in membranes coexpressing rH<sub>2</sub>R and G<sub>saS</sub>, ~1 pmol mg<sup>-1</sup> in membranes coexpressing gpH<sub>2</sub>R and G<sub>saS</sub>, and ~1 pmol mg<sup>-1</sup> in membranes coexpressing hH<sub>2</sub>R and G<sub>saS</sub>.

### 7.3.2 Efficacies and potencies of agonists at H<sub>2</sub>R-G<sub>saS</sub> species isoforms

#### derived from the GTPase assay

Efficacies and potencies of compounds **1-16** and **22** at H<sub>2</sub>R-G<sub>saS</sub> fusion proteins of human, guinea pig, rat, and canine are summarized in Table 7.1. The small H<sub>2</sub>R agonists acted as full (**1-3**) or as nearly full (**4**) agonists at the four receptors with approximately similar efficacies. HA (**1**) and DIM (**2**) were equipotent at human, guinea pig, and rat H<sub>2</sub>R-G<sub>saS</sub>, but showed lower EC<sub>50</sub> values at cH<sub>2</sub>R-G<sub>saS</sub>. AMT (**3**) was slightly more potent at cH<sub>2</sub>R-G<sub>saS</sub> than at hH<sub>2</sub>R-G<sub>saS</sub> and gpH<sub>2</sub>R-G<sub>saS</sub>. At rH<sub>2</sub>R-G<sub>saS</sub>, the potency of AMT (**3**) was further decreased. BET (**4**) acted with increased potencies at gpH<sub>2</sub>R-G<sub>saS</sub> and cH<sub>2</sub>R-G<sub>saS</sub>, compared to hH<sub>2</sub>R-G<sub>saS</sub> and rH<sub>2</sub>R-G<sub>saS</sub>. In agreement with previous studies (Kelley et al., 2001; Xie et al., 2006a, b), *N*-[3-(1*H*-imidazol-4-yl)propyl]guanidines (**8-10**) and their *N*<sup>G</sup>-acylated analogs (**11-16**) were more potent and more efficacious at gpH<sub>2</sub>R-G<sub>saS</sub> than at hH<sub>2</sub>R-G<sub>saS</sub>. At gpH<sub>2</sub>R-G<sub>saS</sub>, UR-PG222A (**13**) was more efficacious than HA (**1**). At hH<sub>2</sub>R-G<sub>saS</sub> and rH<sub>2</sub>R-G<sub>saS</sub> the compounds exhibited similar efficacies and potencies. Only UR-PG214 (**11**) was slightly more potent at rH<sub>2</sub>R-G<sub>saS</sub> than at hH<sub>2</sub>R-G<sub>saS</sub>. Apart from ARP (**9**) and its *N*<sup>G</sup>-acylated analog UR-PG136 (**15**) that acted with similar efficacies at cH<sub>2</sub>R-G<sub>saS</sub> and hH<sub>2</sub>R-G<sub>saS</sub>, compounds **8-16** were more efficacious at cH<sub>2</sub>R-G<sub>saS</sub> than at hH<sub>2</sub>R-G<sub>saS</sub>. Compounds **8-16** were also more potent at cH<sub>2</sub>R-G<sub>saS</sub> than at hH<sub>2</sub>R-G<sub>saS</sub>. An exception of this rule was UR-PG123 (**14**) that exhibited the largest efficacy increase (~4-fold) but was somewhat less potent at cH<sub>2</sub>R-G<sub>saS</sub> than at hH<sub>2</sub>R-G<sub>saS</sub>. In summary, small H<sub>2</sub>R agonists **1-4** acted with similar efficacies at all H<sub>2</sub>R-G<sub>saS</sub> species isoforms investigated, but were more potent at cH<sub>2</sub>R-G<sub>saS</sub> compared to hH<sub>2</sub>R-G<sub>saS</sub>, gpH<sub>2</sub>R-G<sub>saS</sub>, and rH<sub>2</sub>R-G<sub>saS</sub>. Guanidines and *N*<sup>G</sup>-acylated guanidines **8-16** acted with increased efficacies and potencies at gpH<sub>2</sub>R-G<sub>saS</sub> and cH<sub>2</sub>R-G<sub>saS</sub> compared to hH<sub>2</sub>R-G<sub>saS</sub>, whereas no selectivity was observed between rH<sub>2</sub>R-G<sub>saS</sub> and hH<sub>2</sub>R-G<sub>saS</sub>.

**Table 7.1:** Agonist efficacies ( $E_{\text{Max}}$ ) and potencies at H<sub>2</sub>R-G<sub>saS</sub> species isoforms in the GTPase assay. GTPase activity in Sf9 membranes was determined as described in chapter 6.4. Data shown are the means  $\pm$  S.D. of three to five experiments performed in duplicate. Efficacies and potencies, respectively, of ligands at hH<sub>2</sub>R-G<sub>saS</sub> were compared with the corresponding parameters at gpH<sub>2</sub>R-G<sub>saS</sub>, rH<sub>2</sub>R-G<sub>saS</sub>, and cH<sub>2</sub>R-G<sub>saS</sub>, respectively, using one-way ANOVA.

Cpd.	hH <sub>2</sub> R-G <sub>saS</sub>		gpH <sub>2</sub> R-G <sub>saS</sub>		rH <sub>2</sub> R-G <sub>saS</sub>		cH <sub>2</sub> R-G <sub>saS</sub>	
	$E_{\text{Max}}^a$	EC <sub>50</sub> (nM)	$E_{\text{Max}}^a$	EC <sub>50</sub> (nM)	$E_{\text{Max}}^a$	EC <sub>50</sub> (nM)	$E_{\text{Max}}^a$	EC <sub>50</sub> (nM)
1	1.00	990 $\pm$ 92	1.00	850 $\pm$ 340	1.00	1200 $\pm$ 16	1.00	290 $\pm$ 50 <sup>++</sup>
2	0.85 $\pm$ 0.02	910 $\pm$ 430	0.94 $\pm$ 0.06 <sup>*</sup>	740 $\pm$ 360	0.89 $\pm$ 0.03	1100 $\pm$ 92	0.90 $\pm$ 0.04	480 $\pm$ 82
3	0.91 $\pm$ 0.02	190 $\pm$ 50	1.04 $\pm$ 0.01 <sup>**</sup>	190 $\pm$ 42	0.91 $\pm$ 0.03	360 $\pm$ 100 <sup>+</sup>	0.82 $\pm$ 0.03 <sup>**</sup>	110 $\pm$ 66
4	0.81 $\pm$ 0.07	44000 $\pm$ 8900	0.72 $\pm$ 0.02	28000 $\pm$ 4400 <sup>+</sup>	0.71 $\pm$ 0.03	47000 $\pm$ 9100	0.78 $\pm$ 0.08	27000 $\pm$ 6900 <sup>+</sup>
5	0.45 $\pm$ 0.05	13000 $\pm$ 1000	0.26 $\pm$ 0.01 <sup>**</sup>	6800 $\pm$ 1900 <sup>++</sup>	0.43 $\pm$ 0.01	13000 $\pm$ 1000	0.68 $\pm$ 0.02 <sup>**</sup>	13000 $\pm$ 1200
6	0.54 $\pm$ 0.08	240 $\pm$ 41	0.43 $\pm$ 0.02 <sup>*</sup>	310 $\pm$ 62	0.43 $\pm$ 0.02 <sup>*</sup>	400 $\pm$ 81 <sup>+</sup>	0.77 $\pm$ 0.03 <sup>**</sup>	260 $\pm$ 18
7	0.16 $\pm$ 0.01	14000 $\pm$ 12000	0.17 $\pm$ 0.02	12000 $\pm$ 3600	0.18 $\pm$ 0.02	15000 $\pm$ 2100	0.40 $\pm$ 0.01 <sup>**</sup>	11000 $\pm$ 210
8	0.82 $\pm$ 0.02	160 $\pm$ 42	0.96 $\pm$ 0.06	18 $\pm$ 9 <sup>++</sup>	0.99 $\pm$ 0.06 <sup>*</sup>	110 $\pm$ 9	0.99 $\pm$ 0.10 <sup>*</sup>	41 $\pm$ 18 <sup>++</sup>
9	0.84 $\pm$ 0.03	72 $\pm$ 9	0.94 $\pm$ 0.05 <sup>*</sup>	7 $\pm$ 1 <sup>++</sup>	0.80 $\pm$ 0.03	90 $\pm$ 7 <sup>++</sup>	0.84 $\pm$ 0.07	10 $\pm$ 1 <sup>++</sup>
10	0.71 $\pm$ 0.11	130 $\pm$ 13	0.87 $\pm$ 0.05	43 $\pm$ 10 <sup>++</sup>	0.70 $\pm$ 0.04	140 $\pm$ 22	0.88 $\pm$ 0.05 <sup>*</sup>	46 $\pm$ 6 <sup>++</sup>
11	0.91 $\pm$ 0.08	130 $\pm$ 45	0.94 $\pm$ 0.05	25 $\pm$ 10 <sup>++</sup>	1.03 $\pm$ 0.06	84 $\pm$ 8	1.00 $\pm$ 0.06	28 $\pm$ 8 <sup>++</sup>
12	0.80 $\pm$ 0.04	120 $\pm$ 45	0.94 $\pm$ 0.05 <sup>*</sup>	14 $\pm$ 4 <sup>++</sup>	0.82 $\pm$ 0.06	96 $\pm$ 12	0.99 $\pm$ 0.05 <sup>**</sup>	40 $\pm$ 10 <sup>++</sup>
13	0.90 $\pm$ 0.04	18 $\pm$ 6	1.18 $\pm$ 0.08 <sup>**</sup>	5 $\pm$ 1 <sup>++</sup>	0.93 $\pm$ 0.01	13 $\pm$ 1	0.98 $\pm$ 0.03	3 $\pm$ 2 <sup>++</sup>
14	0.14 $\pm$ 0.03	250 $\pm$ 13	0.40 $\pm$ 0.02 <sup>**</sup>	220 $\pm$ 22	0.15 $\pm$ 0.02	250 $\pm$ 48	0.59 $\pm$ 0.02 <sup>**</sup>	340 $\pm$ 33 <sup>+</sup>
15	0.82 $\pm$ 0.05	100 $\pm$ 9	1.02 $\pm$ 0.11 <sup>*</sup>	29 $\pm$ 10 <sup>++</sup>	0.73 $\pm$ 0.02	100 $\pm$ 16	0.86 $\pm$ 0.08	52 $\pm$ 4 <sup>++</sup>
16	0.86 $\pm$ 0.05	15 $\pm$ 4	0.97 $\pm$ 0.18	14 $\pm$ 6	0.73 $\pm$ 0.02	14 $\pm$ 1	0.92 $\pm$ 0.03	5 $\pm$ 3 <sup>+</sup>
22	-0.08 $\pm$ 0.01	1400 $\pm$ 900	-0.06 $\pm$ 0.01	750 $\pm$ 460	-0.04 $\pm$ 0.01 <sup>**</sup>	670 $\pm$ 510	0.06 $\pm$ 0.01 <sup>**</sup>	21000 $\pm$ 2200 <sup>++</sup>

<sup>a</sup> Efficacy relative to HA (= 1.00)

<sup>\*</sup> comparison with the efficacy at hH<sub>2</sub>R-G<sub>saS</sub>; <sup>\*</sup>  $p < 0.05$ ; <sup>\*\*</sup>  $p < 0.01$

<sup>+</sup> comparison with the EC<sub>50</sub> value at hH<sub>2</sub>R-G<sub>saS</sub>; <sup>+</sup>  $p < 0.05$ ; <sup>++</sup>  $p < 0.01$



Compounds **5** and **6** are representatives of H<sub>1</sub>R agonists with partial H<sub>2</sub>R agonism (Seifert et al., 2003). Both compounds were less efficacious at gpH<sub>2</sub>R-G<sub>saS</sub> than at hH<sub>2</sub>R-G<sub>saS</sub> and similarly efficacious at rH<sub>2</sub>R-G<sub>saS</sub> and hH<sub>2</sub>R-G<sub>saS</sub> (Table 7.1). In the GTPase assay at H<sub>2</sub>R-G<sub>saS</sub> fusion proteins, burimamide (**7**) was a weak partial agonist with similar efficacies at human, guinea pig, and rat species. Strikingly, compounds **5**, **6**, and **7** acted with significantly increased efficacies at cH<sub>2</sub>R-G<sub>saS</sub> compared to hH<sub>2</sub>R-G<sub>saS</sub>. Apart from 2-benzylhistamine (**5**) with ~2-fold increased potency at gpH<sub>2</sub>R-G<sub>saS</sub>, the potencies of **5-7** did not significantly differ between the species investigated. Taken together, partial H<sub>2</sub>R agonists were considerably more efficacious at cH<sub>2</sub>R-G<sub>saS</sub> than at human, guinea pig, and rat H<sub>2</sub>R-G<sub>saS</sub>.

### 7.3.3 Potencies and inverse agonist efficacies of antagonists at H<sub>2</sub>R-G<sub>saS</sub>

#### species isoforms derived from the GTPase assay

$K_B$  values and inverse agonist efficacies of the H<sub>2</sub>R antagonists CIM (**17**), RAN (**18**), FAM (**19**), APT (**20**), and IAPT (**21**) are listed in Table 7.2. The compounds decreased GTPase activities below basal values and thus acted as inverse agonists at all four species. At hH<sub>2</sub>R-G<sub>saS</sub> and gpH<sub>2</sub>R-G<sub>saS</sub> compounds **17-21** decreased the basal GTPase signal (0%) by ~10% if the maximum stimulatory effect of 100  $\mu$ M HA was set to 100%. At rH<sub>2</sub>R-G<sub>saS</sub> the inverse agonist efficacies of **17-21** were somewhat smaller. At cH<sub>2</sub>R-G<sub>saS</sub> all compounds except CIM (**17**) showed a significantly higher reduction of the basal GTPase activity by ~20%. The  $K_B$  values of **17-21** were similar at hH<sub>2</sub>R-G<sub>saS</sub> and gpH<sub>2</sub>R-G<sub>saS</sub>. At rH<sub>2</sub>R-G<sub>saS</sub>, **17-19** were less potent, and **20** and **21** were similarly potent compared to hH<sub>2</sub>R-G<sub>saS</sub>. By contrast, all compounds except FAM (**19**) were less potent at cH<sub>2</sub>R-G<sub>saS</sub> than at hH<sub>2</sub>R-G<sub>saS</sub>. Taken together, most of the H<sub>2</sub>R antagonists studied displayed increased inverse agonist efficacies and decreased potencies at cH<sub>2</sub>R-G<sub>saS</sub> compared to hH<sub>2</sub>R-G<sub>saS</sub>.

**Table 7.2:** Potencies and inverse agonist efficacies of antagonists at H<sub>2</sub>R-G<sub>saS</sub> species isoforms in the GTPase assay. Reaction mixtures contained Sf9 membranes expressing fusion proteins, 1  $\mu$ M HA as agonist and antagonists at concentrations from 1 nM to 100  $\mu$ M as appropriate to generate saturated competition curves. To determine the inverse agonist efficacies (Inv. Eff.), the effects of antagonists at fixed concentrations (10  $\mu$ M of **18-21**; 100  $\mu$ M of **17**) on basal GTPase activity were assessed and referred to the stimulatory effect of 100  $\mu$ M HA (= 1.00). Data shown are the means  $\pm$  S.D. of three experiments performed in duplicates.  $K_B$  values and inverse agonist efficacies, respectively, of antagonists at hH<sub>2</sub>R-G<sub>saS</sub> were compared with the corresponding parameters at gpH<sub>2</sub>R-G<sub>saS</sub>, rH<sub>2</sub>R-G<sub>saS</sub>, and cH<sub>2</sub>R-G<sub>saS</sub>, respectively, using one-way ANOVA.

Cpd.	hH <sub>2</sub> R-G <sub>saS</sub>		gpH <sub>2</sub> R-G <sub>saS</sub>		rH <sub>2</sub> R-G <sub>saS</sub>		cH <sub>2</sub> R-G <sub>saS</sub>	
	$K_B$ (nM)	Inv. Eff.	$K_B$ (nM)	Inv. Eff.	$K_B$ (nM)	Inv. Eff.	$K_B$ (nM)	Inv. Eff.
<b>17</b>	1700 $\pm$ 430	-0.08 $\pm$ 0.01	1300 $\pm$ 270	-0.09 $\pm$ 0.02	2800 $\pm$ 340*	-0.06 $\pm$ 0.01	7500 $\pm$ 400**	-0.07 $\pm$ 0.02
<b>18</b>	840 $\pm$ 94	-0.09 $\pm$ 0.01	1000 $\pm$ 170	-0.08 $\pm$ 0.01	2100 $\pm$ 410**	-0.06 $\pm$ 0.01 <sup>++</sup>	1500 $\pm$ 160*	-0.18 $\pm$ 0.01 <sup>++</sup>
<b>19</b>	48 $\pm$ 10	-0.10 $\pm$ 0.02	38 $\pm$ 3	-0.10 $\pm$ 0.01	91 $\pm$ 7**	-0.07 $\pm$ 0.01 <sup>+</sup>	59 $\pm$ 1	-0.22 $\pm$ 0.01 <sup>++</sup>
<b>20</b>	180 $\pm$ 12	-0.09 $\pm$ 0.01	260 $\pm$ 43*	-0.09 $\pm$ 0.01	170 $\pm$ 27	-0.06 $\pm$ 0.01 <sup>+</sup>	620 $\pm$ 49**	-0.20 $\pm$ 0.01 <sup>++</sup>
<b>21</b>	35 $\pm$ 7	-0.10 $\pm$ 0.01	26 $\pm$ 4	-0.10 $\pm$ 0.01	32 $\pm$ 8	-0.07 $\pm$ 0.01 <sup>++</sup>	83 $\pm$ 21**	-0.22 $\pm$ 0.01 <sup>++</sup>

\* comparison with the  $K_B$  value at hH<sub>2</sub>R-G<sub>saS</sub>; \*  $p < 0.05$ ; \*\*  $p < 0.01$

+ comparison with Inv. Eff. at hH<sub>2</sub>R-G<sub>saS</sub>; +  $p < 0.05$ ; ++  $p < 0.01$

### 7.3.4 Constitutive activities of hH<sub>2</sub>R-G<sub>saS</sub>, gpH<sub>2</sub>R-G<sub>saS</sub>, rH<sub>2</sub>R-G<sub>saS</sub>, and cH<sub>2</sub>R-G<sub>saS</sub> in the GTPase assay

As was reported for a constitutively activated mutant of the  $\beta_2$ AR (Samama et al., 1993), the following major hallmarks distinguish constitutively active GPCRs from not (quiescent) or less constitutively active GPCRs. First, the efficacies of partial agonists are increased at the more constitutively active receptor. To uncover differences in the constitutive activities among H<sub>2</sub>R-G<sub>saS</sub> species, efficacies of partial and full agonists **1-16** and inverse agonist efficacies of antagonists **17-21** were compared at hH<sub>2</sub>R-G<sub>saS</sub> with gpH<sub>2</sub>R-G<sub>saS</sub>, rH<sub>2</sub>R-G<sub>saS</sub>, and cH<sub>2</sub>R-G<sub>saS</sub>, respectively (Figure 7.4 A, C, E). Second, constitutively active receptors exhibit an increased affinity for agonists but not antagonists, with the extent of affinity increase being correlated with the efficacy of the ligand (Lefkowitz et al., 1993). Essentially, the potencies in the GTPase assay represent apparent affinities and can be therefore related, as logEC<sub>50</sub> differences between hH<sub>2</sub>R-G<sub>saS</sub> and the other H<sub>2</sub>R species isoforms, to the corresponding

efficacies at hH<sub>2</sub>R-G<sub>saS</sub> (Figure 7.4 B, D, F). Finally, at receptors with increased constitutive activity inverse agonists have an elevated inhibitory effect on GTP hydrolysis (Seifert et al., 1998b).

Similar inverse agonist efficacies of antagonists **17-21** and the absence of selectivity in the efficacies of partial agonists **5-7** and **14** indicate equal magnitudes of constitutive activities for gpH<sub>2</sub>R-G<sub>saS</sub> and hH<sub>2</sub>R-G<sub>saS</sub> (Figure 7.4 A). As Figure 7.4 B illustrates, a poor but significant correlation ( $r^2 = 0.27$ ,  $p = 0.016$ ) was observed between the log (potency ratio) of these species and the efficacies of compounds **1-21** at hH<sub>2</sub>R-G<sub>saS</sub>. However, this correlation was determined by ligand-specific interactions, namely the high potencies of guanidines (**8-10**) and *N*<sup>G</sup>-acylguanidines (**11-16**) at gpH<sub>2</sub>R-G<sub>saS</sub> (Kelley et al., 2001; Xie et al., 2006a, b), and disappeared if only compounds **1-7** and **17-21** were considered ( $r^2 = 0.04$ ,  $p = 0.527$ ). The efficacies of compounds **1-21** at rH<sub>2</sub>R-G<sub>saS</sub> and hH<sub>2</sub>R-G<sub>saS</sub> were almost identical (Figure 7.4 C). Moreover, no correlation between the log (potency ratio) and the efficacies at hH<sub>2</sub>R-G<sub>saS</sub> was evident ( $r^2 = 0.16$ ,  $p = 0.077$ ) (Figure 7.4 D). Thus, in the steady-state GTPase assay, rH<sub>2</sub>R-G<sub>saS</sub> and hH<sub>2</sub>R-G<sub>saS</sub> exhibited similar levels of constitutive activities. By contrast, cH<sub>2</sub>R-G<sub>saS</sub> showed the hallmarks of a GPCR with increased constitutive activity compared to hH<sub>2</sub>R-G<sub>saS</sub>. Specifically, partial agonists **5-7** and **14** were considerably more efficacious at cH<sub>2</sub>R-G<sub>saS</sub> and the inverse agonist efficacies of antagonists **18-21** were increased compared to hH<sub>2</sub>R-G<sub>saS</sub> (Figure 7.4 E). A highly significant correlation between the log (potency ratio) and the efficacies of compounds **1-21** at hH<sub>2</sub>R-G<sub>saS</sub> was determined ( $r^2 = 0.77$ ,  $p < 0.0001$ , Figure 7.4 F). It is noteworthy that this correlation was independent of distinct interactions of guanidines and *N*<sup>G</sup>-acylguanidines with cH<sub>2</sub>R-G<sub>saS</sub> as omitting compounds **8-16** did not change the fit ( $r^2 = 0.75$ ,  $p = 0.0003$ ).

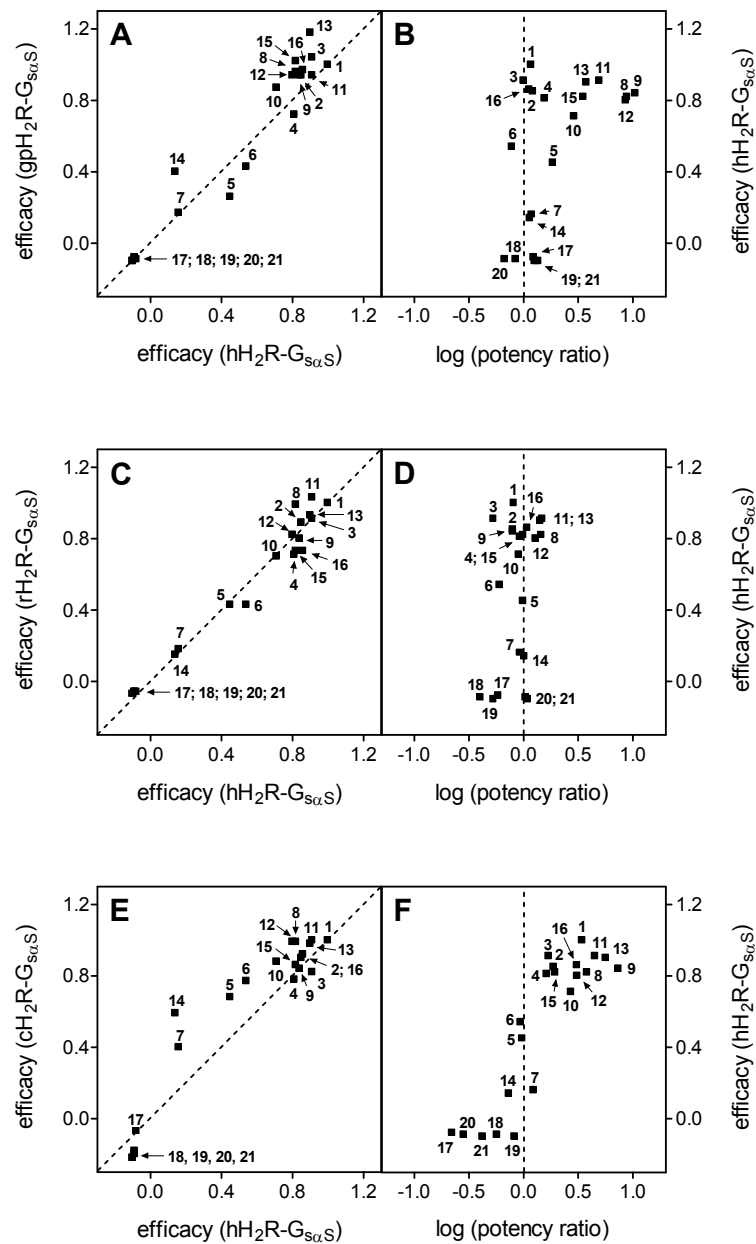


**Figure 7.4:** Efficacies and potencies of ligands **1-21** at hH<sub>2</sub>R-G<sub>sa</sub>S in pairwise comparison with gpH<sub>2</sub>R-G<sub>sa</sub>S, rH<sub>2</sub>R-G<sub>sa</sub>S, and cH<sub>2</sub>R-G<sub>sa</sub>S, respectively, as determined in the steady-state GTPase assay. A, C, E, relation between the efficacies of compounds **1-21** at hH<sub>2</sub>R-G<sub>sa</sub>S vs. gpH<sub>2</sub>R-G<sub>sa</sub>S (A), rH<sub>2</sub>R-G<sub>sa</sub>S (C), and cH<sub>2</sub>R-G<sub>sa</sub>S (E), respectively. The dashed line has a slope of 1.0 and represents a theoretical curve of identical efficacies in both systems. B, D, F, relation between log (potency ratio) of compounds **1-21** at gpH<sub>2</sub>R-G<sub>sa</sub>S (B), rH<sub>2</sub>R-G<sub>sa</sub>S (D), and cH<sub>2</sub>R-G<sub>sa</sub>S (F), respectively, and the corresponding efficacies at hH<sub>2</sub>R-G<sub>sa</sub>S. The potency ratio is the ratio of EC<sub>50</sub> values of full and partial agonists (**1-16**) at hH<sub>2</sub>R-G<sub>sa</sub>S and at gpH<sub>2</sub>R-G<sub>sa</sub>S, rH<sub>2</sub>R-G<sub>sa</sub>S, and cH<sub>2</sub>R-G<sub>sa</sub>S, respectively. Accordingly, the potency ratio of antagonists (**17-21**) is the ratio of the corresponding K<sub>B</sub> values at hH<sub>2</sub>R-G<sub>sa</sub>S and at gpH<sub>2</sub>R-G<sub>sa</sub>S, rH<sub>2</sub>R-G<sub>sa</sub>S, and cH<sub>2</sub>R-G<sub>sa</sub>S, respectively. The vertical dashed line intersects the abscissa at 0.0 and represents a theoretical curve of identical potencies in both systems.

### 7.3.5 Ambiguous response of metiamide in the GTPase assay

At hH<sub>2</sub>R-G<sub>saS</sub>, metiamide (**22**) decreased the basal GTPase signal by  $8 \pm 1\%$  and thus acted as weak inverse agonist (Table 7.1; Figure 7.5). At gpH<sub>2</sub>R-G<sub>saS</sub> and rH<sub>2</sub>R-G<sub>saS</sub>, metiamide inhibited the basal GTPase signals by  $6 \pm 1\%$  and  $4 \pm 1\%$ , respectively, and was ~2-fold more potent than at hH<sub>2</sub>R-G<sub>saS</sub>. Intriguingly, at cH<sub>2</sub>R-G<sub>saS</sub> metiamide did not act as an inverse agonist but rather as a very weak partial agonist (efficacy of  $6 \pm 1\%$ ). This is in marked contrast to the results of antagonists **18-21** reducing the basal GTPase signal at cH<sub>2</sub>R-G<sub>saS</sub> (increased constitutive activity) more effectively than at the other less constitutively active species. Furthermore, the potency of **22** was lowered by approximately 15-fold compared to hH<sub>2</sub>R-G<sub>saS</sub> and not increased as would have been expected for a partial agonist (Samama et al., 1993). Attempts to detect changes in AC activity upon stimulation with metiamide in membranes coexpressing cH<sub>2</sub>R and G<sub>saS</sub> failed due to the much lower sensitivity of this system compared to the GTPase activity assay using fusion proteins (data not shown).

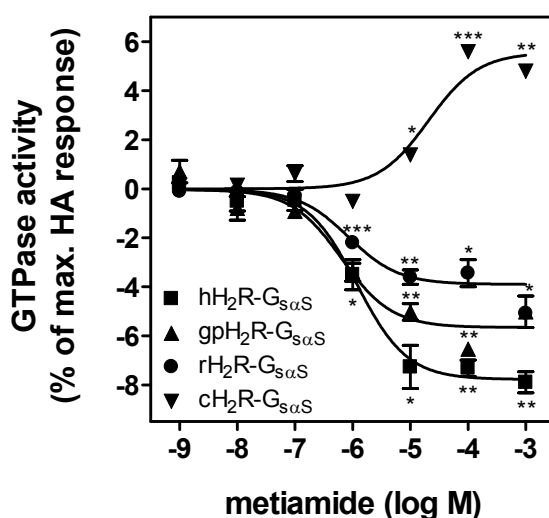


**Figure 7.5:** Effects of metiamide on GTPase activity in membranes expressing H<sub>2</sub>R-G<sub>saS</sub> species isoforms. Data are expressed as percentage change in GTPase activity induced by metiamide compared to the GTPase activity stimulated by HA (100  $\mu$ M). Data shown are the means  $\pm$  S.E.M. of three independent experiments performed in duplicates. The significance of the deviation from zero was calculated for each mean value using the t-test; \*  $p < 0.05$ ; \*\*  $p < 0.01$ ; \*\*\*  $p < 0.001$ .

### 7.3.6 Regulation of AC activities in membranes expressing fused and non-fused H<sub>2</sub>R species isoforms

AC activity was measured in Sf9 cell membranes expressing H<sub>2</sub>Rs (coupling to endogenous G<sub>sa</sub>-like G proteins), in membranes coexpressing H<sub>2</sub>R and mammalian G<sub>saS</sub>, and in membranes expressing H<sub>2</sub>R-G<sub>saS</sub> fusion proteins. Basal AC activities were similar in membranes expressing hH<sub>2</sub>R, gpH<sub>2</sub>R, and rH<sub>2</sub>R (Table 7.3) and ~2-fold higher in the case of the cH<sub>2</sub>R. GTP (10  $\mu$ M) by itself increased AC activities at all four H<sub>2</sub>R species by ~2-fold above the basal level. HA (**1**) further increased, and IAPT (**21**) inhibited this GTP-dependent signal increase, indicative for constitutive activity of all four H<sub>2</sub>R species isoforms in Sf9 membranes (Figure 7.6 A-D). These observations are in agreement with previous studies at the  $\beta_2$ AR (Seifert et al., 1998a). The stimulatory effects of GTP, as determined by relating the effects of GTP (10  $\mu$ M) to the effects of HA (100  $\mu$ M) plus GTP (10  $\mu$ M), were largest at cH<sub>2</sub>R and rH<sub>2</sub>R, compared to hH<sub>2</sub>R and gpH<sub>2</sub>R. Both the high basal AC activity and the strong stimulation with GTP indicate an elevated level of constitutive activity in membranes expressing the cH<sub>2</sub>R relative to membranes expressing hH<sub>2</sub>R, gpH<sub>2</sub>R, and rH<sub>2</sub>R. Notably, the constitutive activity of rH<sub>2</sub>R seemed to be slightly increased compared to hH<sub>2</sub>R and gpH<sub>2</sub>R. The GPCR/G protein stoichiometry affects the magnitude of response (Kenakin, 2001). In H<sub>2</sub>R membranes coexpressing mammalian G<sub>saS</sub>, 5- to 18-fold increased basal levels of AC activity were measured relative to membranes expressing H<sub>2</sub>R alone (Table 7.3). Basal AC activities were ~6-fold higher at cH<sub>2</sub>R plus G<sub>saS</sub> and ~2-fold higher at rH<sub>2</sub>R plus G<sub>saS</sub>, respectively, compared to hH<sub>2</sub>R plus G<sub>saS</sub>. With gpH<sub>2</sub>R plus G<sub>saS</sub>, the basal AC activity was somewhat lower than with hH<sub>2</sub>R plus G<sub>saS</sub>. As was observed in membranes expressing H<sub>2</sub>R alone, the highest stimulatory effects of GTP in the coexpression system were observed with cH<sub>2</sub>R and rH<sub>2</sub>R compared to gpH<sub>2</sub>R and hH<sub>2</sub>R. The inverse agonist IAPT (10  $\mu$ M) decreased the GTP-dependent increases of AC activity at all species isoforms (Figure 7.6 E-H), but even strongly reduced basal AC activities at the lowest concentrations of added GTP. These effects were probably due to traces of GDP being converted to GTP by the action of nucleoside diphosphate kinase, and were most prominent in membranes expressing cH<sub>2</sub>R plus G<sub>saS</sub> (~69% reduction below basal) and rH<sub>2</sub>R plus G<sub>saS</sub> (~59% reduction), compared to hH<sub>2</sub>R plus G<sub>saS</sub> (~29% reduction) and gpH<sub>2</sub>R plus G<sub>saS</sub> (~23% reduction). Taken together, among H<sub>2</sub>R species isoforms coexpressed with G<sub>saS</sub>, cH<sub>2</sub>R was the most constitutively active GPCR.

Due to the efficient coupling of the signaling partners in GPCR-G<sub>sa</sub> fusion proteins (Seifert et al., 1999), in membranes expressing H<sub>2</sub>R-G<sub>saS</sub>, strongly elevated basal AC activities were measured, compared to membranes expressing non-fused H<sub>2</sub>Rs coexpressing G<sub>saS</sub> (Table 7.3).

**Table 7.3:** AC activities in Sf9 membranes expressing H<sub>2</sub>R species isoforms without or with G<sub>saS</sub>, and in Sf9 membranes expressing H<sub>2</sub>R-G<sub>saS</sub> fusion proteins. Basal AC activities and the effects of GTP and HA on AC activity were assessed. Reaction mixtures contained Sf9 membranes expressing 20 to 100 µg protein/tube as appropriate and distilled water (basal), GTP (10 µM), or GTP (10 µM) and HA (100 µM). Data shown are the means ± S.D. of three to four experiments performed in triplicates. To calculate the stimulatory effect of GTP (Rel. GTP Effect), the effect of GTP (10 µM) was referred to the effect of GTP (10 µM) plus HA (100 µM).

Construct	Basal	GTP 10 µM	GTP 10 µM + HA 100 µM	Rel. GTP Effect
	AC activity (pmol mg <sup>-1</sup> min <sup>-1</sup> )			%
<b>hH<sub>2</sub>R</b>	0.3 ± 0.0	0.6 ± 0.1	3.4 ± 0.2	10
<b>gpH<sub>2</sub>R</b>	0.3 ± 0.1	0.5 ± 0.0	2.6 ± 0.2	9
<b>rH<sub>2</sub>R</b>	0.4 ± 0.0	0.8 ± 0.1	3.1 ± 0.2	15
<b>cH<sub>2</sub>R</b>	0.7 ± 0.1	1.5 ± 0.2	4.3 ± 0.7	22
<b>hH<sub>2</sub>R + G<sub>saS</sub></b>	2.3 ± 0.4	6.3 ± 0.8	11.8 ± 0.5	42
<b>gpH<sub>2</sub>R + G<sub>saS</sub></b>	1.5 ± 0.3	4.4 ± 0.5	10.8 ± 1.5	31
<b>rH<sub>2</sub>R + G<sub>saS</sub></b>	4.9 ± 0.4	11.1 ± 1.3	16.1 ± 0.7	55
<b>cH<sub>2</sub>R + G<sub>saS</sub></b>	12.8 ± 1.9	24.7 ± 4.1	31.1 ± 3.7	65
<b>hH<sub>2</sub>R-G<sub>saS</sub></b>	12.1 ± 2.1	24.3 ± 4.8	28.7 ± 5.3	73
<b>gpH<sub>2</sub>R-G<sub>saS</sub></b>	13.4 ± 3.1	25.0 ± 0.6	28.5 ± 2.2	77
<b>rH<sub>2</sub>R-G<sub>saS</sub></b>	30.5 ± 2.6	43.5 ± 1.7	44.4 ± 3.0	94
<b>cH<sub>2</sub>R-G<sub>saS</sub></b>	26.3 ± 3.6	41.9 ± 5.3	40.9 ± 5.2	107

In agreement with the results obtained for membranes expressing non-fused H<sub>2</sub>R<sub>s</sub>, among the four species isoforms, cH<sub>2</sub>R-G<sub>saS</sub> and rH<sub>2</sub>R-G<sub>saS</sub> exhibited the highest basal AC activities. As shown in Figure 7.6 K-L, GTP increased AC activity in those membranes so effectively that HA could not produce a further increase, reflecting exhaustion of the limiting pool of AC molecules (Seifert et al., 1998a). At hH<sub>2</sub>R-G<sub>saS</sub> and gpH<sub>2</sub>R-G<sub>saS</sub>, GTP induced only smaller increases, allowing HA to further enhance AC activity. By contrast, in the absence of added GTP, HA (100 µM) yielded a reduction of basal AC activities at all four species (Figure 7.6 I-L). Very similar effects were observed previously for the β<sub>2</sub>AR-G<sub>saS</sub> fusion protein (Seifert et al., 1998b) and are due to dissociation of GDP from G<sub>saS</sub> following agonist binding to the receptor without subsequent binding of GTP. Since G<sub>saS</sub>-GDP is more effective in activating AC than nucleotide-free G<sub>sa</sub>, AC activity was reduced below basal. Due to much less efficient coupling in membranes coexpressing receptors and G<sub>saS</sub> (Seifert et al., 1998a; Houston et

al., 2002; Gille and Seifert, 2003), in this case HA did not reduce basal AC activity (Figure 7.6 E-H). Similar differences in the coupling efficiencies between fusion proteins and non-fused expression systems were observed in terms of ternary complex formation, guanosine 5'-O-(3-thio)triphosphate binding, GTP hydrolysis, and AC activation in the presence of GTP (Gille and Seifert, 2003; Seifert et al., 1998a; Wenzel-Seifert et al., 2002). Thus, in membranes expressing H<sub>2</sub>R-G<sub>sαS</sub> fusion proteins the apparent constitutive activities were considerably higher than in membranes expressing non-fused H<sub>2</sub>Rs. In the case of cH<sub>2</sub>R-G<sub>sαS</sub> and rH<sub>2</sub>R-G<sub>sαS</sub>, saturation of AC molecules became manifest upon agonist (HA) stimulation.

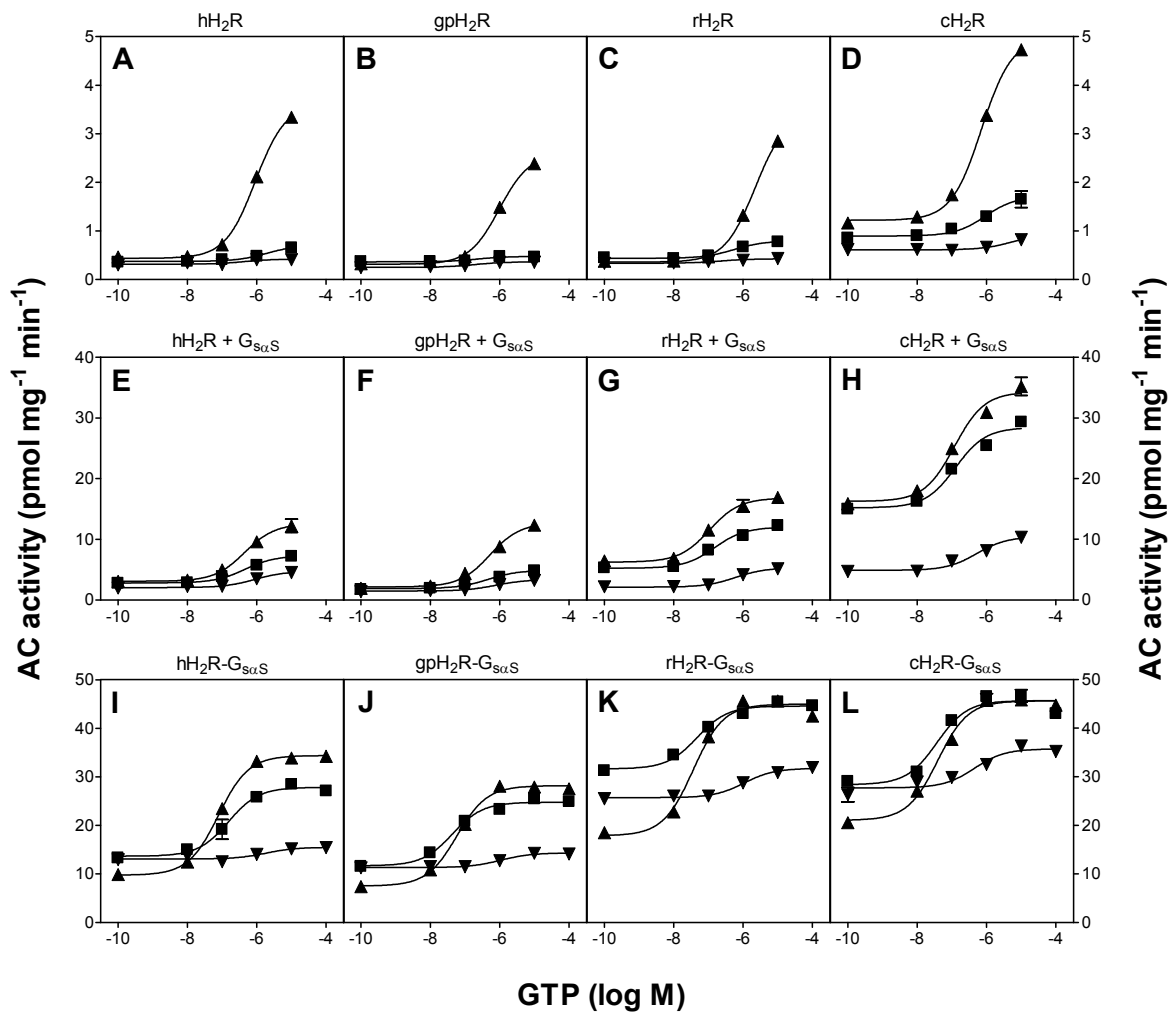


**Figure 7.6:** Regulation of AC activities in Sf9 membranes expressing H<sub>2</sub>R species isoforms (A-D), H<sub>2</sub>R species isoforms plus G<sub>sαS</sub> (E-H), or H<sub>2</sub>R-G<sub>sαS</sub> fusion proteins (I-L). Reaction mixtures contained Sf9 membranes expressing the proteins indicated on top of each panel and GTP at concentrations indicated at the abscissa. Reaction mixtures additionally contained H<sub>2</sub>O (■), HA (100 μM) (▲), or IAPT (10 μM) (▼). Data shown are the means ± S.E.M. of one representative experiment performed in duplicates. The statistical analysis of AC activities is provided in Table 7.3.



## 7.4 Discussion

### 7.4.1 Increased constitutive activity of the cH<sub>2</sub>R compared to hH<sub>2</sub>R, gpH<sub>2</sub>R, and rH<sub>2</sub>R

The use of GPCR-G<sub>sα</sub> fusion protein in combination with the determination of GTPase activity in Sf9 cell membranes was previously shown to be an appropriate system to quantify constitutive activity (Seifert et al., 1998b; Seifert and Wenzel-Seifert, 2002). This system fixes GPCR/G protein coupling and stays at a proximal level, thus avoiding potential bias caused by more downstream effects, such as effector activation or changes in gene expression. Moreover, due to the defined 1:1 stoichiometry of receptor and G<sub>sα</sub> in fusion proteins, ligand potencies and efficacies in the steady-state GTPase assay are independent of the expression levels, allowing for the comparison of various membrane preparations with different expression levels (Seifert et al., 1999; Milligan, 2000).

We comprehensively characterized the human, guinea pig, rat, and canine H<sub>2</sub>R species isoforms in steady-state GTPase assays in Sf9 cell membranes expressing H<sub>2</sub>R-G<sub>sαS</sub> fusion proteins. Structurally diverse H<sub>2</sub>R full and partial agonists and antagonists unmasked considerable differences in the constitutive activities of the receptors. Specifically, cH<sub>2</sub>R-G<sub>sαS</sub> but neither rH<sub>2</sub>R-G<sub>sαS</sub> nor gpH<sub>2</sub>R-G<sub>sαS</sub> displayed the hallmarks of increased constitutive activity compared with hH<sub>2</sub>R-G<sub>sαS</sub> (Samama et al., 1993; Lefkowitz et al., 1993); (i) increased efficacies of partial agonists, (ii) increased potencies of agonists with the extent of potency increase being correlated with the efficacy, and (iii) increased inverse agonist efficacies and decreased potencies of antagonists.

The determination of AC activity in Sf9 cell membranes is an alternative and sensitive method to investigate constitutive activity of GPCRs (Seifert et al., 1998a). With respect to AC, differences in the basal activity and in the magnitudes of signal increases upon stimulation with GTP are indicators for various levels of constitutive activity. In the AC activity assay with membranes expressing non-fused H<sub>2</sub>R species isoforms either without or together with mammalian G<sub>sαS</sub>, both effects were most pronounced for canine relative to human, guinea pig, and rat, corroborating the outstanding role of cH<sub>2</sub>R in terms of constitutive activity.

However, our analysis of AC activity in membranes expressing H<sub>2</sub>R species isoforms also illustrates the limitations of this system. Most importantly, the low concentration levels of AC molecules constrain the maximal signal output, thereby yielding large stimulatory effects of GTP and large inhibitory effects of inverse agonists on AC activity. In contrast, the stimulatory effects of the agonist HA are small if at all detectable. Additionally, in the case of the rH<sub>2</sub>R, basal AC activities and the increases of AC activity upon stimulation with GTP were

moderately higher compared to the hH<sub>2</sub>R, whereas in the GTPase activity assay rH<sub>2</sub>R-G<sub>saS</sub> and hH<sub>2</sub>R-G<sub>saS</sub> showed similar constitutive activities. The accumulation of rH<sub>2</sub>R in Sf9 cell membrane microdomains rich in AC molecules could be an explanation for the observed effects (Ostrom and Insel, 2004).

It is now widely accepted that GPCR activation involves disruption of an ionic lock between Asp(3.49) and Arg(3.50) of the highly conserved (E/D)RY motif in TM3 and Glu(6.30) in the cytoplasmatic extension of TM6 (Ballesteros et al., 2001; Visiers et al., 2002; Shapiro et al., 2002). The effects of mutations in the DRY motif on constitutive activity and structural instability of the rat H<sub>2</sub>R were shown previously (Alewijns et al., 2000). Asp-115(3.49), Arg-116(3.50), and Glu-228/229(6.30) are conserved among all H<sub>2</sub>R species isoforms. However, preceding Glu-229(6.30) in hH<sub>2</sub>R and gpH<sub>2</sub>R and the corresponding Glu-228(6.30) in rH<sub>2</sub>R, human, guinea pig, and rat H<sub>2</sub>Rs exhibit an arginine(6.29), compared to a glycine(6.29) in cH<sub>2</sub>R. Strikingly, many class 1 GPCRs contain a basic amino acid at the corresponding position, and accordingly, a stabilizing role of this residue in the network of ionic interactions was proposed (Ballesteros et al., 2001). According to a dynamic model of the hH<sub>2</sub>R (chapters 4.3.1.2 and 5.3.2.3), the lack of this additional constraint in cH<sub>2</sub>R could facilitate the transition from the inactive to an active state, thus resulting in the observed enhancement in constitutive activity.

Other differences in amino acid sequences could contribute to the differences in constitutive activity as well. Specifically, in G649, an allelic variant of the hH<sub>2</sub>R, Asn-217 in i3 is replaced by Asp-217. This mutant displays low basal activity and is resistant to upregulation upon antagonist exposure (Fukushima et al., 2001). Intriguingly, Asn-217 is conserved within hH<sub>2</sub>R, gpH<sub>2</sub>R and rH<sub>2</sub>R but replaced by a histidine in cH<sub>2</sub>R. Moreover, major variations in the sequences of H<sub>2</sub>R species isoforms occur in the C-terminal domain. Since the C-terminus of H<sub>2</sub>R is important for G<sub>s</sub> protein activation (Smit et al., 1996b), the observed variations in the constitutive activities may alternatively or additionally be due to differences in this domain. In fact, an influence of the C-terminus on the constitutive activities of various GPCRs was described previously (Prezeau et al., 1996; Wenzel-Seifert and Seifert, 2003).

#### 7.4.2 Ligand-specific interactions at H<sub>2</sub>R species isoforms

In the GTPase activity assay, *N*-[3-(1*H*-imidazol-4-yl)propyl]guanidines and their *N*<sup>G</sup>-acylated analogs were more potent and more efficacious at gpH<sub>2</sub>R-G<sub>saS</sub> than at hH<sub>2</sub>R-G<sub>saS</sub> which is in agreement with previous studies (Kelley et al., 2001; Xie et al., 2006a). Since both species isoforms exhibit similar constitutive activities, our present data further support the concept of distinct interactions as a rationale for this species-selectivity. As was predicted by molecular modelling studies and subsequently verified by site-directed mutagenesis, the species-

selectivity of guanidine-type agonists is based on two distinct amino acids, Tyr-17(1.31) in TM1 and Asp-271(7.36) in TM7 in the gpH<sub>2</sub>R, presumably interacting via a charge assisted H-bond and thereby stabilizing an active agonist-bound conformation (Kelley et al., 2001). In the hH<sub>2</sub>R (Cys-17(1.31), Ala-271(7.36)) and the rH<sub>2</sub>R (Leu-17(1.31), Gly-270(7.36)) this interaction is impossible. Consistently, the guanidine-type agonists were similarly efficacious and potent at rH<sub>2</sub>R-G<sub>saS</sub> and hH<sub>2</sub>R-G<sub>saS</sub>. Both cH<sub>2</sub>R and hH<sub>2</sub>R contain Cys-17(1.31) and Ala-271(7.36) and the differences in potencies and efficacies of the compounds between cH<sub>2</sub>R-G<sub>saS</sub> and hH<sub>2</sub>R-G<sub>saS</sub> were not specific to the guanidines. Thus, these differences can be explained by the increased constitutive activity of cH<sub>2</sub>R-G<sub>saS</sub> rather than by distinct ligand/GPCR interactions.

Recently, certain *N*<sup>G</sup>-acylated guanidines have shown to be more efficacious than HA at gpH<sub>2</sub>R-G<sub>saS</sub> in the GTPase assay (Xie et al., 2006b), similar to the observations made with UR-PG222A (**13**) in the present study. These effects can be attributed to the concept of ligand-specific gpH<sub>2</sub>R conformations as well, *i.e.* these compounds stabilize active gpH<sub>2</sub>R conformations that lead to more efficient interactions with G<sub>saS</sub> than achieved with the endogenous ligand HA. By analogy, at the β<sub>2</sub>AR labeled with a fluorescent probe, the synthetic ligand isoproterenol induced a stronger change in fluorescence intensity than the endogenous ligand norepinephrine (Swaminath et al., 2004).

A further example of ligand-specific interactions at H<sub>2</sub>R species isoforms is given by metiamide, acting as a weak partial agonist with low potency at cH<sub>2</sub>R-G<sub>saS</sub> in the GTPase assay compared to being an inverse agonist with increased potency at human, guinea pig, and rat H<sub>2</sub>R-G<sub>saS</sub>. Moreover, in contrast to increased inverse agonist efficacies of antagonists **18-21** at cH<sub>2</sub>R-G<sub>saS</sub> relative to hH<sub>2</sub>R-G<sub>saS</sub>, gpH<sub>2</sub>R-G<sub>saS</sub>, and rH<sub>2</sub>R-G<sub>saS</sub>, the inverse agonist efficacies of cimetidine (**17**), a cyanoguanidine analog of metiamide, were similar at all four species whereas its potency was significantly decreased at cH<sub>2</sub>R-G<sub>saS</sub>. Presumably because of the common 2[(5-methylimidazol-4-yl)methylthio]ethyl moiety, both metiamide and cimetidine stabilize distinct conformations in cH<sub>2</sub>R relative to the other species isoforms, thus leading to an altered interaction with G<sub>saS</sub>, which, in the extreme case of metiamide, causes weak partial agonism rather than increased inverse agonism.

### 7.4.3 Conclusion

In the present study we demonstrate that the cH<sub>2</sub>R exhibits increased constitutive activity compared to hH<sub>2</sub>R, gpH<sub>2</sub>R, and rH<sub>2</sub>R. Species-specific differences in constitutive activity were previously reported for the cholecystokinin-B/gastrin receptor that, like the H<sub>2</sub>R, stimulates gastric H<sup>+</sup> production (Kopin et al., 2000). Thus, differences in constitutive activities of GPCRs regulating H<sup>+</sup> production may reflect species-specific requirements for

“basal” and peak H<sup>+</sup> secretion in the stomach. For example, following stimulation with HA, gastric acid secretion rates in dogs exceed those of the human (Kararli, 1995). Moreover, by studying the H<sub>2</sub>R antagonist metiamide, further evidence for ligand-specific conformations of H<sub>2</sub>R species isoforms was obtained. The present study validates the notion that quantitative comparison of species isoforms of GPCRs provides unique insight into the molecular mechanisms of GPCR activation and ligand/GPCR interactions.

## 7.5 References

- Alewijnse AE, Smit MJ, Hoffmann M, Verzijl D, Timmerman H and Leurs R (1998) Constitutive activity and structural instability of the wild-type human H<sub>2</sub> receptor. *J Neurochem* **71**:799-807.
- Alewijnse AE, Timmerman H, Jacobs EH, Smit MJ, Roovers E, Cotecchia S and Leurs R (2000) The effect of mutations in the DRY motif on the constitutive activity and structural instability of the histamine H<sub>2</sub> receptor. *Mol Pharmacol* **57**:890-898.
- Ballesteros JA, Jensen AD, Liapakis G, Rasmussen SG, Shi L, Gether U and Javitch JA (2001) Activation of the  $\beta_2$ -adrenergic receptor involves disruption of an ionic lock between the cytoplasmic ends of transmembrane segments 3 and 6. *J Biol Chem* **276**:29171-29177.
- Dove S, Elz S, Seifert R and Buschauer A (2004) Structure-activity relationships of histamine H<sub>2</sub> receptor ligands. *Mini Rev Med Chem* **4**:941-954.
- Fukushima Y, Oka Y, Saitoh T, Katagiri H, Asano T, Matsushashi N, Takata K, van Breda E, Yazaki Y and Sugano K (1995) Structural and functional analysis of the canine histamine H<sub>2</sub> receptor by site-directed mutagenesis: N-glycosylation is not vital for its action. *Biochem J* **310**:553-558.
- Fukushima Y, Asano T, Saitoh T, Anai M, Funaki M, Ogihara T, Katagiri H, Matsushashi N, Yazaki Y and Sugano K (1997) Oligomer formation of histamine H<sub>2</sub> receptors expressed in Sf9 and COS7 cells. *FEBS Lett* **409**:283-286.
- Fukushima Y, Saitoh T, Anai M, Tsukuda K, Onishi Y, Sakoda H, Inukai K, Ogihara T, Funaki M, Ono H, Fujishiro M, Ishikawa T, Nagai R, Omata M and Asano T (2001) G649, an allelic variant of the human H<sub>2</sub> receptor with low basal activity, is resistant to upregulation upon antagonist exposure. *Pharmacogenomics J* **1**:78-83.
- Gantz I, Schäffer M, DelValle J, Logsdon C, Campbell V, Uhler M and Yamada T (1991a) Molecular cloning of a gene encoding the histamine H<sub>2</sub> receptor. *Proc Natl Acad Sci U S A* **88**:429-433.
- Gantz I, Munzert G, Tashiro T, Schäffer M, Wang L, DelValle J and Yamada T (1991b) Molecular cloning of the human histamine H<sub>2</sub> receptor. *Biochem Biophys Res Commun* **178**:1386-1392.
- Gantz I, DelValle J, Wang LD, Tashiro T, Munzert G, Guo YJ, Konda Y and Yamada T (1992) Molecular basis for the interaction of histamine with the histamine H<sub>2</sub> receptor. *J Biol Chem* **267**:20840-20843.
- Ghorai, P (2005) Arpromidine-related acylguanidines: synthesis and structure-activity relationships of a new class of guanidine-type histamine H<sub>2</sub> receptor agonists with reduced basicity. Doctoral thesis. University of Regensburg, Germany.  
<http://www.opus-bayern.de/uni-regensburg/volltexte/2006/561/>
- Gille A and Seifert R (2003) Co-expression of the  $\beta_2$ -adrenoceptor and dopamine D<sub>1</sub>-receptor with G<sub>sα</sub> proteins in Sf9 insect cells: limitations in comparison with fusion proteins. *Biochim Biophys Acta* **1613**:101-114.
- Graziano MP, Freissmuth M and Gilman AG (1989) Expression of G<sub>sα</sub> in *Escherichia coli*. Purification and properties of two forms of the protein. *J Biol Chem* **264**:409-418.

- Hill SJ, Ganellin CR, Timmerman H, Schwartz JC, Shankley NP, Young JM, Schunack W, Levi R and Haas HL (1997) International Union of Pharmacology. XIII. Classification of histamine receptors. *Pharmacol Rev* **49**:253-278.
- Houston C, Wenzel-Seifert K, Bürckstümmer T and Seifert R (2002) The human histamine H<sub>2</sub>-receptor couples more efficiently to Sf9 insect cell G<sub>s</sub>-proteins than to insect cell G<sub>q</sub>-proteins: limitations of Sf9 cells for the analysis of receptor/G<sub>q</sub>-protein coupling. *J Neurochem* **80**:678-696.
- Kararli TT (1995) Comparison of the gastrointestinal anatomy, physiology, and biochemistry of humans and commonly used laboratory animals. *Biopharm Drug Dispos* **16**:351-380.
- Kelley MT, Bürckstümmer T, Wenzel-Seifert K, Dove S, Buschauer A and Seifert R (2001) Distinct interaction of human and guinea pig histamine H<sub>2</sub>-receptor with guanidine-type agonists. *Mol Pharmacol* **60**:1210-1225.
- Kenakin T (2001) Inverse, protean, and ligand-selective agonism: matters of receptor conformation. *FASEB J* **15**:598-611.
- Kopin AS, McBride EW, Schaffer K, Beinborn M (2000) CCK receptor polymorphisms: an illustration of emerging themes in pharmacogenomics. *Trends Pharmacol Sci* **21**:346-353.
- Lefkowitz RJ, Cotecchia S, Samama P and Costa T (1993) Constitutive activity of receptors coupled to guanine nucleotide regulatory proteins. *Trends Pharmacol Sci* **14**:303-307.
- Milligan G (2000) Insights into ligand pharmacology using receptor-G-protein fusion proteins. *Trends Pharmacol Sci* **21**:24-28.
- Nederkoorn PH, van Gelder EM, Donne-Op den Kelder GM and Timmerman H (1996) The agonistic binding site at the histamine H<sub>2</sub> receptor. II. Theoretical investigations of histamine binding to receptor models of the seven  $\alpha$ -helical transmembrane domain. *J Comput Aided Mol Des* **10**:479-489.
- Ostrom RS and Insel PA (2004) The evolving role of lipid rafts and caveolae in G protein-coupled receptor signaling: implications for molecular pharmacology. *Br J Pharmacol* **143**:235-245.
- Prezeau L, Gomeza J, Ahern S, Mary S, Galvez T, Bockaert J and Pin JP (1996) Changes in the carboxyl-terminal domain of metabotropic glutamate receptor 1 by alternative splicing generate receptors with differing agonist-independent activity. *Mol Pharmacol* **49**:422-429.
- Ruat M, Traiffort E, Arrang JM, Leurs R and Schwartz JC (1991) Cloning and tissue expression of a rat histamine H<sub>2</sub>-receptor gene. *Biochem Biophys Res Commun* **179**:1470-1478.
- Samama P, Cotecchia S, Costa T and Lefkowitz RJ (1993) A mutation-induced activated state of the  $\beta_2$ -adrenergic receptor. Extending the ternary complex model. *J Biol Chem* **268**:4625-4636.
- Seifert R and Wenzel-Seifert K (2002) Constitutive activity of G-protein-coupled receptors: cause of disease and common property of wild-type receptors. *Naunyn Schmiedebergs Arch Pharmacol* **366**:381-416.
- Seifert R, Lee TW, Lam VT and Kobilka BK (1998a) Reconstitution of  $\beta_2$ -adrenoceptor-GTP-binding-protein interaction in Sf9 cells: High coupling efficiency in a  $\beta_2$ -adrenoceptor-G<sub>s</sub> $\alpha$  fusion protein. *Eur J Biochem* **255**:369-382.
- Seifert R, Wenzel-Seifert K, Lee TW, Gether U, Sanders-Bush E and Kobilka BK (1998b) Different effects of G<sub>s</sub> $\alpha$  splice variants on  $\beta_2$ -adrenoreceptor-mediated signaling. The  $\beta_2$ -adrenoreceptor coupled to the long splice variant of G<sub>s</sub> $\alpha$  has properties of a constitutively active receptor. *J Biol Chem* **273**:5109-5116.
- Seifert R, Wenzel-Seifert K and Kobilka BK (1999) GPCR-G<sub>o</sub> fusion proteins: molecular analysis of receptor-G-protein coupling. *Trends Pharmacol Sci* **20**:383-389.
- Seifert R, Wenzel-Seifert K, Bürckstümmer T, Pertz HH, Schunack W, Dove S, Buschauer A and Elz S (2003) Multiple differences in agonist and antagonist pharmacology between human and guinea pig histamine H<sub>1</sub>-receptor. *J Pharmacol Exp Ther* **305**:1104-1115.
- Shapiro DA, Kristiansen K, Weiner DM, Kroeze WK and Roth BL (2002) Evidence for a model of agonist-induced activation of 5-hydroxytryptamine<sub>2A</sub> serotonin receptors that involves the disruption of a strong ionic interaction between helices 3 and 6. *J Biol Chem* **277**:11441-11449.

- Smit MJ, Leurs R, Alewijnse AE, Blauw J, Van Nieuw Amerongen GP, Van De Vrede Y, Roovers E and Timmerman H (1996a) Inverse agonism of histamine H<sub>2</sub> antagonist accounts for upregulation of spontaneously active histamine H<sub>2</sub> receptors. *Proc Natl Acad Sci U S A* **93**:6802-6807.
- Smit MJ, Timmerman H, Blauw J, Beukers MW, Roovers E, Jacobs EH, Hoffmann M and Leurs R (1996b) The C terminal tail of the histamine H<sub>2</sub> receptor contains positive and negative signals important for signal transduction and receptor down-regulation. *J Neurochem* **67**:1791-1800.
- Swaminath G, Xiang Y, Lee TW, Steenhuis J, Parnot C and Kobilka BK (2004) Sequential binding of agonists to the  $\beta_2$  adrenoceptor. Kinetic evidence for intermediate conformational states. *J Biol Chem* **279**:686-691.
- Traiffort E, Vizuite ML, Tardivel-Lacombe J, Souil E, Schwartz JC and Ruat M (1995) The guinea pig histamine H<sub>2</sub> receptor: gene cloning, tissue expression and chromosomal localization of its human counterpart. *Biochem Biophys Res Commun* **211**:570-577.
- Visiers I, Ebersole B, Dracheva S, Ballesteros JA, Sealfon S and Weinstein H (2002) Structural motifs as functional microdomains in G-protein-coupled receptors: Energetic considerations in the mechanism of activation of the serotonin 5-HT<sub>2A</sub> receptor by disruption of the ionic lock of the arginine cage. *Int J Quantum Chem* **88**:65-75.
- Wenzel-Seifert K and Seifert R (2003) Functional differences between human formyl peptide receptor isoforms 26, 98, and G6. *Naunyn Schmiedeberg's Arch Pharmacol* **367**:509-515.
- Wenzel-Seifert K, Liu HY and Seifert R (2002) Similarities and differences in the coupling of human  $\beta_1$ - and  $\beta_2$ -adrenoceptors to G<sub>sα</sub> splice variants. *Biochem Pharmacol* **64**:9-20.
- Xie SX, Ghorai P, Ye QZ, Buschauer A and Seifert R (2006a) Probing ligand-specific histamine H<sub>1</sub>- and H<sub>2</sub>-receptor conformations with N<sup>G</sup>-acylated imidazolylpropylguanidines. *J Pharmacol Exp Ther* **317**:139-146.
- Xie SX, Kraus A, Ghorai P, Ye QZ, Elz S, Buschauer A and Seifert R (2006b) N<sup>1</sup>-(3-cyclohexylbutanoyl)-N<sup>2</sup>-[3-(1H-imidazol-4-yl)propyl]guanidine (UR-AK57), a potent partial agonist for the human histamine H<sub>1</sub>- and H<sub>2</sub>-receptors. *J Pharmacol Exp Ther* **317**:1262-1268.

## Chapter 8

# Point Mutations of Cys-17 and Ala-271 in the Human Histamine H<sub>2</sub> Receptor

### 8.1 Introduction

The histamine H<sub>2</sub> receptor (H<sub>2</sub>R) is a biogenic amine receptor that belongs to the class 1 of the family of GPCRs. Following stimulation by histamine (HA, **1**, Figure 8.1) the H<sub>2</sub>R couples to G<sub>s</sub> proteins to activate adenylyl cyclase (AC). H<sub>2</sub>Rs mediate regulation of gastric acid secretion in parietal cells, cardiac contractility, and myeloid cell differentiation (Del Valle and Gantz, 1997).

*N*-[3-(1*H*-imidazol-4-yl)propyl]guanidines are the most potent agonists at the H<sub>2</sub>R known so far (up to 400 times more active than HA at the guinea pig right atrium) and possibly useful as positive inotropic drugs for the treatment of severe congestive heart failure, as agents inducing cell differentiation in acute myelogenous leukemia, and as anti-inflammatory drugs (Dove et al., 2004). Guanidines are less potent and efficient agonists at the H<sub>2</sub>R of human neutrophils than at the H<sub>2</sub>R of the guinea pig right atrium (Burde et al., 1989, 1990). In a membrane steady-state GTPase activity assay with fusion proteins of H<sub>2</sub>R and the short splice variant of G<sub>sa</sub>, G<sub>saS</sub>, these compounds are considerably more potent and efficacious at gpH<sub>2</sub>R-G<sub>saS</sub> than at hH<sub>2</sub>R-G<sub>saS</sub> (Kelley et al., 2001). Recently, a novel class of *N*<sup>G</sup>-acylated imidazolylpropylguanidines was developed (Ghorai, 2005). The introduction of an electron-withdrawing carbonyl group adjacent to the guanidine moiety reduces the basicity of the compounds (pK<sub>a</sub> ca. 8). This structural modification does not change the species-selectivity between hH<sub>2</sub>R-G<sub>saS</sub> and gpH<sub>2</sub>R-G<sub>saS</sub> (Xie et al., 2006a).

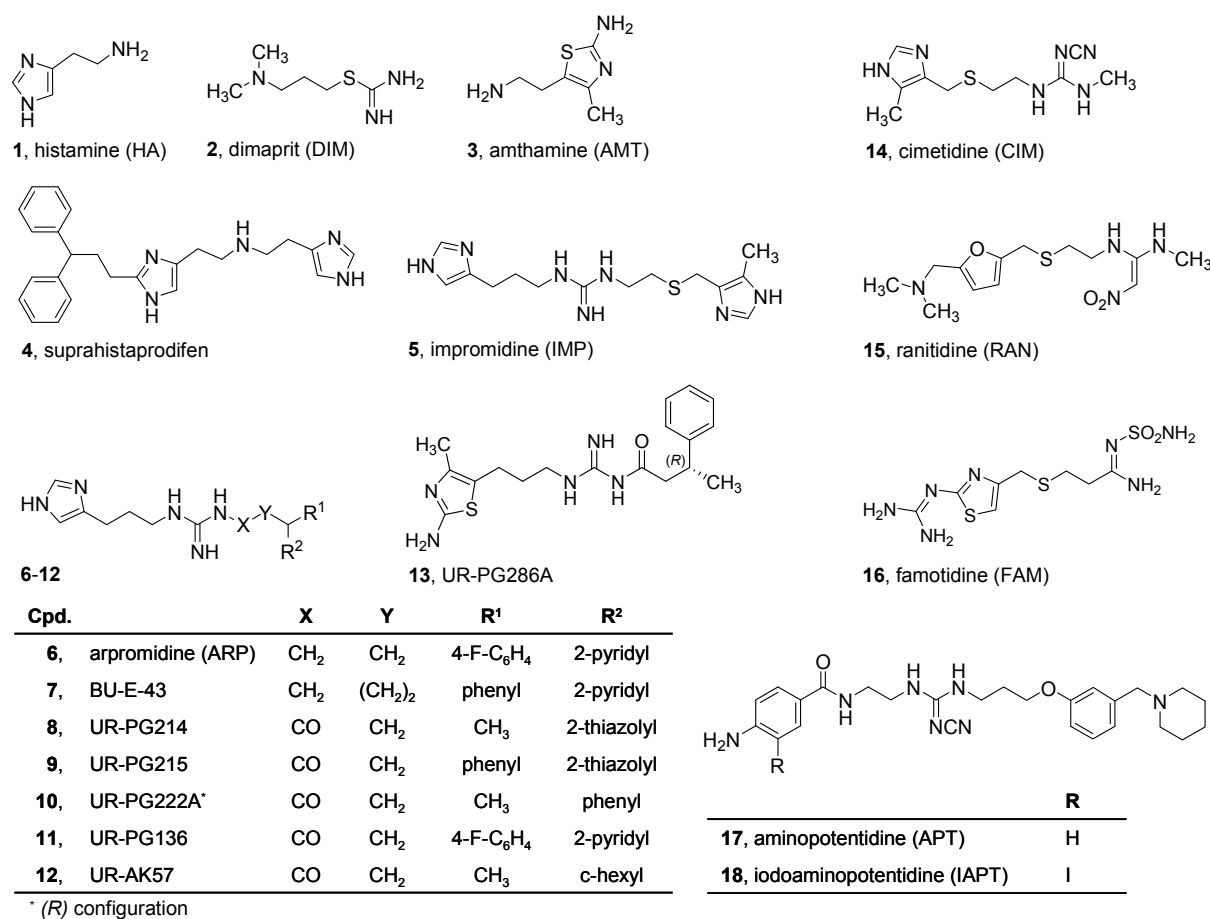


**Figure 8.1:** Structures of H<sub>2</sub>R agonists and inverse agonists. **1-3**, small H<sub>2</sub>R agonists; **4**, H<sub>1</sub>R agonist with partial agonism at the H<sub>2</sub>R; **5-7**, guanidine-type H<sub>2</sub>R agonists; **8-12**, N<sup>G</sup>-acylated N-[3-(1H-imidazol-4-yl)propyl]guanidines with agonistic H<sub>2</sub>R activity; **13**, (R)-N-[3-(2-amino-4-methylthiazol-5-yl)propyl]-N'-(3-phenylbutanoyl)guanidine, an H<sub>2</sub>R agonist; and **14-18**, H<sub>2</sub>R inverse agonists.

By contrast, HA and the small H<sub>2</sub>R agonists dimaprit (**2**, DIM) and amthamine (**3**, AMT) do not exhibit species-selectivity.

A three-dimensional homology model of the gpH<sub>2</sub>R suggested that the nonconserved Asp-271(7.36) in transmembrane domain (TM) 7 confers high potency to the guanidines which was subsequently confirmed by an Ala-271(7.36)→Asp-271(7.36) mutation in hH<sub>2</sub>R-G<sub>saS</sub> (hH<sub>2</sub>R-A271D-G<sub>saS</sub>) (Kelley et al., 2001). However, the efficacies of guanidines at this mutant and at hH<sub>2</sub>R/gpH<sub>2</sub>R chimeras were lower than at gpH<sub>2</sub>R, demonstrating that guanidine efficacy depends on additional or other interactions. As a rationale, an interhelical H-bond between Tyr-17(1.31) in TM1 and Asp-271(7.36) was predicted from the model, stabilizing an active guanidine-bound conformation only in gpH<sub>2</sub>R but not in hH<sub>2</sub>R (containing Cys-17(1.31) and Ala-271(7.36)) (Kelley et al., 2001).

To test this hypothesis, we generated an hH<sub>2</sub>R-G<sub>saS</sub> mutant with a Cys-17(1.31)→Tyr-17(1.31) exchange and a double mutant with Cys-17(1.31)→Tyr-17(1.31) and



Ala-271(7.36)→Asp-271(7.36) exchanges in the sequence of hH<sub>2</sub>R. Sf9 cell membranes expressing mutant and wild-type H<sub>2</sub>R-G<sub>saS</sub> were used to measure steady-state GTPase activity as this system was previously shown to be reliable and very sensitive to analyze ligand potencies and efficacies (Seifert et al., 1999; Milligan, 2000). Due to the defined 1:1 stoichiometry of receptor and G<sub>sa</sub> in fusion proteins, ligand potencies and efficacies in the steady-state GTPase assay are independent of the expression levels, allowing for the comparison of various membrane preparations with different expression levels. We also assessed AC activity in Sf9 membranes as a sensitive readout to compare distinct levels of constitutive activity of mutant and wild-type H<sub>2</sub>R-G<sub>saS</sub> fusion proteins. Figure 8.1 shows the structures of H<sub>2</sub>R agonists examined in the present study. Impromidine (IMP, **5**), arpromidine (ARP, **6**), and BU-E-43 (**7**) are representatives of *N*-[3-(1*H*-imidazol-4-yl)propyl]guanidines. Their *N*<sup>G</sup>-acylated derivatives contain diverse diarylpropanoyl (**9**, **11**), 3-(hetero)arylbutanoyl (**8**, **10**), and 3-(cyclohexylbutanoyl) (**12**) groups. Compound **13** contains a 2-amino-4-methylthiazol-5-yl group and exhibits enhanced selectivity relative to the H<sub>3</sub>R (Ghorai, 2005). Compounds **10** and **13** are the pure (*R*)-enantiomers. In addition, the inverse agonists cimetidine (CIM, **14**), ranitidine (RAN, **15**), famotidine (FAM, **16**), aminopotentidine (APT, **17**), and iodoaminopotentidine (IAPT, **18**) were studied (Hill et al., 1997; Dove et al., 2004).

## 8.2 Materials and Methods

### 8.2.1 Materials

The generation of pGEM-3Z-SF-hH<sub>2</sub>R-G<sub>saS</sub>, pGEM-3Z-SF-hH<sub>2</sub>R-A271D-G<sub>saS</sub>, and pVL1392-SF-hH<sub>2</sub>R-G<sub>saS</sub> was described previously (Kelley et al., 2001). The generation of the baculoviruses encoding hH<sub>2</sub>R-G<sub>saS</sub> and gpH<sub>2</sub>R-G<sub>saS</sub> was described previously (Kelley et al., 2001; Houston et al., 2002). A description of the preparation of all remaining materials is given in chapter 6.1.

### 8.2.2 Construction of the cDNA for hH<sub>2</sub>R-C17Y-G<sub>saS</sub>

The Cys-17(1.31)→Tyr-17(1.31) exchange in hH<sub>2</sub>R was generated by sequential overlap-extension PCRs. With pGEM-3Z-SF-hH<sub>2</sub>R-G<sub>saS</sub> as template, PCR 1A was used to amplify a DNA fragment consisting of the cleavable signal peptide from influenza hemagglutinin (S), the FLAG epitope (F) recognized by the M1 monoclonal antibody, and the N-terminal portion of the hH<sub>2</sub>R. The sense primer annealed with 18 bp of pGEM-3Z prior to the 5'-end of SF.

The antisense primer encoded the sequence GATCTTATATGCGGTAGAGTCTAGAC-AAAAGGAAGAGGCTG to generate the Cys-17(1.31)→Tyr-17(1.31) exchange and a new *Xba* I site (TCTAGA). In PCR 1B, the DNA sequence of the hH<sub>2</sub>R, a hexahistidine tag, and the entire sequence of G<sub>saS</sub> was amplified using pGEM-3Z-SF-hH<sub>2</sub>R-G<sub>saS</sub> as template. The sense primer encoded the sequence CTTTGTICTAGACTCTACCGCATATAAGAT-CACCATCACCG to generate the Cys-17(1.31)→Tyr-17(1.31) exchange and the new *Xba* I site. The antisense primer annealed with the cDNA encoding the 5 C-terminal amino acids of G<sub>saS</sub>, the stop codon, and an *Xba* I site. In PCR 2, the products of PCR 1A and 1B annealed in the region encoding the newly created Cys-17(1.31)→Tyr-17(1.31) exchange and the new *Xba* I site. Here, the sense primer of PCR 1A and the antisense primer of PCR 1B were used. In that way, the complete cDNA for the hH<sub>2</sub>R-C17Y-G<sub>saS</sub> fusion protein was amplified. The product of PCR 2 was digested with *Sac* I and *Kpn* I and cloned into pGEM-3Z-SF-hH<sub>2</sub>R-G<sub>saS</sub> digested with *Sac* I and *Kpn* I. pGEM-3Z-SF-hH<sub>2</sub>R-C17Y-G<sub>saS</sub> was digested with *Sac* I and *EcoN* I and cloned into the baculovirus transfer vector pVL1392-SF-hH<sub>2</sub>R-G<sub>saS</sub> digested with *Sac* I and *EcoN* I. PCR-generated DNA sequences were confirmed by extensive restriction enzyme analysis and enzymatic sequencing.

### 8.2.3 Construction of the cDNA for hH<sub>2</sub>R-C17Y-A271D-G<sub>saS</sub>

To generate the DNA for fusion proteins with two amino acid exchanges Cys-17(1.31)→Tyr-17(1.31) and Ala-271(7.36)→Asp-271(7.36), pGEM-3Z-SF-hH<sub>2</sub>R-A271D-G<sub>saS</sub> was digested with *Kpn* I and *Bgl* II and cloned into pGEM-3Z-SF-hH<sub>2</sub>R-C17Y-G<sub>saS</sub> digested with *Kpn* I and *Bgl* II. pGEM-3Z-SF-hH<sub>2</sub>R-C17Y-A271D-G<sub>saS</sub> was digested with *Nco* I and *Bgl* II and cloned into the baculovirus transfer vector pVL1392-SF-hH<sub>2</sub>R-G<sub>saS</sub> digested with *Nco* I and *Bgl* II.

### 8.2.4 Reverse transcription

mRNA was extracted from Sf9 cells expressing recombinant proteins using the RNeasy Kit (Qiagen, Hilden, Germany). Corresponding cDNA was generated by reverse transcription using MMLV reverse transcriptase (Invitrogen, Carlsbad, CA). In a subsequent PCR a sense primer annealing with 29 bp of the 5'-end of hH<sub>2</sub>R and an antisense primer annealing with 15 bp of the 3'-end of G<sub>saS</sub> were used to generate double-stranded DNA of the full-length fusion proteins.

### **8.2.5 Generation of recombinant baculoviruses, cell culture, and membrane preparation**

A description is given in chapter 6.2.

### **8.2.6 SDS-PAGE and immunoblot analysis**

A description is given in chapter 6.3.

### **8.2.7 Steady-state GTPase activity assay**

A description is given in chapter 6.4.

### **8.2.8 AC activity assay**

A description is given in chapter 6.5.

## **8.3 Results**

### **8.3.1 Immunological detection of recombinant proteins in Sf9 cell membranes**

In Sf9 cells hH<sub>2</sub>R-C17Y-G<sub>saS</sub> and hH<sub>2</sub>R-C17Y-A271D-G<sub>saS</sub> were well expressed (Figure 8.2 A, B). Monomeric non-fused H<sub>2</sub>R expressed in Sf9 cells migrates as a ~33 kDa band in SDS-PAGE (Fukushima et al., 1997; Houston et al., 2002), and the apparent molecular mass of G<sub>saS</sub> is ~45 kDa (Graziano et al., 1989). SDS-PAGE analysis of membranes expressing hH<sub>2</sub>R-C17Y-A271D-G<sub>saS</sub> yielded intense bands at ~80 kDa, recognized by both the anti-FLAG and the anti-6His antibodies, that coincide with the expected apparent molecular masses of H<sub>2</sub>R-G<sub>saS</sub> monomers (Kelley et al., 2001; Houston et al., 2002). Both bands appeared somewhat diffuse, representing different glycosylation forms of the proteins. With the anti-6His antibody, an additional doublet band was detected at ~45 kDa not recognized by the anti-FLAG antibody which is presumably due to a lack of epitope exposure. By contrast, SDS-PAGE of membranes expressing hH<sub>2</sub>R-C17Y-G<sub>saS</sub> yielded strong and diffuse bands at ~40 kDa and lacked the expected bands at ~80 kDa. These bands could either represent atypically migrating glycosylated forms of H<sub>2</sub>R-G<sub>saS</sub> monomers or degraded proteins. Since the anti-FLAG Ig recognizes the N-terminus and the anti-6His Ig the C-terminus of the H<sub>2</sub>R, it can be concluded that for either case the complete amino acid

sequence of hH<sub>2</sub>R-C17Y was expressed. Additional diffuse bands at ~110 kDa may correspond to GPCR dimers or higher oligomers and were also observed in wild-type hH<sub>2</sub>R-G<sub>saS</sub> fusion proteins (Kelley et al., 2001). Comparison with the peak intensities of calibrated Sf9 membranes expressing the  $\beta_2$ AR at 7.5 pmol mg<sup>-1</sup> (as determined by [<sup>3</sup>H]dihydroalprenolol saturation binding) revealed approximately similar expression levels of ~2 pmol mg<sup>-1</sup> for hH<sub>2</sub>R-C17Y-G<sub>saS</sub> and hH<sub>2</sub>R-C17Y-A271D-G<sub>saS</sub>.

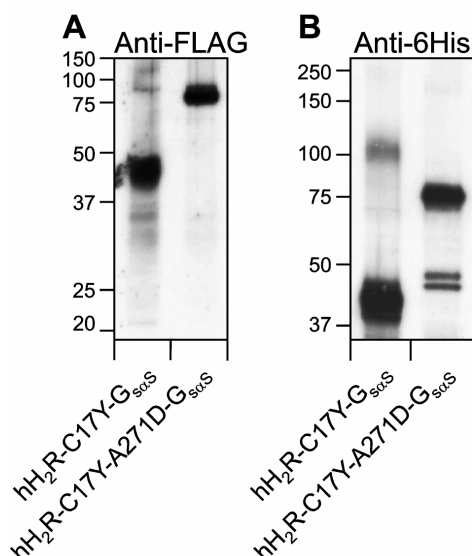


**Figure 8.2:** Immunological detection of recombinant proteins in Sf9 cells. Sf9 membranes expressing various proteins were prepared, separated by SDS-PAGE on gels containing 12% (w/v) acrylamide, transferred onto Immobilon P membranes, and probed with the respective Ig indicated on top of each panel. In each lane, 10  $\mu$ g of membrane protein was loaded onto the gel. Numbers on the left of membranes designate masses of marker proteins in kDa.

### 8.3.2 Analysis of the mRNA in Sf9 membranes expressing hH<sub>2</sub>R-C17Y-G<sub>saS</sub> and hH<sub>2</sub>R-C17Y-A271D-G<sub>saS</sub>

Reverse transcriptase PCR of isolated mRNA and subsequent amplification of the corresponding cDNA yielded DNA sequences that displayed the expected bands of 2240 bp for the full-length fusion proteins of both receptor mutants after separation in agarose gel electrophoresis (Figure 8.3 A, lane 2 and 4). Restriction digestion with *EcoR* V and *Xba* I yielded the specific fragments of 1341 bp and 862 bp for hH<sub>2</sub>R-C17Y-G<sub>saS</sub> (Figure 8.3 A, B; lane 1) and 1341 bp and 780 bp for hH<sub>2</sub>R-C17Y-A271D-G<sub>saS</sub> (Figure 8.3 A, B; lane 3), verifying the existence of the desired point mutations. The 1341 bp bands in lanes 1 and 3 migrated slightly differently in the two gels for unknown reason. In lane 3, the expected band at 82 bp was not detectable.

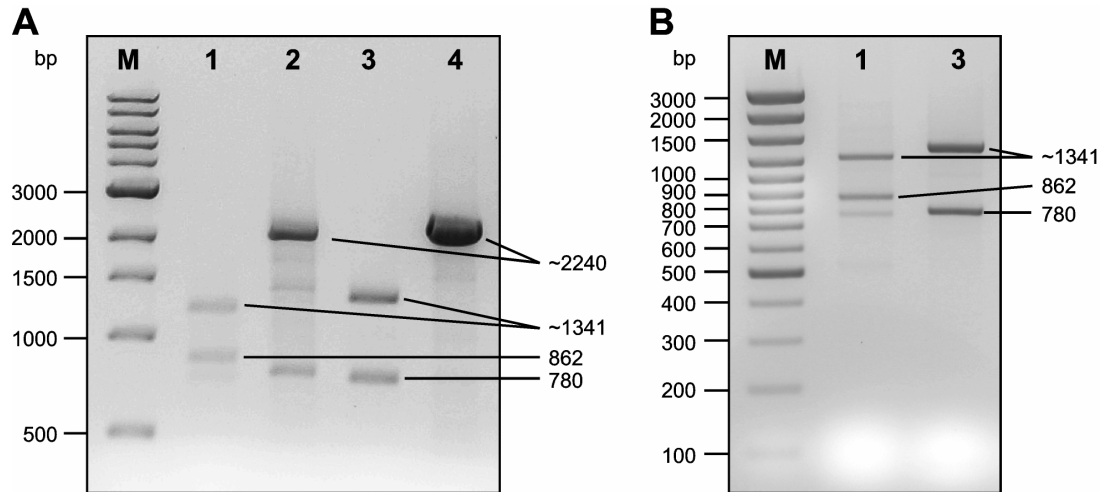


**Figure 8.3:** Analysis of the mRNA in Sf9 cells expressing hH<sub>2</sub>R-C17Y-G<sub>sαS</sub> (lanes 1 and 2) and hH<sub>2</sub>R-C17Y-A271D-G<sub>sαS</sub> (lanes 3 and 4). Lanes 1 and 3, digestion with *EcoR* V and *Xba* I; lanes 2 and 4, undigested DNA fragment. The DNA fragments were separated on gels containing 1% (A) or 2% (B) agarose. M, DNA marker.

### 8.3.3 Efficacies and potencies of agonists at hH<sub>2</sub>R-G<sub>sαS</sub>, gpH<sub>2</sub>R-G<sub>sαS</sub>,

#### hH<sub>2</sub>R-C17Y-G<sub>sαS</sub>, and hH<sub>2</sub>R-C17Y-A271D-G<sub>sαS</sub>

The basal GTPase activity of the hH<sub>2</sub>R-G<sub>sαS</sub> amounted to  $0.66 \pm 0.09$  pmol mg<sup>-1</sup> min<sup>-1</sup> (n = 10). Compared to it, the data were similar in membranes expressing gpH<sub>2</sub>R-G<sub>sαS</sub> ( $0.69 \pm 0.19$  pmol mg<sup>-1</sup> min<sup>-1</sup>; n = 8), and hH<sub>2</sub>R-C17Y-G<sub>sαS</sub> ( $0.78 \pm 0.10$  pmol mg<sup>-1</sup> min<sup>-1</sup>; n = 9), respectively, but significantly increased at hH<sub>2</sub>R-C17Y-A271D-G<sub>sαS</sub> ( $1.67 \pm 0.38$  pmol mg<sup>-1</sup> min<sup>-1</sup>; n = 9;  $p < 0.01$ ). At the fusion proteins of both wild-type receptors and at hH<sub>2</sub>R-C17Y-A271D-G<sub>sαS</sub>, stimulation with 100 μM HA yielded GTPase activities 400 to 600% of the basal levels. By contrast, at hH<sub>2</sub>R-C17Y-G<sub>sαS</sub> maximum HA GTPase activities amounted to just 140% of the basal signal, thereby yielding lower signal-to-noise ratios for the analysis of agonists (Figure 8.4).

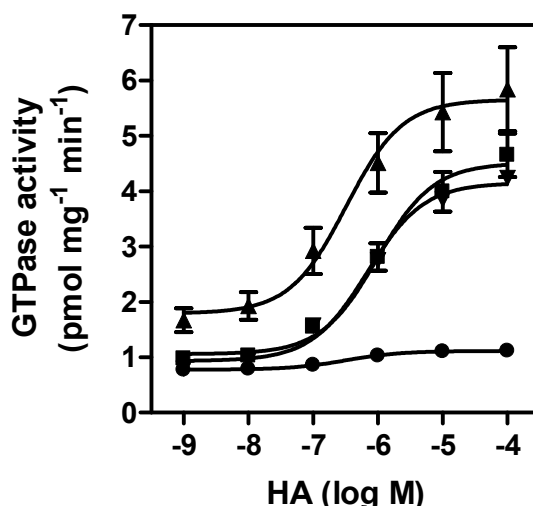


**Figure 8.4:** Concentration-dependent increase of GTPase activity by HA in membranes expressing hH<sub>2</sub>R-G<sub>saS</sub> (■), gpH<sub>2</sub>R-G<sub>saS</sub> (▼), hH<sub>2</sub>R-C17Y-G<sub>saS</sub> (●), and hH<sub>2</sub>R-C17Y-A271D-G<sub>saS</sub> (▲). GTPase activity in Sf9 membranes was determined as described in chapter 6.4. Reaction mixtures contained membranes (10 µg of protein/tube) expressing fusion proteins and HA at concentrations indicated on the abscissa. Data shown are the means ± S.E.M. of three independent experiments performed in duplicates. Data were analyzed by nonlinear regression and were best fitted to sigmoidal concentration/response curves.

Efficacies and potencies of compounds **1-13** are summarized in Table 8.1. The efficacies of the small agonists DIM (**2**) and AMT (**3**) were similar at hH<sub>2</sub>R-G<sub>saS</sub> and hH<sub>2</sub>R-C17Y-G<sub>saS</sub>, and slightly increased at gpH<sub>2</sub>R-G<sub>saS</sub> and hH<sub>2</sub>R-C17Y-A271D-G<sub>saS</sub>. HA (**1**) was ~3-fold more potent at hH<sub>2</sub>R-C17Y-G<sub>saS</sub> and hH<sub>2</sub>R-C17Y-A271D-G<sub>saS</sub> than at hH<sub>2</sub>R-G<sub>saS</sub> and gpH<sub>2</sub>R-G<sub>saS</sub> (Figure 8.4). The potencies of **2** and **3** were similar at hH<sub>2</sub>R-C17Y-G<sub>saS</sub> and the wild-type receptors but were increased at hH<sub>2</sub>R-C17Y-A271D-G<sub>saS</sub>. The H<sub>1</sub>R-selective agonist suprahistaprodifen (**4**) (Seifert et al., 2003) acted as a partial agonist with similar efficacies and potencies at hH<sub>2</sub>R-G<sub>saS</sub>, gpH<sub>2</sub>R-G<sub>saS</sub>, and hH<sub>2</sub>R-C17Y-A271D-G<sub>saS</sub> and with increased efficacy and potency at hH<sub>2</sub>R-C17Y-G<sub>saS</sub>.

In agreement with previous studies (Kelley et al., 2001, Xie et al., 2006a, b), *N*-[3-(1*H*-imidazol-4-yl)propyl]guanidines **5-7** and most of their *N*<sup>G</sup>-acylated derivatives **8-13** were more efficacious and more potent at gpH<sub>2</sub>R-G<sub>saS</sub> than at hH<sub>2</sub>R-G<sub>saS</sub>. Except for IMP (**5**) being more efficacious at hH<sub>2</sub>R-C17Y-A271D-G<sub>saS</sub>, the efficacies of **5-7** were not significantly changed at both receptor mutants if compared with wild-type hH<sub>2</sub>R-G<sub>saS</sub>. The differences in the efficacies of the *N*<sup>G</sup>-acylated imidazolylpropylguanidines (**8-13**) between hH<sub>2</sub>R-C17Y-G<sub>saS</sub> and hH<sub>2</sub>R-G<sub>saS</sub> were not significant.

**Table 8.1:** Agonist efficacies ( $E_{\text{Max}}$ ) and potencies at hH<sub>2</sub>R-G<sub>saS</sub>, gpH<sub>2</sub>R-G<sub>saS</sub>, hH<sub>2</sub>R-C17Y-G<sub>saS</sub>, and hH<sub>2</sub>R-C17Y-A271D-G<sub>saS</sub> in the GTPase assay. GTPase activity in Sf9 membranes was determined as described in chapter 6.4. Data shown are the means  $\pm$  S.D. of three to six experiments performed in duplicates or triplicates. Efficacies and potencies, respectively, of ligands at hH<sub>2</sub>R-G<sub>saS</sub> were compared with the corresponding parameters at gpH<sub>2</sub>R-G<sub>saS</sub>, hH<sub>2</sub>R-C17Y-G<sub>saS</sub>, and hH<sub>2</sub>R-C17Y-A271D-G<sub>saS</sub>, respectively, using the t-test.

Cpd.	hH <sub>2</sub> R-G <sub>saS</sub>		gpH <sub>2</sub> R-G <sub>saS</sub>		hH <sub>2</sub> R-C17Y-G <sub>saS</sub>		hH <sub>2</sub> R-C17Y-A271D-G <sub>saS</sub>	
	$E_{\text{Max}}^a$	EC <sub>50</sub> (nM)	$E_{\text{Max}}^a$	EC <sub>50</sub> (nM)	$E_{\text{Max}}^a$	EC <sub>50</sub> (nM)	$E_{\text{Max}}^a$	EC <sub>50</sub> (nM)
1	1.00	990 $\pm$ 92	1.00	850 $\pm$ 340	1.00	260 $\pm$ 110 <sup>+++</sup>	1.00	320 $\pm$ 9 <sup>+++</sup>
2	0.85 $\pm$ 0.02	910 $\pm$ 430	0.94 $\pm$ 0.06 <sup>*</sup>	740 $\pm$ 360	0.92 $\pm$ 0.14	670 $\pm$ 420	0.98 $\pm$ 0.01 <sup>***</sup>	370 $\pm$ 36 <sup>+</sup>
3	0.91 $\pm$ 0.02	190 $\pm$ 50	1.04 $\pm$ 0.01 <sup>**</sup>	190 $\pm$ 42	0.86 $\pm$ 0.19	120 $\pm$ 20	0.97 $\pm$ 0.01 <sup>**</sup>	65 $\pm$ 6 <sup>+</sup>
4	0.54 $\pm$ 0.08	240 $\pm$ 41	0.43 $\pm$ 0.02	310 $\pm$ 62	0.79 $\pm$ 0.12 <sup>*</sup>	120 $\pm$ 52 <sup>+</sup>	0.61 $\pm$ 0.02	320 $\pm$ 11 <sup>+</sup>
5	0.82 $\pm$ 0.02	160 $\pm$ 40	0.96 $\pm$ 0.06 <sup>*</sup>	18 $\pm$ 9 <sup>++</sup>	0.73 $\pm$ 0.16	43 $\pm$ 9 <sup>++</sup>	0.95 $\pm$ 0.02 <sup>**</sup>	37 $\pm$ 5 <sup>+</sup>
6	0.84 $\pm$ 0.03	72 $\pm$ 9	0.94 $\pm$ 0.05 <sup>*</sup>	7 $\pm$ 1 <sup>+++</sup>	0.78 $\pm$ 0.15	68 $\pm$ 26	0.87 $\pm$ 0.02	39 $\pm$ 4 <sup>++</sup>
7	0.71 $\pm$ 0.11	130 $\pm$ 13	0.87 $\pm$ 0.05	43 $\pm$ 10 <sup>+++</sup>	0.52 $\pm$ 0.16	30 $\pm$ 22 <sup>++</sup>	0.73 $\pm$ 0.01	150 $\pm$ 6 <sup>+</sup>
8	0.91 $\pm$ 0.08	130 $\pm$ 45	0.94 $\pm$ 0.05	25 $\pm$ 10 <sup>++</sup>	1.14 $\pm$ 0.30	57 $\pm$ 33 <sup>+</sup>	0.92 $\pm$ 0.09	44 $\pm$ 13 <sup>+</sup>
9	0.80 $\pm$ 0.04	120 $\pm$ 45	0.94 $\pm$ 0.05 <sup>*</sup>	14 $\pm$ 4 <sup>++</sup>	0.72 $\pm$ 0.17	68 $\pm$ 35	0.83 $\pm$ 0.04	46 $\pm$ 21
10	0.90 $\pm$ 0.04	18 $\pm$ 6	1.18 $\pm$ 0.08 <sup>**</sup>	5 $\pm$ 1 <sup>+</sup>	1.11 $\pm$ 0.22	9 $\pm$ 3 <sup>+</sup>	1.01 $\pm$ 0.04 <sup>**</sup>	13 $\pm$ 5
11	0.82 $\pm$ 0.05	100 $\pm$ 9	1.02 $\pm$ 0.11 <sup>*</sup>	29 $\pm$ 10 <sup>+++</sup>	0.62 $\pm$ 0.18	200 $\pm$ 33 <sup>++</sup>	0.92 $\pm$ 0.04 <sup>*</sup>	66 $\pm$ 5 <sup>++</sup>
12	0.86 $\pm$ 0.05	15 $\pm$ 4	0.97 $\pm$ 0.18	14 $\pm$ 6	0.83 $\pm$ 0.16	27 $\pm$ 9	0.78 $\pm$ 0.03	21 $\pm$ 10
13	0.55 $\pm$ 0.06	49 $\pm$ 9	0.82 $\pm$ 0.02 <sup>***</sup>	12 $\pm$ <sup>++</sup>	0.58 $\pm$ 0.25	74 $\pm$ 118	0.68 $\pm$ 0.06	29 $\pm$ 16

<sup>a</sup> Efficacy relative to HA (= 1.00)

<sup>\*</sup> comparison with the efficacy at hH<sub>2</sub>R-G<sub>saS</sub>; <sup>\*</sup>  $p < 0.05$ ; <sup>\*\*</sup>  $p < 0.01$ ; <sup>\*\*\*</sup>  $p < 0.001$

<sup>+</sup> comparison with the EC<sub>50</sub> value at hH<sub>2</sub>R-G<sub>saS</sub>; <sup>+</sup>  $p < 0.05$ ; <sup>++</sup>  $p < 0.01$ ; <sup>+++</sup>  $p < 0.001$

Whereas mutation into Tyr-17(1.31) did not change the potency of ARP, the N<sup>G</sup>-acylated analog **11** was less potent at hH<sub>2</sub>R-C17Y-G<sub>saS</sub> than at hH<sub>2</sub>R-G<sub>saS</sub>. By contrast, **11** but not ARP was more efficacious and both were more potent at hH<sub>2</sub>R-C17Y-A271D-G<sub>saS</sub> than at wild-type hH<sub>2</sub>R-G<sub>saS</sub>. Compounds **8** and **9** share a 2-thiazolyl moiety and were more potent at both receptor mutants compared to hH<sub>2</sub>R-G<sub>saS</sub> although for compound **9** the difference was

not significant. When the 2-thiazolyl group was replaced by a cyclohexyl group (**12**) the selectivity for the mutants was lost. Compound **10** was more potent at hH<sub>2</sub>R-C17Y-G<sub>saS</sub> than at hH<sub>2</sub>R-G<sub>saS</sub>. Taken together, the small H<sub>2</sub>R agonists **1-3** were considerably more potent at hH<sub>2</sub>R-C17Y-A271D-G<sub>saS</sub> than at the wild-type human and guinea pig H<sub>2</sub>R-G<sub>saS</sub>. Some guanidines and *N*<sup>6</sup>-acylated guanidines displayed enhanced potencies at the mutant receptor compared to hH<sub>2</sub>R-G<sub>saS</sub>. However, these compounds were all less potent at hH<sub>2</sub>R-C17Y-A271D-G<sub>saS</sub> than at gpH<sub>2</sub>R-G<sub>saS</sub>, and the efficacies varied between the corresponding values at both wild-type receptors.

#### 8.3.4 Potencies and inverse agonist efficacies of antagonists at hH<sub>2</sub>R-G<sub>saS</sub>,

##### gpH<sub>2</sub>R-G<sub>saS</sub>, hH<sub>2</sub>R-C17Y-G<sub>saS</sub>, and hH<sub>2</sub>R-C17Y-A271D-G<sub>saS</sub>

At wild-type and mutant H<sub>2</sub>R-G<sub>saS</sub>, CIM (**14**), RAN (**15**), FAM (**16**), APT (**17**), and IAPT (**18**) decreased GTPase activities below basal and thus acted as inverse agonists (Table 8.2). All compounds exhibited similar inverse agonist efficacies at hH<sub>2</sub>R-C17Y-G<sub>saS</sub> and at both wild-type receptors. By contrast, at hH<sub>2</sub>R-C17Y-A271D-G<sub>saS</sub> inverse agonist efficacies of **14-18** were significantly increased. Because inverse agonists stabilize an inactive receptor conformation (Milligan et al., 1995), the differences in inverse agonist efficacies reflect an increased level of constitutive activity of hH<sub>2</sub>R-C17Y-A271D-G<sub>saS</sub> relative to wild-type receptors. The magnitudes of constitutive activity measured critically depend on the relative stoichiometry of GPCR and G-protein in the system (Kenakin, 2001). Physical tethering of H<sub>2</sub>R with G<sub>saS</sub> in the fusion proteins used provides a fixed 1:1 stoichiometry of both partners, allowing for a direct comparison of the efficacies in an expression-independent manner (Milligan, 2000). **16** and **18** were slightly more potent at hH<sub>2</sub>R-C17Y-A271D-G<sub>saS</sub> than at the wild-type receptors, whereas no significant differences in the *K<sub>B</sub>* values were observed for **14**, **15**, and **17**. By comparison, **15-18** were more potent at hH<sub>2</sub>R-C17Y-G<sub>saS</sub> than at hH<sub>2</sub>R-G<sub>saS</sub> and gpH<sub>2</sub>R-G<sub>saS</sub>.



**Table 8.2:** Potencies and inverse agonist efficacies of antagonists at hH<sub>2</sub>R-G<sub>saS</sub>, gpH<sub>2</sub>R-G<sub>saS</sub>, hH<sub>2</sub>R-C17Y-G<sub>saS</sub>, and hH<sub>2</sub>R-C17Y-A271D-G<sub>saS</sub> in the GTPase assay. Reaction mixtures contained Sf9 membranes expressing fusion proteins, 1  $\mu$ M HA as agonist and antagonists at concentrations from 1 nM to 1 mM as appropriate to generate saturated competition curves. To determine the inverse agonist efficacies (Inv. Eff.), the effects of antagonists at fixed concentrations (10  $\mu$ M of cpds. **15** to **18**; 100  $\mu$ M of cpd. **14**) on basal GTPase activity were assessed and referred to the stimulatory effect of 100  $\mu$ M HA (= 1.00). Data shown are the means  $\pm$  S.D. of three experiments performed in duplicates.  $K_B$  values and inverse agonist efficacies, respectively, of antagonists at hH<sub>2</sub>R-G<sub>saS</sub> were compared with the corresponding parameters at gpH<sub>2</sub>R-G<sub>saS</sub>, hH<sub>2</sub>R-C17Y-G<sub>saS</sub>, and hH<sub>2</sub>R-C17Y-A271D-G<sub>saS</sub>, respectively, using the t-test.

Cpd.	hH <sub>2</sub> R-G <sub>saS</sub>		gpH <sub>2</sub> R-G <sub>saS</sub>		hH <sub>2</sub> R-C17Y-G <sub>saS</sub>		hH <sub>2</sub> R-C17Y-A271D-G <sub>saS</sub>	
	$K_B$ (nM)	Inv. Eff.	$K_B$ (nM)	Inv. Eff.	$K_B$ (nM)	Inv. Eff.	$K_B$ (nM)	Inv. Eff.
<b>14</b>	1700 $\pm$ 430	-0.08 $\pm$ 0.01	1300 $\pm$ 270	-0.09 $\pm$ 0.02	2000 $\pm$ 1900	-0.08 $\pm$ 0.13	1400 $\pm$ 19	-0.25 $\pm$ 0.04 <sup>++</sup>
<b>15</b>	840 $\pm$ 94	-0.09 $\pm$ 0.01	1000 $\pm$ 170	-0.08 $\pm$ 0.01	140 $\pm$ 73 <sup>***</sup>	-0.09 $\pm$ 0.08	1000 $\pm$ 64	-0.21 $\pm$ 0.05 <sup>++</sup>
<b>16</b>	48 $\pm$ 10	-0.10 $\pm$ 0.02	38 $\pm$ 3	-0.10 $\pm$ 0.01	22 $\pm$ 1 <sup>**</sup>	-0.12 $\pm$ 0.09	29 $\pm$ 2 <sup>*</sup>	-0.27 $\pm$ 0.06 <sup>++</sup>
<b>17</b>	180 $\pm$ 12	-0.09 $\pm$ 0.01	260 $\pm$ 43 <sup>*</sup>	-0.09 $\pm$ 0.01	65 $\pm$ 61 <sup>*</sup>	-0.10 $\pm$ 0.08	200 $\pm$ 31	-0.26 $\pm$ 0.05 <sup>++</sup>
<b>18</b>	35 $\pm$ 7	-0.10 $\pm$ 0.01	26 $\pm$ 4	-0.10 $\pm$ 0.01	7 $\pm$ 3 <sup>**</sup>	-0.11 $\pm$ 0.04	12 $\pm$ 2 <sup>**</sup>	-0.27 $\pm$ 0.05 <sup>+++</sup>

<sup>\*</sup> comparison with the  $K_B$  value at hH<sub>2</sub>R-G<sub>saS</sub>; <sup>\*</sup>  $p < 0.05$ ; <sup>\*\*</sup>  $p < 0.01$ ; <sup>\*\*\*</sup>  $p < 0.001$

<sup>+</sup> comparison with Inv. Eff. at hH<sub>2</sub>R-G<sub>saS</sub>; <sup>+</sup>  $p < 0.05$ ; <sup>++</sup>  $p < 0.01$ ; <sup>+++</sup>  $p < 0.001$

### 8.3.5 Regulation of AC activities in membranes expressing hH<sub>2</sub>R-G<sub>saS</sub>,

#### gpH<sub>2</sub>R-G<sub>saS</sub>, hH<sub>2</sub>R-C17Y-G<sub>saS</sub>, and hH<sub>2</sub>R-C17Y-A271D-G<sub>saS</sub>

AC activities were measured in Sf9 membranes expressing hH<sub>2</sub>R-C17Y-G<sub>saS</sub> and hH<sub>2</sub>R-C17Y-A271D-G<sub>saS</sub>, and they were compared with results at wild-type human and guinea pig H<sub>2</sub>R-G<sub>saS</sub> (Table 8.3). hH<sub>2</sub>R-G<sub>saS</sub> and gpH<sub>2</sub>R-G<sub>saS</sub> were similarly expressed in Sf9 cells (at  $\sim$ 3 and 1 pmol mg<sup>-1</sup>, respectively) and produced similar basal AC activities. By contrast, basal AC activities were increased  $\sim$ 3-fold at hH<sub>2</sub>R-C17Y-A271D-G<sub>saS</sub>. At both mutant and both wild-type receptors, GTP (10  $\mu$ M) by itself increased AC activities above the basal level (Figure 8.5), indicating constitutive activity of these receptors (Seifert et al., 1998a, b; Gille and Seifert, 2003). Accordingly, at all four H<sub>2</sub>Rs, the inverse agonist IAPT (**18**) reduced this GTP-dependent AC activity. At hH<sub>2</sub>R-G<sub>saS</sub> and gpH<sub>2</sub>R-G<sub>saS</sub>, AC activity increases by 10  $\mu$ M GTP achieved 73% and 77%, respectively, of the signal increases by

**Table 8.3:** AC activities in Sf9 membranes expressing hH<sub>2</sub>R-G<sub>sαS</sub>, gpH<sub>2</sub>R-G<sub>sαS</sub>, hH<sub>2</sub>R-C17Y-G<sub>sαS</sub>, and hH<sub>2</sub>R-C17Y-A271D-G<sub>sαS</sub>. Reaction mixtures contained Sf9 membranes (20 µg protein/tube) expressing fusion proteins and distilled water (basal), GTP (10 µM), or GTP (10 µM) plus HA (100 µM). Data shown are the means ± S.D. of three experiments performed in triplicates. To calculate the stimulatory effect of GTP (Rel. GTP Effect), the effect of GTP (10 µM) was referred to the effect of GTP (10 µM) plus HA (100 µM).

Construct	Basal	GTP (10 µM)	GTP (10 µM) + HA (100 µM)	Rel. GTP Effect
	AC activity (pmol mg <sup>-1</sup> min <sup>-1</sup> )			%
hH <sub>2</sub> R-G <sub>sαS</sub>	12.1 ± 2.1	24.3 ± 4.8	28.7 ± 5.3	73
gpH <sub>2</sub> R-G <sub>sαS</sub>	13.4 ± 3.1	25.0 ± 0.6	28.5 ± 2.2	77
hH <sub>2</sub> R-C17Y-G <sub>sαS</sub>	0.8 ± 0.2	2.4 ± 0.4	7.0 ± 0.8	26
hH <sub>2</sub> R-C17Y-A271D-G <sub>sαS</sub>	42.5 ± 2.2	66.9 ± 4.2	66.4 ± 3.3	100

10 µM GTP plus 100 µM HA. Strikingly, at hH<sub>2</sub>R-C17Y-A271D-G<sub>sαS</sub>, HA did not further enhance the GTP effect. Both higher basal AC activity and a strong stimulation by GTP caused exhaustion of the limiting pool of AC molecules in Sf9 cells and reflect an increased level of constitutive activity of hH<sub>2</sub>R-C17Y-A271D-G<sub>sαS</sub>, compared to the wild-type fusion proteins. Similar reduced agonist-responsiveness due to high constitutive activity was shown for other aminergic GPCRs, *e.g.* β<sub>2</sub>AR-G<sub>sα</sub> fusion proteins (Seifert et al., 1998a) and mutants of the 5-HT<sub>4</sub> receptor (Claeysen et al., 1999). At hH<sub>2</sub>R-C17Y-G<sub>sαS</sub> much lower basal AC activities and a much smaller stimulatory effect of GTP were determined. In this case, GTP on its own caused only 26% of the effect with HA addition.

At hH<sub>2</sub>R-G<sub>sαS</sub>, gpH<sub>2</sub>R-G<sub>sαS</sub>, and hH<sub>2</sub>R-C17Y-A271D-G<sub>sαS</sub>, HA (100 µM) reduced the basal AC activities in the absence of added GTP (Figure 8.5 A-C). Similar effects were observed at β<sub>2</sub>AR-G<sub>sαS</sub> fusion proteins (Seifert et al., 1998b) and are due to dissociation of GDP from G<sub>sαS</sub> following agonist binding to the receptor without subsequent binding of GTP. G<sub>sαS</sub>-GDP is more effective in activating AC than nucleotide-free G<sub>sα</sub>, and therefore AC activities were decreased.

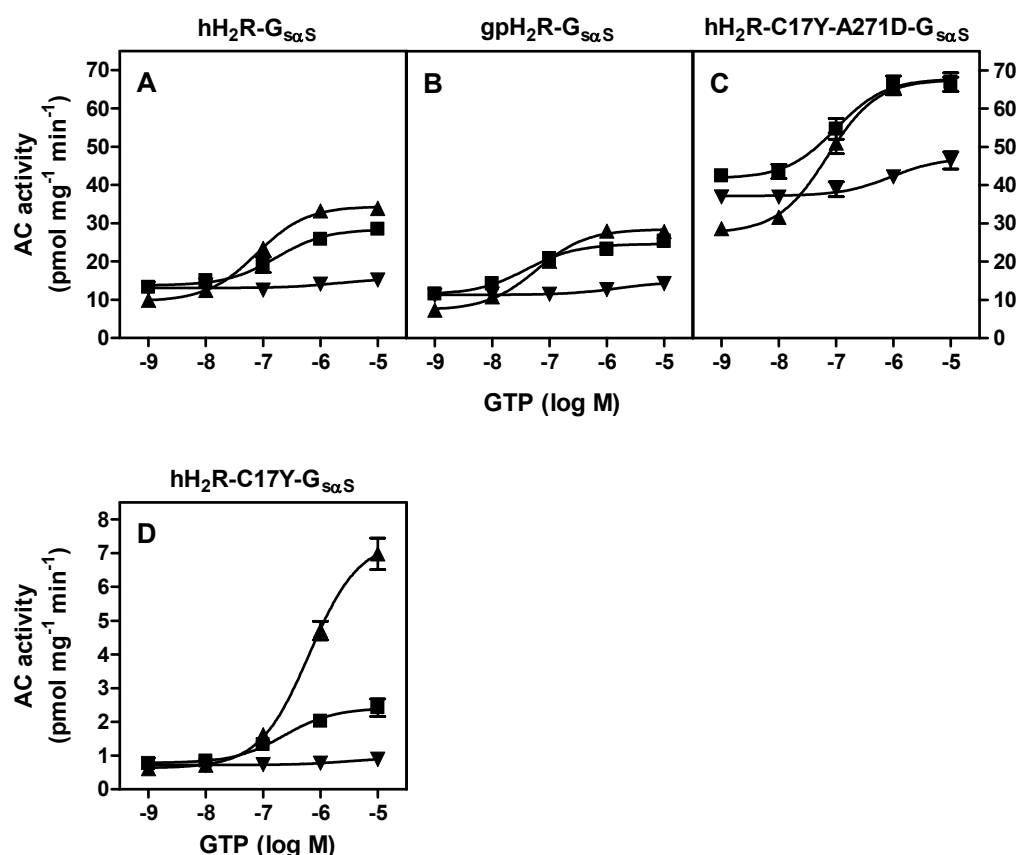


**Figure 8.5:** Regulation of AC activities in Sf9 membranes expressing hH<sub>2</sub>R-G<sub>sα</sub>S (A), gpH<sub>2</sub>R-G<sub>sα</sub>S (B), hH<sub>2</sub>R-C17Y-A271D-G<sub>sα</sub>S (C), and hH<sub>2</sub>R-C17Y-G<sub>sα</sub>S (D). Reaction mixtures contained Sf9 membranes expressing the proteins indicated on top of each panel and GTP at concentrations indicated at the abscissa. Reaction mixtures additionally contained H<sub>2</sub>O (■), HA (100 μM) (▲), or IAPT (10 μM) (▼). Data shown are the means ± S.E.M. of one representative experiment performed in triplicates. The statistical analysis of AC activities is provided in Table 8.3. Please note the different scale of the ordinate in D.

## 8.4 Discussion

### 8.4.1 Impaired coupling in membranes expressing hH<sub>2</sub>R-C17Y-G<sub>sα</sub>S

In Sf9 cells expressing hH<sub>2</sub>R-C17Y-G<sub>sα</sub>S the increases of GTPase activity upon agonist stimulation were much lower than in the wild-type H<sub>2</sub>R-G<sub>sα</sub>S species. Moreover, the basal AC activities and the stimulatory effects of GTP on AC activity were largely reduced and were similar to the values typical for Sf9 membranes expressing non-fused H<sub>2</sub>R species (Houston et al., 2002). However, in the GTPase assay potencies and efficacies of agonists and inverse

agonists were similar or even increased, compared to hH<sub>2</sub>R-G<sub>sαS</sub> and gpH<sub>2</sub>R-G<sub>sαS</sub>, indicating functionality of hH<sub>2</sub>R-C17Y. This is corroborated by substantial stimulatory effects of HA and inhibitory effects of IAPT on the GTP-dependent AC activity increases. Strikingly, the anti-FLAG and the anti-6His antibodies recognized similarly migrating diffuse proteins in SDS-PAGE which verifies the existence of the full-length amino acid sequence of hH<sub>2</sub>R-C17Y. It can therefore be concluded that in membranes expressing hH<sub>2</sub>R-C17Y-G<sub>sαS</sub> the coupling of hH<sub>2</sub>R-C17Y to G<sub>sαS</sub> was much less efficient than is characteristic for GPCR-G<sub>sα</sub> fusion proteins (Gille and Seifert, 2003; Seifert et al., 1999). As a rationale, G<sub>sαS</sub> could be incorrectly expressed or degraded in Sf9 cells. Instead, hH<sub>2</sub>R-C17Y possibly coupled to endogenous G<sub>sα</sub>-like G-proteins with much lower efficiency.

However, several findings argue against degradation or proteolysis of G<sub>sαS</sub> in hH<sub>2</sub>R-C17Y-G<sub>sαS</sub>. First, basal GTPase activities were not reduced relative to hH<sub>2</sub>R-G<sub>sαS</sub> and gpH<sub>2</sub>R-G<sub>sαS</sub> as would have been expected for membranes expressing non-fused H<sub>2</sub>R without or with recombinant G<sub>sαS</sub>, according to studies with Sf9 membranes expressing non-fused β<sub>2</sub>ARs or β<sub>2</sub>AR-G<sub>sα</sub> fusion proteins (Seifert et al., 1998a). Second, although being lower than at H<sub>2</sub>R-G<sub>sαS</sub>, GTPase activity increases with the mutant fusion protein upon agonist stimulation were ~2-fold higher than in membranes expressing non-fused hH<sub>2</sub>R (Houston et al., 2002). Third, the immunoreactive bands observed at ~40 kDa did not coincide with the expected bands for monomeric H<sub>2</sub>R at ~33 kDa (Fukushima et al., 1997), and additional bands at ~110 kDa may correspond to H<sub>2</sub>R-G<sub>sαS</sub> dimers or oligomers (Kelley et al., 2001). Notably, the use of GPCR-G<sub>sα</sub> fusion proteins expressed in Sf9 cells is a well established pharmacological method and proteolysis has not been observed so far (Milligan, 2000; Seifert and Wenzel-Seifert, 2002).

Considering that only a fraction of mutant receptors may be fused with G<sub>sαS</sub> or a deficiency of functional G proteins in Sf9 cells, the potencies (apparent affinities) of agonists and inverse agonists may increase (receptor reserve). This could explain the mostly higher potencies of agonists and inverse agonists at hH<sub>2</sub>R-C17Y-G<sub>sαS</sub> relative to wild-type hH<sub>2</sub>R-G<sub>sαS</sub>, since the large distance between Tyr-17(1.31) and the putative binding site of the gpH<sub>2</sub>R renders a direct interaction with ligands unlikely.

#### 8.4.2 Increased constitutive activity in membranes expressing

##### **hH<sub>2</sub>R-C17Y-A271D-G<sub>sαS</sub>**

In membranes expressing hH<sub>2</sub>R-C17Y-A271D-G<sub>sαS</sub> high efficiency coupling was observed as GTPase activities were increased upon agonist stimulation similar to hH<sub>2</sub>R-G<sub>sαS</sub> and gpH<sub>2</sub>R-G<sub>sαS</sub>. Moreover, with this receptor mutant enhanced basal GTPase activities,

increased potencies of the agonists, as well as increased inverse agonist efficacies of antagonists were detected, representing the hallmarks of enhanced constitutive activity compared to the wild-type proteins (Lefkowitz et al., 1993). The determination of AC activity in Sf9 cell membranes has previously shown to be an alternative and sensitive system to quantify differences in the constitutive activities of GPCRs (Seifert et al., 1998a). In membranes expressing hH<sub>2</sub>R-C17Y-A271D-G<sub>sαS</sub> the high basal AC activities and the strong AC activity increases upon stimulation with GTP additionally reflect high constitutive activity compared to hH<sub>2</sub>R-G<sub>sαS</sub>, gpH<sub>2</sub>R-G<sub>sαS</sub>, and hH<sub>2</sub>R-C17Y-G<sub>sαS</sub>.

The discovery of increased constitutive activity at hH<sub>2</sub>R-C17Y-A271D-G<sub>sαS</sub> further supports the concept of an H-bond between Tyr-17(1.31) in TM1 and Asp-271(7.36) in TM7 (Kelley et al., 2001) as basis for the distinct pharmacological properties of human and guinea pig H<sub>2</sub>Rs. Our data suggest that this interhelical interaction stabilizes an active receptor conformation not only when agonists are bound but also when ligands are absent. However, gpH<sub>2</sub>R-G<sub>sαS</sub> containing Tyr-17(1.31) and Asp-271(7.36) also was similarly constitutively active as hH<sub>2</sub>R-G<sub>sαS</sub> which is presumably due to additional intramolecular interactions constraining the gpH<sub>2</sub>R in an inactive conformation and thereby compensating for the activating function of both residues.

Of interest, the tertiary structure of the α<sub>1b</sub>-adrenergic receptor (α<sub>1b</sub>-AR) contains Lys-331(7.36) in TM7 corresponding to Ala-271(7.36) in hH<sub>2</sub>R. Strikingly, α<sub>1b</sub>-AR mutants with Lys-331(7.36) exchanged by alanine or glutamate were more constitutively active than wild-type α<sub>1b</sub>-AR (Porter et al., 1996), suggesting a general role of an amino acid at this position for the activation mechanism of related GPCRs.

#### **8.4.3 Species-selectivity of guanidines and *N*<sup>G</sup>-acylguanidines at wild-type and mutant H<sub>2</sub>R-G<sub>sαS</sub>**

The main intention of this study was to elucidate the impact of Cys-17(1.31)/Tyr-17(1.31) and Ala-271(7.36)/Asp-271(7.36) on the species-selectivity of *N*-[3-(1*H*-imidazol-4-yl)propyl]guanidines and *N*<sup>G</sup>-acylated imidazolylpropylguanidines between hH<sub>2</sub>R and gpH<sub>2</sub>R. In our GTPase activity experiments some of these agonists were more potent and more efficacious at hH<sub>2</sub>R-C17Y-A271D-G<sub>sαS</sub> than at hH<sub>2</sub>R-G<sub>sαS</sub>, and some compounds were not selective. Overall, the potencies and efficacies of the agonists were still higher at gpH<sub>2</sub>R-G<sub>sαS</sub> than at hH<sub>2</sub>R-C17Y-A271D-G<sub>sαS</sub>. The following conclusions can be drawn from these results. First, both Tyr-17(1.31) and Asp-271(7.36) contribute to the enhanced potencies and efficacies of guanidines and *N*<sup>G</sup>-acylguanidines at the gpH<sub>2</sub>R. This investigation adds to a previous study at an hH<sub>2</sub>R-A271D-G<sub>sαS</sub> mutant conferring high potency to guanidines without

affecting the efficacies (Kelley et al., 2001). However, the pharmacological differences between hH<sub>2</sub>R-C17Y-A271D-G<sub>saS</sub> and gpH<sub>2</sub>R-G<sub>saS</sub> indicate that more than these two amino acids determine the species-selectivity of agonists and will have to be identified in further mutagenesis studies (chapter 9).

Second, the concept of ligand-specific conformations (Kenakin, 2003) in H<sub>2</sub>R species (Kelley et al., 2001; Xie et al., 2006a) is further supported. The variable side chains of the compounds distinctly interact with wild-type and mutant H<sub>2</sub>R-G<sub>saS</sub> which is represented by compounds **8** and **9** containing a 2-thiazolyl group and being more potent at hH<sub>2</sub>R-C17Y-A271D-G<sub>saS</sub> than at hH<sub>2</sub>R-G<sub>saS</sub> in contrast to compound **10** with a cyclohexyl group being similarly potent at both proteins. The 5-methyl-1*H*-imidazol-4-yl group in IMP (**5**) presumably directly interacts with Asp-271(7.36) (Kelley et al., 2001) thus yielding the high potency increase of ~4-fold at hH<sub>2</sub>R-C17Y-A271D-G<sub>saS</sub> vs. hH<sub>2</sub>R-G<sub>saS</sub>.

GPCRs with enhanced constitutive activity exhibit an increased affinity for agonists with the affinity increase being correlated with the efficacy of the ligand (Samama et al., 1993). Accordingly, the parameter of constitutive activity not only affects elevated potencies of small H<sub>2</sub>R agonists at hH<sub>2</sub>R-C17Y-A271D-G<sub>saS</sub> but also potency increases of the guanidines and *N*<sup>G</sup>-acylguanidines. Different magnitudes of constitutive activity therefore add to the complexity of the system for the analysis of species-selective ligand/GPCR interactions. Moreover, inverse agonists are less potent at constitutively active than at quiescent GPCRs (Kenakin, 2001). Accordingly, **14-18** were expected to be less potent at the more constitutively active hH<sub>2</sub>R-C17Y-A271D-G<sub>saS</sub> than at hH<sub>2</sub>R-G<sub>saS</sub>. However, the potencies of inverse agonists were not decreased, and **16** and **18** were even more potent at the mutant receptor, assuming that not only guanidine-type agonists but also inverse agonists could stabilize ligand-specific conformations in H<sub>2</sub>R species isoforms.

#### 8.4.4 Conclusion

In the present study we demonstrate that an hH<sub>2</sub>R-G<sub>saS</sub> fusion protein with mutations of Cys-17(1.31)→Tyr-17(1.31) in TM1 and Ala-271(7.36)→Asp-271(7.36) in TM7 displayed enhanced constitutive activity compared to hH<sub>2</sub>R-G<sub>saS</sub> and gpH<sub>2</sub>R-G<sub>saS</sub>. We additionally showed that an interaction between Tyr-17(1.31) and Asp-271(7.36) in gpH<sub>2</sub>R contributes to the species-selective action of *N*-[3-(1*H*-imidazol-4-yl)propyl]guanidines and their *N*<sup>G</sup>-acylated derivatives. Distinct potencies and efficacies of agonists and inverse agonists further support the concept of ligand-specific conformations in wild-type and mutant H<sub>2</sub>R-G<sub>saS</sub> fusion proteins. A single point mutation of Cys-17(1.31)→Tyr-17(1.31) was devoid of efficient GPCR-G-protein coupling. By analogy, point mutations of Phe-153→Leu-153 or Ile-433→Val-433 in the hH<sub>1</sub>R (hH<sub>1</sub>R→gpH<sub>1</sub>R) resulted in functional inactivity, whereas a

Phe-153→Leu-153/Ile-433→Val-433 double mutant was functionally active (Seifert et al., 2003). The reasons for the annihilating effects of the single point mutations at hH<sub>1</sub>R and hH<sub>2</sub>R are not known, but they illustrate the limitations of site-directed mutagenesis experiments. The characterization of closely related wild-type GPCR species isoforms is, therefore, an important alternative approach to relate distinct pharmacological properties to relatively few molecular determinants.

## 8.5 References

- Burde R, Seifert R, Buschauer A and Schultz G (1989) Histamine inhibits activation of human neutrophils and HL-60 leukemic cells via H<sub>2</sub>-receptors. *Naunyn Schmiedeberg's Arch Pharmacol* **340**:671-678.
- Burde R, Buschauer A and Seifert R (1990) Characterization of histamine H<sub>2</sub>-receptors in human neutrophils with a series of guanidine analogues of impromidine. Are cell type-specific H<sub>2</sub>-receptors involved in the regulation of NADPH oxidase? *Naunyn Schmiedeberg's Arch Pharmacol* **341**:455-461.
- Claeysen S, Sebben M, Becamel C, Bockaert J and Dumuis A (1999) Novel brain-specific 5-HT<sub>4</sub> receptor splice variants show marked constitutive activity: role of the C-terminal intracellular domain. *Mol Pharmacol* **55**:910-920.
- Del Valle J and Gantz I (1997) Novel insights into histamine H<sub>2</sub> receptor biology. *Am J Physiol* **273**:G987-996.
- Dove S, Elz S, Seifert R and Buschauer A (2004) Structure-activity relationships of histamine H<sub>2</sub> receptor ligands. *Mini Rev Med Chem* **4**:941-954.
- Fukushima Y, Asano T, Saitoh T, Anai M, Funaki M, Ogihara T, Katagiri H, Matsushashi N, Yazaki Y and Sugano K (1997) Oligomer formation of histamine H<sub>2</sub> receptors expressed in Sf9 and COS7 cells. *FEBS Lett* **409**:283-286.
- Ghorai P (2005) Arpromidine-related acylguanidines: synthesis and structure-activity relationships of a new class of guanidine-type histamine H<sub>2</sub> receptor agonists with reduced basicity. Doctoral thesis. University of Regensburg, Germany.  
<http://www.opus-bayern.de/uni-regensburg/volltexte/2006/561/>.
- Gille A and Seifert R (2003) Co-expression of the  $\beta_2$ -adrenoceptor and dopamine D<sub>1</sub>-receptor with G<sub>sα</sub> proteins in Sf9 insect cells: limitations in comparison with fusion proteins. *Biochim Biophys Acta* **1613**:101-114.
- Graziano MP, Freissmuth M and Gilman AG (1989) Expression of G<sub>sα</sub> in *Escherichia coli*. Purification and properties of two forms of the protein. *J Biol Chem* **264**:409-418.
- Hill SJ, Ganellin CR, Timmerman H, Schwartz JC, Shankley NP, Young JM, Schunack W, Levi R and Haas HL (1997) International Union of Pharmacology. XIII. Classification of histamine receptors. *Pharmacol Rev* **49**:253-278.
- Houston C, Wenzel-Seifert K, Bürckstümmer T and Seifert R (2002) The human histamine H<sub>2</sub>-receptor couples more efficiently to Sf9 insect cell G<sub>s</sub>-proteins than to insect cell G<sub>q</sub>-proteins: limitations of Sf9 cells for the analysis of receptor/G<sub>q</sub>-protein coupling. *J Neurochem* **80**:678-696.
- Kelley MT, Bürckstümmer T, Wenzel-Seifert K, Dove S, Buschauer A and Seifert R (2001) Distinct interaction of human and guinea pig histamine H<sub>2</sub>-receptor with guanidine-type agonists. *Mol Pharmacol* **60**:1210-1225.
- Kenakin T (2001) Inverse, protean, and ligand-selective agonism: matters of receptor conformation. *FASEB J* **15**:598-611.

- Kenakin T (2003) Ligand-selective receptor conformations revisited: the promise and the problem. *Trends Pharmacol Sci* **24**:346-354.
- Lefkowitz RJ, Cotecchia S, Samama P and Costa T (1993) Constitutive activity of receptors coupled to guanine nucleotide regulatory proteins. *Trends Pharmacol Sci* **14**:303-307.
- Milligan G (2000) Insights into ligand pharmacology using receptor-G-protein fusion proteins. *Trends Pharmacol Sci* **21**:24-28.
- Milligan G, Bond RA and Lee M (1995) Inverse agonism: pharmacological curiosity or potential therapeutic strategy? *Trends Pharmacol Sci* **16**:10-13.
- Porter JE, Hwa J and Perez DM (1996) Activation of the  $\alpha_{1b}$ -adrenergic receptor is initiated by disruption of an interhelical salt bridge constraint. *J Biol Chem* **271**:28318-28323.
- Samama P, Cotecchia S, Costa T and Lefkowitz RJ (1993) A mutation-induced activated state of the  $\beta_2$ -adrenergic receptor. Extending the ternary complex model. *J Biol Chem* **268**:4625-4636.
- Seifert R and Wenzel-Seifert K (2002) Constitutive activity of G-protein-coupled receptors: cause of disease and common property of wild-type receptors. *Naunyn Schmiedebergs Arch Pharmacol* **366**:381-416.
- Seifert R, Lee TW, Lam VT and Kobilka BK (1998a) Reconstitution of  $\beta_2$ -adrenoceptor-GTP-binding-protein interaction in Sf9 cells: High coupling efficiency in a  $\beta_2$ -adrenoceptor-G<sub>sα</sub> fusion protein. *Eur J Biochem* **255**:369-382.
- Seifert R, Wenzel-Seifert K, Lee TW, Gether U, Sanders-Bush E and Kobilka BK (1998b) Different effects of G<sub>sα</sub> splice variants on  $\beta_2$ -adrenoreceptor-mediated signaling. The  $\beta_2$ -adrenoreceptor coupled to the long splice variant of G<sub>sα</sub> has properties of a constitutively active receptor. *J Biol Chem* **273**:5109-5116.
- Seifert R, Wenzel-Seifert K and Kobilka BK (1999) GPCR-G<sub>o</sub> fusion proteins: molecular analysis of receptor-G-protein coupling. *Trends Pharmacol Sci* **20**:383-389.
- Seifert R, Wenzel-Seifert K, Bürckstümmer T, Pertz HH, Schunack W, Dove S, Buschauer A and Elz S (2003) Multiple differences in agonist and antagonist pharmacology between human and guinea pig histamine H<sub>1</sub>-receptor. *J Pharmacol Exp Ther* **305**:1104-1115.
- Xie SX, Ghorai P, Ye QZ, Buschauer A and Seifert R (2006a) Probing ligand-specific histamine H<sub>1</sub>- and H<sub>2</sub>-receptor conformations with *N*<sup>6</sup>-acylated Imidazolylpropylguanidines. *J Pharmacol Exp Ther* **317**:139-146.
- Xie SX, Kraus A, Ghorai P, Ye QZ, Elz S, Buschauer A and Seifert R (2006b) *N*<sup>1</sup>-(3-cyclohexylbutanoyl)-*N*<sup>2</sup>-[3-(1*H*-imidazol-4-yl)propyl]guanidine (UR-AK57), a potent partial agonist for the human histamine H<sub>1</sub>- and H<sub>2</sub>-receptors. *J Pharmacol Exp Ther* **317**:1262-1268.



## Chapter 9

# Point Mutations in the Second Extracellular Loops of Human and Guinea Pig Histamine H<sub>2</sub> Receptors

### 9.1 Introduction

The histamine H<sub>2</sub> receptor (H<sub>2</sub>R) is a biogenic amine receptor that belongs to the class 1 (rhodopsin-like) of G protein coupled receptors (GPCRs) (Foord et al., 2005). GPCRs represent the largest class of cell surface receptors and are predicted to share a common molecular structure consisting of seven  $\alpha$ -helical transmembrane domains (TM1-TM7) connected by three intracellular and three extracellular loops (Kristiansen, 2004). Many aminergic class 1 GPCRs are predicted to bind endogenous small molecule ligands via a cavity formed by TM3 to TM7 (Shi and Javitch, 2002). The crystal structure of bovine rhodopsin (Palczewski et al., 2000) suggests that in addition to amino acids within the TM domains residues in the second extracellular loop (e2) contact the endogenous ligand retinal. Due to the considerable homology with rhodopsin, a participation of e2 residues to the binding pocket was proposed for members of class 1 GPCRs, too (Shi and Javitch, 2002). To date, experimental evidence for a contribution of e2 on ligand binding has been provided for the dopamine D<sub>2</sub> receptor (Shi and Javitch, 2004), the adenosine A<sub>2a</sub> receptor (Kim et al., 1996), and the M<sub>3</sub> muscarinic acetylcholine receptor (Scarselli et al., 2007).

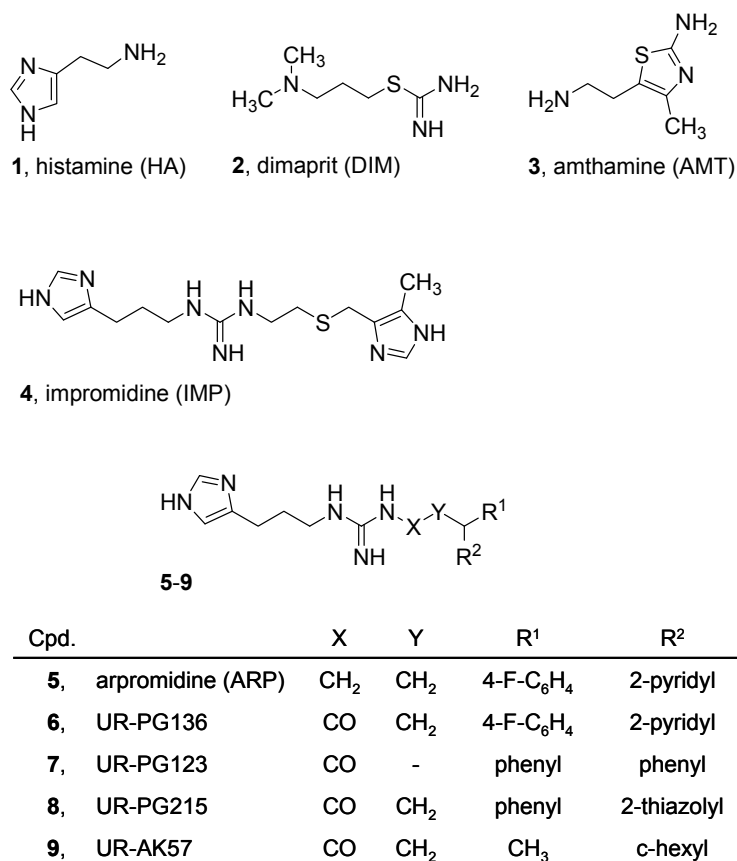


**Figure 9.1:** Structures of H<sub>2</sub>R agonists. **1-3**, small H<sub>2</sub>R agonists; **4-5**, H<sub>2</sub>R agonistic *N*-[3-(1*H*-imidazol-4-yl)propyl]guanidines; **6-9**, H<sub>2</sub>R agonistic *N*<sup>G</sup>-acylated *N*-[3-(1*H*-imidazol-4-yl)propyl]guanidines.

The endogenous H<sub>2</sub>R ligand histamine (**1**, HA; Figure 9.1) and related small agonists dimaprit (**2**, DIM) and amthamine (**3**, AMT) similarly interact with the binding site of the H<sub>2</sub>R. The amino group of HA forms an ionic interaction with Asp-98(3.32) in TM3 (Gantz et al., 1992), and the imidazolyl ring presumably interacts with Tyr-182(5.38) and Asp-186(5.42) in TM5 (Nederkoorn et al., 1996). The guanidine-type H<sub>2</sub>R agonists impromidine (**4**, IMP), arpromidine (**5**, ARP), and the *N*<sup>G</sup>-acylated derivatives **6-9** share a common *N*-[3-(1*H*-imidazol-4-yl)propyl]guanidine moiety that mimics binding of HA and thus is crucial for agonistic activity (Dove et al., 2004). The variable side chains of compounds **4-9** are supposed to interact with a pocket formed by multiple residues in TM2, TM3, TM6, and TM7 (chapter 4.3.2.1). Strikingly, *N*-[3-(1*H*-imidazol-4-yl)propyl]guanidines and *N*<sup>G</sup>-acylguanidines but not the small H<sub>2</sub>R agonists are considerably more potent and efficacious at fusion proteins of the guinea pig H<sub>2</sub>R coupled to the short splice variant of G<sub>sa</sub>, G<sub>saS</sub>, (gpH<sub>2</sub>R-G<sub>saS</sub>) than at the human isoforms (hH<sub>2</sub>R-G<sub>saS</sub>). Tyr-17(1.31) in TM1 and Asp-271(7.36) in TM7 of gpH<sub>2</sub>R (Cys-17(1.31) and Ala-271(7.36) in hH<sub>2</sub>R) have been shown to contribute to this species-selectivity (chapter 8). However, the results from this study also suggest participation of additional as yet unidentified residues as molecular basis for the selective agonist activities.



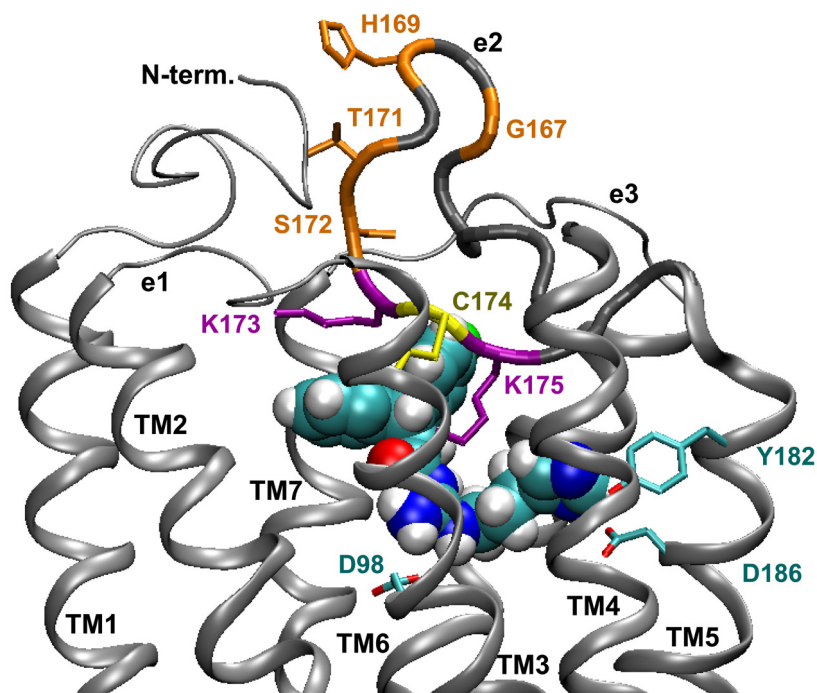


**Figure 9.3:** Side-view of a 3D model of the hH<sub>2</sub>R in complex with UR-PG136. The model was generated as described in chapter 4.2. The putative agonist binding site and the extracellular components of the hH<sub>2</sub>R are shown. UR-PG136 is shown as space-filling representation. e2 is shown as a thick line. Residues differing in the e2 sequences of hH<sub>2</sub>R and gpH<sub>2</sub>R are shown in orange. Adjacent to the highly conserved Cys-174 (yellow) forming a disulfide bond to Cys-91(3.25), Lys-173 and Lys-175 (both magenta) are predicted to face the binding pocket and were mutated into alanine within this study. Asp-98(3.32), Tyr-182(5.38), and Asp-186(5.42) designate the main interaction sites of agonists with the H<sub>2</sub>R.

## 9.2 Materials and Methods

### 9.2.1 Materials

The generation of pGEM-3Z-SF-hH<sub>2</sub>R-G<sub>saS</sub>, pGEM-3Z-SF-gpH<sub>2</sub>R-G<sub>saS</sub>, and pVL1392-SF-hH<sub>2</sub>R-G<sub>saS</sub> was described previously (Kelley et al., 2001). The generation of the baculoviruses encoding hH<sub>2</sub>R-G<sub>saS</sub> and gpH<sub>2</sub>R-G<sub>saS</sub> was described previously (Kelley et al., 2001; Houston et al., 2002). A description of all remaining materials is given in chapter 6.1.

### 9.2.2 Construction of the cDNA for gpH<sub>2</sub>R-hE2-G<sub>saS</sub>

The point mutations in the sequence of the gpH<sub>2</sub>R were generated by sequential overlap-

extension PCRs. With pGEM-3Z-SF-gpH<sub>2</sub>R-G<sub>saS</sub> as template, PCR 1A was used to amplify a DNA fragment consisting of the cleavable signal peptide from influenza hemagglutinin (S), the FLAG epitope (F) recognized by the M1 monoclonal antibody, and the N-terminal part of the gpH<sub>2</sub>R. The sense primer annealed with 18 bp of pGEM-3Z prior to the 5'-end of SF. The antisense primer encoded the sequence CTTACTAGTGGTATGATTGCCCTTGCTGGTCTCATTCC to generate the amino acid exchanges Asp-167→Gly-167, Asp-169→His-169, Ile-171→Thr-171, and Val-172→Ser-172, and a new *Spe* I site (ACTAGT). In PCR 1B, the DNA sequence for the C-terminal part of gpH<sub>2</sub>R, a hexahistidine tag, and the entire sequence of G<sub>saS</sub> was amplified using pGEM-3Z-SF-gpH<sub>2</sub>R-G<sub>saS</sub> as template. The hexahistidine tag was included to allow future purification and to provide additional protection against proteolysis (Seifert et al., 1998). The sense primer encoded the sequence GGCAATCATACCACTAGTAAGTGCAAAGTCCAGGTC to generate the amino acid exchanges Asp-167→Gly-167, Asp-169→His-169, Ile-171→Thr-171, and Val-172→Ser-172, and the new *Spe* I site. The antisense primer annealed with the cDNA encoding the 5 C-terminal amino acids of G<sub>saS</sub>, the stop codon, and an *Xba* I site. In PCR 2, the products of PCR 1A and 1B annealed in the region of the newly created point mutations and the new *Spe* I site. Here, the sense primer of PCR 1A and the antisense primer of PCR 1B were used. In that way, the complete cDNA for the gpH<sub>2</sub>R-hE2-G<sub>saS</sub> fusion protein was amplified. The product of PCR 2 was digested with *Nco* I and *Xba* I and cloned into pGEM-3Z-SF-hH<sub>2</sub>R-G<sub>saS</sub> digested with *Nco* I and *Xba* I. pGEM-3Z-SF-gpH<sub>2</sub>R-hE2-G<sub>saS</sub> was digested with *Nco* I and *EcoR* I and cloned into the baculovirus transfer vector pVL1392-SF-hH<sub>2</sub>R-G<sub>saS</sub> digested with *Nco* I and *EcoR* I. PCR-generated DNA sequences were confirmed by extensive restriction enzyme analysis and enzymatic sequencing.

### 9.2.3 Construction of the cDNA for hH<sub>2</sub>R-gpE2-G<sub>saS</sub>

The strategy for the generation of the cDNA for the epitope-tagged hH<sub>2</sub>R-gpE2-G<sub>saS</sub> was analogous to the strategy for the generation of the cDNA for gpH<sub>2</sub>R-hE2-G<sub>saS</sub>. With pGEM-3Z-SF-hH<sub>2</sub>R-G<sub>saS</sub> as template, PCR 1A was used to amplify a DNA fragment encoding SF and the N-terminal part of the hH<sub>2</sub>R. The sense primer annealed with 18 bp of pGEM-3Z prior to the 5'-end of SF. The antisense primer encoded the sequence CTTAACGATCGTATCATTATCCTTGCTGGTCTCGTTCC to generate the amino acid exchanges Gly-167→Asp-167, His-169→Asp-169, Thr-171→Ile-171, and Ser-172→Val-172, and a new *Pvu* I site (CGATCG). In PCR 1B, the DNA sequence for the C-terminal part of hH<sub>2</sub>R, the hexahistidine tag, and the entire sequence of G<sub>saS</sub> was amplified using pGEM-3Z-SF-hH<sub>2</sub>R-G<sub>saS</sub> as template. The sense primer encoded the sequence GATAATGATACGATCGTTAAGTGCAAAGTCCAGGTC to generate the amino acid

exchanges Gly-167→Asp-167, His-169→Asp-169, Thr-171→Ile-171, and Ser-172→Val-172, and the new *Pvu* I site. The antisense primer annealed with the cDNA encoding the 5 C-terminal amino acids of G<sub>saS</sub>, the stop codon, and an *Xba* I site. In PCR 2, the products of PCR 1A and 1B annealed in the region of the newly created point mutations and the new *Pvu* I site. Here, the sense primer of PCR 1A and the antisense primer of PCR 1B were used. In that way, the complete cDNA for the hH<sub>2</sub>R-gpE2-G<sub>saS</sub> was amplified. The product of PCR 2 was digested with *Nco* I and *Xba* I and cloned into pGEM-3Z-SF-hH<sub>2</sub>R-G<sub>saS</sub> digested with *Nco* I and *Xba* I. pGEM-3Z-SF-hH<sub>2</sub>R-gpE2-G<sub>saS</sub> was digested with *Nco* I and *EcoR* I and cloned into the baculovirus transfer vector pVL1392-SF-hH<sub>2</sub>R-G<sub>saS</sub> digested with *Nco* I and *EcoR* I.

#### 9.2.4 Construction of the cDNA for hH<sub>2</sub>R-K173A-G<sub>saS</sub>

With pGEM-3Z-SF-hH<sub>2</sub>R-G<sub>saS</sub> as template, PCR 1A was used to amplify a DNA fragment encoding SF and the N-terminal part of the hH<sub>2</sub>R. The sense primer annealed with 18 bp of pGEM-3Z prior to the 5'-end of SF. The antisense primer encoded the sequence CTTTGCACGCACTAGTGGTATGATTGCCCTTGC to generate the Lys-173→Ala-173 exchange and a new *Spe* I site. In PCR 1B, the DNA sequence for the C-terminal part of hH<sub>2</sub>R, the hexahistidine tag, and the entire sequence of G<sub>saS</sub> was amplified using pGEM-3Z-SF-hH<sub>2</sub>R-G<sub>saS</sub> as template. The sense primer encoded the sequence CATACCACTAGTGCGTGCAAAGTCCAGGTCAATG to generate the Lys-173→Ala-173 exchange and the new *Spe* I site. The antisense primer annealed with the cDNA encoding the 5 C-terminal amino acids of G<sub>saS</sub>, the stop codon, and an *Xba* I site. In PCR 2, the products of PCR 1A and 1B annealed in the region of the newly created Lys-173→Ala-173 exchange and the new *Spe* I site. The product of PCR 2 was digested with *Nco* I and *Xba* I and cloned into pGEM-3Z-SF-hH<sub>2</sub>R-G<sub>saS</sub> digested with *Nco* I and *Xba* I. pGEM-3Z-SF-hH<sub>2</sub>R-K173A-G<sub>saS</sub> was digested with *Nco* I and *EcoR* I and cloned into the baculovirus transfer vector pVL1392-SF-hH<sub>2</sub>R-G<sub>saS</sub> digested with *Nco* I and *EcoR* I.

#### 9.2.5 Construction of the cDNA for hH<sub>2</sub>R-K175A-G<sub>saS</sub>

With pGEM-3Z-SF-hH<sub>2</sub>R-G<sub>saS</sub> as template, PCR 1A was used to amplify a DNA fragment encoding SF and the N-terminal part of the hH<sub>2</sub>R. The sense primer annealed with 18 bp of pGEM-3Z prior to the 5'-end of SF. The antisense primer encoded the sequence CTTCGTTAAACCTGGACTGCGCACTTAGAGGTGGTATG to generate the Lys-175→Ala-175 exchange and a new *Hpa* I site (GTTAAC). In PCR 1B, the DNA sequence for the C-terminal part of hH<sub>2</sub>R, the hexahistidine tag, and the entire sequence of G<sub>saS</sub> was amplified using

pGEM-3Z-SF-hH<sub>2</sub>R-G<sub>saS</sub> as template. The sense primer encoded the sequence GTGCGCAGTCCAGGTIAACGAAGTGTACGGGCTGGTG to generate the Lys-175→Ala-175 exchange and the new *Hpa* I site. The antisense primer annealed with the cDNA encoding the 5 C-terminal amino acids of G<sub>saS</sub>, the stop codon, and an *Xba* I site. In PCR 2, the products of PCR 1A and 1B annealed in the region of the newly created Lys-175→Ala-175 exchange and the new *Hpa* I site. The product of PCR 2 was digested with *Nco* I and *Xba* I and cloned into pGEM-3Z-SF-hH<sub>2</sub>R-G<sub>saS</sub> digested with *Nco* I and *Xba* I. pGEM-3Z-SF-hH<sub>2</sub>R-K175A-G<sub>saS</sub> was digested with *Nco* I and *EcoR* I and cloned into the baculovirus transfer vector pVL1392-SF-hH<sub>2</sub>R-G<sub>saS</sub> digested with *Nco* I and *EcoR* I.

## 9.2.6 Generation of recombinant baculoviruses, cell culture, and membrane preparation

A description is given in chapter 6.2.

## 9.2.7 SDS-PAGE and immunoblot analysis

A description is given in chapter 6.3.

## 9.2.8 Steady-state GTPase activity assay

A description is given in chapter 6.4.

# 9.3 Results

## 9.3.1 Immunological detection of recombinant proteins in Sf9 cell membranes

In Sf9 cells, hH<sub>2</sub>R-G<sub>saS</sub>, gpH<sub>2</sub>R-G<sub>saS</sub>, gpH<sub>2</sub>R-hE2-G<sub>saS</sub>, hH<sub>2</sub>R-gpE2-G<sub>saS</sub>, hH<sub>2</sub>R-K173A-G<sub>saS</sub>, and hH<sub>2</sub>R-K175A-G<sub>saS</sub> were well expressed (Figure 9.4). In SDS-PAGE, monomeric H<sub>2</sub>Rs migrate as ~33 kDa (Fukushima et al., 1997) and G<sub>saS</sub> as ~45 kDa bands (Graziano et al., 1989). With all fusion proteins, strong bands were detected at ~80 kDa thus representing fusion protein monomers. The bands appeared somewhat diffuse presumably due to differently glycosylated forms of fusion proteins. Comparison with the peak intensities of calibrated Sf9 membranes expressing the β<sub>2</sub>AR at 7.5 pmol mg<sup>-1</sup> (as determined by

[<sup>3</sup>H]dihydroalprenolol saturation binding) revealed expression levels of ~3 pmol mg<sup>-1</sup> for hH<sub>2</sub>R-G<sub>saS</sub>, ~4 pmol mg<sup>-1</sup> for hH<sub>2</sub>R-K175-G<sub>saS</sub>, and ~1 pmol mg<sup>-1</sup> for gpH<sub>2</sub>R-G<sub>saS</sub>, gpH<sub>2</sub>R-hE2-G<sub>saS</sub>, hH<sub>2</sub>R-K173-G<sub>saS</sub>, and hH<sub>2</sub>R-gpE2-G<sub>saS</sub>, respectively.

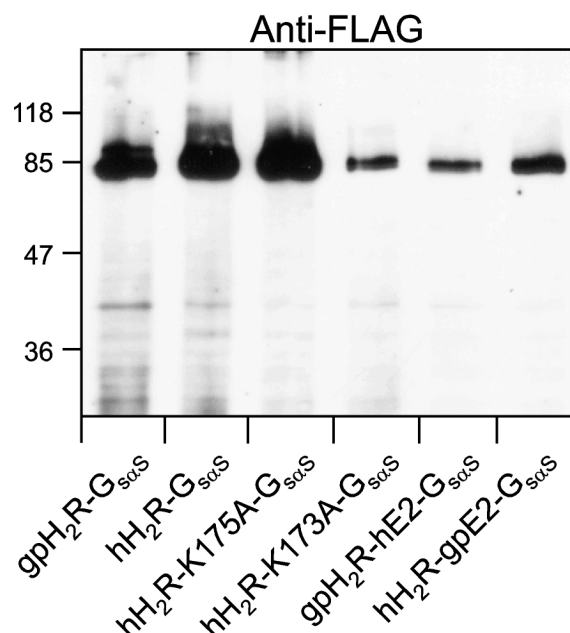


**Figure 9.4:** Immunological detection of recombinant proteins in Sf9 cells. Sf9 membranes expressing various proteins were prepared, separated by SDS-PAGE on gels containing 12% (w/v) acrylamide, transferred onto Immobilon P membranes, and probed with the anti FLAG (M1) antibody. In each lane, 10 µg of membrane protein was loaded onto the gel. Exceptionally, 40 µg of a membrane expressing gpH<sub>2</sub>R-G<sub>saS</sub> was loaded onto the gel. Numbers on the left of membranes designate masses of marker proteins in kDa.

### 9.3.2 GTPase activities in Sf9 membranes expressing wild-type and mutant

#### H<sub>2</sub>R-G<sub>saS</sub>

The basal GTPase activities were approximately similar in Sf9 membranes expressing both wild-type and all mutant H<sub>2</sub>R-G<sub>saS</sub> fusion proteins. At wild-type hH<sub>2</sub>R-G<sub>saS</sub>, stimulation with 100 µM HA yielded GTPase activities approximately 450% of the basal levels (Figure 9.5 A). The maximum HA-stimulated GTPase activities were slightly reduced at hH<sub>2</sub>R-gpE2-G<sub>saS</sub> and strongly reduced at hH<sub>2</sub>R-K173A-G<sub>saS</sub> and hH<sub>2</sub>R-K175A-G<sub>saS</sub>. By contrast, HA stimulation was similar at gpH<sub>2</sub>R-G<sub>saS</sub> and gpH<sub>2</sub>R-hE2-G<sub>saS</sub> (Figure 9.5 B). Apparently, these values were independent of the different expression levels in Sf9 cells (chapter 9.3.1).



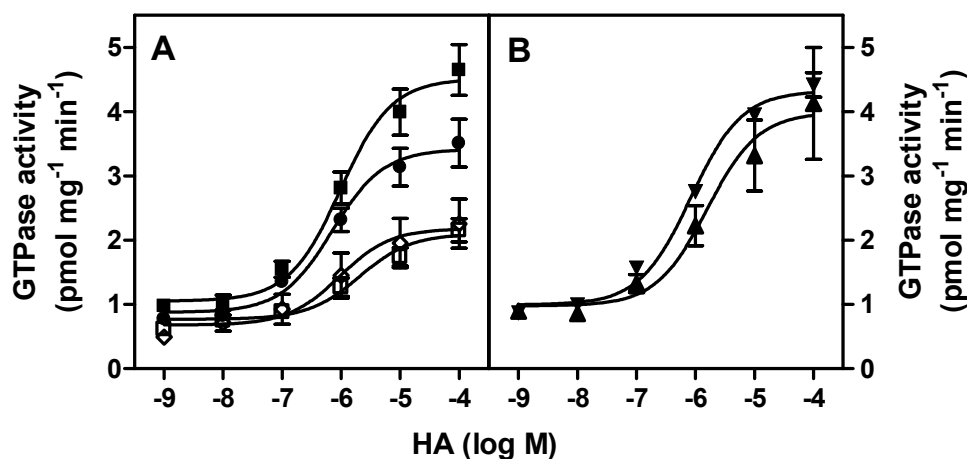


**Figure 9.5:** Concentration-dependent increase of GTPase activity by HA in membranes expressing wild-type and mutant H<sub>2</sub>R-G<sub>saS</sub> fusion proteins. A, hH<sub>2</sub>R-G<sub>saS</sub> (■), hH<sub>2</sub>R-gpE2-G<sub>saS</sub> (●), hH<sub>2</sub>R-K173A-G<sub>saS</sub> (◇), hH<sub>2</sub>R-K175A-G<sub>saS</sub> (□); B, gpH<sub>2</sub>R-G<sub>saS</sub> (▼), gpH<sub>2</sub>R-hE2-G<sub>saS</sub> (▲). GTPase activity in Sf9 membranes was determined as described in chapter 6.4. Reaction mixtures contained membranes (10 µg of protein/tube) expressing fusion proteins and HA at concentrations indicated on the abscissa. Data shown are the means ± S.E.M. of three independent experiments performed in duplicates or triplicates.

Efficacies and potencies of compounds **1-9** at wild-type hH<sub>2</sub>R-G<sub>saS</sub> and at hH<sub>2</sub>R-gpE2-G<sub>saS</sub>, hH<sub>2</sub>R-K173A-G<sub>saS</sub>, and hH<sub>2</sub>R-K175A-G<sub>saS</sub> are listed in Table 9.1. In Table 9.2, the corresponding values at gpH<sub>2</sub>R-G<sub>saS</sub> and gpH<sub>2</sub>R-hE2-G<sub>saS</sub> are shown. The small agonists HA (**1**), DIM (**2**), and AMT (**3**) were similarly efficacious and potent at hH<sub>2</sub>R-G<sub>saS</sub>, hH<sub>2</sub>R-gpE2-G<sub>saS</sub>, and hH<sub>2</sub>R-K173A-G<sub>saS</sub>. Whereas HA (**1**) and DIM (**2**) were less potent at hH<sub>2</sub>R-K175A-G<sub>saS</sub> than at hH<sub>2</sub>R-G<sub>saS</sub>, the potencies of AMT (**3**) did not differ between both proteins. DIM (**2**) and AMT (**3**) were similarly efficacious at hH<sub>2</sub>R-K175A-G<sub>saS</sub> and at hH<sub>2</sub>R-G<sub>saS</sub>. The majority of guanidines (**4**, **5**) and *N*<sup>G</sup>-acylguanidines (**6-9**) was similarly efficacious and potent at hH<sub>2</sub>R-gpE2-G<sub>saS</sub>, hH<sub>2</sub>R-K173A-G<sub>saS</sub>, and hH<sub>2</sub>R-K175A-G<sub>saS</sub>, respectively, compared to the human wild-type receptor. However, IMP (**4**) was 2.5-fold (not significant) more and ARP (**5**) and compound **9** slightly less potent at hH<sub>2</sub>R-K175A-G<sub>saS</sub> than at hH<sub>2</sub>R-G<sub>saS</sub>. The potency of compound **7** was somewhat higher at hH<sub>2</sub>R-gpE2-G<sub>saS</sub> vs. hH<sub>2</sub>R-G<sub>saS</sub>. In agreement with previous studies, guanidines and *N*<sup>G</sup>-acylguanidines were more potent and more efficacious at gpH<sub>2</sub>R-G<sub>saS</sub> than at hH<sub>2</sub>R-G<sub>saS</sub> (Kelley et al., 2001; Xie et al., 2006a, b). Most of the agonists tended to be less potent at gpH<sub>2</sub>R-hE2-G<sub>saS</sub> than at gpH<sub>2</sub>R-G<sub>saS</sub> but these differences were only significant for ARP (**5**). All compounds studied were similarly efficacious at gpH<sub>2</sub>R-hE2-G<sub>saS</sub> and gpH<sub>2</sub>R-G<sub>saS</sub>.

**Table 9.1:** Agonist efficacies ( $E_{\text{Max}}$ ) and potencies at hH<sub>2</sub>R-G<sub>saS</sub>, hH<sub>2</sub>R-gpE2-G<sub>saS</sub>, hH<sub>2</sub>R-K173A-G<sub>saS</sub>, and hH<sub>2</sub>R-K175A-G<sub>saS</sub> in the GTPase assay. GTPase activity in Sf9 membranes was determined as described in chapter 6.4. Data shown are the means  $\pm$  S.D. of three to five experiments performed in duplicates or triplicates. Efficacies and potencies, respectively, of ligands at hH<sub>2</sub>R-G<sub>saS</sub> were compared with the corresponding parameters at hH<sub>2</sub>R-gpE2-G<sub>saS</sub>, hH<sub>2</sub>R-K173A-G<sub>saS</sub>, and hH<sub>2</sub>R-K175A-G<sub>saS</sub>, respectively, using one-way ANOVA.

Cpd.	hH <sub>2</sub> R-G <sub>saS</sub>		hH <sub>2</sub> R-gpE2-G <sub>saS</sub>		hH <sub>2</sub> R-K173A-G <sub>saS</sub>		hH <sub>2</sub> R-K175A-G <sub>saS</sub>	
	$E_{\text{Max}}^a$	EC <sub>50</sub> (nM)	$E_{\text{Max}}^a$	EC <sub>50</sub> (nM)	$E_{\text{Max}}^a$	EC <sub>50</sub> (nM)	$E_{\text{Max}}^a$	EC <sub>50</sub> (nM)
1	1.00	990 $\pm$ 92	1.00	700 $\pm$ 190	1.00	990 $\pm$ 430	1.00	2400 $\pm$ 870*
2	0.85 $\pm$ 0.02	910 $\pm$ 430	0.88 $\pm$ 0.04	1000 $\pm$ 230	0.86 $\pm$ 0.04	1200 $\pm$ 240	0.91 $\pm$ 0.05	2600 $\pm$ 1500*
3	0.91 $\pm$ 0.02	190 $\pm$ 50	0.94 $\pm$ 0.05	140 $\pm$ 30	0.89 $\pm$ 0.01	130 $\pm$ 14	0.94 $\pm$ 0.04	180 $\pm$ 36
4	0.82 $\pm$ 0.02	160 $\pm$ 42	0.83 $\pm$ 0.06	140 $\pm$ 65	0.85 $\pm$ 0.05	130 $\pm$ 67	0.95 $\pm$ 0.08	63 $\pm$ 10
5	0.84 $\pm$ 0.03	72 $\pm$ 9	0.88 $\pm$ 0.08	77 $\pm$ 4	0.85 $\pm$ 0.03	69 $\pm$ 7	0.84 $\pm$ 0.04	87 $\pm$ 8*
6	0.82 $\pm$ 0.05	100 $\pm$ 8	0.76 $\pm$ 0.08	89 $\pm$ 7	0.82 $\pm$ 0.02	88 $\pm$ 25	0.91 $\pm$ 0.09	150 $\pm$ 81
7	0.14 $\pm$ 0.03	250 $\pm$ 13	0.09 $\pm$ 0.03	110 $\pm$ 52*	0.14 $\pm$ 0.02	150 $\pm$ 68	0.22 $\pm$ 0.06	270 $\pm$ 41
8	0.80 $\pm$ 0.04	120 $\pm$ 45	0.74 $\pm$ 0.03	96 $\pm$ 32	0.81 $\pm$ 0.02	120 $\pm$ 49	0.85 $\pm$ 0.07	150 $\pm$ 61
9	0.86 $\pm$ 0.05	15 $\pm$ 4	0.76 $\pm$ 0.13	12 $\pm$ 3	0.85 $\pm$ 0.07	17 $\pm$ 8	0.98 $\pm$ 0.10	27 $\pm$ 6*

<sup>a</sup> Efficacy relative to HA (= 1.00)

\* comparison with the EC<sub>50</sub> value at hH<sub>2</sub>R-G<sub>saS</sub>; \*  $p < 0.05$

**Table 9.2:** Agonist efficacies ( $E_{\text{Max}}$ ) and potencies at gpH<sub>2</sub>R-G<sub>saS</sub> and gpH<sub>2</sub>R-hE2-G<sub>saS</sub> in the GTPase

Cpd.	gpH <sub>2</sub> R-G <sub>saS</sub>		gpH <sub>2</sub> R-hE2-G <sub>saS</sub>	
	$E_{\text{Max}}^a$	EC <sub>50</sub> (nM)	$E_{\text{Max}}^a$	EC <sub>50</sub> (nM)
1	1.00	850 $\pm$ 340	1.00	1400 $\pm$ 280
2	0.94 $\pm$ 0.06	740 $\pm$ 360	0.96 $\pm$ 0.04	1500 $\pm$ 480
3	1.04 $\pm$ 0.01	190 $\pm$ 42	0.94 $\pm$ 0.06	310 $\pm$ 110
4	0.96 $\pm$ 0.06	18 $\pm$ 9	0.98 $\pm$ 0.02	41 $\pm$ 19
5	0.94 $\pm$ 0.05	7 $\pm$ 1	0.97 $\pm$ 0.03	18 $\pm$ 3**
6	1.02 $\pm$ 0.11	29 $\pm$ 10	1.02 $\pm$ 0.10	27 $\pm$ 2
7	0.40 $\pm$ 0.02	220 $\pm$ 22	0.37 $\pm$ 0.07	250 $\pm$ 79
8	0.94 $\pm$ 0.05	14 $\pm$ 4	1.00 $\pm$ 0.05	26 $\pm$ 10
9	0.97 $\pm$ 0.18	14 $\pm$ 6	0.97 $\pm$ 0.08	15 $\pm$ 1

<sup>a</sup> Efficacy relative to HA (= 1.00)

\* comparison with the EC<sub>50</sub> value at hH<sub>2</sub>R-G<sub>saS</sub>; \*\*  $p < 0.01$

assay. Please consider the legend of Table 9.1 for experimental conditions. Efficacies and potencies, respectively, of ligands at gpH<sub>2</sub>R-G<sub>saS</sub> were compared with the corresponding parameters at gpH<sub>2</sub>R-hE2-G<sub>saS</sub>, using the t-test.

## 9.4 Discussion

Several reports showed that e2 contributes to the ligand-specificity in aminergic and nucleoside-binding GPCRs. For example, a single residue in e2 was sufficient to interconvert ketanserin specificity between canine and human 5-HT<sub>1D</sub> receptors (Wurch and Pauwels, 2000). Additionally, three adjacent residues in e2 were identified to be responsible for  $\alpha_1$ -adrenergic receptor subtype-selective antagonist binding (Zhao et al., 1996). Moreover, the distal eleven amino acids of the e2 determined the selectivity of agonist and antagonist binding to A<sub>1</sub>/A<sub>3</sub> adenosine receptors (Olah et al., 1994).

In the steady-state GTPase activity assay, efficacies and potencies of the small H<sub>2</sub>R agonists HA, DIM, AMT, and the more bulky *N*-[3-(1*H*-imidazol-4-yl)propyl]guanidines and *N*<sup>G</sup>-acylated derivatives did neither significantly differ between hH<sub>2</sub>R-gpE2-G<sub>saS</sub> and hH<sub>2</sub>R-G<sub>saS</sub>, nor between gpH<sub>2</sub>R-hE2-G<sub>saS</sub> and gpH<sub>2</sub>R-G<sub>saS</sub>. From this follows that selective interactions of guanidine-type agonists with human and guinea pig H<sub>2</sub>R species isoforms are not determined by the specific e2 loop sequences differing in the four non-conservative exchange positions 167, 169, 171 and 172. Presumably, residues at these positions do not directly face the agonist binding pockets of hH<sub>2</sub>R and gpH<sub>2</sub>R. At the most, the slightly reduced potencies of the small agonists and the non-*N*<sup>G</sup>-acylated guanidines at gpH<sub>2</sub>R-hE2-G<sub>saS</sub> vs. gpH<sub>2</sub>R-G<sub>saS</sub> may be due to minor conformational modifications of the gpH<sub>2</sub>R binding pocket.

The high-resolution structure of bovine rhodopsin revealed that e2 folds down into the transmembrane domain and forms part of the ligand binding surface for retinal (Palczewski et al., 2000). Characteristically, a disulfide bond in rhodopsin between Cys-187 in e2 and Cys-110 in TM3 is highly conserved among class 1 GPCRs. The obvious suggestion that the structure of e2 in the region around the conserved cysteine is similar in rhodopsin and aminergic receptors was supported by SCAM (substituted-cysteine accessibility method) studies at the dopamine D<sub>2</sub> receptor (Shi and Javitch, 2004). Additionally, the M<sub>3</sub> muscarinic acetylcholine receptor (Scarselli et al., 2007), the adenosine A<sub>2a</sub> receptor (Kim et al., 1996), the  $\alpha_{1A}$  and  $\alpha_{1B}$  adrenoceptors (Zhao et al., 1996), and the 5-HT<sub>1D</sub> receptor (Wurch and Pauwels, 2000) contain residues in the corresponding regions of e2 that directly participate in the binding of ligands. Adjacent to Cys-174 in e2 forming a disulfide bond with Cys-91(3.25) in TM3, the hH<sub>2</sub>R contains Lys-173 and Lys-175. In hH<sub>2</sub>R-G<sub>saS</sub>, substitution of Lys-173 by alanine did not affect the efficacies and potencies of small and bulky agonists in the GTPase assay. The role of Lys-175 in the hH<sub>2</sub>R-G<sub>saS</sub> is ambiguous since alanine mutation significantly reduced the potencies of HA, DIM, ARP, and UR-AK57, but slightly increased the potency of IMP. These results clearly demonstrate the non-existence of electrostatic interactions between the amine group of Lys-173 and Lys-175, respectively, with the agonists. However,

the homology model of the hH<sub>2</sub>R proposes Lys-175 to be in close proximity to the small agonist binding pocket including TM3 and TM5 (see Figure 9.3). Corresponding weak interactions may occur that could be partly counterbalanced by entropic effects. Moreover, it cannot be ruled out that alanine by itself maintains some interaction potential.

At hH<sub>2</sub>R-K173A-G<sub>sαS</sub> and hH<sub>2</sub>R-K175A-G<sub>sαS</sub>, the HA-stimulated increases in GTPase activity were strongly reduced compared to hH<sub>2</sub>R-G<sub>sαS</sub>. Thus, with both mutant receptors agonist-bound active conformations are stabilized that activate G<sub>sαS</sub> less efficiently than the corresponding activated wild-type hH<sub>2</sub>R. Possibly, the two lysines in e2 undergo distinct ionic or H-bonding interactions in the active state whose disruption impairs the coupling to G<sub>sαS</sub>.

Taken together, in the present study we show that the second extracellular loop does not contribute to the species-selective interactions of *N*-[3-(1*H*-imidazol-4-yl)propyl]guanidines and *N*<sup>G</sup>-acylated derivatives with human and guinea pig H<sub>2</sub>R species isoforms, thereby broadening our understanding of the molecular basis for this pharmacological phenomenon. The six mutated amino acids presumably do not directly face the H<sub>2</sub>R binding pocket of guanidine-type agonists, indicating that participation of residues in the distal part of e2 to the binding pocket may apply for many (Shi and Javitch, 2002) but possibly not for all class 1 GPCRs. Despite the constraining function of the conserved disulfide bond between two cysteines in e2 and TM3, the loop regions are much more flexible than the backbone of the TM domains. It is therefore generally difficult to state precise predictions about backbone structures and side chain conformations of loop regions in 3D structural models which emphasizes the need for supplementing molecular pharmacological studies.

## 9.5 References

- Dove S, Elz S, Seifert R and Buschauer A (2004) Structure-activity relationships of histamine H<sub>2</sub> receptor ligands. *Mini Rev Med Chem* **4**:941-954.
- Foord SM, Bonner TI, Neubig RR, Rosser EM, Pin JP, Davenport AP, Spedding M and Harmar AJ (2005) International Union of Pharmacology. XLVI. G protein-coupled receptor list. *Pharmacol Rev* **57**:279-288.
- Fukushima Y, Asano T, Saitoh T, Anai M, Funaki M, Ogihara T, Katagiri H, Matsushashi N, Yazaki Y and Sugano K (1997) Oligomer formation of histamine H<sub>2</sub> receptors expressed in Sf9 and COS7 cells. *FEBS Lett* **409**:283-286.
- Gantz I, Munzert G, Tashiro T, Schaffer M, Wang L, DelValle J and Yamada T (1991) Molecular cloning of the human histamine H<sub>2</sub> receptor. *Biochem Biophys Res Commun* **178**:1386-1392.
- Gantz I, DelValle J, Wang LD, Tashiro T, Munzert G, Guo YJ, Konda Y and Yamada T (1992) Molecular basis for the interaction of histamine with the histamine H<sub>2</sub> receptor. *J Biol Chem* **267**:20840-20843.

- Graziano MP, Freissmuth M and Gilman AG (1989) Expression of G<sub>sα</sub> in *Escherichia coli*. Purification and properties of two forms of the protein. *J Biol Chem* **264**:409-418.
- Houston C, Wenzel-Seifert K, Bürckstümmer T and Seifert R (2002) The human histamine H<sub>2</sub>-receptor couples more efficiently to Sf9 insect cell G<sub>s</sub>-proteins than to insect cell G<sub>q</sub>-proteins: limitations of Sf9 cells for the analysis of receptor/G<sub>q</sub>-protein coupling. *J Neurochem* **80**:678-696.
- Kelley MT, Bürckstümmer T, Wenzel-Seifert K, Dove S, Buschauer A and Seifert R (2001) Distinct interaction of human and guinea pig histamine H<sub>2</sub>-receptor with guanidine-type agonists. *Mol Pharmacol* **60**:1210-1225.
- Kim J, Jiang Q, Glashofer M, Yehle S, Wess J and Jacobson KA (1996) Glutamate residues in the second extracellular loop of the human A<sub>2a</sub> adenosine receptor are required for ligand recognition. *Mol Pharmacol* **49**:683-691.
- Kristiansen K (2004) Molecular mechanisms of ligand binding, signaling, and regulation within the superfamily of G-protein-coupled receptors: molecular modeling and mutagenesis approaches to receptor structure and function. *Pharmacol Ther* **103**:21-80.
- Milligan G (2000) Insights into ligand pharmacology using receptor-G-protein fusion proteins. *Trends Pharmacol Sci* **21**:24-28.
- Nederkoorn PH, van Gelder EM, Donne-Op den Kelder GM and Timmerman H (1996) The agonistic binding site at the histamine H<sub>2</sub> receptor. II. Theoretical investigations of histamine binding to receptor models of the seven alpha-helical transmembrane domain. *J Comput Aided Mol Des* **10**:479-489.
- Olah ME, Jacobson KA and Stiles GL (1994) Role of the second extracellular loop of adenosine receptors in agonist and antagonist binding. Analysis of chimeric A<sub>1</sub>/A<sub>3</sub> adenosine receptors. *J Biol Chem* **269**:24692-24698.
- Palczewski K, Kumasaka T, Hori T, Behnke CA, Motoshima H, Fox BA, Le Trong I, Teller DC, Okada T, Stenkamp RE, Yamamoto M and Miyano M (2000) Crystal structure of rhodopsin: A G protein-coupled receptor. *Science* **289**:739-745.
- Scarselli M, Li B, Kim SK and Wess J (2007) Multiple residues in the second extracellular loop are critical for M<sub>3</sub> muscarinic acetylcholine receptor activation. *J Biol Chem* **282**:7385-7396.
- Seifert R, Lee TW, Lam VT and Kobilka BK (1998) Reconstitution of β<sub>2</sub>-adrenoceptor-GTP-binding-protein interaction in Sf9 cells: High coupling efficiency in a β<sub>2</sub>-adrenoceptor-G<sub>sα</sub> fusion protein. *Eur J Biochem* **255**:369-382.
- Seifert R, Wenzel-Seifert K and Kobilka BK (1999) GPCR-G<sub>α</sub> fusion proteins: molecular analysis of receptor-G-protein coupling. *Trends Pharmacol Sci* **20**:383-389.
- Shi L and Javitch JA (2002) The binding site of aminergic G protein-coupled receptors: the transmembrane segments and second extracellular loop. *Annu Rev Pharmacol Toxicol* **42**:437-467.
- Shi L and Javitch JA (2004) The second extracellular loop of the dopamine D<sub>2</sub> receptor lines the binding-site crevice. *Proc Natl Acad Sci U S A* **101**:440-445.
- Traiffort E, Vizuite ML, Tardivel-Lacombe J, Souil E, Schwartz JC and Ruat M (1995) The guinea pig histamine H<sub>2</sub> receptor: gene cloning, tissue expression and chromosomal localization of its human counterpart. *Biochem Biophys Res Commun* **211**:570-577.
- Wurch T and Pauwels PJ (2000) Coupling of canine serotonin 5-HT<sub>1B</sub> and 5-HT<sub>1D</sub> receptor subtypes to the formation of inositol phosphates by dual interactions with endogenous G<sub>i/o</sub> and recombinant G<sub>α15</sub> proteins. *J Neurochem* **75**:1180-1189.
- Xie SX, Ghorai P, Ye QZ, Buschauer A and Seifert R (2006a) Probing ligand-specific histamine H<sub>1</sub>- and H<sub>2</sub>-receptor conformations with N<sup>G</sup>-acylated imidazolylpropylguanidines. *J Pharmacol Exp Ther* **317**:139-146.
- Xie SX, Kraus A, Ghorai P, Ye QZ, Elz S, Buschauer A and Seifert R (2006b) N<sup>1</sup>-(3-cyclohexylbutanoyl)-N<sup>2</sup>-[3-(1H-imidazol-4-yl)propyl]guanidine (UR-AK57), a potent partial agonist for the human histamine H<sub>1</sub>- and H<sub>2</sub>-receptors. *J Pharmacol Exp Ther* **317**:1262-1268.

Zhao MM, Hwa J and Perez DM (1996) Identification of critical extracellular loop residues involved in  $\alpha_1$ -adrenergic receptor subtype-selective antagonist binding. *Mol Pharmacol* **50**:1118-1126.

## Chapter 10

### Summary

The histamine H<sub>2</sub> receptor (H<sub>2</sub>R) is a biogenic amine receptor that belongs to the class 1 of G protein coupled receptors. *N*-[3-(1*H*-imidazol-4-yl)propyl]guanidines such as arpromidine are the most potent H<sub>2</sub>R agonists known so far and might be useful as positive inotropic drugs. Recently, less basic *N*<sup>G</sup>-acylated derivatives with improved pharmacokinetic properties, *i.e.* oral bioavailability and the capability of penetrating across the blood-brain-barrier, have been developed. Guanidines and *N*<sup>G</sup>-acylguanidines are more potent and efficacious agonists at the guinea pig (gp) than at the human (h) H<sub>2</sub>R species isoform.

The aim of this thesis was to investigate molecular mechanisms underlying distinct functions of H<sub>2</sub>R species isoforms. Structural models of hH<sub>2</sub>R and gpH<sub>2</sub>R were expected to provide insight into the binding mode of guanidine-type agonists and to explore the molecular basis for the species-selectivity of these agonists. Predictions emerging from molecular modelling provided a basis for subsequent experimental molecular pharmacological studies.

Three-dimensional homology models of hH<sub>2</sub>R and gpH<sub>2</sub>R were generated using the crystal structure of bovine rhodopsin as template. With these models, conserved intramolecular interactions were reproduced according to present concepts of GPCR structure and function. Analysis of the binding site predicted amino acids within the transmembrane (TM)-spanning domains TM2, TM3, TM5, TM6, and TM7, as well as Lys-173 and Lys-175 of the second extracellular loop for interactions with guanidine-type agonists. An interaction between the non-conserved Tyr-17 in TM1 and Asp-271 in TM7 was selectively formed in the gpH<sub>2</sub>R model and proposed to determine the species-selectivity of the compounds. A virtual screening approach with the program LUDI resulted in the development of alkyl-branched *N*<sup>G</sup>-(phenylalkanoyl)guanidines with enhanced potencies at the hH<sub>2</sub>R.

The hH<sub>2</sub>R model was subjected to molecular dynamics simulations both in its ligand-free form and in complex with arpromidine. A hydrated 1-palmitoyl-2-oleoyl-*sn*-glycero-3-

phosphatidylcholine bilayer was added to the model to realistically simulate the membrane environment of the receptor. The selective formation and deletion of interactions dependent on the presence or absence of arpromidine in the binding pocket was proposed to represent perturbations that are necessary for the transition from an inactive towards an active receptor state. The results from simulations help on further refining dynamic models of the binding mode of guanidine-type agonists.

In the experimental part of this thesis H<sub>2</sub>R species isoforms of human, guinea pig, rat and canine were pharmacologically characterized. Recombinant proteins were expressed using a baculovirus/Sf9 insect cells expression system. In a steady-state GTPase activity assay at membranes expressing fusion proteins of the H<sub>2</sub>R and the short splice variant of G<sub>sα</sub> (G<sub>sαS</sub>), only canine H<sub>2</sub>R exhibited an increased level of constitutive activity compared to hH<sub>2</sub>R. Moreover, in membranes expressing fused and non-fused receptors the highest basal and GTP-dependent increases in adenylyl cyclase activity were observed with canine H<sub>2</sub>R. From H<sub>2</sub>R modelling, the constitutive activities of H<sub>2</sub>R species isoforms were predicted to depend on the presence or absence of interactions requiring the non-conserved Arg-228.

Characterization of a mutant hH<sub>2</sub>R-G<sub>sαS</sub> fusion protein with Cys-17 and Ala-271 mutated into the corresponding gpH<sub>2</sub>R residues, Tyr-17 and Asp-271, confirmed the selective formation of an interaction between both amino acids in the gpH<sub>2</sub>R and the critical role of this interaction in determining the species-selectivity of guanidine-type agonists. An hH<sub>2</sub>R-G<sub>sαS</sub> fusion protein with the four amino acids in the second extracellular loop differing in human and guinea pig mutated into the gpH<sub>2</sub>R sequence, and a gpH<sub>2</sub>R-G<sub>sαS</sub> protein with the corresponding point mutations into the hH<sub>2</sub>R sequence, were generated. Efficacies and potencies of agonists were similar in the GTPase assay at these mutants and the wild-type receptors indicating that the second extracellular loop does not contribute to the species-selectivity. With two additional mutant hH<sub>2</sub>R-G<sub>sαS</sub> proteins bearing single point mutations of Lys-173→Ala-173 and Lys-175→Ala-175, respectively, agonist activities remained unchanged, suggesting that both amino acids do not participate in direct ligand-receptor interactions.

The complementary application of three-dimensional structural models and molecular pharmacological studies provided striking insight into molecular mechanisms and species-selectivity of H<sub>2</sub>R functions and ligand-receptor interactions. An improved knowledge of the binding mode of guanidine-type agonists may facilitate the development of more potent and selective derivatives. Moreover, results from this thesis are not restricted to the H<sub>2</sub>R subclass but may also apply to other members of the G protein coupled receptor family.



# Chapter 11

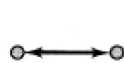
## Appendix

### Appendix 1: Principles of Molecular Mechanics and MD Simulations

#### Empirical force field methods: molecular mechanics

For modelling of proteins and protein-ligand interactions empirical force fields are commonly used to approximate reasonable low-energy structures. The core of any force field is a potential energy function which describes the relationship of a molecular structure to the energy ( $V$ ) of the system of interest. For an exhaustive description of all nuclei and electrons in the system, high-level quantum mechanical methods would be required. With increasing complexity of the molecular system, these methods will become infeasible due to the large time-consumption of the calculations required. Force field methods ignore the electronic motions and calculate the energy of a system as a function of the nuclear positions only. This simplification is permitted by the Born-Oppenheimer approximation, separating the Schrödinger equation into the parts of electron motion and the motion of atomic nuclei.

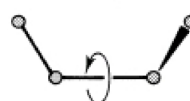
Typically, the potential energy function of the system contains additive contributions of bonded and non-bonded interactions (Figure 11.1). Bonded interactions can be subdivided into terms describing bond stretching ( $V_{\text{stretch}}$ ), angle bending ( $V_{\text{bend}}$ ), and bond rotation ( $V_{\text{torsion}}$ ). Non-bonded interactions are calculated between all pairs of atoms ( $i$  and  $j$ ) that are in different molecules or in the same molecule but separated by at least three bonds. The non-bonded term is usually modelled using a Coulomb potential term for electrostatic interactions ( $V_{\text{elec}}$ ) and a Lennard-Jones potential for van der Waals interactions ( $V_{\text{vdW}}$ ). Depending on the force field, additional terms are included.

**Bonded interactions:**

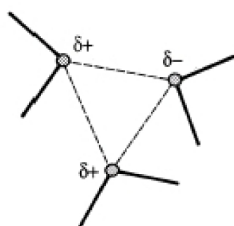
bond stretching



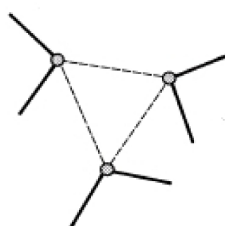
angle bending



bond rotation (torsion)

**Non-bonded interactions:**

electrostatic interactions



van der Waals interactions

**Figure 11.1:** Bonded and non-bonded interactions between atoms calculated in a force field potential.

The total potential energy in the system is given by:

$$V = V_{\text{stretch}} + V_{\text{bend}} + V_{\text{torsion}} + V_{\text{elec}} + V_{\text{vdW}} + \dots \quad (11.1)$$

The potential due to variations in bond length between atoms  $i$  and  $j$  is usually modelled as a harmonic spring:

$$V_{\text{stretch}}(r_{ij}) = \frac{k_{ij}^b}{2} (r_{ij} - r_{ij}^0)^2 \quad (11.2)$$

where  $k_{ij}^b$  is the bond-stretching force constant and  $r_{ij}^0$  is the equilibrium bond length. In more refined force fields a cubic term (Allinger, 1977), a quartic function (Allinger et al., 1989; Lii and Allinger, 1989a, b), or a Morse function (Morse, 1929) have been included. In a similar way, angle stretching for the atoms  $i, j, k$  (where  $j$  is the central atom) can be described by

$$V_{\text{bend}}(\theta_{ijk}) = \frac{k_{ijk}^\theta}{2} (\theta_{ijk} - \theta_{ijk}^0)^2 \quad (11.3)$$

with  $\theta_{ijk}^0$  being the equilibrium bend angle and  $k_{ijk}^\theta$  the angle-bending force constant. The potential energy associated with the rotation of a bond is usually expressed as

$$V_{\text{torsion}}(\phi_{ijkl}) = k_{jk}^{\phi} [1 + \cos(n\phi - \phi^0)] \quad (11.4)$$

with the torsion angle  $\phi$  defined by the atoms  $i, j, k, l$  (where atoms  $j$  and  $k$  form the bond). The multiplicity  $n$  determines the number of minima and barriers during a full rotation and  $\phi^0$  their positions.  $k_{jk}^{\phi}$  is the force constant.

To adjust the geometry of planar groups such as aromatic rings or ester functions, improper torsion and out-of-plane bending terms are usually added to the potential energy function.

The Lennard-Jones potential describes the interaction of two non-bonded atoms using both an attractive dispersive (van der Waals interactions) and a strong repulsive contribution important on short distances:

$$V_{\text{vdW}}(r_{ij}) = 4\epsilon_{ij} \left[ \left( \frac{\sigma_{ij}}{r_{ij}} \right)^{12} - \left( \frac{\sigma_{ij}}{r_{ij}} \right)^6 \right] \quad (11.5)$$

with  $r_{ij}$  being the distance between the atoms  $i$  and  $j$ ,  $\sigma_{ij}$  the collision diameter, and  $\epsilon_{ij}$  the well depth. The electrostatic interaction between two charged particles can be calculated by Coulomb's law:

$$V_{\text{elec}}(r_{ij}) = \frac{q_i q_j}{4\pi\epsilon_0 \epsilon_r r_{ij}} \quad (11.6)$$

$q_i$  and  $q_j$  are the charges, separated by the distance  $r_{ij}$ , and  $\epsilon_0$  and  $\epsilon_r$  are the dielectric constant of free space and the relative permittivity, respectively.

There are several force fields for protein modelling implemented in software programs. The most frequently used methods are AMBER (Weiner et al., 1984, 1986), CVFF (Dauber-Osguthorpe et al., 1988), CHARMM (Brooks et al., 1983), and GROMOS (van Gunsteren and Berendsen, 1987).

## Energy minimization

Energy minimization techniques are commonly used to optimize the geometry of molecular structures into a minimum state. Considering the entire energy hypersurface of a macromolecule comprising a very large number of local minima, energy minimization protocols approach the energy minimum that is closest to the starting structure rather than

the global energy minimum (Figure 11.2). Hence, energy minimizations are generally limited to explore only a small fraction of the energy hypersurface. Energy minimization methods can be divided into the classes of solely energy-based methods like simplex, first-derivative techniques like steepest-descent and conjugate gradient, and second-derivative methods like the Newton-Raphson and related algorithms. The simplex method is useful for initial geometry optimizations in systems with very high energy, whereas first derivative methods are most often used for subsequent minimizations of large biomolecules.

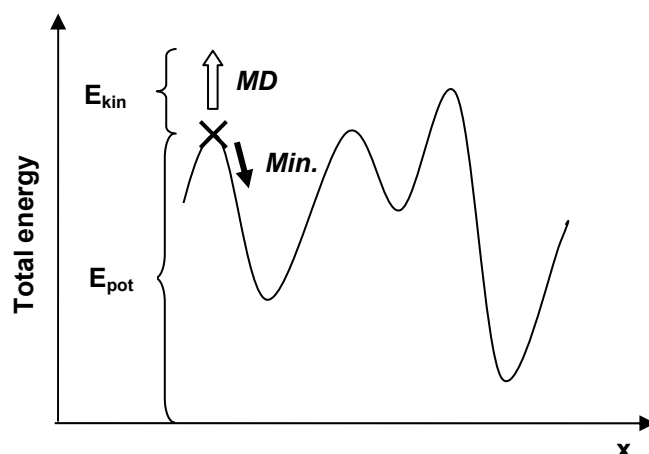


**Figure 11.2:** Principles of energy minimization (*Min.*) and MD simulation (*MD*), illustrated as a walk on the total energy hypersurface (shown in only one dimension).

## Molecular dynamics (MD) simulations

The aim of MD simulations is to reproduce the time-dependent motional behavior of a molecule containing  $N$  interacting atoms by integrating Newton's equations of motion

$$m_i \frac{\partial^2 r_i}{\partial t^2} = m_i \frac{\partial v_i}{\partial t} = F_i \quad i = 1 \dots N \quad (11.7)$$

where  $r_i(t)$  is the position and  $v_i(t)$  the velocity of the atom  $i$ . The momentary force  $F_i$  on each atom is calculated from the derivative of the potential energy function  $V$  in the force field,

$$F_i = -\frac{\partial V}{\partial r_i}. \quad (11.8)$$

For most MD simulations the Verlet algorithm (Verlet, 1967) is used for integration. With this approach, velocities and accelerations of the atoms are assumed to be constant over the time step  $\Delta t$  of integration. Usually, a time step of 1 fs is applied corresponding to vibrational movements of bonds (fastest vibration: C-H stretch  $\sim 10$  fs). The Verlet algorithm is based on the addition and subtraction of the Taylor expansions for the time dependence of the coordinates  $r_i$  at the times  $t - \Delta t$  and  $t + \Delta t$ . A slightly modified algorithm of the Verlet algorithm is the Leap-Frog scheme (Hockney and Eastwood, 1981),

$$v_i(t + \Delta t/2) = v_i(t - \Delta t/2) + \frac{\Delta t}{m_i} F_i \quad (11.9)$$

$$r_i(t + \Delta t) = r_i(t) + v_i(t + \Delta t/2)\Delta t \quad (11.10)$$

The velocities  $v_i$  and coordinates  $r_i$  are calculated at alternating half and whole time steps.

In MD simulations, velocities are generated acting on all atoms depending on the adjusted temperature, thus kinetic energy is supplied to the system. Hence, with MD simulations local energy maxima in the energy hypersurface can be overcome enabling exploration of the conformational space of molecules rather than approaching the closest energy minimum (Figure 11.2).

The reference temperature  $T_0$  in a system is controlled by rescaling the atom velocities every time step with a calculated factor  $\lambda$ :

$$\lambda = \sqrt{1 + \frac{\Delta t}{\tau_T} \left( \frac{T_0}{T} - 1 \right)} \quad (11.11)$$

with the temperature coupling constant  $\tau_T$ . This weak coupling scheme (Berendsen et al., 1984) produces an exponential relaxation to the reference temperature. Similarly, the pressure  $P$  in the system can be controlled through a coupling method scaling the coordinates of all atoms and the box size every time step with a factor  $\mu$ :

$$\mu = \sqrt[3]{1 + \frac{\Delta t}{\tau_P} \beta (P - P_0)} \quad (11.12)$$

where  $\beta$  is the isothermal compressibility of the system,  $\tau_P$  the time constant for pressure coupling, and  $P_0$  the reference pressure.

## References

- Allinger NL (1977) Conformational analysis. 130. MM2. A hydrocarbon force field utilizing  $V_1$  and  $V_2$  torsional terms. *J Am Chem Soc* **99**:8127-8134.
- Allinger NL, Yuh YH and Lii J-H (1989) Molecular mechanics. The MM3 force field for hydrocarbons. 1. *J Am Chem Soc* **111**:8551-8566.
- Berendsen HJ, Postma JPM, DiNola A and Haak JR (1984) Molecular dynamics with coupling to an external bath. *J Chem Phys* **81**:3684-3690.
- Brooks BR, Brucoleri RE, Olafson BD, States DJ, Swaminathan S and Karplus M (1983) CHARMM: A program for macromolecular energy, minimization, and dynamics calculations. *J Comput Chem* **4**:187-217.
- Dauber-Osguthorpe P, Roberts VA, Osguthorpe DJ, Wolff J, Genest M and Hagler AT (1988) Structure and energetics of ligand binding to proteins: *Escherichia coli* dihydrofolate reductase-trimethoprim, a drug-receptor system. *Proteins* **4**:31-47.
- Hockney RW and Eastwood JW (1981) *Computer simulations using particles*, McGraw-Hill, London, 1981.
- Lii J-H and Allinger NL (1989a) Molecular mechanics. The MM3 force field for hydrocarbons. 2. Vibrational frequencies and thermodynamics. *J Am Chem Soc* **111**:8566-8576.
- Lii J-H and Allinger NL (1989b) Molecular mechanics. The MM3 force field for hydrocarbons. 3. The van der Waals' potentials and crystal data for aliphatic and aromatic hydrocarbons. *J Am Chem Soc* **111**:8576-8582.
- Morse PM (1929) Diatomic Molecules According to the Wave Mechanics. II. Vibrational Levels. *Phys Rev* **34**:57-64.
- van Gunsteren WF and Berendsen HJC (1987) *Gromos-87 manual*. Biomos BV Nijenborgh 4, 9747 AG Groningen, The Netherlands 1987.
- Verlet L (1967) Computer "Experiments" on Classical Fluids. I. Thermodynamical Properties of Lennard-Jones Molecules. *Phys Rev* **159**:98-103.
- Weiner SJ, Kollman PA, Case DA, Singh UC, Ghio C, Alagona G, Profeta SJ and Weiner P (1984) A new force field for molecular mechanical simulation of nucleic acids and proteins. *J Am Chem Soc* **106**:765-784.
- Weiner SJ, Kollman PA, Nguyen DT and Case DA (1986) An all atom force field for simulations of proteins and nucleic acids. *J Comput Chem* **7**:230-252.

## Appendix 2: Parameters for MD simulations in GROMACS

**Table 11.1:** Example of a GROMACS input file containing run parameters for MD simulations. Description of parameters was adapted from the GROMACS user manual version 3.2.

Parameter	Value	Description
VARIOUS PREPROCESSING OPTIONS:		
title	md2	Title of the MD simulation.
cpp	/lib/cpp	Location of the preprocessor.
include		Directories to include in the topology.
define		Enables the option of including positional restraints on atom positions.
RUN CONTROL PARAMETERS:		
integrator	md	Application of a leap-frog algorithm for integrating Newton's equations of motions.
tinit (ps)	0	Starting time of the MD run.
dt (ps)	0.002	Time step for integration.
nsteps	1250000	Number of steps to integrate. The simulation period results from the equation $0.002 \text{ ps} \cdot 1250000 \text{ steps} = 2500 \text{ ps}$ .
comm-mode	Linear	Remove center of mass translation.
nstcomm (steps)	1	Frequency for center of mass removal.
comm-grps		Groups for center of mass removal; default is the whole system.
OUTPUT CONTROL OPTIONS:		
nstxout (steps)	500	Frequency to write coordinates to the output trajectory file.
nstvout (steps)	500	Frequency to write velocities to the output trajectory file.
nstlog (steps)	250	Frequency to write energies to the log file.
nstenergy (steps)	250	Frequency to write energies to the energy file.
nstxtcout (steps)	500	Frequency to write coordinates to an xtc file.
xtc-precision	1000	Precision to write an xtc file.
energygrps	Protein POP SOL	Groups to write to the energy file.
NEIGHBORSEARCHING PARAMETERS:		
nstlist (steps)	10	Frequency to update the neighbor list.

ns_type	grid	Make a grid in the box and only check atoms in neighboring grid cells when constructing a new neighbor list every nstlist steps.
pbcb	xyz	Use periodic boundary conditions in all directions.
rlist (nm)	1.0	Cut-off distance for the short-range neighbor list.
OPTIONS FOR ELECTROSTATICS AND VDW:		
coulombtype	PME	Use Particle-Mesh Ewald electrostatics to calculate long-range electrostatic interactions.
rcoulomb (nm)	1.0	Distance for the Coulomb cut-off.
vdwtype	Cut-off	Apply twin-range cut-off's for van der Waals interactions.
rvdw (nm)	1.4	Distance for the Lennard-Jones cut-off.
fourierspacing (nm)	0.12	Maximum grid spacing for the Fast Fourier Transform grid when using PME.
pme_order	4	Interpolation order for PME.
ewald_rtol	1e-05	Relative strength of the Ewald-shifted direct potential.
ewald_geometry	3d	Geometry to use for Ewald summations.
OPTIONS FOR WEAK COUPLING ALGORITHMS:		
tcoupl	berendsen	Temperature coupling with a Berendsen-thermostat to a bath with temperature ref_t and the time constant tau_t.
tc-grps	Protein ARP POP SOL CI	Groups to couple separately to the temperature bath.
tau_t (ps)	0.1 0.1 0.1 0.1 0.1	Time constants for coupling the temperature for each group separately.
ref_t (K)	300 300 300 300 300	Reference temperatures for each group.
pcoupl	berendsen	Exponential relaxation pressure coupling using a time constant tau_p.
pcoupltype	anisotropic	Anisotropic pressure coupling.
tau_p (ps)	5.0 5.0 5.0 0.0 0.0 0.0	Time constant for anisotropic pressure coupling for the xx, yy, zz, xy/yx, xz/zx, and yz/zy components.
compressibility (bar <sup>-1</sup> )	4.5e-5 4.5e-5 4.5e-5 0.0 0.0 0.0	Compressibilities for anisotropic pressure coupling. A value of 4.5 e-5 bar <sup>-1</sup> corresponds to the compressibility of water at 1 atm and 300 K.
ref_p (bar)	1.0 1.0 1.0 0.0 0.0 0.0	Reference pressure.



---

**GENERATE VELOCITIES FOR STARTUP RUN:**

gen_vel	no	Do not generate velocities but use velocities from the previous run.
gen-temp (K)		Temperature for Maxwell distribution.
gen-seed		Used to initialize random generator for random velocities.

---

**OPTIONS FOR BONDS:**

constraints	all-bonds	Constrain all bonds for using the LINCS algorithm.
constraint_algorithm	lincs	Apply the Linear Constraint Solver (LINCS) algorithm to allow for the usage of a time step for integration of 2 fs.

---

**NMR refinement stuff:**

disre	simple	Application of distance restraints of pairs of atoms.
disre_weighting	equal	Divide the restraint force equally over all atom pairs in the restraint.
disre_mixed	no	The violation used in the calculation of the restraint force is the time averaged violation.
disre_fc (kJ mol <sup>-1</sup> nm <sup>-2</sup> )	1000	Force constant for distance restraints.

---

## Appendix 3: List of publications and presentations

### Publications:

Preuss H, Ghorai P, Kraus A, Dove S, Buschauer A, Seifert R (2007) Point Mutations in the Second Extracellular Loop of the Histamine H<sub>2</sub> Receptor do not affect the Species-Selective Activity of Guanidine-Type Agonists. *Naunyn Schmiedeberg's Arch Pharmacol* (in revision).

Preuss H, Ghorai P, Kraus A, Dove S, Buschauer A, Seifert R (2007) Mutations of Cys-17 and Ala-271 in the Human Histamine H<sub>2</sub> Receptor Determine the Species-Selectivity of Guanidine-Type Agonists and Increase Constitutive Activity.

*J Pharmacol Exp Ther* **321**: 975-982.

Preuss H, Ghorai P, Kraus A, Dove S, Buschauer A, Seifert R (2007) Constitutive Activity and Ligand Selectivity of Human, Guinea Pig, Rat, and Canine Histamine H<sub>2</sub> Receptors.

*J Pharmacol Exp Ther* **321**: 983-995.

### Short lecture and poster presentations:

"The binding-site of histamine H<sub>2</sub> receptor agonists: molecular modelling and site-directed mutagenesis", short lecture at the occasion of the evaluation of the Research Training Group (Graduiertenkolleg GRK 760) by the Deutsche Forschungsgemeinschaft, University of Regensburg, January 10, 2006.

Preuss H, Ghorai P, Kraus A, Schneider E, Buschauer A, Seifert R, The canine histamine H<sub>2</sub> receptor is more constitutively active than the human, the guinea-pig, and the rat H<sub>2</sub> receptor, poster contribution, 3<sup>rd</sup> Summer School Medicinal Chemistry, University of Regensburg, September 25-27, 2006.

Preuss H, Dove S, Seifert R, Buschauer A, The binding site of guanidine-type H<sub>2</sub>R agonists: molecular modeling and site-directed mutagenesis, poster contribution at the occasion of the evaluation of the Research Training Group (Graduiertenkolleg GRK 760) by the Deutsche Forschungsgemeinschaft, University of Regensburg, January 10, 2006.

Preuss H, Buschauer A, Dove S, The Human Histamine H<sub>2</sub> Receptor in a POPC Bilayer: Molecular Dynamics Simulations and Structural Analysis, poster contribution, Annual Meeting of the German Pharmaceutical Society (DPhG), Johannes Gutenberg University of Mainz, October 5-8, 2005.

Preuss H, Buschauer A, Dove S, Molecular Dynamics Simulations of the Human Histamine H<sub>2</sub> Receptor in a Hydrated POPC Bilayer, poster contribution, 19. Darmstädter Molecular Modelling Workshop, Friedrich Alexander University of Erlangen, May 3-4, 2005.

Preuss H, Xie SX, Seifert R, Buschauer A, Dove S, Histamine H<sub>2</sub> Agonistic Guanidines: Structural Basis for Species Selective Ligand-Receptor Interactions, poster contribution, Annual Meeting and Joint Meeting of the German Pharmaceutical Society (DPhG), University of Regensburg, October 6-9, 2004.

Preuss H, Buschauer A, Dove S, Analysis of the Species Selectivity of Guanidine-type Histamine H<sub>2</sub>-Receptor Agonists by GPCR Modeling, poster contribution, The 15<sup>th</sup> European Symposium on Quantitative Structure-Activity Relationships & Molecular Modelling, Istanbul, Turkey, September 5-10, 2004.

Preuss H, Dove S, Buschauer A, A model of the interaction of guanidine-type agonists with the guinea-pig histamine H<sub>2</sub> receptor, poster contribution, Fachgruppentagung der GDCh und DPhG Pharmazeutische/Medizinische Chemie („Frontiers in Medicinal Chemistry“), Friedrich Alexander University of Erlangen, March 15-17, 2004.